Feasibility of Multi-Component Spatio-Temporal Modeling of Cognitively Generated EEG Data and its Potential Application to Research in Functional Anatomy and Clinical Neuropathology

By

Philip Michael Zeman
B.Eng., University of Victoria, 2000

A Dissertation Submitted in Partial Fulfillment of the
Requirements of the Degree of

DOCTOR OF PHILOSOPHY

in the Department of Interdisciplinary Studies
with the involvement of the Departments of Electrical Engineering, Biology, and Psychology

Feasibility of Multi-Component Spatio-Temporal Modeling of Cognitively Generated EEG Data and its Potential Application to Research in Functional Anatomy and Clinical Neuropathology

By

Philip Michael Zeman
B.Eng., University of Victoria, 2000

Supervisory Committee

Dr. Ronald W. Skelton, Supervisor
(Department of Psychology)

Dr. Nigel J. Livingston, Co-Supervisor
(Department of Biology)

Dr. Dorothy H. Paul, Committee Member
(Department of Biology)

Dr. Peter F. Driessen, Committee Member
(Department of Electrical Engineering)

Dr. Gary Birch, Additional Member
(Adjunct, Department of Electrical Engineering)

Supervisory Committee

Dr. Ronald W. Skelton, Supervisor
(Department of Psychology)

Dr. Nigel J. Livingston, Co-Supervisor
(Department of Biology)

Dr. Dorothy H. Paul, Committee Member
(Department of Biology)

Dr. Peter F. Driessen, Committee Member
(Department of Electrical Engineering)

Dr. Gary Birch, Additional Member
(Adjunct, Department of Electrical Engineering)

ABSTRACT

This dissertation is a compendium of multiple research papers that, together, address two main objectives. The first objective and primary research question is to determine whether or not, through a procedure of independent component analysis (ICA)-based data mining, volume-domain validation, and source volume estimation, it is possible to construct a meaningful, objective, and informative model of brain activity from scalp-acquired EEG data. Given that a methodology to construct such a model can be created, the secondary objective and research question investigated is whether or not the sources derived from the EEG data can be used to construct a model of complex brain function associated with the spatial navigation and the virtual Morris Water Task (vMWT).

The assumptions of the signal and noise characteristics of scalp-acquired EEG data were discussed in the context of what is currently known about functional brain activity to identify appropriate characteristics by which to separate the activities comprising EEG data into parts. A new EEG analysis methodology was developed using both synthetic and real EEG data that encompasses novel algorithms for (1) data-mining of the EEG to obtain the activities of individual areas of the brain, (2) anatomical modeling of brain sources that provides information about the 3-dimensional volumes from which each of

the activities separated from the EEG originates, and (3) validation of data mining results to determine if a source activity found via the data-mining step originates from a distinct modular unit inside the head or if it is an artefact. The methodology incorporating the algorithms developed was demonstrated for EEG data collected from study participants while they navigated a computer-based virtual maze environment. The brain activities of participants were meaningfully depicted via brain source volume estimation and representation of the activity relationships of multiple areas of the brain. A case study was used to demonstrate the analysis methodology as applied to the EEG of an individual person. In a second study, a group EEG dataset was investigated and activity relationships between areas of the brain for participants of the group study were individually depicted to show how brain activities of individuals can be compared to the group.

The results presented in this dissertation support the conclusion that it is feasible to use ICA-based data mining to construct a physiological model of coordinated parts of the brain related to the vMWT from scalp-recorded EEG data. The methodology was successful in creating an objective and informative model of brain activity from EEG data. Furthermore, the evidence presented indicates that this methodology can be used to provide meaningful evaluation of the brain activities of individual persons and to make comparisons of individual persons against a group.

In sum, the main contributions of this body of work are 5 fold. The technical contributions are: (1) a new data mining algorithm tailored for EEG, (2) an EEG component validation algorithm that identifies noise components via their poor representation in a head model, (3) a volume estimation algorithm that estimates the region in the brain from which each source waveform found via data mining originates, (4) a new procedure to study brain activities associated with spatial navigation. The main contribution of this work to the understanding of brain function is (5) evidence of specific functional systems within the brain that are used while persons participate in the vMWT paradigm (Livingstone and Skelton, 2007) examining spatial navigation.

TABLE OF CONTENTS

Supervisory Committee ii
Abstract iii
Table of Contents v
List of Terms vi
List of Symbols ix
Acknowledgements x
Preface xi
Section I: Introduction D1
Chapter 1. Background, Rationale, Objectives, and Document Organization D2
Section II: Background of EEG Methodology D29
Chapter 2. Understanding and Improving ICA Source Separation of EEG Data D30
Section III: Development of New EEG Methodologies D75
Chapter 3. Beamform Volume Projection of EEG ICA Topographies D78
Chapter 4. Beamform Volume Projection of ICA Components of Scalp EEG: Volume-Domain Uniqueness of Components D121
Chapter 5. Volume Domain Validation of ICA-Derived EEG Sources D145
Chapter 6. Spectral Shaping to Relax ICA Assumptions to Facilitate Decomposition of EEG D196
Section IV: The Novelty, Utility, and Context of the Methodological Advancements D246
Chapter 7. Building a Multi-Component Spatio-Temporal Model Using Scalp-EEG Data D248
Section V: Application of New Methods D293
Chapter 8. Feasibility of System Analysis of Brain Activity for Spatial Navigation using Scalp-EEG D294
Section VI: Discussion and Conclusions D379
Chapter 9. General Discussion and Conclusions D380
References D412
Appendix A: Volume Estimation and Validation: University of Lethbridge Study D433

LIST OF TERMS

alpha waves	electromagnetic oscillations in the frequency range of 8-12 Hz arising from synchronous and coherent electrical activity thought to arise from thalamic pacemaker cells
anatomy	the structure of an organism or any of its parts
behavior	the aggregate of responses to internal and external stimuli
bilateral	pertaining to, involving, or affecting both sides (left and right hemispheres of the brain)
blind source separation	the separation of a set of signals from a set of mixed signals, without the aid of information about the source signals of the mixing process
bottom-up	strategy for information processing were high-level processes do not influence low-level process as pertaining to brain physiology; low-level process might, in fact, influence high-level processes
Brodmann	a region of the cortex defined based on its cytoarchitecture
clinical	concerned with of based on actual observation and treatment of disease in patients
cognition	the mental process of knowing, including aspects such as awareness, perception, reasoning, and judgment
conscious	the part of the mind comprising psychic material of which the individual is aware
correlation	indicates the strength and direction of a linear relationship between two random variables
cytoarchitecture	the cellular composition of a bodily structure
data-mining	the automatic extraction of useful, often previously unknown information
diagnostics and statistical manual of mental disorders	a categorization of psychiatric diagnoses published by the American Psychiatric Association. Also lists causes of

	these disorders, statistics in terms of gender, age at onset, and prognosis as well as some research concerning the optimal treatment approaches
distal	situated away from the point of origin
electroencephalograph	an instrument that measures electrical potentials on the scalp and generates a record of that electrical activity
failed separation distortion	when two sources are not appropriately split during the blind source separation process
feasible	capable of being done, effected, or accomplished
features	a prominent or conspicuous part or characteristic
foetal alcohol spectrum disorder	a continuum of permanent birth defects caused by maternal consumption of alcohol during pregnancy
forced independence distortion	when source activities are forced to be statistically independent during the blind source separation process when the bona fide activities are not
grey matter	greyish nervous tissue containing cell bodies, glia, synapses as well as fibres; forms the cerebral cortex consisting of unmyelinated neurons
inference	the process of arriving at some conclusion that, though it is not logically derivable from the assumed premises, possesses some degree of probability relative to the premises
modular	a self-contained unit
modulate	in telecommunications: to cause the amplitude, frequency, phase, or intensity of (a carrier) wave to vary in accordance with a sound wave of other signal
neuroanatomy	the branch of anatomy dealing with the nervous system
neurophysiology	the branch of physiology dealing with functions of the nervous system
over-determined	has fewer unknowns that equations
paradigm	a set of assumptions, concepts, values, and practices that

	constitutes a way of viewing reality
pathology	any deviation from a healthy, normal, or efficient condition
phenomenon	a fact, occurrence, or circumstance observed or observable
physiology	the branch of biology dealing with the functions and activities
proximal	situated toward the point of origin
psychology	the science of human and animal behaviour
stationary	a stochastic process with a joint probability distribution does not change when shifted in time or space. as a result, parameters such as the mean and variance, if they exist, also do not change over time or space
statistical independence	the occurrence of one event makes it neither more nor less probable that the other occurs
source	any thing or place from where something comes
top-down	strategy for information processing were high-level processes influence low-level process as pertaining to brain physiology
trials	repetitions of a similar set of stimuli to elicit a behaviour
under-determined	has more unknowns that equations
validation	to give official sanction, confirmation, or approval to; the active of finding or testing the truth of something
voxel	the smallest distinguishable box-shaped part of a three-dimensional space
volume	a mass or quantity that occupies physical space
volumetric spectrum	the set of coefficients that defines the value of variance at each location inside the head model
white matter	nerve tissue of the brain which primarily contains myelinated fibres and is nearly white in color

LIST OF SYMBOLS

A	matrix of ICA mixing weights (mixing matrix)
s	matrix containing source waveform activities (source matrix)
W	matrix containing estimated coefficients to separate mixture (weight matrix)
P	matrix containing weights used to sphere the EEG mixture (sphereing matrix)
C(x)	covariance matrix of the data matrix x
H	matrix containing lead field coefficients describing characteristics of the model head
q	index of a grid location in the head model
tr{**C**(x)}	trace of the covariance matrix of x
m(**q**)	matrix describing the x,y,z moment of position q in the head model
V	
r	vector containing the volume-projected coefficients obtained from an ICA scalp topography (volumetric spectrum)
Q	matrix describing covariance of a noise matrix
K	number of time samples
M	number of electrodes
N(*t*)	matrix of time-varying noise
i, j, k	indices
P	number of grid points inside a head model
G(*t*)	Matrix of idealized data used by the beamformer
T	threshold calculated for separating noise contained in the volumetric spectrum from estimated source volumes

ACKNOWLEDGEMENTS

Thank-you to John, Melinda, Lucy, and Claire Minkley for inspiring this project.

I would also like to thank Sunny Mahajan for the many hours in the lab during which we explored the intricacies of brain activity analysis and devised schemes to create something profound.

I would also like to thank my friends and family. Thank-you for understanding that writing is a solitary endeavour. If I ever tackle a project such as this again, I know you will support and encourage me.

PREFACE

The format of this dissertation is atypical. The Ph.D. committee has required that this dissertation be a compendium of journal paper manuscripts. The dissertation thus contains some repetition; each component of the dissertation is a complete and independent work. To facilitate this format, two page numbering systems are present because the pages of each manuscript are numbered with their own numbering system. Page numbers for individual manuscripts are provided at the top of each page. Page numbering for the dissertation is provided at the bottom of each page with the prefix 'D'.

Section I: Introduction

This section of the dissertation describes the inspiration and insights that led to the investigation of the Ph.D. research question and provides a 'big-picture' context for the larger problems to which the results of this research can be applied. A description of current EEG analysis methods, their limitations, and how the current research might be used to address some of these limitations is provided. This section is concluded with a description of the components of the research and how they relate.

Chapter 1: Background, Rationale, Objectives, and Document Organization

I. INTRODUCTION

Electrical recordings from the scalp of humans, called an electroencephalograph (EEG), are used in a variety of medical and research settings to examine activities of the brain. Medically, the EEG has proven valuable in detecting compromised brain function often visible as epileptic spike-wave activity in the EEG. It has also been useful for providing information for making decisions about the level of brain function present; for example, in identification of coma. The EEG has also proven valuable in characterizing the multiple stages of sleep. The EEG has been adopted as a mechanism by which to understand the relationship between brain activity and overt human behaviour, and to understand how brain function supports cognitive processes.

However, while the activities of the brain can be measured at the scalp as EEG activity, standard scalp-EEG analytical methods do not use the EEG to directly describe brain function. Within current research methodologies, EEG data are typically used to create inference-based models of brain activity; predictions are made of the measured change in electrical field activity at the scalp that corresponds to strategic manipulations of well-studied behavioural paradigms. Such predictions are tested as hypotheses based on prior knowledge obtained from experiments that similarly examine the relationship between scalp field activity and human behaviour. Such experiments examine a small number of features of the EEG that vary in amplitude and latency between similar human behaviours. Their findings are interpreted and validated by statistically relating EEG results across multiple participants and data collection sessions. Findings of individual experiments are interpreted together, with other non-EEG data, via a meta analysis or literature review to draw conclusions about how the scalp field activity relates to human behaviour and brain function. Attempts are made to explain the scalp-measured electric fields in terms of anatomical source regions by semi-automated trial and error dipole fitting. Such methods attempt to model the possible locations of areas of the brain that project activities from inside the head to the surface of the scalp by using point-source electric-field dipoles positioned at strategic locations in a model head to account for the electric field variance at the scalp. Together, multiple studies and anatomical brain

modelling methods provide a more complete model of brain function than can be established from any one experiment alone. The major drawback to this methodology, however, is that obtaining knowledge about the brain requires a complex repeated cycle of prediction, EEG feature measurement, behavioural manipulation, anatomical modelling, and statistical analysis. Moreover, potentially important data describing individual differences between experiments and subjects are lost.

In this dissertation, a new direct methodology of analyzing scalp-acquired EEG data to describe brain function is presented. The objective of this methodology is to extract as much information as possible from the EEG data, with minimal researcher interference, to meaningfully reveal the functional brain activities contained in the EEG data. The methodology attempts to maximize the information that can be obtained in a single experiment. By this method, the data collected from a single person can be analyzed to make conclusions about their functional brain activity and, similarly, the brain activities of multiple persons can be compared in a single experiment. The proposed methodology encompasses the following steps, which will each be explained in subsequent chapters. First, EEG data that are revealing of brain function and are appropriate for data-mining are obtained. Second, the acquired EEG data are mined using characteristics of the time-domain EEG to reveal the individual activities of modular macroscopic regions of the brain. This step attempts to isolate activities originating from specific anatomical areas of the brain, such as specific cyto-architectonically defined Brodmann areas. Third, the data-mining results consisting of a description of the time-varying electric field at the scalp for each component of the EEG are mathematically transformed into volumetric representations inside the head. Fourth, each possible brain source found via data-mining is validated to ascertain the likelihood that it is not an EEG artefact. This is done via a procedure of scoring the volumetric representations of each possible brain source. Since validation is accomplished using the characteristics of the data itself rather than external measures, information about activities of the brain are immediately available. Fifth, physical 3-dimensional modular brain source volumes pertaining to the validated brain sources are calculated. This step provides meaningful representation of active areas of the brain to facilitate interpretation of brain function. Finally, the dynamic coordination of

activities of these brain volumes is estimated to provide a system-level view of brain function. These brain volumes and respective coordinated activities are then depicted graphically for interpretation. This perspective is appropriate to provide information about information transfer in the brain such as processing of stimuli, and top-down control of high functioning brain areas to evaluate attention and memory processes.

MOTIVATION

This project began with an investigation of scalp-EEG with the intent of using it to construct a brain-computer interface and has concluded with the development of a new EEG analysis methodology to extract meaningful information from the scalp-EEG.

This research was inspired by the necessity to understand the unique brain physiology of a young woman named Claire Minkley. Abnormal brain development left Claire without the ability to speak and without skilled use of her limbs. Having these disabilities she was still able to communicate, however, not without a care-aid worker acting as an interpreter. The 'Claire Project' was created to create a device to provide her from some autonomy. One concept for providing this autonomy was to develop an EEG-driven device that would detect specific brain activities and use them to control a computer. However, in order to use her EEG as the input to such a device it was necessary to identify suitable cognitively controllable brain activities visible as 'features' in the EEG. It turns out that there are many different features to choose from, each with advantages and disadvantages.

The CanAssist group at the University of Victoria, a successor of the Claire Project, conducted some initial investigation to determine what suitable brain activity features might be available in the EEG. Alpha waves (activities in the alpha frequency band) were identified as a possible EEG feature to facilitate 'yes'/'no' communication. However, while it is known that alpha waves can be modulated by attention (Jackson GM and Everly DA, 1982; Mulholland, 1969), and the CanAssist group was able to show that alpha waves can easily be detected in the scalp-EEG, doubt remained as to the

effectiveness of the use of alpha band activities in this particular application. Alpha band activities are generally large amplitude making them easy to detect. The fundamental issue is that alpha waves accompany many types of processing in the brain. This includes such processes as semantic memory recall (Klimesch, 1999) and limb movement preparation (Andrew and Pfurtscheller, 1997). Alpha band activities are also generated as a result of a neurophysiological mechanism called focal event-related desynchronization/surround event-related synchronization (Pfurtscheller and Neuper, 1994; Suffczynski et al., 1999) of cortical activities. This is thought to occur whenever a specific part of the cortex is to be utilized in a behavioural function; the portion of the cortex to be utilized becomes desynchronized in the alpha band (decreased alpha band power), while the surrounding areas become synchronized in the alpha band (increased alpha band power). This poses a problem for an alpha wave based communication system because any 'non-target' area of the cortex that is not directly related to the target human behaviour might generate alpha band activities. Another weakness of using alpha band signals relates to susceptibility to wide band noise fluctuations. Generally, any increases in wide-band power, if narrow band filtered, appear at the output of the narrow band filter as an increased amplitude sinusoidal signal. In such a case, an increase in alpha band brain activity is indiscernible from an increase in wide band noise. Thus, to effectively use the amplitude of alpha waves as a means of communication also requires an estimate of the wide-band noise level to determine what amount of activity through the alpha band filter might be accounted for by fluctuating noise levels. It is, however, difficult to determine what part of the EEG spectrum should be monitored to quantify fluctuating wide-band noise levels. This is because the, 'wide band noise' might actually be the bona fide activities of other neural processes that create randomly fluctuating EEG amplitudes. For these reasons, use of alpha band activities for 'yes/no' communication was abandoned.

Other methods that use scalp-measured brain activities to control a computer have utilized features found in the EEG that occur coincidently with hand movement (Birch et al., 1988; Borisoff et al., 2004). While success has been demonstrated using their approach, the feature detection block of their method has a large false positive rate. They

have compensated for these false positives via a processing block that asserts a 'switch de-bouncing' period after each event is detected; there is a window of time after an event is detected for which all other features detected are ignored. This additional processing block has decreased the false positive rate and increased the reliability of their system, however, the fundamental issues underlying the multiple feature detections have not been directly addressed; this multiple feature detection problem has a possible neurophysiological basis. The false positives detected might actually true detection of the brain activities of interest; there may be a burst of multiple events related to the planning stage of generating limb movement rather than the 'single feature event' for which the feature detection processing block is designed. This may have a relation to how the brain plans limb movements; movement planning is thought to be automatic and occurring independently of movement execution (Glover, 2004) and multiple 'planning events' may accompany each single movement execution. For at least some types of limb movements, the intentional gating to transition from the movement planning stage to the movement execution stage has been shown to be facilitated by sub-cortical brain structures such as the basal ganglia.

Another EEG signal that could be used as an input to a brain communication device is the sensory evoked potential. It has been shown to be a good indicator of a person's attention to particular stimuli and thus, a system whereby various visual stimuli are presented and the brain response is monitored might provide a means for selection of visually presented menu options. This signal originates from brain areas such as the visual or auditory cortices and its amplitude is modulated by higher-level cognitive brain areas (Kim et al., 2007; Zani and Proverbio, 1997; Trenado et al., 1997). Modulation of the sensory evoked potential by high-level brain areas results in a small amplitude EEG peak at the presentation of a stimulus if the person does have 'interest' in the stimulus and directs attention towards the stimulus. If there is 'no interest' or attention towards the stimulus, the amplitude of the EEG peak is reduced. However, in most situations this evoked potential generally requires between 30 to 100 trials of stimulus presentation, the counterbalancing of trial presentations with other non-interesting stimuli, and averaging

of the data of each trial, to be able to discern these activities of 'interest' versus 'non-interest' from interfering background brain activities.

Clearly, to design a reliable brain-computer interface, it is important to identify appropriate features in the EEG. These features should be under full conscious and cognitive control of the person who is to generate them and should be specific enough that they are not unintentionally generated by non-target cognitive and behavioural processes. It is thus important to consider the fundamental cognitive and non-cognitive operations of the brain and the features in the EEG might accompany them. To do this, requires good knowledge of brain function and the relationship between behaviour and brain function. For this reason, the focus of this investigation shifted from construction of a brain computer interface to understanding brain function and finding a way to reliably detect specific cognitively generated signals from the brain.

A review of available literature to identify possible EEG features that might be present given Claire's specific brain function revealed only very general information. This provided for an important insight. It became apparent to me that the EEG is investigated as one would study a phenomenon, and from this phenomenon, brain function is inferred. In my opinion, the EEG is underutilized to describe specific characteristics of brain function, such as which areas of the brain coordinate with each other and how they coordinate to facilitate human behaviour. Current standard EEG methods do not exploit the detail in the EEG to maximize the information that can be derived. Their findings are based on averages across subjects and averages across experimental trials to identify abstract characteristics of the EEG that relate to behaviour. These methods are not designed to reveal unique brain activities relating to the way each individual person's brain processes information. This insight, combined with the expressed frustration of Claire's father that nobody could provide him with concrete information regarding Claire's brain function (for example, her perceived physical pain related to her physical condition) put me on a path to devise some new EEG analysis methods.

RESEARCH GOALS

The EEG analysis methodology described in this dissertation has been developed to facilitate examination of brain function of individual persons and to provide directly interpretable information by which to draw conclusions about brain function in individual experiments. By using this methodology in future cases similar to Claire's, we might be able to characterize the brain activities underlying the scalp-EEG, better understand the brain disorder, and be better prepared for any necessary treatment. Secondarily, this methodology would serve as the first step in designing a robust brain-computer interface as it provides a means to identify and characterize specific activities of the brain that are present in the EEG and under specific cognitive and/or behavioural control.

Stemming from the proposal that EEG data can be more effectively utilized for understanding brain activities, I have defined a set of hierarchical goals to direct my research. My ultimate and far-reaching vision is to be able to capture the functional brain characteristics of single subjects, map these characteristics to a meaningful representation, and if applicable and available, compare such representations against those of a 'healthy' or 'control' population. Given this ability, it might be possible to better understand brain pathologies and to improve on traditional neuropsychological diagnostic tests. For example, such diagnostic tests could use a patient's brain activity itself for comparison against a continuous-scale standardized database of brain activities; current diagnostic tests use scoring and database comparison based on observation of overt behaviour or pen and paper tests to make diagnostic assessment of brain function (DSM-IV, 1994). This is a lofty goal requiring some small 'first steps' towards it. The primary and direct goal, as it applies to this PhD dissertation, is to examine the feasibility of building a meaningful functional model of the brain activity that takes place in relation to behaviour during a single EEG experiment, and ideally, a single EEG recording session.

In order to develop such an EEG analysis methodology, I was required to obtain an appropriate set of EEG data. This was accomplished by posting inquires on the internet.

Patricia Sorensen, directed by Robert Sutherland, at the University of Lethbridge, Canadian Centre for Behavioural Neuroscience, was examining scalp-EEG data collected during a virtual spatial navigation task called the virtual Morris Water Task (vMWT) (Hamilton et al., 2003). Their data analysis approach using traditional EEG analysis methods to identify scalp-EEG field differences among the different cognitive conditions of the spatial navigation task proved unsuccessful; the main issue, it seems, is that the EEG of the vMWT is comprised of activities from many parts of the brain creating a complex problem for traditional analysis methods. Having failed to yield results using standard methods, they employed a recently developed experimental method, independent component analysis (ICA) (available with the EEGLab software package (Makeig et al., 1996) to make sense of the EEG data. Again however, they were unable to obtain interpretable results from existing ICA methods. Their greatest challenges were how to determine which components of an ICA decomposition of EEG likely represent brain activities and which ones were artefacts, and how to make comparisons across subjects and behavioural groups.

The development and initial evaluation of the methods described in this dissertation has been done using the University of Lethbridge EEG dataset. To evaluate these methods on an independent dataset, I have used EEG data collected at the University of Victoria collected using the virtual spatial navigation paradigm of Ron Skelton and Sharon Livingstone. Evaluation of the methods using multiple datasets collected in different environments using different EEG acquisition equipment can be used to show if results found using the methods are sensitive and possibly caused by these factors. Ideally, the location, and equipment used should have little impact on the result, assuming the behaviour and brain activities measured are the same.

Developing these methods using datasets collected using a vMWT paradigm is fortuitous for one additional reason. That is, behavioural measures obtained using such paradigms have been shown to be effective at revealing behavioural and cognitive deficits. For this reason, such a task should be suitable to be used in conjunction with the proposed EEG analysis methodology for determining diagnostic criteria for brain pathologies. Hence,

this EEG can successfully be analyzed these methods with the vMWT behavioural paradigm provide a means of diagnostic assessment.

Our primary research question is whether or not, through a procedure of data-mining using ICA, validation, and source volume estimation, it is possible to construct a meaningful, objective, and informative model of brain activity from the EEG data. Standard EEG analysis is typically directed by predetermined conclusions or theoretical constructs based on results obtained from similar EEG studies; for example, in modelling a scalp field by placing dipole sources inside a head model, researchers will often try multiple dipoles at multiple theoretically driven locations to get the best fit of scalp variance. (For example, see (D'arcy et al., 2004).) In contrast, our objective is to obtain information about the brain using as little of this prior knowledge and theory as possible; it is not assumed which areas of the brain will be active given a particular behavioural paradigm. Given that such a model can be constructed, can the cross-correlation of ICA derived sources be used to construct a physiologically accurate model of transiently co-operating parts of the brain? Can this be done for complex brain function such as that associated with the virtual Morris Water Task (vMWT)? Can a computer model describing the interaction of multiple parts of the brain over time be constructed from the brain activities of individual persons? Can this be done to compare the EEG of individual persons to a group? In addressing these questions, a step-wise data analysis methodology has been developed that incorporates the steps of: obtaining EEG, mining the EEG, validating results of the data-mining and representing brain activity sources as modular volumes.

EVOLUTION OF EEG METHODOLOGIES

The proposed methodology is a logical advancement of three main classic analytical methods. These are the standard and most widely-known methods used for both experimental study and clinical assessment. Two alternate methods of analysis are the evoked potential (EP) and the event-related potential (ERP). The third method is generally known as analysis of the continuous EEG and is herein referred to as EEGc.

Analysis using EP and ERP methods is fundamentally based on acquiring EEG data during multiple presentations of a strategic stimulus and the ensemble averaging the EEG data of each stimulus trial collected to obtain an average result. For example, during each stimulus presentation, a waveform is recorded from the scalp. The waveforms generated from many stimulus presentations are trial-averaged together to form the EP or ERP waveforms. By averaging the scalp activity related to brain activity response to each stimulus presentation, a representation of the average scalp activity is obtained. The random brain response inconsistencies and random interfering noise activities are reduced in the average waveform. Analysis using EPs assumes the scalp potential arises from activities of well-known sensory pathway neuroanatomy of the brain that provides sensory feature detection and does not rely on high-level psychological processes. For example, studies of auditory-evoked brain waves examine the amplitude and latency of stimulus-locked waveform peaks occurring between 0 and 150 ms, post stimulus use the EP model. In contrast to the EP, the ERP encompasses both the brain activities considered by the EP and also those that are traditionally thought to arise from post-sensory neural activities. The ERP is used to study the brain activities of psychological events where the sensory stimuli are combined and analyzed in the brain with the constructs of expectation, memory, and stimulus identification. ERP-type analysis generally examines waveform peak properties in the range 150-600 ms, post stimulus. For both the EP and the ERP, the amplitude and latency of the stimulus-locked waveform peaks revealed by the ensemble averaging process are studied.

Unlike the EP and the ERP, EEGc methods utilize raw data from individual trials of an experiment, without ensemble averaging trials of data and do not require the use of specific stimuli. This method has its origins in the study of human sleep behaviours or states including hyperventilation and coma, and brain activity changes related to environmental conditions such as room temperature and oxygen supply. The assumptions behind EEGc analysis consider the activity measured at the scalp as an abstract electrical phenomenon that does not necessarily relate to a specific neuroanatomical processing pathway.

Each method has a second stage of analysis from which inferences are drawn. These secondary processing methods are similar for EP, ERP and EEGc analysis methods. For example second-stage analysis of the EEGc by covariance and correlation of activities from multiple different parts of the scalp can be used in an attempt to infer the degree to which the activities of the brain are synchronized. Similarly, frequency band power analysis can be employed to determine the amount of processing required for a particular stimulus or in relation to a behavioural state. For example, it is generally assumed that greater average power in the gamma frequency band relates to greater brain processing.

These classic analytical methods were originally designed to analyze data collected from a single electrode. However, the availability of multi-channel recording, providing full-coverage recording of activity at the scalp, allowed for some significant analysis advancements such as correlation analysis of the EEG among different electrodes. Unfortunately, the time-varying electric field activities obtained at many of the scalp sensors are highly correlated due to volume conduction (Nunez et al., 1997) and not necessarily because the activities of differing brain areas generating the EEG are correlated. Volume conduction in the scalp leads to mixing of various brain source activities such that activity at a particular electrode is the sum of multiple brain sources; activity at a given electrode does not necessarily represent the activity of a single modular area of the brain.

Second order statistical factoring of the multi-channel recordings using Principal Component Analysis (PCA) was introduced for the purpose of separating the EEG activities into more easily interpretable parts. This statistical method was introduced to identify uncorrelated factors of brain activities among the EEG recorded for multiple behavioural conditions (Donchin, 1966). More recent advances were subsequently made to improve PCA analysis of EEG data such as the addition of secondary processing steps such as Varimax (Kaiser, 1958), Weighted Varimax, and Promax rotations (Cureton and Stanley, 1975). By using PCA methods, multi-channel recordings can be used to separate

the EEG scalp field into uncorrelated parts, providing a significant advancement over prior single channel and multi-channel analytical methods.

To facilitate interpretation of multi-channel scalp recordings and the PCA factors identified, source modelling methods were developed that links scalp field variance to brain anatomy. Using such methods, regions of the brain with activities projecting to the scalp are modelled as point-source dipoles. Iteratively, by optimization, the positions of such dipoles are adjusted to maximally account for the scalp-field variance (Scherg and Berg, 1996). An alternative to iterative optimization is Least-Constrained Minimum Variance (LCMV) beamforming, which uses a closed-form mathematical solution that maps scalp surface variance to variance within a volume head model. It was introduced as a means to both factor the multi-channel EEG using second-order statistics and simultaneously identify the centers of mass of source locations (Van Veen et al., 1997).

More recently, a method called independent component analysis (ICA) was introduced as an alternative to PCA methods to separate the sources comprising the EEG data mixture (Makeig et al., 1996). Source separation by this method identifies maximally statistically independent sources that comprise the EEG data. The time-domain activities of such sources are uncorrelated, as are those found by time-domain PCA methods, and they are also statistically independent. Statistical independence means that the time-domain activities of one source can not be predicted from the activities of other sources.

Our proposed EEG analysis methodology builds on current experimental ICA and beamform methodologies. While our method is similar to prior ICA methods, our goal is fundamentally different. In particular, our goal is to mine the EEG data for the activities of modular brain areas and resolve them as realistic brain volumes. Differing from the previous methods, the EEG data are mined using custom source separation criteria (rather than the criteria used by strict PCA or ICA) in an attempt to identify activities in the scalp EEG that originate from physically modular volumes within the brain. Our custom criteria do not require that brain source activities are uncorrelated or statistically independent in the standard sense. Thus, the components of the EEG identified, are not

in the standard sense, necessarily uncorrelated or statistically independent (described in Chapter 6). The location and volumes of activities of modular brain sources are found by our custom beamforming volume-domain projection algorithm (Chapter 3). Characteristics derived from the volume-domain projection of EEG components are used to identify them as either brain activity or as an artefact (Chapter 5).

Our processing methodology is essentially a first step before applying the EP, ERP or EEGc analysis methods. Because our method isolates the activities of individual brain areas, EP, ERP and EEGc analysis methods can be applied more effectively than on the raw EEG data from individual electrodes. Correlation analysis, trial averaging of waveforms, and waveform peak amplitude and latency comparisons can all be used as though the data were recorded from a single electrode, however, in this case, the activities of specific parts of the brain have been isolated and separated from the interference of other areas. The center of mass location and volume of the brain from which the waveform activities originate are also known and validated thus making this processing step an important contribution to scalp EEG analysis methods.

ADDRESSING LIMITATIONS OF CURRENT METHODS

The proposed methodology where will herein refer to as Multi-Component Spatio-temporal Modelling for EEG (MCST-EEG) is an attempt to address some fundamental limitations of standard methods. The end result is that the EEG is treated less like a phenomenological process that varies according across different behavioural paradigms and more like a system of measurement of activities of specific volumes within the head. The MCST-EEG methodology processes the scalp EEG so that the measured activities are directly represented in a functionally meaningful way-- as activities of specific areas of the brain with specific functional relationships.

The foremost weakness of current methods is the reliance on hypothesis testing and multiple studies to provide new understanding of brain function. They do not easily and directly allow for the discovery of new results because each result must be anticipated

prior to its discovery in the data to qualify as a statistically valid finding. Using these methods, a conclusion based on as much prior information as possible is assumed, and then tested for correctness. To assume a result is valid without an established hypothesis can be considered 'fishing'. In addition, hypothesis testing requires that statistical power be balanced and conserved. Hence, in a single experiment, there is a limit imposed on the number of possible statistically significant findings. Because of the statistically-based nature of results, replicate experiments are required to determine if findings are bona fide or an 'artefact' of the experiment. Hence, to gain a small amount of knowledge that can be used in the treatment process of a clinical patient or clinical group, numerous experiments measuring the same effect are required.

It is difficult to interpret the EEG to make statements about an individual's brain function in the absence of statistics across subjects and a correlative relationship of the EEG to a behavioural or psychological measure. By themselves, EEG data are difficult to interpret. Two characteristics are usually used for interpretation: the consistency of brain activity in relation to a specific behaviour, and the relation of brain activity to psychological and pathological classifications. The consistency of brain activity in relation to a behaviour provides a direct point of interpretation. It is available when group behavioural data, such as button press times, are found to be correlated with some group characteristic of the EEG. Generating statistics across multiple study participants or data-recording sessions also provides a measure of consistency. It is assumed that features in the EEG that are consistent across different subjects and data-recording sessions must be related to the average brain activity and the behaviour of interest. Psychological parameters or pathological group characteristics obtained via DSM-IV criteria, (a behaviour and personality characterization process used by neuropsychologists), provide a way to describe broader characteristics of brain activity by a classification of behaviour. For example, a reduced ERP peak might be correlated to the level of performance on a memory task. Those with poor memories (pathological group) have small peaks while those with normal memories (control group) have large peaks. All of these measures which are external to the EEG provide a 'ground-truth' for

the EEG measurement; i.e., those measures ensure that the features in the EEG have some relation to human behaviour and are not random noise.

As will be explained in Chapter 7, the MCST-EEG method uses as little prior information and behavioural data as possible to generate results while maximizing information from the EEG data to facilitate interpretation. We do not look for particular features but are open to the discovery and study of all qualified brain activity features present in the data. Our validation methodology offers some protection against confounding artefactual results that arise from noise and not the brain activity. The validation methodology has criteria that are fundamentally different from those of data-mining. Where the data-mining is based only on the time-domain activities of the brain, the criteria by which data-mining results are weighed are anatomically meaningful; results of data-mining are validated by physical volume domain characteristics of the results themselves. A result may only be regarded as valid and be used to draw conclusions if it meets the validation criteria. Since the results of the data mining are not obtained via the standard hypothesis testing methodology, statistical power is reserved for testing of specific detail of the EEG, validated using the validation algorithm. Therefore, if an effect is well represented in the dataset and is validated by its logical physical characteristics, the EEG feature is considered real and knowledge of it can be used in the diagnosis and treatment of an individual.

Standard established EP, ERP, and EEGc methods require data of minimal complexity. Analysis by these standard methods is facilitated when the number of active brain areas during a time interval is low, increasing the likelihood the waveform peak examined originates from a finite number of brain locations (ideally, one location). ERP methods have an additional constraint in that the brain activity being examined must occur time-locked to a stimulus, thus allowing the average EEG and average behaviour across multiple trials to be studied. For these methods, the EEG collection paradigm is designed to make the brain activity of each trial the same and thus the EEG in each trial is expected to be the same. The requirements of these methods limit the richness of the data and how

closely the data collection paradigm can imitate real life experiences and the behaviour studied.

The MCST-EEG method is designed to allow the study of highly complex data with multiple active brain areas. We determine which areas of the brain are active, when they are active, and how they cooperate with or inhibit each other. The single-trial details of brain area activities are used to create a time-domain graphical map of coordinated activities and how this coordination evolves over time. While we examine single trial activities, trial average results can also be calculated. It is thus possible to make comparison to standard classical methods. Single trial analysis allows for the study of brain activity associated with learning related to task repetition and brain activity variability related to behavioural variation in strategy selection.

Results found using classical methods usually describe a subtractive difference between conditions rather than what actually occurs in the brain. For example, some condition **A** might be associated with a larger amplitude feature such as an ERP peak (or EEGc waveform) than condition **B**. Dipole localization may be used to infer a possible anatomical locus of the peak, however in general there can be no conclusion as to what neural processing the feature relates to. For example, it might be inferred that a difference between **A** and **B** indicates a difference in the amount of processing of a single brain region between the behaviours (D'arcy et al., 2004; Rugg and Coles, 1997). Alternatively, the amplitude of the feature corresponding to condition **A** might represent the sum of two or more brain source activities while the amplitude of the feature corresponding to condition **B** represents the activity of only one brain source. The assumption here is that multiple active brain sources generate greater ERP peak amplitudes than a single active brain source. In this way, a subtractive difference of the ERP is used to interpret the EEG of different behavioural conditions (D'arcy et al., 2004). The only direct interpretation however is that the two conditions are as different as the subtractive waveform (**A**-**B**). This subtractive difference does not reflect what actually happened in the brain for a given behaviour.

Processing EEG data using the MCST-EEG method attempts to provide results that represent what is actually happening in the brain. These results are distinctly interpretable without the (**A**-**B**) subtractive contrast. By providing a complete picture, it is possible to see a system-level logical progression of activities through the brain in relation to anatomy. This provides the ability to understand how the active parts of the brain functions with regards to a given overt behaviour. For example, if a task of visual memory of objects and memory processing is of primary research interest, the data will show both those activities solely related to memory processing and also the activities related to visual processing. Thus the activities of visual and memory areas can be understood within the context of activities of the visual system.

To addresses our main goal of maximizing the interpretability of EEG data by revealing how the brain works as a system, we use correlation measures similar to those that would have traditionally been used between the activities measured at individual electrodes. However, for this case the activities of individual parts of the brain are identified via data-mining and validation processing steps. Doing so allows for the detection of time intervals during which areas of the brain are highly correlated and involved in some coordinated functional processing.

II. SPECIFIC CONTRIBUTION AND METHODOLOGY

The main research question investigating the feasibility of an EEG analysis methodology that incorporates data-mining, validation, and source volume estimation to construct meaningful models of brain activity from EEG data and the analysis of data for the vMWT paradigm is addressed in a series of 7 research papers organized as dissertation chapters. Together, these research papers provide four main technical contributions to the fields of engineering and neuroscience. They show (1) a new data-mining method that is appropriate for separating biological contributors to the EEG data in an anatomically and physiologically meaningful way, (2) an EEG component validation

methodology that uses anatomically relevant scoring criteria in the validation process, (3) an algorithm to estimate the physical modular source volumes of components of the EEG to provide a more meaningful depiction of the active areas of the brain, (4) that the activities related to eye-movements during spatial cognition can effectively be detected and interpreted.

The elements of our primary research question, "is it is possible to construct a meaningful, objective, and informative model of brain activity from the EEG data", and the secondary question investigating the ability to analyze EEG data of the vMWT paradigm have been divided into sections to show a clear step-wise progression of findings and contributions. The current section has described the motivation for this work and the issues it potentially addresses. A fundamental component of the research question is finding a solution to the problem of accurately estimating the activities of bona fide brain sources via blind source separation and data-mining methods. Section II provides background into the details of gross brain function and the technical issues surrounding the blind source separation problem. In Section III, a set of tools is developed to obtain more information from scalp EEG data and by which to further understand and measure the impact of our efforts to address the source separation problem. In Section IV, use of the MCST-EEG methodology to calculate a meaningful representation of brain activity from EEG data is described and a comparison the methodology with other recently proposed methodologies is given. In Section V, the complete methodology is demonstrated and the calculated results are related to eye-tracking data to demonstrate a link between estimated brain activities and observable behaviour. Finally, a discussion of the collective findings and concluding remarks are provided in Section VI. Here, all important concepts described throughout the body of the dissertation are related and linked to the primary research question.

Each chapter provides a specific contribution towards addressing the analysis problems described previously. In Chapter 2 of Section II, the details of gross brain function and how they relate to blind source separation using ICA are examined. We show that current ICA methods are not necessarily appropriate to separate the activities of the brain

into meaningful parts; the parts that current source separation method separate EEG do not necessarily relate to physically distinct modular areas of the brain. The primary issue being that the activities of spatially distinct parts of the brain are sometimes correlated—ICA assumes that brain activities are uncorrelated and independent. The work presented in this chapter demonstrates that brain activity estimates via ICA methods can be improved by considering the characteristics of brain activity and brain function and adapting the ICA source separation algorithm.

In the chapters contained in Section 3, the procedure of data-mining, validation, and volume estimation is described. In Chapter 3, a means to maximize the meaning derived from the scalp surface EEG data is investigated. In doing so, a method to calculate volume-domain characteristics of ICA-derived EEG components and determine the regions of the brain from which these components of the EEG are originating is created. In Chapter 4, a volume estimation method using real EEG data is demonstrated and a method to objectively determine the relative overlap of volume-projected sources to demonstrate that the physical brain sources have been truly separated is described. Then, in Chapter 5, a procedure to determine the relative quality of components as they represent physical modular brain sources is described. The work leading up to this indicated that estimates of overlap of volumes, and multiple other logical volume-domain characteristics of sources can be used for determining the relative quality of components as representing brain sources. In Chapter 6 we propose a new algorithm for improving the separation of EEG into brain activity components that correspond to physical modular brains sources. We used our observation from Chapter 2 that the correlation can be reduced prior to calculating source separation matrices to improve separation results of the original EEG data. We found that our algorithm does indeed provide better source separation than the standard ICA algorithm while also demonstrating application of our volume domain analysis and validation methods. The methods developed in this section used a combination of real EEG data obtained from the University of Lethbridge, and synthetic EEG data created in the lab.

In Section IV, Chapter 7, we then compare the MCST-EEG methodology with related methods that are new and not currently standard in clinical or experimental EEG analysis. In this section, real EEG data obtained from the University of Lethbridge was used to develop the methods.

In Section V, Chapter 8, the MCST-EEG methodology is applied to data collected in our own lab at the University of Victoria. The data collection paradigm used is similar to that used at the University of Lethbridge. In addition to EEG collection, we also collect eye-position data and use it to validate our EEG analysis methodology. We show that the results of our EEG analysis methodology provides results that meaningfully relate to eye-movement and we show that this relationship fits within current understanding of the cognitive brain activity associated with the cognition of spatial navigation. We demonstrate that the brain activities of each individual subject examined in this single experiment can be meaningfully compared within the group.

Finally, In Chapter 9 of Section VI, an overall discussion and summary of the findings is provided and how these findings have addressed the research question is discussed. The results of each of the dissertation chapters are linked and how this research will impact the study of brain activity using EEG in the future is discussed. Chapter 9 is closed with a statement of the conclusions drawn from the results and inferences of each component of this research.

While reading this text it is helpful to keep four main ideas in mind. The first is the goal to advance current EEG analysis methods and overcome some fundamental problems. Namely, to move beyond current standard methods that use EEG as a phenomenology that differentiates behaviours by inferring brain activity from the EEG through statistical relationships across groups of study participants; it is more effective to first maximize the information gained from the EEG in relation to brain physiology and anatomy and then use statistics to determine the consistency of a specific bona fide brain activity across multiple trials in a single experiment or to determine the consistency of brain activity across a population. The second idea is that we wish to develop an algorithm that

separates the EEG into its individual contributors rather than separating it into uncorrelated or statistically independent parts. Since the ultimate goal is to examine the correlated activities of parts of the brain, it is not appropriate to force the components of the EEG to be uncorrelated or statistically independent. The third idea is that there is currently no direct way to determine if a new algorithm for separating the brain activities contributing to the EEG into parts offers improvement over standard methods; a method to do this must be created. Fourth and finally, there is currently no effective way to analyze the EEG data collected during the vMWT. Standard ERP methods have not been successful in finding meaningful differences between brain activities underlying behaviours associated with spatial navigation in the vMWT paradigm because navigation does not easily lend itself to ERP analysis since it has a continuous rather than a repeated trial process. For example, there is natural variation of behaviour across sequential trials and the EEG is comprised of activities from many parts of the brain. Prior analysis attempts using ICA have also failed because there is no objective way to determine which components of a decomposition are good and which ones are artefact making it difficult to make sense of data-mining results.

An appendix is provided to demonstrate results obtained by application of the methods developed in Section III on real EEG data to reinforce the findings provided in the body of this dissertation. They are not included with the body of the dissertation because these results will be published by a different principal author at the University of Lethbridge. These results include the volume-domain validation plots and the modular source volume estimation plots for the Lethbridge FASD study.

A summary of the format of the dissertation with section and chapter headings is given below. Those chapters that correspond to manuscripts written for publication have been labelled.

Section I: Introduction

Chapter 1. Introduction: Background, rationale, objectives, and overview of dissertation.

Section II: Background of EEG Methodology

Chapter 2. Understanding and Improving ICA Source Separation of EEG Data (for publication)

Section III: Development of New EEG Methodologies

Chapter 3. Beamform Volume Projection of EEG ICA Topographies (for publication)

Chapter 4. Beamform Volume Projection of ICA Components of Scalp EEG: Volume-Domain Uniqueness of Components (for publication)

Chapter 5. Volume Domain Validation of ICA-Derived EEG Sources (for publication)

Chapter 6. Spectral Shaping to Relax ICA Assumptions to Facilitate Decomposition of EEG (for publication)

Section IV: The novelty, utility, and context of the methodological advancements.

Chapter 7. Building a Multi-Component Spatio-Temporal Model Using Scalp-EEG Data (for publication)

Section V: Application of New Methods

Chapter 8. Feasibility of System Analysis of Brain Activity for Spatial Navigation using Scalp-EEG (for publication)

Section VI: Discussion and Conclusions

Chapter 9. General Discussion and Conclusion

Appendix A: Volume Estimation and Validation Results: University of Lethbridge FASD Study

III. REFERENCES

Andrew CM, Pfurtscheller G. On the existence of different alpha band rhythms in the hand area of man. Neuroscience Letters 1997;222:103-106.

Birch GE, Lawrence PD, Hare RD. Extraction of motor related activity from single trial EEG. Departments of Electrical Engineering and Psychology, University of British Columbia, Vancouver, B.C., Canada. 1988.

Borisoff JF, Mason GS, Bashashati A, Birch GE. Brain-computer Interface Design for Asynchronous Control Applications: Improvements to the LF-ASD Asynchronous Brain Switch. IEEE Transactions on Biomedical Engineering 2004; 51(6):985-992.

Cureton EE, Mulaik SA. The weighted varimax rotation and the promax rotation. Psychometrika 1975;40(2):183-195.

D'arcy RCN, Connolly JF, Service E, Hawco CS, Houlihan ME. Separating Phonological and Semantic Processing in Auditory Sentence Processing: A High-Resolution Event-Related Brain Potential Study. Human Brain Mapping 2004;22:40-51.

Diagnostic and Statistical Manual of Mental Disorders, 4th Ed. American Psychiatric Association, 1400 K Street, N.W.,Washington, DC, American Psychiatric Association, 1994.

Donchin E. A multivariate approach to the analysis of average evoked potentials. IEEE Transactions on Bio-Medical Engineering 1966; BME-13:131-139.

Glover S. Separate visual representations in the planning and control of action. Behavioural and Brain Sciences 2004;27:3-78.

Hamilton DA, Kodituwakku P, Sutherland RJ, Savage DD. Children with Fetal Alcohol Syndrome are impaired at place learning but not cued-navigation in a virtual Morris water task. Behavioural Brain Research 2003, 143:85-94.

Jackson GM, Eberly DA. Facilitation of performance on an arithmetic task as a result of the application of a biofeedback procedure to suppress alpha wave activity. Applied Psychology and Biofeedback 1982;7(2):211-221.

Kaiser HF. The Varimax Criterion for Analytic Rotation in Factor Analysis. Psychometrika 1958;23(3):187-200.

Kim YJ, Grabowecky M, Paller KA, Muthu K, Suzuki S. Attention induces synchronization-based response gain in steady-state visual evoked potentials. Nature Neuroscience 2007;10:117-125.

Klimesch W. EEG alpha and theta oscillations reflect cognitive and memory performance: a review and analysis. Brain Research Reviews 1999;29:169-195.

Nunez PL, Srinivasan R, Westdorp AF, Wijesinghe RS, Tucker DM, Silberstein RB, Cadusch PJ. EEG coherency I: statistics, reference electrode, volume condition, Laplacians, cortical imaging, and interpretation at multiple scales. Electroencephalography and Clinical Neurophysiology 1997;103(5):499-515.

Makeig S, Bell A, Jung T, Sejnowski, T. Independent component analysis of electroencephalographic data. In: Touretzky D, Mozer M, Hasselmo M (Eds). Advances in Neural Information Processing Systems. MIT Press, 1996;8:145-151.

Mulholland TB. The concept of attention and the electroencephalographic alpha rhythm. In: Evans CR, Mulholland TB (Eds.) Attention in Neurophysiology. London Butter-worths, 1969.

Pfurtscheller G, Neuper C. Event-Related synchronization of mu rhythm in the EEG over the cortical hand area in man. Neuroscience Letters 1994;174:93-96.

Rugg MD, Coles MGH. Electrophysiology of Mind: Event-Related Brain Potentials and Cognition. Oxford University Press, Oxford, New York, 2002.

Scherg M, Berg P. New concepts of brain source imaging and localization. In: Barber C, Celesia G, Comi GC, Maguiere F, eds. Functional Neuroscience. Amsterdam: Elsevier Science B.V. 1996; 127-137.

Suffczynski P, Pijn J P M, Pfurtscheller G, Lopes da Silva F H. Event-related dynamics of alpha band rhythms: a neuronal network model of focal ERD/surround ERS. In: Pfurtscheller and Lopes da Silva Eds. Handbook of Electroencephalography and Clinical Neurophysiology: Event-Related Desynchronization. Revised Series, v6. Amsterdam, The Netherlands:Elsevier, 1999.

Trenado C, Haab L, Strauss DJ. Modeling Neural Correlates of Auditory Attention in Evoked Potentials using Corticothalamic Feedback Dynamics. Proceedings of the 29th Annual International Conference of the IEEE EMBS. Cite Internationale, Lyon, France. Aug. 2007.

Zani A, Proverbio AM. Attention modulation of C1 and P1 components of visual evoked potentials. Electroencephalography and Clinical Neurophysiology 1997;103(1):97-97.

Zeman PM, Sorensen PL, Livingstone SA, Skelton RW, Livingston NJ. Understanding and Improving ICA Source Separation of EEG Data. (for publication) 2008a.

Zeman PM, Mahajan SV, Livingstone SA, Driessen PF, Skelton RW, Livingston NJ. Beamform Volume Projection of EEG ICA Topographies. (for publication) 2008b.

Zeman PM, Mahajan SV, Sorensen PL, Driessen PF, Skelton RW, Livingston NJ. Beamform Volume Projection of ICA Components of Scalp EEG: Volume-Domain Uniqueness of Components. (for publication) 2007c.

Zeman PM, Mahajan SV, Livingstone SA, Driessen PF, Skelton RW, Livingston NJ. Volume Domain Validation of ICA-Derived EEG Sources. (for publication) 2008d.

Zeman PM, Mahajan SV, Livingstone SA, Livingston NJ, Skelton RW. Spectral Shaping to Relax ICA Assumptions to Facilitate Decomposition of EEG. (for publication). 2008e.

Zeman PM, Livingstone SA, Livingston NJ, Skelton RW. Building a Multi-Component Spatio-Temporal Model Using Scalp-EEG Data. (for publication). 2008f.

Zeman PM, Livingstone SA, Livingston NJ, Skelton RW. Feasibility of System Analysis of Brain Activity for Spatial Navigation using Scalp-EEG. (for publication). 2008g.

Section II: Background of EEG Methodology

In the previous section, the background, rationale, motivation, and objectives of the dissertation were described. Together, these provide the foundation and impetus for the development of an EEG analysis methodology that maximises information obtained from the EEG to describe how parts of the brain work together as a system. This methodology should be appropriate for (1) identifying the characteristics of brain activity from the EEG collected from a single person and (2) for comparing the brain activities of individual persons in a group.

The proposed analysis methodology and research goals were given in the context of the development and history of EEG analysis methods. Some fundamental issues relating to current accepted methods were identified and from these issues some direction to improve on these methods was described. This new direction includes: (1) moving away from hypothesis-based methods that require cross-subject or cross-experiment validation to make sense of scalp EEG waveforms, and to (2) improve source separation methods so that the bona fide activities of specific parts of the brain can be isolated. Steps in this new direction will ultimately make the EEG easier to understand and interpret reducing source distortion, and improving signal-to-noise ratios. This should lead to the ability to analyze and interpret the EEG data collected from single persons associated with complex behaviours, and ultimately, provide the foundation for better use of EEG for understanding brain function.

The current section discusses brain activity and the scalp EEG in detail and makes recommendations for the development of a new EEG analysis method. A description of this new EEG analysis methodology incorporating all component algorithms developed is provided in Section IV. A comparison of the complete methodology with other closely related methodologies is also provided in Section IV.

Chapter 2: Understanding and Improving ICA Source Separation of EEG Data

This chapter sets out to clearly describe the Independent Component Analysis (ICA) source separation process and how source separation assumptions relate to the quality of brain source estimates. A common misconception that the simple act of collecting and analyzing more EEG data provides for better brain source activity estimates is discussed. Analyzing more data does provide for reduction of brain source estimation error due to random noise however it does not necessarily reduce estimation error related to correlated brain source activities; it does not improve the separation of activities of the brain that are correlated. To demonstrate this and to identify ways to reduce brain source estimation error, brain activity characteristics and their relation to the assumptions of ICA source separation are examined. A standard algorithm that uses Infomax ICA principles (Bell and Sejnowski, 1995) called runica (Makeig et al., 1997) is evaluated in the context of what is currently known about brain function and scalp acquired EEG data. Simulated EEG data are then used to model and examine ICA source estimation error with respect to analysis window duration and amplitude of momentary periods of correlated activity. Simulation shows that coordinated brain function of multiple spatially distinct areas of the brain that occurs as zero-lag correlated activity leads to ICA source separation error. Methods to reduce this estimation error such as variation of analysis window size, window location, and frequency notching are examined.

Article Title: Understanding and Improving ICA Source Separation of EEG Data

Philip M. Zeman[1,3,4], Sharon A. Livingstone[3], Ron W. Skelton[3] , Patricia L. Sorensen[2], Nigel J. Livingston[1]

[1] CanAssist, University of Victoria, BC, Canada
[2] Department of Neuroscience, Canadian Centre of Behavioural Neuroscience, University of Lethbridge, AB, Canada
[3] Department of Psychology, University of Victoria, BC, Canada
[4] Department of Electrical Engineering, University of Victoria, BC, Canada

Correspondence may be addressed to Philip Zeman:
(voice) +1-250-589-4234 / (fax) +1-250-721-6611 / pzeman@alumni.uvic.ca

Alternate Title: Improving Independent Component Analysis of EEG

Abstract

Objective: To clearly describe the Infomax (Bell and Sejnowski, 1995) ICA source separation process and how its assumptions relate to the quality of brain source estimates. To show how coordinated brain function is a potential barrier to source separation via ICA. To demonstrate methods to improve the estimate of brain source activities.
Method: An overview of Infomax ICA assumptions with respect to brain activity properties is given. Simulated EEG data are then used to model and examine ICA source estimation error with respect to duration and amplitude of momentary periods of correlated activity. Variation of analysis window size, window location, and frequency notching are examined to reduce source estimate error.
Results: Source estimate errors increase when brain activities are temporally correlated. Our analysis demonstrates that ICA source waveform estimation errors decrease as the ratio of duration of momentary correlation vs. duration of source independence decreases. Error is also reduced by removal of frequencies of correlation or removal of intervals of correlation prior to calculation of source separation matrices.
Conclusions: Correlated activities of spatially distinct areas of the brain are a barrier to accurate source estimation. By appropriately modifying the data on which the ICA source separation matrices are calculated, the source estimate error caused by correlation can be reduced.

Keywords: EEG; ICA; correlation; *runica*; functional analysis; brain activity model

(I) INTRODUCTION

Recently, independent component analysis (ICA) of EEG has emerged as a powerful methodology for identifying how different parts of the brain participate in different cognitive processes. ICA provides a means to blindly separate the activities of individual contributors (sources) to the EEG (Bell and Sejnowski, 1995) based on the separation criteria of statistical independence. Delorme and Makeig, (2004), and others (Contreras-Vidal and Kerick, 2004; Makeig et al., 2004; Jung et al., 2001; Makeig et al, 1996) have established the ICA approach in the analysis of brain activity by showing many cases where the analysis method proves feasible in human studies and in source estimation of simulated EEG (Makeig et al., 2000; Ghahremani et al., 1996).

ICA is effective at finding statistically independent sources in the EEG mixture. The waveforms of such components in the EEG mixture have been used in the ICA work described above to study a variety of brain functions. ICA is also an effective tool for the removal of non-biological artifacts from the EEG as they are generally statistically independent of the biological contribution to the EEG.

ICA is not necessarily effective at accurately separating partially correlated and dependent sources from the EEG mixture. Prior work examining EEG obtained at electrodes implanted in the cortex has shown that the activities of distinct parts of the brain are not necessarily independent but are in some circumstances correlated and dependent (Roelfsema et al., 1997). However, ICA by its very nature identifies only components that are independent from one another, distorting or failing to separate sources that are partially correlated. When ICA is used to separate a mixture of partially correlated and dependent sources, it yields waveform activities that are uncorrelated and statistically independent, whether or not the bona fide parts that comprise the mixture are statistically independent. In cases where anatomically distinct brain areas have activities that are highly correlated, ICA separation criteria fails to accurately identify their activities (Zeman et al., 2008e).

Brain source activities found via ICA are thus an approximation. They are the statistically independent analogs of the bona fide sources. In the best cases, when the ICA assumption of statistical independence closely fits the actual brain source activities, the distortion introduced by the assumption of independence is low. If this assumption is not closely satisfied by the brain source activities, the distortion is large and problematic. It is thus generally appropriate to assume that the sources found by ICA have some amount of unknown error. By minimizing the distortion effects caused by brain areas having temporally correlated activities, this error can be minimized. It is thus worthwhile to understand the circumstances in which correlation distorts ICA brain source estimation and to do so requires a clear understanding of brain activities and their relation to the assumptions of ICA source estimation.

Previous studies have investigated the relationship between ICA and partially correlated brain sources. For example, using synthetic EEG, Makeig et al (2000) examined the relationship between partially correlated source activities and source separation error using ICA. They that found for spatially distinct sources with partially correlated time-domain activities, ICA identified a single topography representing the two distinct sources as a single correlated source component. This suggests that in cases where the activities of distinct brain areas are coordinated and correlated as in a 'multi-node network' involving multiple distinct areas of the brain, ICA will identify the topographies and time-activities of the entire 'network' as a single component and not necessarily separate the activities of each distinct 'network node' into different components. This has in fact been demonstrated by Summerfield and Mangels, (2005).

It is not necessarily clear how to obtain good brain source estimates using ICA. For example, one might assume that if enough data are available, the ICA criteria that the sources to be separated are statistically independent will be satisfied by the dynamic and non-deterministic nature of EEG data. This assumption relies on the property that the correlated activities of spatially distinct brain areas do not consistently occur in a large fixed percentage of trials. This correlated activity might actually be a fundamental characteristic of brain function, related to the transfer of information from the primary

visual cortices to high-level cortical areas (Roelfsema et al., 1997), and thus will exist in every trial (or most trials) of data collected. Hence, this effect on the measure of independence can not be minimized by adding more trials of data to the analysis. The 'non-deterministic nature' of EEG data that has facilitated brain source separation in past research might largely be related to the random noise that exists in tandem with activities of the brain. Thus, the assumption above essentially relies on some non-quantified noise parameter of the EEG that makes the brain source activities more closely approximate statistical independence.

Our position is that direct steps can be taken to improve the accuracy and reliability of brain source estimations. We propose that estimation error can be addressed by reducing the influence of parasitic correlations on the ICA separation process. To examine and justify this assertion we discuss the assumptions and requirements of signal processing using Infomax ICA and relate them to brain activity, and show how the characteristics of a conceptual brain activity model relate to the signal processing assumptions of ICA. Finally, we show, using synthetic EEG data, how some modifications to the data can reduce ICA source estimation error. The key idea for improving ICA separation of sources is that the brain sources to be identified should be made to appear as statistically independent as possible for construction of the spatial separation matrices. Since this paper was first drafted, we have demonstrated, using real EEG data, steps can be taken to reduce source estimation errors associated with correlated brain activities (Makeig et al., 2000; Zeman et al., 2008e).

(II) PART A: RELATING SIGNAL PROCESSING TO BRAIN ACTIVITIES

There are varied levels of detail and numerous properties by which to conceptually model and characterize brain activity. For example, a signal processing perspective of brain activity at individual electrodes (Parra and Sajda, 2003) considers brain activity as a non-Gaussian, non-white, and temporally non-stationary random process. In addition to these characteristics, Makeig et al., (1997) has assumed the property that brain sources that contribute to the EEG are spatially stationary. That is, neural tissues that project

activities to the scalp do not move about the cranium during EEG recording. While these assumptions seem reasonable to the person versed in brain anatomy, physiology, and single electrode EEG analysis methods, there are some additional important characteristics to consider from the signal processing perspective.

Assumptions and Mathematics of ICA

The separation of sources from within scalp-recorded EEG data is thought to be analogous to the so-called 'Cocktail Party Problem' (Makeig 2005). An excellent description of the Cocktail Party Problem is provided by Haykin and Chen (2005). In this problem there are n people in a room, all speaking simultaneously, with each voice considered as a time-varying source signal, $\mathbf{s}_n(t)$. It is assumed that all persons remain in spatially stationary locations; that is, they do not move about the room. Further, it is assumed that their voices originate from discrete regions in the room, (their mouths). There are also $\boldsymbol{m}$ microphones in the room, fixed at particular unique locations, with each microphone recording an observation of the mixture, $\mathbf{x}_m(t)$. Thus, each microphone receives a mixture of all the voices, with each voice amplitude-weighted by a factor of their relative distance from the microphone. The source signals are not observable in isolation because each microphone responds only to some mixture of the sources. The task, then, is to recover both the mixing characteristics, **A,** and each voice source in the room $\mathbf{s}_n(t)$ knowing only the recorded observations of mixed voices $\mathbf{x}_m(t)$.

This analogy is carried forward to understand how ICA can be used to separate EEG data into component sources. In this case, there is assumed to be some number of brain regions, (or sources) located at specific, fixed, locations within the head. It is assumed that each of these brain regions emits a 'voice' that sums as a part of a mixture of voices measured at numerous electrodes at the scalp. Here, the EEG recording electrodes provide a set of observations in the same way as the microphones in the cocktail party analogy.

A popular approach to the EEG source separation problem uses the Infomax ICA algorithm (Bell and Sejnowski, 1995) that calculates an unmixing matrix of scalar

weights based on an instantaneous mixing model. This unmixing matrix is then used to separate the EEG into component sources having statistically independent time-domain activities. The *runica* (Makeig et al., 1997) implementation of the Infomax algorithm has been demonstrated as sufficient to address the Cocktail Party Problem, as it has been described, and is available with the EEGLAB toolbox of Delorme and Makeig, (2004; http://sccn.ucsd.edu/eeglab).

The Infomax ICA mathematical definition used by runica is intimately linked to the assumptions of the source mixture and to the sources themselves. Equation 1 models the observed time-domain activities of the source mixture $\mathbf{x}(t)$ as a linear combination of unknown time-domain source activities $\mathbf{s}(t)$ and an unknown mixing matrix, $\mathbf{A}$ of m x n scalar mixing coefficients, such that

$$\mathbf{x}(t) = \mathbf{A}\mathbf{s}(t) \qquad (1)$$

where $\mathbf{x}(t) = [x_1(t), x_2(t), \ldots x_m(t)]^T$ and $\mathbf{s}(t) = [s_1(t), s_2(t), \ldots s_n(t)]^T$.

The number of observation electrode channels is indicated by m, while the number of sources to be estimated is given as n. For source separation, it is required that there are at least as many sensors as there are sources, $m \geq n$. Each row of $\mathbf{x}(t)$ corresponds to the time-domain activities measured at individual electrodes while each row of $\mathbf{s}(t)$ corresponds to the time-domain activities of individual sources comprising the mixture. It is assumed that the observations $\mathbf{x}(t)$, and the sources comprising the mixture, $\mathbf{s}(t)$, both have zero mean. The zero-mean criterion for the observations is easily satisfied by subtracting the mean from each observation channel over the time window of analysis. The topographies relating to each individual source waveform are directly available from the estimate of $\mathbf{A}$. Each row of $\mathbf{A}$ relates to how the sources combine to form a particular observed signal while each column of $\mathbf{A}$ relates to how a particular source is distributed among the observed signals.

A weight matrix **W** is used to solve for the source activities comprising the mixture, as in Equation 2,

$$\mathbf{s}(t) = \mathbf{W}\hat{\mathbf{x}}(t) \tag{2}$$

where $\hat{\mathbf{x}}(t)$ is a whitened version of $\mathbf{x}(t)$. The matrix **W** adjusts the variance of the whitened data such that the time-domain activities of one source cannot be used to predict the activities of another.

The first step (after the mean of the analysis window for each electrode is removed) is thus the calculation of a sphering matrix to whiten the observed EEG. The process of whitening rotates and scales the data such that the cross-correlation values of all channels of the whitened data $\hat{\mathbf{x}}(t)$ are exactly zero and the variance of each observation channel is unity. The sphering matrix **P**, is calculated from the data as in Equation 3,

$$\mathbf{P} = \mathbf{C}^{-\frac{1}{2}}(\mathbf{x}(t)) \tag{3}$$

where $\mathbf{C}^{-\frac{1}{2}}(\mathbf{x}(t))$ is the matrix square-root of the inverse of the covariance estimate of the observed data within a temporal analysis window. Covariance is equivalent to a measure of zero-mean correlation. Since the mean of each channel has been previously removed, we can regard covariance and correlation equally. The sphering matrix is used, as in Equation 4, to create the whitened data, $\hat{\mathbf{x}}(t)$.

$$\hat{\mathbf{x}}(t) = \mathbf{P}\mathbf{x}(t) \tag{4}$$

By default, the *runica* (Makeig et al., 1997) implementation of Infomax calculates the sphering matrix **P**, and then uses the sphered data in successive iterations to estimate **W**. Thus the estimation of W has a reliance on a correct **P**. In turn, creation of **P** relies on the calculation of covariance, **C(x)**, which characterizes the relationship between sensor pairs using the variance of **x** measured in the temporal analysis window. Hence, a correct

correlation estimate is important for a correct ICA outcome. The relationship between these parameters is illustrated in Equation 5, where the (*t*) notation has been dropped for succinctness.

$$\mathbf{s} = \mathbf{W}\hat{\mathbf{x}} = \mathbf{WPx} \tag{5}$$

The component source activities **s** and the weight matrix **W** are solved for simultaneously by runica via an iterative process that searches for a **W** that minimizes the dependence among the source activities in **s**. The details of the runica algorithm are evident by inspection of the runica code available with EEGLab (Makeig et al., 1997).

Once the unmixing matrix **W** has been found, the mixing matrix **A** can be calculated as in Equation 6.

$$\mathbf{A} = [\mathbf{WP}]^{-1} \tag{6}$$

Because the ICA methodology scales the variance of the dimensions to unity in the sphering step, the estimated sources must be re-scaled to recover their scalp-domain magnitudes. This process is referred to as 'back-projection' of the component. To back-project a single source waveform to the scalp, the source matrix **s** is set to contain all zeros except for those entries corresponding to the source waveform of interest. By setting all other entries to zero, all of the unwanted signal vectors are eliminated. Thus, by using this modified version of **s** in Equation 1, any single source can be projected back to the scalp-domain. Since the back-projection of **s** exists on ***m*** electrodes, it is appropriate to project the variance to the scalp using the electrode of greatest variance in further analysis and is analogous to measuring an interference free signal from a single scalp electrode. While back-projection restores the scalp-domain variance, it does not restore the scalp-domain covariance. By this process, only one source is projected to the scalp at a time and the shape of each back-projected source waveform is the same as it was before back-projection.

Relating ICA and Brain Activity

Correct identification of sources comprising the EEG relies heavily on an appropriate estimate of covariance (and correlation) as the sphering matrix **P**, which is calculated from the covariance of the EEG data, is important in the calculation of both the source waveforms **s**, and the weight matrix **W**. It is an important step which cannot be avoided. The mathematics of Equation 5 can be summarized in words as two steps. The first step is the sphering of the data. After sphering the data using an estimate of covariance, the sources comprising the mixture are largely identified; it is only a matter of appropriately assigning variance amongst the dimensions of analysis through a second step of rotating the sphered data. The second step rotates the sphered data to assign variance to dimensions via the assumption of statistical independence. If the researcher using runica chooses to not sphere the data (an option of *runica*), runica still computes Equation 3 as the starting point for the estimate of the weight matrix, **W**. Alternatively, the *runica* implementation allows researchers to provide their own starting weight matrix, however, even given this user-supplied matrix, its calculation would most likely be some attempt at a calculation of covariance. In all these conditions, a calculation of covariance impacts the source separation process.

Because of the non-stationary temporal characteristic of EEG data and the brain activities it contains, the estimate of covariance and of statistical independence depends on the size and position of the temporal analysis window. The temporal analysis window is the 'window' or epoch of data selected on which to calculate the source separation matrices **W** and **P**. For example, an EEG researcher might choose to analyze 100 trials of data for the trial epoch, defined -1000 to 2500 ms in their experiment where the trial onset is 0 ms. The researcher could have just as easily selected an epoch of 0 to 1000 ms, or -500 to 500 ms.

Selection of an appropriate ICA pre-processing steps to minimize source estimation error requires some knowledge of the brain sources of interest. A 'brain perspective' on the problem is taken in the investigation provided the subsequent paragraphs to help the

researcher make data preparation decisions and to identify what modifications to the data might lead to the best results. This investigation provides some background on brain function and describes why some ICA studies are more successful at identifying brain activities relating to specific areas of the brain than others.

Luria's serial model of information processing in the human brain proposes that a stimulus is processed first in a primary zone that constructs the perception of a sensory input, then in a secondary zone that recognizes the context of the sensory input, and then in a tertiary zone that provides understanding and assessment of the stimulus (Luria, 1973). Luria's model is the foundation for analysis of EEG in response to stimulus, known as event-related potential (ERP) analysis. An example is the clinical assessment of auditory function using a monaural auditory event-related potential (ERP) data collection paradigm (Streletz et al., 1977). To examine auditory processing from each ear separately, the clinician presents an auditory stimulus of approximately 10,000 clicks, each click separated by an interval of approximately 50 ms. The EEG resulting from each click stimulus is averaged over trials to generate the auditory ERP waveform. By averaging the data across trials, the random 'noise' in each trial is cancelled while that which is not random (the brain activity of interest) is emphasized. The 5 early peaks of the ERP (1.5 ms to 15 ms post stimulus) are known as the brainstem auditory evoked response. Wave peaks I and II indicate activity at the VIIIth cranial nerve, while wave peak V indicates activity originating in the lateral lemniscus and inferior colliculus. This sequence of waves is believed to illustrate the sequential function of the underlying physiology of the auditory path. Each wave peak is thought to represent the arrival and processing of some aspect of the stimulus in sequential brain areas. The conceptual model that follows from this is a set of processing blocks connected by a feed-forward path. It is assumed that each region of the brain is either active or inactive as information is discretely passed from one brain area to another. It suggests that activities of the brain related to processing of a stimulus have no temporal overlap, and thus the activities of these blocks, while having a lock-step activation relationship, are not correlated at zero-lag.

While a serial model of brain activity may be appropriate to describe very simple (or early sensory) brain function, it cannot adequately describe function associated with more complex human behaviour. There is considerable evidence that the fundamental nature of brain function underlying human behaviour requires the activity of parallel and reciprocally connected active brain areas (Parvizi et al., 2006; Takada et al., 1998). Conceptually, a parallel-distributed model that includes complex feed-forward and reciprocal feed-back connections rather than the simple connectivity of the serial model supports a more complete description of brain activity and can account for and describe co-activation of multiple brain areas.

As early as 1869, John Hughlings Jackson argued in favor of a multi-level, distributed model of brain function. More recently, Fellman and van Essen (1991) developed a parallel-distributed hierarchical model of brain activity whereby sensory motor and association areas are linked by both feed-forward and feedback connectivity. According to this model, information processing is not limited to sequences of serial activities, nor is information flow in one direction. Thus, there are at least 3 mechanisms by which brain activities can be correlated. First, multiple areas that are not necessarily connected to each other but do receive the same or related inputs might have correlated activities. For example, auditory stimulus presented at both ears would generate correlated activities in bilateral auditory areas. In this case, they process the same stimulus input at the same time. Areas of the brain that have direct reciprocal connections may also have correlated activities. For example, outputs of brain processing modules have direct feedback to their inputs or to prior processing blocks, to notify the driving brain circuitry of their level of output. Such connections can lead to closed-loop oscillatory activity between multiple, sequentially connected, areas of the brain. In the third case, an unknown region or nucleus of the brain may send information to multiple brain areas in parallel causing the activities of multiple areas to similarly modulated, even if no actual direct connections exist between them. This could occur via changes in neuromodulator outputs projecting to multiple areas of the cortex or could be directly related to gating of cortical projections from subcortical areas via the thalamus. In all three cases, correlation

results when multiple areas of the brain are active and have some coordinated relationship that can be considered network brain activity.

Network activity of the brain has been implicated by observations of multi-channel scalp EEG recordings. Michel et al., (1999) and Mesulam, (1998) described that information processing is realized through a sequence of moments or "microstates" that represent concurrent processing involving multiple distinct areas of the brain. The term, microstate, stems from the observation that moments of 'stable' scalp topographies appear in the multi-electrode topographical representation of the ERP. They are generally shown in literature as a time-sequence of scalp topography images over the duration of stimulus presentation and subsequent multi-stage brain processing of the stimulus. The appearance of these microstates in the trial averaged ERP indicates some characteristics of the brain activities that create them. First, it indicates that the average brain activity contributing the microstate ERP is temporally stationary across trials (at least for the 1^{st}-order statistic). Second, the duration of these microstates define an interval of time-domain stationarity of brain activities (again, at least for the 1^{st}-order statistic). Third, the appearance of microstates from ensemble averaged trial data reveals that the concerted activation of multiple distinct areas of the brain is somewhat consistent across trials.

Specific frequency bands of the EEG may contain brain activities that are more correlated than others. For example, Başar, (2005) suggests that the brain uses frequency-domain multiplexing of information to send a variety of types of information between areas of the brain. This premise comes from established findings that activities in the theta, delta, alpha, beta, and gamma frequency bands have distinct behavioral correlates. Thus, at some frequencies, statistical relationships might be correlated and dependent, while at other frequencies, statistical relationships might be uncorrelated and independent. It has been theorized that the frequency band of correlated activities of distinct areas of the brain might have some relation to the path lengths between brain areas. Nunez, (1989) attempted to predict the oscillatory characteristics of pathways of various lengths using a mathematical wave-theory model. His model suggests that long distance pathways, such

as those involving white matter fascicules projecting between anterior and posterior cortical areas, will exhibit low frequency oscillations, while short pathways, such as those that project short distances within the lamina of the cortex, will oscillate at high frequencies. Perhaps knowledge of the frequencies at which correlated activities among distinct areas of the brain occurs can be used to reduce their impact on source separation.

The properties of brain activity described above suggest a persistent and unchanging level of correlation between the activities of distinct areas of the brain at each and every stimulus presentation in a multi-trial experiment. However, we have not yet accounted for how these correlations or the activities of the brain in general change as a function of repeated use in an experimental paradigm. For example, Henson and Rugg, (2003) found reduced haemodynamic activity in brain areas that are repeatedly used for processing indicating that the sudden time-local influx of oxygen uptake that is visible by fMRI, for repeated processing, is not necessarily needed by brain anatomy during the moment the brain function is required (e.g., to facilitate a button pressing behaviour). They suggest that this is evidence of priming. How this impacts the activation coordination among areas of the brain is not known and it isn't evident if this would increase the duration of measured correlation in an experiment or if it would decrease the correlation with decreased activation. However, what is clear is that the brain activities associated with each and every trial are not necessarily equal. This fact may be leveraged to create an improved source separation solution to reduce source separation error caused by correlation among the activities of distinct brain areas.

Whether or not the EEG and underlying brain activities have a predictable, deterministic time-structure been a topic of disagreement among researchers. If the EEG is generally deterministic, then the activities contributing to the EEG can be modeled by predictable waveform activities and knowing the characteristics of activities at one moment in time, one can successfully predict activities in the future. If the EEG are not deterministic, (or are considered purely stochastic) the activities contributing to the EEG can only be modeled by statistical processes that are independent of time. Discrepancy between studies investigating the deterministic characteristics of EEG data seems to be related to

the methods used to measure determinism. Jeong et al., (2002) investigated the deterministic nature of EEG by examining the statistical differentiability of the EEG state-space from multiple EEG channels uniformly spaced across the scalp. Data were collected while participants were seated, at rest, with their eyes closed. Results of their investigation demonstrated that the EEG was not predictable over time and they concluded that the EEG and underlying brain activity is not deterministic. In a similar study, Stepien, (2002) investigated determinism of the EEG using non-linear prediction methods. Analysis of multi-channel EEG collected while study participants were seated, at rest, with their eyes open revealed that the EEG was not deterministic but actually stochastic for all 21 participants examined. In contrast, when examining the EEG of participants with eyes closed, 3 of the participants presented EEG with deterministic characteristics. A study by Meghdadi et al., (2006) which decomposed the EEG into principal components before applying state-space analysis found EEG is both deterministic and stochastic. They found principal components that account for the largest percentage of total variance in the data were deterministic while other components accounting for a small percentage of the total variance in the data were purely stochastic. They concluded that components accounting for a large percentage of the variance were related to actual brain activities while components accounting for only a small percentage of the total variance were related to various noise sources. The results of this final study explain some of the discrepancies between the earlier two. It is possible that the noise contained in the EEG was leading to the conclusions that brain activity is stochastic. When the noise and the brain activity were ostensibly separated, it was the brain activity that was characterized as deterministic while the noise was characterized as stochastic.

It might advantageous to define the causes of variability in the EEG data separately as either ‘behavioral’ or as ‘external noise’. Differentiating between the two might lead to a more thorough understanding of brain function, learning, and the noise contribution to the EEG. For example, the ‘behavioral’ component of ‘randomness’ of brain activities seen across trials of an experiment might be fully explained by factors that are under experimental control such as attention, learning, priming, and arousal, which can all be manipulated by the paradigm. These factors should be accounted for by variables in the

analysis and modeling procedure to best understand the brain activities contained in the EEG. The component of the 'randomness' that can be accounted for by noise should also be explained and modeled so that the signal-to-noise ratio of the EEG data and the related reliability of the brain activity estimates can be known.

The discussion above reveals three important characteristics of brain activity to understand and analyze brain function. The EEG has been identified as (1) containing both deterministic and stochastic characteristics. It is assumed that those contributions to the EEG that are deterministic relate to brain activity while the stochastic component relates to noise. In terms of activation relationships of distinct areas of the brain, in paradigms that are not as simple as a monaural auditory evoked response, (2) activities of distinct areas of the brain should be considered as having momentary periods of correlation. Additionally, while the activities of the brain are generally considered non-stationary, (3) there are moments of stationarity that may or may not encompass the coordinated activities of multiple areas of the brain.

Three methods were identified to reduce the negative impact of this correlatedness and interdependence on ICA source separation. Our investigation suggests that to reduce estimation error: (1) the time window of analysis can be moved or resized to avoid capturing momentarily correlated activities, (2) the data used to calculate source separation matrices can be adjusted to reduce the impact of those frequencies with highly correlated activities, or (3) data from the inter-trial interval can be included in order to provide paradigm relevant source activities resulting from priming effects that may have minimal correlations.

(III) PART B: EXAMINING MOMENTARY CORRELATION AND ICA ERROR

In order to illustrate the kind of ICA errors that can be introduced by momentary correlated activities, we have modeled an EEG data collection and ICA analysis scenario within which momentary correlation between two distinct areas of the brain is present.

Synthetic EEG data were constructed to model the worst-case correlation problem typically seen: correlation associated with the coordination of distinct brain areas at the onset of behavioral trials, i.e., the part of the trial that is generally of research interest.

The model EEG data collection paradigm simulates data collection in a signaled response task. In this task, one of two 1 second directive stimuli (A or B) precedes an imperative stimulus by 1 second. The directive stimuli A and B respectively indicate whether the participant should press the left button with their left and or the right button with their right hand as quickly as possible at the appearance of the imperative stimulus (a "+"). All stimuli are presented in the center of the screen and the participant's arms remain on the armrests of their chair until the imperative signal is given. There is a variable inter-trial interval of approximately 10000 ms (+/- 1000 ms), post button press.

In this paradigm, multiple regions of the brain must cooperate towards the behavioral objective and distinct brain regions are required to coordinate and transfer information. Because this task presumably requires multiple parallel distributed networks of the brain, the EEG is then a mixture of activities originating from multiple physically distinct brain locations. Each brain location contains both independent and correlated activities. For example, it is assumed that brain activities of visual areas are integrated/coordinated with the activities of other brain areas as illustrated in Figure 1.

Specifically, our simulation models coordination of the left orbito-frontal cortex (designated as $\mathbf{s}_1$) and the left medial-temporal cortex (designated as $\mathbf{s}_2$). Further, the simulation EEG includes activity of an area of the brain (designated as $\mathbf{s}_3$) that is active for the paradigm but is not coordinated with either $\mathbf{s}_1$ or $\mathbf{s}_2$. Figure 1 illustrates the how the activities of multiple brain areas might be temporally coordinated as a sequence of microstates of momentary networks of information processing. For clarity, the diagram is simplified to highlight only three active brain areas, which are examined in further detail. These expectations of multiple co-active and coordinated brain areas are consistent with models of working memory (Baddeley and Hitch, 1974; Baddeley, 2000)

and visuomotor integration (Glover, 2004). As well, electrophysiological evidence supports the integration of sensory stimuli with motor action (Lim et al., 2006).

The time-domain waveform activities for the simulated brain sources are given in Figure 2. Sources $\mathbf{s}_1$ and $\mathbf{s}_2$ have tonic operating characteristics modeled as a square wave and a sawtooth wave, respectively. These particular tonic waveform were selected to provide for easy visual discrimination between source activities and because they meet the ICA assumption of uncorrelatedness and statistical independence. The state of tonic excitation after the trial onset results from the repetition of the paradigm behaviour over multiple trials and the participant's maintenance of a behavioural context, reflecting the assumption that the activity state of the brain regions used repeatedly does not drop to the background level of normal brain activity. For easy visual inspection of waveforms on a realistic time-scale, momentarily coordinated activity is simulated by a delta wave (3 Hz). For simplicity, the synthetic EEG models of only 3 channels and a momentary correlation between only 2 of the 3 sources comprise the mixture. In reality, coordination might include multiple frequency bands and involve more brain areas at multiple time intervals appearing in averaged EEG as microstates of networked brain areas as described earlier, distributed over 30 or more channels of EEG. The simulation includes only a single episode of momentarily correlated activity in each trial, occurring 400 ms before and continuing for 400 ms after the imperative stimulus (movement signal). The third source, $\mathbf{s}_3$ simulates the activity of a brain region that is directly involved with the behavior but does not participate in the momentary network of correlated activity involving $\mathbf{s}_1$ and $\mathbf{s}_2$. The brain source $\mathbf{s}_3$ is not temporally stationary anywhere in the trial but is, but is consistent between trials.

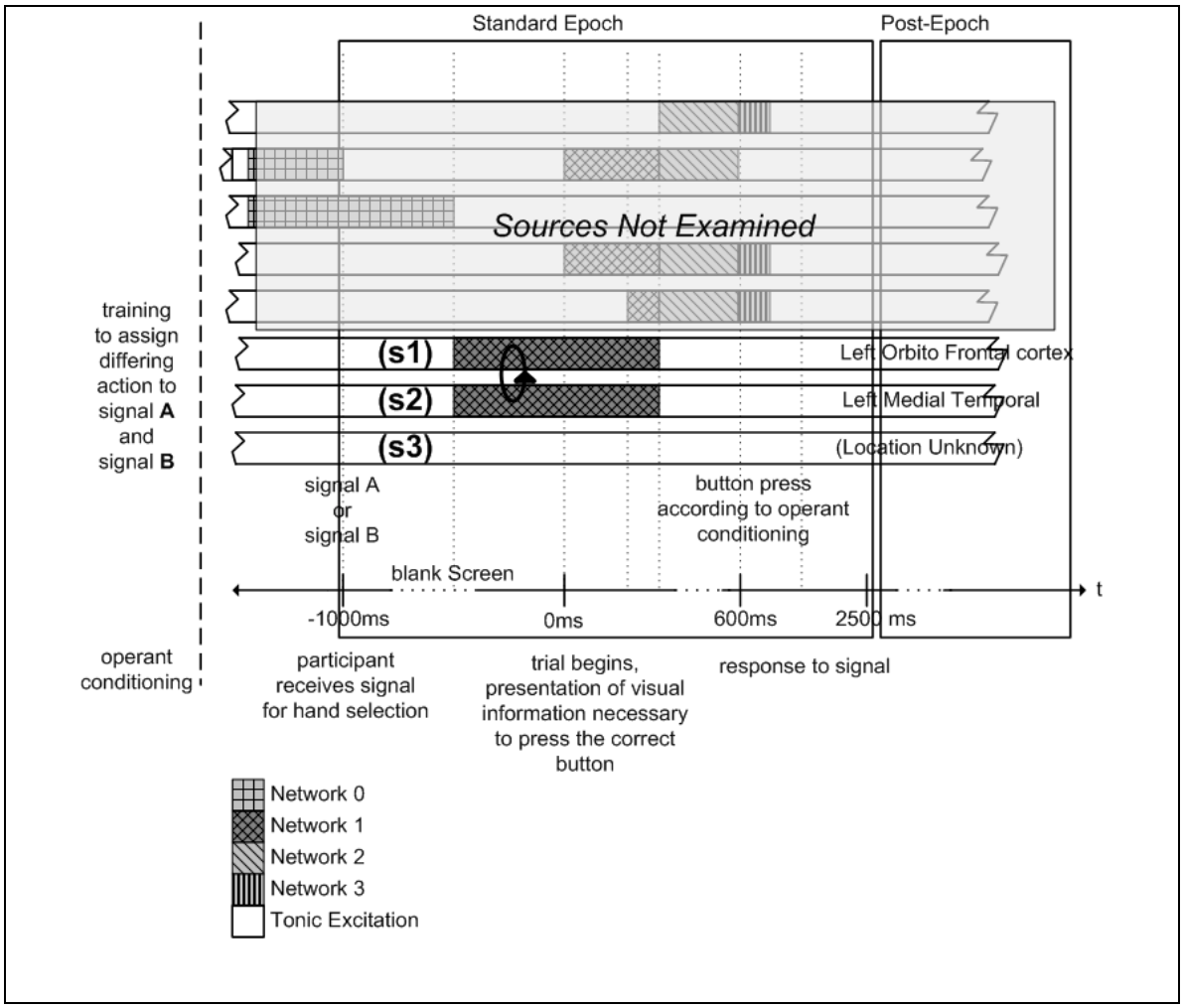

Figure 1. Hypothetical model of parallel-distributed brain activities for the example paradigm. The activity of 8 brain areas (sources) are shown though only 3 are involved in the current simulation. Momentary coordination between brain regions is indicated by shaded areas of similar hatch marks. Tonic excitation is indicated by non-shaded regions. Each characteristic moment of coordination is assigned a unique network number. Brain source regions are discriminated in the vertical axis. Time is indicated on the horizontal axis. A circular arrow indicates coordination of the brain regions being examined. These regions are marked as $\mathbf{s_1}$, $\mathbf{s_2}$ and $\mathbf{s_3}$ in relation to their time-domain activities. Brain regions are not examined but are included to illustrate the presence of other coordinated brain areas and momentary networks involved in the behavioral task.

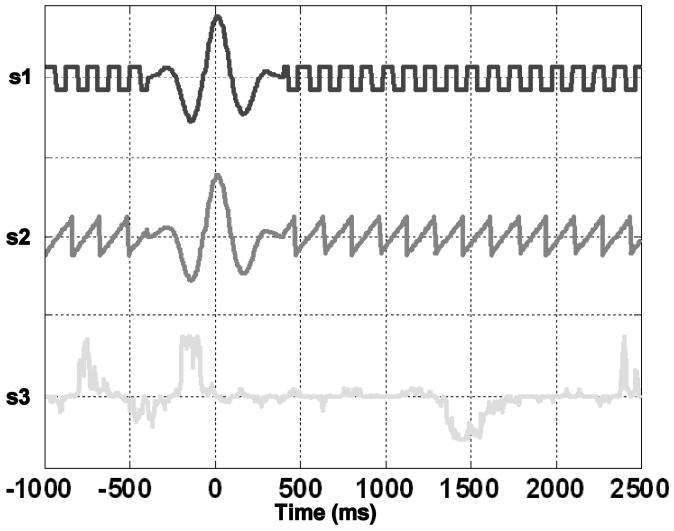

Figure 2. Three simulated sources. Two simulated sources, $\mathbf{s}_1$ and $\mathbf{s}_2$ have minimally correlated tonic activity and a momentary interval of perfect correlation. The third source, $\mathbf{s}_3$ is active during the trial but does not have activities correlated with other sources.

Methods

Synthesis of Simulated EEG

The creation of simulated data is illustrated in Figure 3. Synthetic EEG data were created as a mixture of the 3 brain sources from Figure 2, $\mathbf{s}_j$ appearing on 3 channels of EEG using Equation 7,

$$\mathbf{x} = \sum_{j=1}^{3} [\mathbf{a}_j \mathbf{s}_j] + \mathbf{N} \tag{7}$$

where $\boldsymbol{a}_j$ is a vector corresponding to the mixing weights for each source number $\boldsymbol{j}$ in Table 1. Additive zero-mean Gaussian noise, $\mathbf{N}$, uncorrelated on all channels was added to simulate stochastic sensor noise and complete the simulated EEG. Each simulated trial

of data examined ranged from –1000 to 2500 ms, at 250 samples per second totaling 875 samples (indicated in the 'standard epoch' of Figure 1). A period of correlated activity between $\mathbf{s}_1$ and $\mathbf{s}_2$ occurred in the interval -400 to 400 ms. Otherwise, the activities of $\mathbf{s}_1$, $\mathbf{s}_2$, and $\mathbf{s}_3$ were simulated as tonically excited, having independence activities. The tonic activities of $\mathbf{s}_1$, $\mathbf{s}_2$ and $\mathbf{s}_3$ were scaled to have unit standard deviation. These waveforms were selected to allow easy visual inspection of waveform distortion characteristics when evaluating results. To evaluate the effect of the amplitude of the activities of correlation on corresponding waveform estimate errors, variance of the window of momentary correlation was simulated for both $\sigma^2 = 3$ and $\sigma^2 = 6$, classified as either 'small' or 'large', respectively. These two levels of variance provided for the demonstration of 2 modes of source estimation error reduction. The additive Gaussian noise, used to simulate sensor noise, was at a level 64 dB below the tonic activities of $\mathbf{s}_1$, $\mathbf{s}_2$ and $\mathbf{s}_3$.

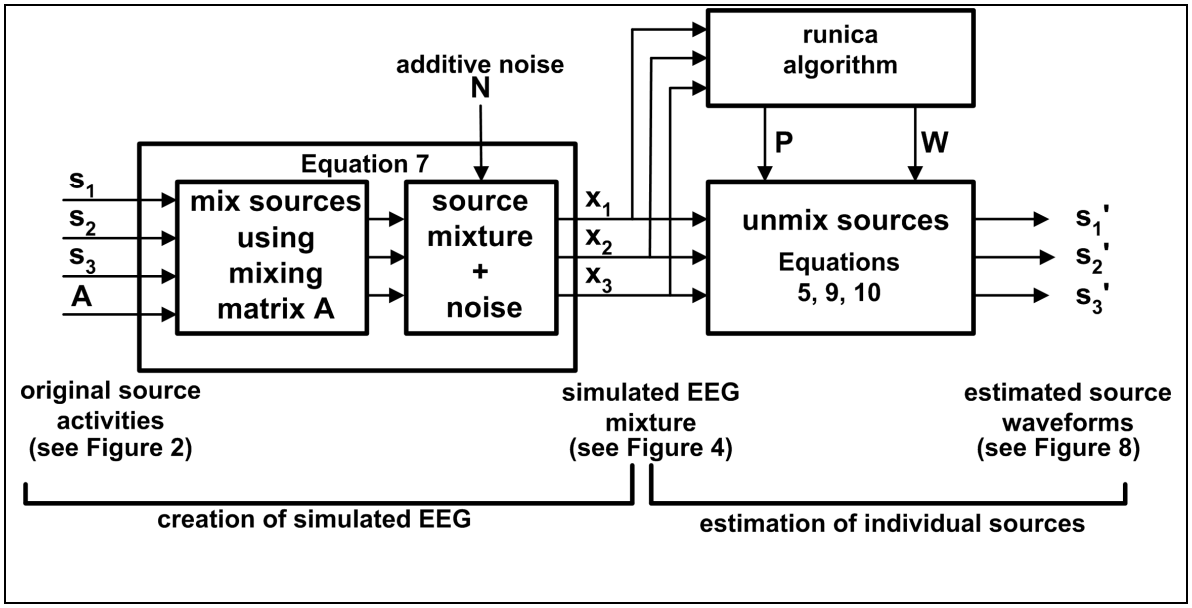

Figure 3. Block diagram illustrating (left-side) creation of simulated EEG and (right-side) the estimation of individual sources from the simulated EEG mixture. Original source waveforms are indicated as $\mathbf{s}_1$, $\mathbf{s}_2$, $\mathbf{s}_3$. Additive simulated sensor noise in given as $\mathbf{N}$. EEG mixture sensors 1 through 3 are indicated as $\mathbf{x}_1$, $\mathbf{x}_2$, $\mathbf{x}_3$. Estimated source waveforms are given as $\mathbf{s}_1'$, $\mathbf{s}_2'$, $\mathbf{s}_3'$. The sphering and weight matrices are given as $\mathbf{P}$ and $\mathbf{W}$ respectively.

mixing vector	weight 1	weight 2	weight 3
$\mathbf{a}_1$	1	2	3
$\mathbf{a}_2$	3	2	1
$\mathbf{a}_3$	1	3	1

Table 1. Mixing weights used in conjunction with Equation 7 to create simulated EEG.

Figure 4 illustrates a single trial of activities for the three channels of simulated EEG, $\mathbf{x}_1$, $\mathbf{x}_2$, and $\mathbf{x}_3$. The momentary period of coordinated activity is visible above the levels of mixed activities of the independent sources. Interestingly, the correlated wave shape appears on all 3 channels of the mixed EEG of Figure 4 in the interval -400 ms to 400 ms.

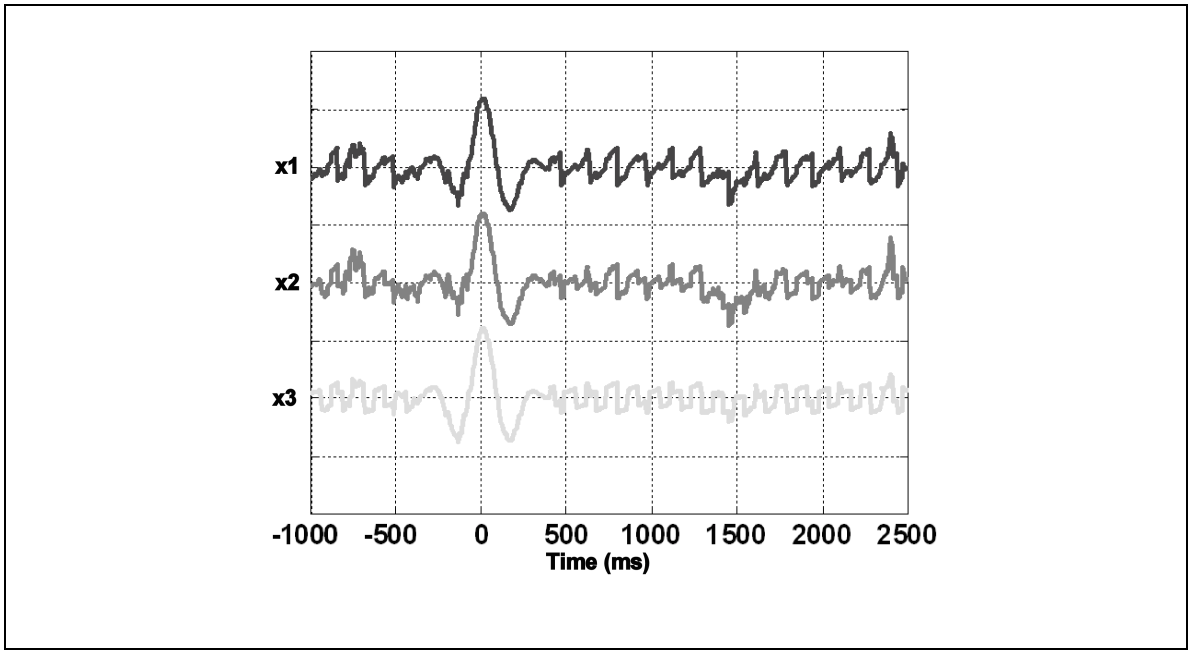

Figure 4. A single trial of raw simulated EEG. The waveforms on observation channels $\mathbf{x}_1$, $\mathbf{x}_2$, $\mathbf{x}_3$ are illustrated.

Analysis of Simulated EEG

Four methods were examined to reduce source estimation errors caused by the momentary correlation of $\mathbf{s}_1$ and $\mathbf{s}_2$ to illustrate limitations of standard ICA (runica) and to identify possible techniques to reduce brain source estimation error. These four methods

were: 1) addition of more trials, 2) increased the epoch size, 3) variation of the time analysis window position, and 4) notch filtering the data prior to ICA decomposition. For each of the methods, the estimated source activities **s'** were calculated from the estimate of the sphering matrix and weight matrix as in Equation 5 or by employing variations described by Equation 9 and Equation 10, presented below.

For the purpose of making waveform comparisons, recovered average source waveforms and original unmixed source waveforms were adjusted to have zero mean and unit standard deviation. Recovered waveforms were manually matched with the original source waveform for comparison and error calculation. Error was calculated as the root-mean-square (RMS) of the difference of the waveform as illustrated in Equation 8 where ***K*** is the number of samples in the epoch and **s'** is the estimate of **s** returned by ICA. The recovered value **s'** is calculated from the mean of all trials when multiple trials are used as in the step 'Addition of More trials' given below.

$$\textbf{RMS error} = \sqrt{\frac{\sum_{j=1}^{K}[\mathbf{s}_j - \mathbf{s}'_j]^2}{K}} \tag{8}$$

ICA parameters

The *runica* algorithm supplied with EEGLab 4.515 (Makeig et al., 1997) was used to estimate the sphering matrix **P**, and the weight matrix **W** from the simulated EEG mixture. The "extended" *runica* parameter implementing the use of the tanh non-linearity was used in the search for the unmixing matrix to separate the temporal sources. This non-linearity was found to be suitable for separating the tonic activities of the simulated sources. EEGLab and Matlab 7 (Mathworks Inc.) were used for all source modeling, source recovery, and error analysis.

Method 1: Addition of More Trials

Here, a scenario was synthesized to demonstrate that momentary correlation does lead to source estimation error and that the addition of more trials does not necessarily address the correlation problem. To evaluate the effect of increasing the number of trials used to calculate the sphering and weight matrices and subsequent source waveform activities, more trials of EEG for the standard epoch size (–1000 to 2500 ms) were systematically added for each execution of *runica* illustrated in Figure 1. A unique seed was used to initialize the random number generator to create unique additive white Gaussian noise in each trial. The characteristics of the source waveforms themselves were held constant. The source waveform estimate errors were calculated using Equation 8. The size of the error was evaluated for a small correlation ($\sigma^2 = 3$) and a large correlation ($\sigma^2 = 6$).

Method 2: Increasing Epoch Size

The effect of increasing the size of the epoch, and hence, the ratio of duration of correlated activity vs. uncorrelated activity on the weight matrix was evaluated. The epoch size was systematically increased such that the first epoch size examined was -1000 to 2500 ms (875 samples) and the second was –1000 to 6000 ms, (1750 samples), continuing until the final epoch length was 18 times the first epoch length evaluated. The source waveform estimate errors for each epoch size evaluated were calculated using Equation 8. The average RMS error was calculated across modeled sources. Trend lines were calculated from the average RMS error. This error was evaluated for a small correlation ($\sigma^2 = 3$) and a large correlation ($\sigma^2 = 6$).

Method 3: Uncorrelated Epoch

The effect of calculating the sphering and weight matrix from a portion of the standard epoch (indicated in Figure 3, Figure 4, and Figure 6) without the momentary correlation was evaluated. The interval, 400 to 2500 ms of the EEG mixture was isolated and used to calculate the sphering and weight matrices, $\mathbf{P}^U$ and $\mathbf{W}^U$, respectively. As a consequence, instead of having 875 samples per trial as in the standard epoch, only 525

samples per trial were available to calculate source separation matrices. These matrices were then used to separate the entire data epoch as in Equation 10, where **x** contains data for the entire epoch, -1000 to 2500 ms. The source waveform errors were calculated using Equation 8.

$$\mathbf{s} = \mathbf{W}^{U}\mathbf{P}^{U}\mathbf{x} \tag{10}$$

Method 4: Notch Filtering

The effect of notch filtering the frequencies relating only to the momentary correlation, while leaving activities at other frequencies intact, was examined as a way to reduce source estimate error. A 120-point, FIR notch filter (2 Hz to 4 Hz) was used to filter the data. The *runica* algorithm was then used to calculate the sphering and weight matrices corresponding to the notch-filtered data. These sphering and weight matrices, $\mathbf{P}^{h}$ and $\mathbf{W}^{h}$, respectively, were then used to separate unfiltered data as in Equation 9, where **x** indicates the unfiltered, simulated EEG data. The source waveform estimate errors were calculated using Equation 8.

$$\mathbf{s} = \mathbf{W}^{h}\mathbf{P}^{h}\mathbf{x} \tag{9}$$

Results

Method 1: Addition of More Trials

Overall, the addition of more trials to reduce source estimation error due to the momentary correlation had little effect (Figure 5). With the addition of two trials, error for $\mathbf{s}_2'$ with a large momentary correlation variance ($\sigma^2 = 6$) decreases, while the error of $\mathbf{s}_1'$ with a high momentary correlation increases slightly. There was no further improvement offered by the inclusion of more than two trials. This effect is also consistent for the case where the variance of the momentary correlation is small ($\sigma^2 = 3$). The results show that the RMS error for each of the sources modeled is not reduced by this method.

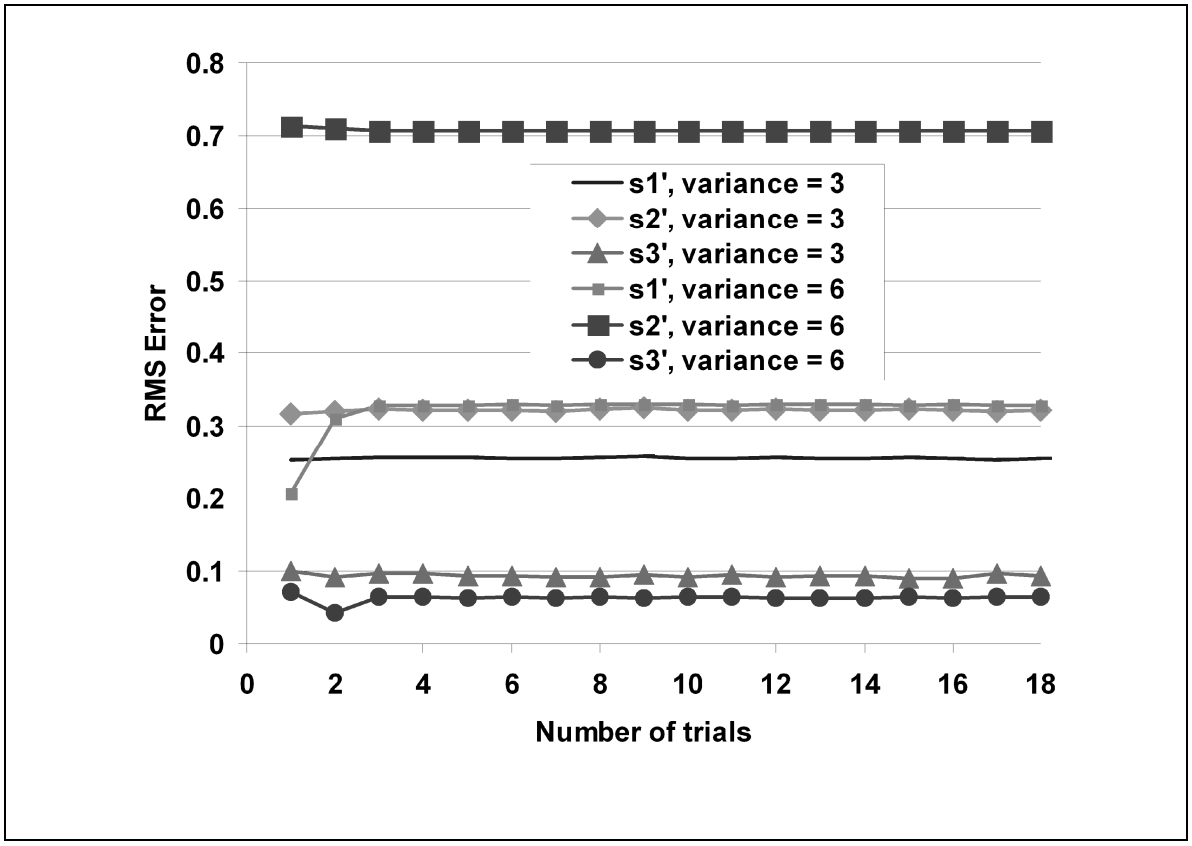

Figure 5: RMS source estimation error with respect to increasing number of trials for both small ($\sigma^2 = 3$) and large ($\sigma^2 = 6$) momentary correlation variances. Sources $\mathbf{s}_1$ and $\mathbf{s}_2$ model activities that are momentarily correlated. Source $\mathbf{s}_3$ models a source with activities that are not correlated with other sources.

Method 2: Increasing Epoch Size

Increasing the epoch length reduced the error associated with the momentary correlation. The plots of Figure 6 illustrate a consistent trend that as the epoch length is increased, the RMS error decreases asymptotically towards zero for a small momentary correlation variance ($\sigma^2 = 3$). The average error is decreased by approximately 65% ((0.23-0.080)/0.023, calculated from Figure 6) when the epoch length is quadrupled (875 to 3500 samples) to extend from -1000 to 13000 ms. (originally -1000 to 2500 ms). The trend of RMS error decrease was modeled as an inverse-linear function of the epoch length.

When the variance of the momentary correlation is large ($\sigma^2 = 6$) a substantial increase in the epoch size is required for a significant decrease in the source estimation error (Figure 7). The RMS difference calculation between the estimated waveforms of $\mathbf{s}_1$ and $\mathbf{s}_2$ (plotted as $\mathbf{s}_1'$-$\mathbf{s}_2'$, using Equation 8), shows a sudden transition between epoch length 875 to 9625 samples (interval A) and epoch length 9625 to 10500 samples (interval B). This transition is also reflected in the individual plots of RMS error of $\mathbf{s}_1'$ and $\mathbf{s}_2'$. The change of error trend follows two modes. The initial trend of the RMS error of $\mathbf{s}_1'$ decreases while the RMS error of $\mathbf{s}_2'$ increases as the epoch size is increased. In contrast to interval A, the plots of the Figure 7 inset (interval B) illustrate a more consistent trend: as the epoch length is further increased, the RMS error decreases asymptotically towards zero. This trend of interval B is similar to the trend for the case of a small variance of the momentary correlation.

Two trends of error suggest two error underlying mechanisms. The error interval A is much larger than the error in interval B. There is also a smaller RMS difference between waveforms for the comparison of of $\mathbf{s}_1'$ - $\mathbf{s}_2'$ in interval A versus the same comparison in interval B. Notably, the transition between between the RMS difference between $\mathbf{s}_1'$ and $\mathbf{s}_2'$ corresponds to the transition in the size of RMS error for of $\mathbf{s}_1'$ and $\mathbf{s}_2'$.

Method 3: Uncorrelated Epoch

Not surprisingly, avoiding the interval of momentary correlation altogether, by calculating the sphering and weight matrix from a portion of the standard epoch without the momentary correlation, eliminated it as a cause of source estimation error. This result also shows that it is not strictly necessary to use the entire dataset to calculate the sources separation matrices. The average RMS error (Figure 6 and Figure 7), when the sphering and weight matrices were calculated from the uncorrelated epoch (400 ms to 2500 ms), is similar to using an epoch 18 times longer than the standard epoch in the small variance condition.

Method 4: Notch Filtering

Notch filtering greatly reduced the source estimation error associated with the momentary correlation of sources. The average RMS error (Figure 6 and Figure 7), when the sphering and weight matrices were calculated from notch-filtered data, was largely reduced for $\mathbf{s}_1'$ and $\mathbf{s}_2'$, and was comparable to having an epoch length approximately 3 to 4 times the standard length, provided the variance of the momentary correlation is small. The error is comparably small for the case when the momentary correlation is large. For both cases, there is slightly more error in the estimate of $\mathbf{s}_3'$ than for $\mathbf{s}_1'$ and $\mathbf{s}_2'$. The reason for the error of $\mathbf{s}_3$ is elaborated upon in the discussion.

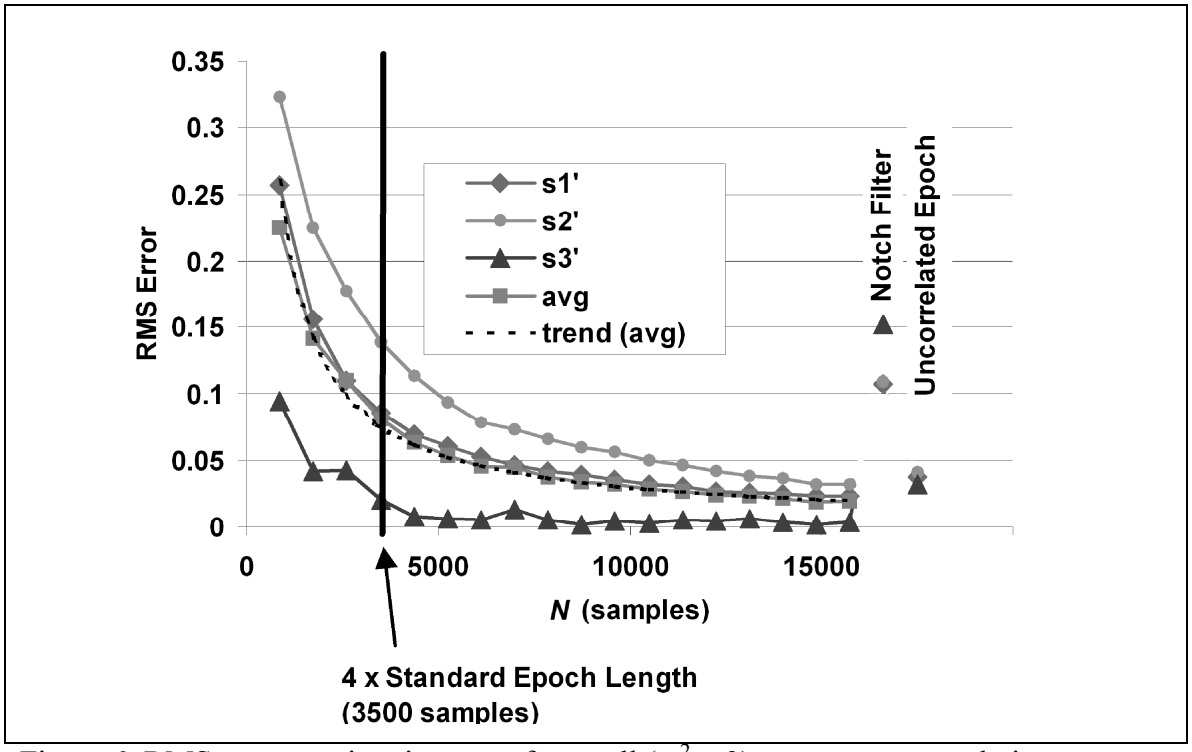

Figure 6: RMS source estimation error for small ($\sigma^2 = 3$) momentary correlation variance. Error is provided for method 2: increasing the epoch length, method 3: utilizing only the uncorrelated portion of the epoch (indicated as 'Uncorrelated Epoch'), and method 4: notch filtering (indicated as 'Notch filter'). These results have been provided on the same plot for comparison purposes. Details for method 2: Epoch lengths of 1 x standard epoch size to 18 x standard epoch size are given. A trend line illustrates the

average of the RMS error for $\mathbf{s}_1$, $\mathbf{s}_2$, $\mathbf{s}_3$. The equation of the trend is **RMS error** = $\mathbf{104.4}N^{-0.88}$.

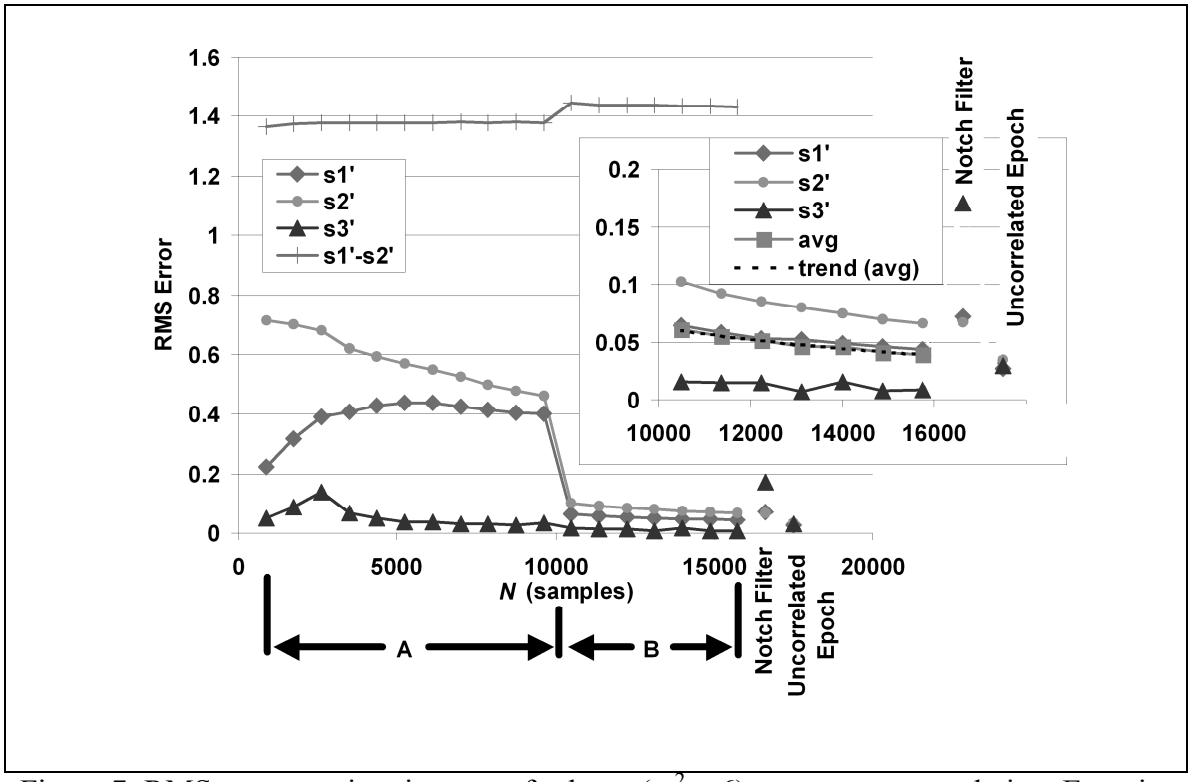

Figure 7: RMS source estimation error for large ($\sigma^2 = 6$) momentary correlation. Error is provided for method 2: increasing the epoch length, method 3: utilizing only the uncorrelated portion of the epoch (indicated as 'Uncorrelated Epoch'), and method 4: notch filtering (indicated as 'Notch filter'). These results have been provided on the same plot for comparison purposes. Details for method 2: Epoch lengths of 1 x standard epoch size (875 samples) to 18 x standard epoch size are given. The difference between $\mathbf{s}_1'$ and $\mathbf{s}_2'$ illustrates an abrupt transition in the trends of the plot. The difference between the estimated $\mathbf{s}_1$ and $\mathbf{s}_2$ plotted as $\mathbf{s}_1'$-$\mathbf{s}_2'$, and calculated as a RMS error illustrates a sudden transition at between epoch length 875 to 9625 (interval A) and epoch length 9625 to 10500 (interval B). This transition is reflected in the general plot of RMS error of $\mathbf{s}_1'$ and $\mathbf{s}_2'$ between intervals A and B. Inset: illustrates plot details of epoch length 12 to 18 x the standard epoch interval. The equation of the trend of the inset is **RMS error** = $\mathbf{1060}N^{-1.1}$.

(V) DISCUSSION

To use ICA to determine the bona fide time-domain activities of spatially distinct brain areas, the characteristics of brain activity must fit the assumptions of ICA as closely as possible. The results of our data analysis indicate that the size of sources waveform estimate errors is related to the degree to which brain activities meet the ICA assumption of statistical independence. Our results show that when the activities of multiple spatially distinct brain areas are correlated at zero-lag, ICA does not necessarily find the bona fide time activities of those spatially distinct brain areas. Given that correlation indicates coordination, our results suggest that those paradigms examining behaviors that require coordination of brain activities will not produce EEG that can easily be separated into constituent brain source activities. This is a serious problem since most behaviours of interest presumably are mediated by multiple, coordinated brain areas. Hence, the assumptions of ICA are not appropriate to brain activity that is best described by the parallel-distributed model. Since brain activities may not always fit the assumptions of ICA, steps can be taken to minimize the effects of coordinated activities. Such steps should take into account the (a) temporal non-stationarity of brain activity, (b) momentary and long-duration correlations, and (c) the frequency bands in which those correlated activities may exist.

Addition of More Trials

The addition of more trials was investigated and found that it does not directly address the correlation problem. The effect of adding more trials to improve the ICA estimate of source waveform activities results in slight shifts in the RMS error. These shifts, however, are not part of a consistent trend towards zero estimation error. For real EEG data, the addition of more trials might decrease error more than in this simulation, however, to a limit; correlation of activities of multiple brain areas may be consistent in the data. For example, if the activities of two brain areas are required to be correlated to facilitate a particular human behaviour, they will be, and this will appear in the data. The first-order statistic, the mean, is consistent enough to appear in averaged trials, thus, so could be the second order statistic, correlation. In this simulation, only a small random

noise-level was used to construct the synthetic data to emphasize the real problem of correlation. For real EEG data, with higher random noise levels, a greater reduction of RMS error would be expected. Thus, while increasing the number of trials is helpful in reducing the effects of random events occurring in individual trials, it does not directly influence errors due to momentary source correlations.

Increasing Epoch Size

The effect of increasing the epoch size to include more data samples where sources are not correlated produced a reliable trend of decreasing the RMS error of the source time-domain activity estimate. When the momentary correlation involved a variance 3 times the variance of the tonic uncorrelated waveform, there was an asymptotic reduction in RMS error as the epoch length increased. When the variance of the momentary correlation was greater however, in this case, 6 times the variance of the tonic uncorrelated waveform, the RMS error reduction trend followed two different modes as the length of the trials were increased. The second mode is similar to that for the case of a variance of 3 (Figure 7, interval B), but the first mode is distinctly different. We attribute this first mode (Figure 7, interval A) as the inability of the algorithm to identify $\mathbf{s}_1$ and $\mathbf{s}_2$ as two distinct sources (with waveform errors). These two sources were regarded by the ICA algorithm as a single source until the epoch length was increased to 12 times the standard length (10,500 samples). We term this first mode as *correlative source splitting distortion* (the two sources were not appropriately split) and *correlative source distortion* (the two sources were appropriately split, but waveform estimation errors due to partial correlation was still present and significant).

We attribute the error of interval A to an inappropriate representation of the data by the sphering matrix. It did not appropriately represent the structure of three separate sources. It isn't until the interval B when the three sources are appropriately represented and the error curve has convergent properties.

In application, if the interval of uncorrelated activity is much greater than the interval of correlated activity, then the impact of the correlated activity on estimation of the covariance matrix, sphering matrix and weight matrix, and the RMS error will be negligible. In this case, the data samples relating to the momentary correlation would be considered outliers of the distribution of all data samples in the time window that is used to calculate the sphering and weight matrices. Thus, estimates of source activities would then be accurate and relate to physically distinct brain areas. This is supported by the simulation experiment of Makeig et al. (2000), where they found that adding more data samples from their simulated 'no-response' behavioural event minimized the importance of the partial correlation on calculating the separation criteria, and source recovery results were improved.

Large epochs improve the estimation of high order statistics such as kurtosis, that itself, can improve source estimates via the ICA weight matrix. Vigário et al., (2000) illustrated how the estimated value of kurtosis changes depending on the epoch length used to characterize a signal. It is thought that the EEG is a mixture of temporally isolated 'events' of physically distinct sources. Therefore, source activities would be short duration increases in activity and long-duration intervals of minimal activity. This is characteristic of positive kurtosis which ICA relies on for calculating source independence. Thus, longer epoch lengths might improve separation of sources by providing a better estimate of the kurtosis.

It is likely that the brain activity associated with many behavioural paradigms have sources that are momentarily correlated in the time interval of research interest. This correlated interval could also be referred to as the primary microstate of the paradigm, for example, the first 400 ms after a stimulus. In this interval, the correlation between distinct brain regions is high and then subsides later in (or after) the trial. ICA methodologies that utilize more of the tonically excited and uncorrelated portion of the data (post standard epoch) of the inter-trial interval may yield better results. This is in agreement with a general consensus among those who use ICA to identify components of EEG that ICA should be applied to non-segmented EEG. In a personal communication,

Arnaud Delorme (1995) stated that when comparing results between ICA applied to concatenated data epochs versus ICA applied to the continuous data, that running ICA on the raw data returns cleaner (and more dipolar) ICA components.

Another reason to use longer epoch lengths is that they should capture a greater variety of microstates and facilitate source estimation. Capturing a greater variety of differing microstates should increase the combinations for which parts of the brain are correlated, and thus more clearly represent independent brain activities in the data. This is consistent with the observation that concatenated data from different conditions facilitates separation of activities of distinct brain areas.

Given the advantages stated above, there are two fundamental drawbacks of increasing epoch lengths. First, it is not known a priori, by how much epoch lengths should be increased to separate all of the sources. Second, increasing epoch lengths require that the duration of the inter-trial interval be extended. In some studies, this interval is kept short so that many hundreds of trials can be collected. If a large inter-trial interval is required, the number of trials then must be limited to provide a reasonable limit on the duration of a data collection session. Thus, increasing epoch length to durations long enough to reduce error to an acceptable level may not be feasible.

Uncorrelated Epoch

If the number of sources in the data remains constant over the entire epoch (that is, sources do not appear or disappear), then it may be appropriate to calculate the unmixing matrix on a sub-section of the epoch to avoid the moment of correlated activity. Avoiding the momentary correlation as though it were an ‘artefact’ was demonstrated by calculating the unmixing and sphering matrices using the interval of tonic uncorrelated activity and then using those results to unmix the data of the entire epoch. When the ‘artefact’ was removed, the source separation improved. This appears to be a viable option for improving ICA results when the exact moment of coordination is known.

In the case of our simulated EEG data, the temporal location of the momentary coordination is known— it is visible in the original source illustrations of Figure 2. The temporal location of the correlation between $\mathbf{s}_1$ and $\mathbf{s}_2$ might even have been inferred from the hypothetical relational diagram of Figure 1 or visible in the simulated EEG mixture of Figure 4. In such a case, one can use the ICA algorithm to construct an appropriate unmixing matrix and sphering matrix for the region of no source correlation. In application, however, there may be no moment when all sources in the EEG are uncorrelated.

Notch Filtering

Generally, notch-filtering the frequencies of momentary correlation prior to calculation of the sphering and weight matrices and then using these matrices to separate sources in the unfiltered data reduced the RMS error for both levels of momentary correlation evaluated. However, this method resulted in a slight error in the estimate of $\mathbf{s}_3$. Overall, the reduction of error is approximately equivalent to having an epoch length 3 to 4 times the standard length.

From this simulation, notch filtering the frequencies relating to long-distance synchronization appears to be a simple way to construct a sphering matrix and weight matrix that appropriately separates the time-domain activities of physically distinct sources. In our example, the estimate of $\mathbf{s}_3$ is poor because $\mathbf{s}_3$ had considerable power in the band that was notch filtered to calculate the unmixing matrix. Ostensibly, there was too little remaining power to obtain the best estimation for this source. To verify this, we examined differing waveforms and a variety of frequencies of correlation (data not shown) and found that we were able to recover all three sources with minimal error if significant uncorrelated variance remained outside those frequencies that were notch filtered. We provide this example to illustrate the point that enough variance, pertaining to each source, that is statistically independent among sources must remain after removing frequencies related to coordination. This variance is necessary to correctly calculate the sphering and weight matrices. We emphasize the necessity that the brain

areas with contributions to the EEG to be identified must have activities with enough variance that lie outside a frequency band that is to be notch filtered or attenuated.

The fundamental drawback to this method is that it is not necessarily known which frequencies bands contain the parasitic levels of correlation that might be removed to calculate the source separation matrices. Studies of the hippocampal complex generally implicate both the theta band (4 - 8 Hz) and gamma band (36 - 44 Hz) frequencies (Bland and Oddie, 2001) for having coordination between spatially distinct parts of the brain. Thus there are multiple frequency bands implicated as possibly containing such correlated activities. The hippocampal complex, however, also exhibits local activities in the beta band (15 - 20 Hz) (Bibbig et al., 2007) and thus the such activities might be enough to provide enough variance to identify brain areas as distinct after notch filtering frequencies of correlated activities. It is however pertinent and necessary to find a methodology that automatically identifies those frequencies of parasitic correlation.

In recent study conducted after this manuscript was prepared, we proposed a method to automatically identify the frequencies of parasitic correlation. The method first identifies the frequencies of correlation and dependence, defining a filter similar to the notch filter described in the current study. Lastly, this filter is used to modify the EEG data prior to calculating the spatial separation matrices (Zeman et al., 2008e) in a manner similar to Equation 9. The results of that study thus supports the rational developed in the current paper to modify the frequency content of the EEG data for the calculation of the spatial separation matrices.

Summary

Our goal has been not to identify the uncorrelated activities of the brain for analysis, but to identify such activities so that spatial separation matrices can be appropriately estimated to separate the bona fide activities originating from different parts of the brain. By identifying activities in this way, both the correlated and uncorrelated activities of different brain areas can be studied.

We have demonstrated that the accuracy in estimating bona fide brain activities using ICA is clearly linked to the correlation of time-domain activities among brain sources. The characterization that brain activities are non-Gaussian, non-white, temporally non-stationary, spatially stationary, and statistically independent is not sufficient to completely characterize the brain activity–ICA relationship. We have identified that in addition to those properties above, brain activities additionally have the following properties: (1) In some time intervals the activities of distinct brain areas are uncorrelated and independent, while in other intervals they are correlated and dependent. (2) There are intervals of short-term temporal stationarity and intervals of short-term non-stationarity. (3) At different frequencies, the correlatedness or dependence relationship differs among distinct brain areas. (4) Areas in the brain that are used repeatedly in consecutive experimental trials might remain active about their usual resting threshold with statistically independent activities during the inter-trial interval. (5) Brain areas used in a behavior may remain active and uncorrelated between trials. (6) The level of correlation and dependence between source activities measured from a data set varies depending on characteristics of the paradigm in which the data were collected. All of these characteristics listed have some bearing on the ICA estimation accuracy of brain activities.

ACKNOWLEDGEMENTS

Funding for this work was provided by the Natural Sciences and Engineering Research Council of Canada, CanAssist, the University of Victoria, and the Alberta Heritage Foundation for Medical Research. Thanks also to our Research Assistant Sunny V. Mahajan, for his work on this project.

(VI) CONCLUSIONS

In evaluating how to improve source estimation accuracy in the presence of momentary correlated activities, we identified three methods to reduce estimation error. Error can be reduced by calculating ICA source separation matrices on data arranged in the following

ways: increasing trial length, removing frequency bands containing activities associated with coordination, or removing the time-window of maximum coordinated activity. Of these methods, increasing trial length to include the inter-trial interval and removal of the frequency bands containing activities associated with coordination of distinct brain areas might prove to be the most effective in future work.

(IV) REFERENCES

Andrew CM, Pfurtscheller G. On the existence of different alpha band rhythms in the hand area of man. Neuroscience Letters 1997;222:103-106.

Andrew C. Quantification of event-related coherence (ERCoh). In: Pfurtscheller G, Lopes da Silva FH (Eds). Handbook of electroencephalography and clinical neurophysiology. Revised Series, v6. Amsterdam, The Netherlands: Elsevier, 1999:119-137.

Anemueller J, Sejnowski TJ, Makeig S. Complex independent component analysis of frequency domain electroencephalographic data. Neural Network 2003;16:1311-1323.

Baddeley AD, Hitch G. (1974). Working memory. In: Bower GH (Ed). The psychology of learning and motivation: Advances in research and theory, v8. New York: Academic Press 1974:47-89.

Baddeley A. The episodic buffer: a new component of working memory? Trends in Cognitive Sciences 2000;4(11):417-423.

Baddeley A, Della Salla S. Working memory and executive control. Philosophical Transactions R. Soc. Lond 1996;351:1397-1404.

Başar, E. Memory as the “whole brain work”: a large-scale model based on “oscillations in super-synergy”. International Journal of Psychophysiology 2005;58:199-226.

Bell A, Sejnowski TJ. An information-maximization approach to blind separation and blind deconvolution. Neural Comp. 1995;7:1129-1159.

Bibbig A, Middleton S, Racca C, Gillies MJ, Garner H, LeBeau FEN, Davies CH, Whittington MA. Beta rhythms (15-20 Hz) generated by non-reciprocal communication in the hippocampus. Journal of Neurophysiology 2007;97:2812-2823.

Bland B H, Oddie S D. Theta band oscillation and synchrony in the hippocampal formation and associated structures: the case for its role in sensorimotor integration. Behavioural Brain Research 2001;127:119-136.

Bressler SL. Large-scale cortical networks and cognition, Brain Research Reviews 1995;20;288-304.

Contreras-Vidal JL, Kerick SE. Independent component analysis of dynamic brain responses during visuomotor adaptation. NeuroImage 2004;21(3):936-945.

Delorme A, Makeig S. EEGLAB: an open source toolbox for analysis of single-trial EEG dynamics including independent component analysis. J. Neuroscience Methods 2004;134:9-21.

Fellman DJ, Van Essen DC. Distributed hierarchical processing in the primate cerebral cortex. Cereb Cortex, 1991;1:1– 47.

Gevins AS, Bressler SL, Morgan NH, Cutillo BA, White RM, Greer DS, Illes J. Event-related covariances during a bimanual visuomotor task. I. Methods and analysis of stimulus- and response-locked data. Electroencephalography and clinical Neurophysiology 1989;74:58–75.

Ghahremani D, Makeig S, Jung T-P, Bell AJ, Sejnowski TJ (Institute for Neural Computation, University of California San Diego. La Jolla CA). Independent Component Analysis of Simulated EEG Using a Three-Shell Spherical Head Model. Technical Report INC-9601, 1996.

Glover S. Separate visual representations in the planning and control of action. Behavioural and Brain Sciences 2004;27:3-78.

Haykin S, Chen Z. The Cocktail Party Problem, Neural Computation 2005;17(9):875-1902.

Hensen RN, Rugg MD. Neural resonse suppression, haemodynamic repetition effects, and behavioural priming. Neuropsychologia 2003;41(3):263-270.

Holzner B. Event-related correlation of EEG activity. MSc. Thesis, Graz University of Technology.

Hyvärinen A, Karhunen J, Oja E. Independent Component Analysis. New York, NY: John Wiley & Sons, 2001.

Jung TP, Makeig S, Westerfield M, Townsend J, Courchesne E, Sejnowki TJ. Analysis and visualization of single-trial event-related potentials. Human Brain Mapping 2001;14(3):166-85.

Knoblauch A, Sommer FT. Synaptic plasticity, conduction delays, and inter-areal phase relations of spike activity in a model of reciprocally connected areas. Neurocomputing 2003; 52(44):301-306.

Kopp F, Schroger E, Lipka S. Neural networks engaged in short-term memory rehearsal are disrupted by irrelevant speech in human subjects. Neuroscience Letters, 2004;354:42-45.

Languis ML, Miller DC. Luria's Theory of brain functioning: A model for research in cognitive psychology. Educational Psycologist 27(4), 493-511, 1992

Leocani, L, Locatelli T, Martinelli V, Rovaris M, Falautano M, Filippi M, Magnani G, Comi G. Electroencephalographic coherence analysis in multiple sclerosis: correlation with clinical, neuropsychological, and MRI findings. Journal of Neurology, Neurosurgery, and Psychiatry 2000;69:192-198.

Luria, AR. The working Brain. Harmondsworth, England: Penguin, 1973.

Makeig S, Delorme A, Westerfield M, Jung TP, Townsend J, Courchesne E, Sejinowski TJ. Electroencephalographic Brain Dynamics Following Manually Responded Visual Targets. PloS Biolog, 2004;2(6):0747-0762.

Makeig S, Bell A, Jung T, Sejnowski, T. Independent component analysis of electroencephalographic data. In: Touretzky D, Mozer M, Hasselmo M (Eds). Advances in Neural Information Processing Systems. MIT Press, 1996;8:145-151.

Makeig S, Jung TP, Ghahremani D, Bell AJ, Sejnowski TJ. Blind separation of auditory event-related brain responses into independent components. Proc Natl Acad Sci USA, 1997;94:10979-10984.

Makeig S, Jung T-P, Ghahremani D, Sejnowski TJ. Independent Component Analysis of Simulated ERP Data. In: Nakada T (Ed). Integrated Human Brain Science: Theory, Method, Applications (Music). Elsevier, 2000.

Makeig S. Beyond Blind Averaging: Analyzing Event-Related Brain Dynamics. Institute for Neural Computation, University of California San Diego, La Jolla, CA. Retrieved April 17, 2007 from http://cogimage.dsi.cnrs.fr/documents/HBM2005_MEEGCourse/Makeig.pdf

Marosi E, Harmony T, Becker J, Reyes A, Bernal J, Fernandez T, Rodriguez M, Silva J, Guerrero V. Electroencephapographic coherences discriminate between children with

different pedagogical evaluation. International Journal of Psychophysiology 1995;19:23-32.

Michel C M, Seeck M, Landis T. Spatiotemporal Dynamics of Human Cognition. News Physiol. Sci, 1999;14:206-214.

Mesulam MM. From sensation to cognition. Brain 1998;121(6),1013-1052.

Nunez LP, Generation of Human EEG by a Combination of Long and Short Range Neocortical Interactions. Brain Topography 1989;1(3): 199-215.

Nunez PL, Neocortical Dynamics and Human EEG Rhythms. New York: Oxford University Press, 1995

Onton J, Delorme A, Makeig S. Frontal midline EEG dynamics during working memory. NeuroImage 2005;17(2):341-356.

Parra L, Sajda P. Converging Evidence of Linear Independent Components in EEG, Proc 1st Int'l IEEE EMBS Conf. Neural Eng 2003;525-528.

Parvizi J, Van Hoesen GW, Buckwalter J, Damasio A. Neural connections of the posteromedial cortex in the macque. PNAS 2006;103(5):1563-1568.

Pfurtscheller G, Neuper C. Simultaneous EEG 10 Hz desynchronization and 40 Hz synchronization during finger movements. Neuroreport 1992;3(12):1057-1060.

Raghavachari S, Kahana MJ, Rizzuto DS, Caplan JB, Kirschen MP, Bourgeois B, Madsen JR, Lisman JE. Gating of Human Theta Oscillations by a Working Memory Task. The Journal of Neuroscience 2001;21(9):3175-3183.

Rodriguez E, George N, Lachaux JP, Martinerie J, Renault B, Varela FJ. Perception's shadow: long-distance synchronization of human brain activity. Letters to nature 1999;397:430-433.

Roelfsema, PR, Engel AK, Konig P, Singer W. Visuomotor integration is associated with zero time-lag synchronization among cortical areas. Nature 1997; 385:157-161.

Sklar B, Hanley J, Simmons WW. An EEG experiment aimed toward identifying dyslexic children. Nature 1972;240:414-416.

Streletz LJ, Katz L, Hohenberger M, Cracco RQ. Scalp recorded auditory evoked potentials and sonomotor responses: an evaluation of components and recording techniques. Electroencephalography and Clinical Neurophysiology 1977;43:192-206.

Summerfield C, Mangels JA. Functional coupling between frontal and parietal lobes during recognition memory. Brain Imaging 2005;8;16(2):117-122.

Takada M, Tokuno H, Nambu A, Inase M. Corticostriatal projections from the somatic motor areas of the frontal cortex in the macaque monkey: segregation versus overlap of input zones from the primary motor cortex, the supplementary motor area, and the premotor cortex. Experimental Brain Research 1998;120:114-128.

Townsend J, Courchesne E. Parietal damage and narrow "spotlight" spatial attention. J Cogn Neurosci 1994;6:220–232.

Varela F, Lachaux JP, Rodriguez E, Martinerie J. The Brainweb: Phase synchronization and large-scale integration. Nature Neuroscience Reviews 2001;2:229-239.

Vigário R, Särelä J, Jousmäki V, Hämäläinen M, Oja E. Independent Component Approach to the Analysis of EEG and MEG Recordings. IEEE transactions on biomedical engineering 2000; 47(5):589-593.

Von Stein A, Sarnthein J. Different frequencies for different scales of cortical integration: from local gamma to long range alpha/theta synchronization. International Journal of Psychophysiology 2000;38:301-313.

Weiss S, Muller HM. The contribution of EEG coherence to the investigation of language. Brain and Language 2003;85:325-343.

Zeman PM, Mahajan SV, Livingstone SA, Livingston NJ, Skelton RW. Spectral Shaping to Relax ICA Assumptions to Facilitate Decomposition of EEG. (for publication). 2008e.

Section III: Development of New EEG Methodologies

The previous section examined some fundamental principles of brain function, ICA, and the typical EEG data collection paradigm. Researchers applying ICA methods to EEG analysis have perhaps oversimplified the properties of brain activity and scalp EEG. The perspective has been that the EEG is a mixture of brain activities that are individually non-Gaussian, non-white, and statistically independent. However, the discussion of neuropsychology and brain activity in the context of the blind source separation problem in the previous chapter has brought to light additional characteristics by which to conceptualize the scalp EEG. Fundamentally, the characteristics of brain activity and the scalp EEG depend on behaviour and not all EEG datasets have equivalent properties. Furthermore, the characteristics of EEG data and the component sources of which it is comprised are driven by the behavioural characteristics of the EEG data recording session. In addition to the standard, and convenient, characteristics of non-Gaussianity, non-white, and statistically independent given above, brain activities exhibit movements of stationarity and correlatedness. It is actually very likely that at the commencement of a behavioural trial, the activities of multiple distinct brain areas will be correlated. As indicated in the previous section, there are also likely differences in the statistics of the EEG for different frequency bands. A simulation to illustrate the problem caused by correlated brain activities provided some theoretical solutions to the correlation problem. First, we showed that, indeed, for blind source separation using ICA, correlated source activities are problematic when the activities of particular parts of the brain are of interest and that when partial correlation of activities is present, source estimation error is also present. We showed that the time interval used to calculate the ICA separation matrices is important to the ICA source separation outcome and thus the accuracy with which brain sources are estimated. When we examined ways to reduce the source estimation error, simulation results suggested three possible ways to accomplish this. These include: (1) lengthening trials, (2) notch filtering frequencies of correlated activities between distinct brain areas, or (3) attenuation of frequencies of correlated activities between distinct sources.

In chapters 3 to 5 of the current section, we develop a set of tools which are intended to provide more information about the brain activity estimates calculated via blind source separation using ICA than is currently available by other methods. In each of these chapters we assume that data mining EEG data using standard ICA methods does provide us with reasonable brain sources (the issue of source estimation accuracy is addressed later in Chapter 6). In chapter 3 we develop a method of mapping scalp surface fields of components of the EEG found via ICA to equivalent volume-domain representations. In their volume-domain representations, components have the properties of 3D volumes that occupy space; they thus have the property, and possibility, of physical overlap with other components of the ICA decomposition. Actual modular areas of the brain that have differing activities however can not have a physical overlap and thus any contradiction a component of the EEG has with a physical property of the brain (such as non-overlap) can be used as criteria by which to evaluate the component. An algorithm to map scalp-acquired brain activity components of the EEG to the volume-domain also provides for the additional ability to estimate the modular volumes of such sources. Thus, in the same chapter, we define a method to estimate the modular brain volumes of ICA components of the EEG data so that the actual origin of component brain activities can be determined. This volume projection of components and the estimate of component volumes is explored using synthetic EEG data. The work in Chapter 4 uses real EEG data to first demonstrate the estimation of modular brain volumes and then to examine how a measure of volume overlap of sources can be used to evaluate source separation. In Chapter 5, a tool is developed that provides validation of components found via ICA source separation as either originating from a brain volume or as artefact. This is also done using synthetic EEG data. The creation of this set of tools makes it possible to evaluate modifications to the standard ICA method to improve source separation of brain activities. Prior to the existence of these tools, there was no direct, objective way to measure brain source estimation improvement using only the EEG data. Thus, these tools provide an important technical contribution to the field of neuroscience.

The technical methods developed in Chapters 3 to 5 have been used by researchers at the University of Lethbridge, Centre for Behavioural Neuroscience to make sense of the EEG

data they have collected during a virtual spatial navigation task. Figures and plots associated with their research that demonstrate the application of the methods developed here, are given with descriptions in Appendix I and Appendix II. These figures and plots demonstrate the usefulness of these methods for processing real EEG data.

Using the tools developed in Chapters 3 to 5, a new method of data mining is introduced in Chapter 6 that uses ICA principles to obtain better estimates of bona fide brain activities than the standard ICA method, runica (Makeig et al., 1997).

Chapter 3: Beamform Volume Projection of EEG ICA Topographies

The following manuscript describes a method of mapping surface fields of components of the scalp EEG to volume-domain representations within a head model. In this representation, components have the properties of center of mass, 3D volume, and occupancy of space. Thus, there exists the property and possibility that, if a component of brain activity is poorly estimated, it might have some physical overlap with other components. The following manuscript shows that surface potentials can be projected to the volume domain with the purpose of identifying the neuroanatomical origin of components of the EEG. These volume-domain projections of component scalp topographies are called the volumetric spectra of the projected EEG components. By this projection method, the spatial surface variance of the scalp topography exists in a 3D head model as 3D spatial variance. The manuscript demonstrates how the overlaps of the modular volumes of components can be calculated using these volumetric spectra. Also demonstrated is that the characteristics of the volume-domain representation of components can be used to differentiate artefacts from bona fide brain source components. This manuscript explores these concepts using synthetic EEG data.

Article Type: Research Article

Article Title: Beamform Volume Projection of EEG ICA Topographies

Philip M. Zeman[1,2,3], Sunny V. Mahajan[1,2], Sharon A. Livingstone[3], Peter F. Driessen[2], Ronald W. Skelton[3], Nigel J. Livingston[1]

[1] CanAssist, University of Victoria, BC, Canada

[2] Department of Electrical and Computer Engineering, University of Victoria, BC, Canada

[3] Department of Psychology, University of Victoria, BC, Canada

Correspondence may be addressed to Philip M. Zeman:
(voice) +1-250-589-4234 / (fax) +1-250-721-6611 / pzeman@alumni.uvic.ca

Abstract

Objectives: We present a methodology that relates topographies calculated via Independent Component Analysis (ICA) of EEG data to volume domain representation not constrained to a single voxel. We investigate the feasibility of using such projections to estimate brain source volumes and volume overlap of source pairs, and determine if neural and artefact sources might be differentiated by their volume domain characteristics.

Methods: Synthetic EEG data were comprised of artefacts and multiple sources within a head model and decomposed into parts using ICA. An adaptation of Linearly-Constrained Minimum-Variance Beamforming, projected ICA-derived topographies into a model brain volume. Additive noise was used to meet the Beamformer requirement for an EEG baseline to remove volume domain bias. Estimates of volume domain noise were used to calculate the edges of modular brain volumes.

Results: Volume projections calculated from synthetic EEG data are similar to actual model source volumes. Estimates of volume modularity are similar to actual volumes for a threshold of 5 standard deviations above the mean volume noise estimate. Components relating to model brain sources placed at unique proximal and distal locations have non-overlapping volumes and high volumetric spectrum peaks. Modelled artefact components have low volumetric spectrum peaks and overlapping volumes.

Conclusions: Our methodology provides a basis for linking time and topography domains of ICA components to physical volume domain representations. Further, volume domain projections provide source information that might be used to differentiate brain activity from artefact components.

Keywords: EEG; ICA; LCMV beamforming; volumetric localization; dipole fitting; blind source separation.

I. INTRODUCTION

Independent Component Analysis (ICA) is widely used in analysis of EEG data and has become a useful tool for blind separation of scalp-EEG to identify functionally independent, modular neural sources (Makeig et al., 1996; Karhunen et al., 2000; Contreras-Vidal and Kerick, 2004; Delorme and Makeig, 2004; Makeig et al., 2004; Onton et al., 2005). The relationship between EEG scalp activities and anatomy is typically inferred using dipole source location modelling of ICA-derived topographies (Delorme and Makeig, 2004). In many studies, only the center of mass and orientation of EEG sources are determined, with little or no information available regarding source volume and the spatial overlap of these volumes. We believe that this volume information is critically important because it can provide an objective and anatomically relevant measure of the separation of ICA components.

Demonstrating that adjacent sources have differing centers of mass does not necessarily prove that they relate to anatomically different brain areas because these sources could have overlapping brain volumes. A measure of the location and volume of each source, and a measure of the volume overlap of source pairs could be particularly useful in cases where it must be demonstrated that two compared waveforms originate from unique brain volumes. These measures could provide a conclusive determination that sources do or do not originate from unique parts of the brain.

We propose and demonstrate a methodology that identifies source locations and volumes. This methodology combines ICA and Linearly-Constrained Minimum-Variance (LCMV) Beamforming in five main steps. First, sources are identified from scalp-acquired EEG by employing the standard ICA methodology (Makeig et al., 1997). The source topographies calculated via the ICA decomposition of EEEG data are then used to create an idealized input to the LCMV Beamformer (Van Veen et al., 1997). This idealized input is projected to the volume-domain via the LCMV Beamformer. The volume-domain projection is then bias corrected. Finally, a modular volume equivalent of each

ICA-derived scalp topography is generated by applying a threshold to the Beamformer output. This threshold is calculated from an estimate of the noise in the spatial volume domain. Thus, for each neural source, we obtain an estimate of the brain volume and location pertaining to each topography and time-domain waveform identified via ICA. The block diagram of Figure 1 provides an overview of this routine and is explained in subsequent sections.

The standard LCMV Beamform approach to EEG source localization natively maps a time-varying EEG field at the scalp to a volume inside the head rather than a single ICA topography. A detailed description of the LCMV Beamformer is provided by Van Veen et al. (1997). Mapping from the scalp domain to the volume domain is done using a linear closed-form solution (Van Veen et al. 1997). Using time-varying data, LCMV Beamforming estimates variances at all locations within a head model to create what we, for reasons of clarity, operationally define as the *volumetric spectrum* (other literature refers to this as the spatial spectrum). By the standard Beamform methodology, the presence of individual, spatially distinct peaks in a volumetric spectrum indicates that there are distinct brain sources.

The special case when EEG data contain only one time-varying source provides the basis for our proposed methodology. In such a case, the maximum of the resulting Beamform volumetric spectrum is analogous to the center of mass of that source (Michel et al., 2004). The source representation is further improved when interfering noise activity is uncorrelated and low-power compared to the source. We hypothesize that the source volume can be defined as the intersection of the fall-off of the volumetric spectrum from the peak to the noise floor. In this special case, the LCMV Beamformer effectively provides a mathematically closed-form relation between the electric field measured at the scalp to a source volume inside a model head. To create this special case from standard EEG data requires separation and isolation of the individual contributors to the EEG through a source unmixing and rank reduction procedure.

Source separation and rank reduction methods have been widely used to reduce the EEG data source space. For example, Koles and Soong (1998) used Principal Component Analysis (PCA) to estimate the number of distinct sources in an EEG dataset. Methods proposed by Schmidt (1986), and Mosher and Leahy (1996) use eigenvalue decomposition to simplify the source space prior to localization. Approaches such as these address the limitation that beamforming use alone can generally only isolate and localize a small number of sources (Van Veen et al., 1997; Michel et al., 2004). The degrees of freedom by which Beamforming natively provides a source separation and localization solution are determined as $K/3$, where K is the number of electrodes. This is in contrast to the PCA source separation methods described above that provide K degrees of freedom for source separation.

ICA has also been used to reduce the source space of EEG data and it provides a viable solution to the source separation problem (Bell and Sejnowski, 1995; Hyvärinen and Oja, 1997; Hyvärinen and Oja, 1999; Hyvärinen and Oja, 2000; Lee et al., 2000). Its application to EEG data has been widely demonstrated (Delorme and Makeig, 2004; Makeig et al., 1996; Ghahremani et al, 1996; De Lucia et al, 2006; Urrestarazu et al, 2006; Leal et al, 2006; Jentzsch, 2004; Tzy-Ping et al., 2001; Makeig et al., 2004; Onton, Delorme and Makeig, 2005). Kobayashi et al., (2002) used ICA of EEG to separate the noise and source space of EEG data prior to localization of epileptiform spike activity by employing the RAP-MUSIC algorithm (Baillet et al., 2000). By their method, ICA was used to separate the EEG data into source and noise spaces. Subsequently, components of the signal space were separated and localized while using the noise space to calculate a noise floor baseline to compensate for Beamformer biases.

We build on this body of research by providing a routine that incorporates the LCMV Beamformer to estimate the locations and volumes pertaining to individual source scalp topographies that have been previously isolated using ICA. In effect, we map scalp topographies to the volume domain without constraining the volume representation of these topographies to a single dipole. In contrast to prior methods, we do not require a

noise space baseline from the scalp-EEG data as baseline normalization and bias correction comes of an inherent property of our routine.

Simulations using model data have provided important information pertaining to the source separation characteristics of ICA (Makeig et al., 2000; Ghahremani et al., 1996). By first determining a relationship between source volumes and ICA-derived EEG components using synthetic data, a further relationship between ICA-derived scalp activities and brain anatomy may then be revealed. Our study uses synthetic data comprised of idealized, uncorrelated sources so that the interpretation of results is not confounded by issues relating to source separation of brain activities. In work stemming from this paper (Zeman et al., 2008c), we demonstrate success in localizing and estimating the volumes of brain areas contributing to scalp-recorded EEG data. In another study, this volume estimation methodology provides a very convincing representation of the left- and right- side ocular muscles that contributed activities to the scalp EEG (Zeman et al., 2008e).

In addition to describing and demonstrating the proposed routine, we show how volume characteristics can provide additional information about ICA-derived EEG components. We show how volume estimates provide a measure of the overlap and physical difference between sources. Finally, we demonstrate how characteristics of the volume representation of EEG components might be used to differentiate between EEG components arising from source volumes within the head from unwanted artefacts.

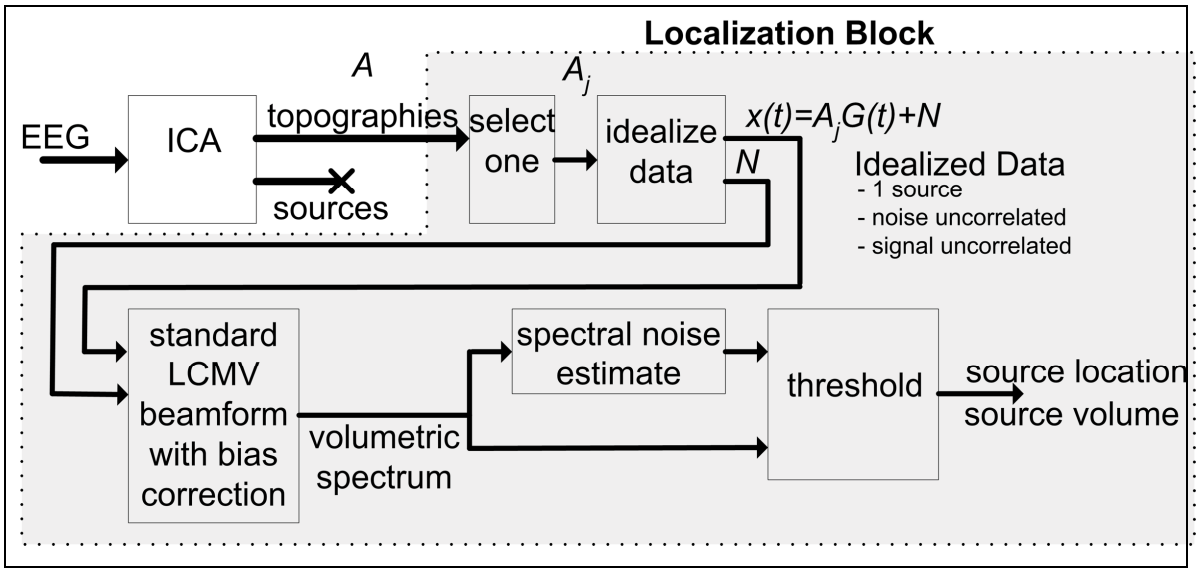

Figure 1. Block diagram of the proposed methodology. The shaded area indicates the localization and volume estimation components. Equation notation is defined in Section II.

II. MATHEMATICAL DESCRIPTION

MATHEMATICS OF ICA

The first step of our routine requires the separation of sources to identify topographies that pertain to modular regions of the brain. This is necessary to generate volumes that can be appropriately localized. ICA can be used to meet this objective, provided the data satisfy some basic assumptions. It is assumed that sources are: linearly mixed, spatially stationary, and have non-Gaussian activities that are zero-mean and statistically independent within the temporal window of analysis (Makeig et al., 1997). We assume that the statistically independent activities of interest that comprise the EEG and relate to activities of the brain, originate from modularly defined volumes. While it might not necessarily be the case that activities from distinct modular brain areas are not exactly statistically independent, it is a reasonable approximation that has in prior work yielded sources that can be related to anatomy via dipole modelling (Delorme and Makeig, 2004).

A variety of ICA algorithms are available to address the source separation problem. A detailed background and description of the general principles of ICA are provided by Stone, (2002); Hyvarinen and Oja, (2000) and Hyvärinen, Karhunen and Oja, (2001). Our proposed algorithm utilizes the *runica* implementation (Makeig et al., 1997) of the InfoMax algorithm (Bell and Sejnowski, 1995), however, any unmixing methodology that yields appropriate topographies may be used.

The general mixture model is given by Equation 1,

$$\mathbf{x}(t) = \mathbf{A}\,\mathbf{s}(t) \tag{1}$$

where $\mathbf{x}(t)$ is the observed mixture and $\mathbf{s}(t)$ describes the sources comprising the mixture. The matrix $\mathbf{A}$ of scalar values, describes the physical characteristics of the mixture. Each row of $\mathbf{A}$ determines how the sources combine to form a particular observed signal, and each column of $\mathbf{A}$ determines how a particular source is distributed among the observed signals. Both $\mathbf{A}$ and $\mathbf{s}$ are generally not known. Noise sources are not explicitly modelled in Equation 1, however, this is thought not to be a major issue because any noise present is extracted as one or more of the independent components (Makeig et al., 1996).

The observed mixture $\mathbf{x}(t)$ contains $\boldsymbol{K}$ rows of spatially distributed, time-domain sensor measurements (Equation 2), while the source matrix $\mathbf{s}(t)$ contains $\boldsymbol{J}$ rows of unknown time-domain sources activities (Equation 3). It is required that there be at least as many electrodes as there are unknown sources, such that $\boldsymbol{K} \geq \boldsymbol{J}$.

$$\mathbf{x}(t) = [\mathbf{x}_1(t), \mathbf{x}_2(t), \ldots \mathbf{x}_K(t)]^{\mathrm{T}} \tag{2}$$

$$\mathbf{s}(t) = [\mathbf{s}_1(t), \mathbf{s}_2(t), \ldots \mathbf{s}_J(t)]^{\mathrm{T}} \tag{3}$$

Given that the assumptions about the sources stated above are satisfied, the problem reduces to the task of finding a linear transform, $\mathbf{W}$, as outlined in Equation 4. The

weight matrix **W**, linearly reduces the mixture into parts and is used by Equation 5 to solve for the mixing matrix **A**, and the scalp topographies of each source held in the columns of the mixing matrix.

$$\mathbf{s}(t) = \mathbf{W}\mathbf{x}(t) \tag{4}$$

$$\mathbf{A} = \mathbf{W}^{-1} \tag{5}$$

MATHEMATICS OF THE LCMV BEAMFORMER

The mathematics of the LCMV Beamformer provides the link between time-varying scalp-EEG data and a volume domain representation. The LCMV Beamformer utilizes the measured covariance between scalp electrodes to provide an estimate of the volume-projected variance at all points within a model head. Equation 6 gives a noiseless forward model for a single source location $\boldsymbol{q_p}$ where $\mathbf{H}(\boldsymbol{q_p})$ is the $\boldsymbol{K}$ x 3 (a separate vector for each x, y, and z direction) transfer matrix from locations inside the head to the surface of the scalp **x,** and $\mathbf{m}(\boldsymbol{q_p})$ is the 3 x 1 vector representing the dipole moment at a given location. There are a total of $\boldsymbol{P}$ grid locations inside the head model for which to assign variances from $\boldsymbol{K}$ scalp electrodes. Following the equations of Van Veen et al. (1997), we have not included the notation of time, '$\boldsymbol{t}$' in our mathematical description.

$$\mathbf{x} = \mathbf{H}(\boldsymbol{q}_p)\mathbf{m}(\boldsymbol{q}_p) \tag{6}$$

For the case of multiple locations or *voxels* within the head model we utilize the summation of Equation 7 where **x** is now the superposition of multiple dipoles projecting to the scalp.

$$\mathbf{x} = \sum_{p=1}^{P} \mathbf{H}(\boldsymbol{q}_p)\mathbf{m}(\boldsymbol{q}_p) \tag{7}$$

Equation 8 describes a mathematical model that relates the observed covariance, $\mathbf{C(x)}$, at the electrodes to the covariance, $\mathbf{C(q}_p\mathbf{)}$, at each location within the head model, and to the head model transfer matrix.

$$\mathbf{C(x)} = \sum_{p=1}^{P} \mathbf{H}(q_p)\mathbf{C}(q_p)\mathbf{H}^T(q_p) \tag{8}$$

The sum of x, y, and, z variances for a dipole moment of a location, q_p, inside the model head, is defined in Equation 9,

$$VAR\{q_p\} = tr\{\mathbf{C}(q_p)\} \tag{9}$$

where $VAR\{q_p\}$ denotes the total variance at location q_p and $tr\{\mathbf{C}(q_p)\}$ is the trace of the covariance matrix at location q_p.

To isolate $\mathbf{C}(q_p)$ we exploit the relationship between the covariance matrix $\mathbf{C}(\mathbf{x})$ and the transfer matrix $\mathbf{H}(q_p)$ for each location q_p to solve the inverse problem illustrated in Equation 12. To do so, Equations 10 and 11 are utilized where $\overline{m}(q_p)$ is the expected value of the moment at a given location q_p and E is the expectation operator.

$$\overline{m}(q_p) = E\{m(q_p)\} \tag{10}$$

$$\mathbf{C}(q_p) = E\{[\mathbf{m}(q_p) - \overline{\mathbf{m}}(q_p)][\mathbf{m}(q_p) - \overline{\mathbf{m}}(q_p)]^T\} \tag{11}$$

The solution to the inverse problem (Equation 12) requires a K x 3 matrix $\mathbf{V}$ that defines a pass-band and stop-band based on $\mathbf{C}(\mathbf{x})$ for the head model characterized by $\mathbf{H}$.

$$\mathbf{m}(q_p) = \mathbf{V}^T\mathbf{x} \tag{12}$$

The solution for **V** is provided as Equation 13. A derivation for this closed-form solution is given by (Van Veen et al., 1997).

$$\mathbf{V}(q_0) = [\mathbf{H}^T(q_p)\mathbf{C}^{-1}(\mathbf{x})\mathbf{H}(q_p)]^{-1}\mathbf{H}^T(q_p)\mathbf{C}^{-1}(\mathbf{x}) \quad (13)$$

Substituting Equations 11 and 12 into 9 yields Equation 14,

$$VAR\{q_p\} = tr\{[\mathbf{H}^T(q_p)\mathbf{C}^{-1}(\mathbf{x})\mathbf{H}(q_p)]^{-1}\} \quad (14)$$

the projection of scalp variance to volume domain variance for a specific location q_p.

The volumetric spectrum comprised of the variances at each location inside the head model for a given $\mathbf{C}^{-1}(\mathbf{x})$ is given as Equation 15,

$$r = [VAR\{q_1\}, VAR\{q_2\}, ..., VAR\{q_P\}] \quad (15)$$

where each voxel in the head model is specified as $q_1, q_2, ..., q_P$.

Standard use of the LCMV Beamformer to allocate variance using Equation 14 suffers from a slight bias of variance. Because the spatial distribution of electrodes is not uniform (there are more electrodes on the top part of the hemisphere than on the bottom) this bias is mostly towards the top of the head model. Electrode non-uniformity might also contribute to left/right or anterior/posterior offsets in the resulting volumetric spectrum of Equation 15. This bias is typically compensated for by an independent baseline measure of brain activity (Van Veen et al., 1997).

Our proposed approach, however, compensates for this bias without requiring a baseline estimate from the scalp-EEG data. The volumetric spectrum relating to the source is normalized using the volumetric spectrum of a known white-noise input that is

uncorrelated on all sensors and is uncorrelated with the data itself. Details of this are provided in the next section. The complete bias-compensated relation is given as Equation 16, whereby the covariance matrix of the known uncorrelated white noise input providing bias compensation is denoted as **Q.** Unity is subtracted from the bias-corrected volumetric spectrum to provide for a zero-valued volumetric spectrum when no location is implicated in the data. Thus, the resulting spectrum is perfectly flat and exactly zero when the time-varying data relating to the numerator of Equation 16 is uncorrelated on all channels (within numerical error of machine floating point representation).

$$VAR\{q_p\} = \frac{tr\{[\mathbf{H}^T(q_p)\mathbf{C}^{-1}(\mathbf{x})\mathbf{H}(q_p)]^{-1}\}}{tr\{[\mathbf{H}^T(q_p)\mathbf{Q}^{-1}\mathbf{H}(q_p)]^{-1}\}} - \mathbf{1} \tag{16}$$

MATHEMATICS OF THE VOLUME ESTIMATE

To determine the volume projections of ICA-derived topographies, we exploit the special case where the EEG data used in conjunction with the LCMV Beamformer contain a single source. This is accomplished by creating idealized Beamformer input data using a normalized version of each ICA-derived topography. This idealized input is created using a synthetic signal corresponding to the topography and known additive uncorrelated noise. Embedded in this idealized input, the topography is projected into the volume domain using the LCMV Beamformer. Thus, the volumetric spectrum representing the topography is generated. The location of the center of mass is found as the peak of the volumetric spectrum and the modular source volume is estimated by appropriately thresholding the volumetric spectrum using an estimate of the volume domain noise-level.

Idealized EEG Data

Given a single source topography $\mathbf{A}_j$ (denoting a row of **A**), a time-domain construct of $\mathbf{A}_j$ that spans the space of electrodes is required to create the beamform input. Idealized data $\tilde{\mathbf{x}}(t)$ are created with known second order stationary statistics using Equation 17,

$$\tilde{\mathbf{x}}(t) = A_j^{\mathrm{T}}\mathbf{G}(t) + \mathbf{N}(t) \tag{17}$$

where $\mathbf{G}(t)$ is a Gaussian process of dimension 1 x M and $\mathbf{N}(t)$ is a white noise process of dimension K x M with exactly zero correlation among the electrodes. The number of time-domain samples is given by M (40,000 samples in our implementation). The Gaussian sequence $\mathbf{G}(t)$ is zero-mean and has unit standard deviation σ_G on each electrode. The noise process $\mathbf{N}(t)$ is zero-mean and is scaled such that it has a standard deviation, $\sigma_N = 0.0001\sigma_G$. This ratio provides separation of the noise used to estimate bias and the projected topography. Numerically, it allows the low power, uncorrelated additive noise $\mathbf{N}(t)$ to be precisely separated from the $A_j^{\mathrm{T}}\mathbf{G}(t)$ term via Equation 16.

This method of calculating idealized data is used for 2 reasons. First, itprovides for a means to compensate for Beamformer bias. Second, it guarantees that the $\mathbf{c}(\mathbf{x})$ calculated in Equation 8 for volume estimation is full-rank, has a guaranteed inverse. Calculation of $\mathbf{c}(\mathbf{x})$ as $[\mathbf{A}_j\mathbf{A}_j^{\mathrm{T}}]$ does not guarantee that $\mathbf{c}(\mathbf{x})$ has an inverse. This scheme to provide assurance that an inverse is available is not unlike Tikhonov regularization (Tikhonov, 1963) for ill-posed problems.

Prior to creating idealized data, the topography $\mathbf{A}_j$ is mean-subtracted (we assume the EEG data were average referenced) and normalized using Equation 18 so that the magnitude of coefficients in the volumetric spectrum calculated via the LCMV Beamformer reflect the relative weights defining the topography in Euclidian space. Each $\mathbf{A}_{j1}$ to $\mathbf{A}_{jK}$ in Equation 18 corresponds to the weights at each of K electrodes. Although mean subtraction of topographies is not an ideal method to average reference for Beamforming (Van Veen et al. 1997) and does result in a small error, we do so here

because it is a common method used to average reference EEG data (Yao D, 2001) and it does not adversely affect our results.

$$\mathbf{A}_j = \frac{\mathbf{A}_j}{\sqrt{\mathbf{A}_{j1}^{\ 2} + \mathbf{A}_{j2}^{\ 2} + \ldots + \mathbf{A}_{jK}^{\ 2}}} \tag{18}$$

The additive white Gaussian noise provides for full-rank, second order, idealized, time-domain data $\tilde{\mathbf{x}}(t)$ and for bias removal of the volumetric spectrum. The matrix **Q** of Equation 16 is calculated as the covariance of the additive noise component **N(*t*)**. To ensure that each channel of additive noise **N(*t*)** and the projected waveform **G(*t*)** have exactly zero correlation, before use in Equation 17, the two are combined in a single matrix, sphered to remove partial correlation and then re-separated. For example, using Equation 19, a matrix **y** is created as the concatenation of **G(*t*)** and **N(*t*)** where $\hat{\mathbf{y}}$ is the sphered result (Hyvärinen, Karhunen, and Oja, 2001). After sphering, all columns of **y** have exactly zero correlation.

$$\hat{\mathbf{y}} = [\mathbf{C}^{-\frac{1}{2}}(\mathbf{y})]\mathbf{y} \tag{19}$$

Noise Estimate

The general ICA model of Equation 1 does not explicitly model noise. Here, random noise is modelled as being present in the ICA-derived topography. This is reflected in our proposed method as in Equation 20 where the ICA-derived topography is separated into a noise-free topography and noise topography, $\mathbf{A}_j^{\mathbf{s}}$ and $\mathbf{A}_j^{\mathbf{n}}$, respectively.

$$\mathbf{A}_j = \mathbf{A}_j^{\mathbf{s}} + \mathbf{A}_j^{\mathbf{n}} \tag{20}$$

This topographical noise is also represented in the volume. The volume-projected topography is represented by the coefficients of the volumetric spectrum as in Equation

21 where the source volume and the volume domain noise are expressed as $\mathbf{r}^s$ and $\mathbf{r}^n$, respectively. In addition to accounting for noise in a topography, this volume distinction of signal and noise also allows for accounting of inaccuracies resulting from projecting an average referenced topography into a model head of fixed grid sizes and locations.

$$\mathbf{r} = \mathbf{r}^s + \mathbf{r}^n \tag{21}$$

The large number of voxels (5439 in this implementation) in the volume space provides for a statistical noise-level estimate. To make this estimate, the coefficients of the volumetric spectrum are considered as observations of a single population. The statistics contained in the population relate to both the volume domain noise and the projected source volume. It is assumed the source volume is represented by relatively few coefficients, whereas the noise is present in most of the coefficients. In this way, the statistics of the spectrum largely represent noise. Formally, the variance relating to the source volume $\tilde{r}$ is different from the noise and is contained in L voxels where L is much, much less than the total number of voxels, P in the head model.

To demonstrate the principle of thresholding without clouding the methods with discussion of robust statistical estimators, it is assumed the contribution of the coefficients relating to the brain volumes on the statistics of the volumetric spectrum is minimal. Thus, in this demonstration, generic calculation of mean $\bar{\mathbf{r}}$ and standard deviation σ_r corresponding to a specified topography, $\mathbf{A}_j$ are calculated.

By identifying the statistics of the noise, those voxels that relate to the source volume are also identified. The threshold T (Equation 22) at which the source variance intersects the noise variance is calculated as R standard deviations from the mean of the volumetric spectrum as in Equation 22. Those voxels with coefficients greater than the threshold T relate to the brain volume estimate.

$$T = R\sigma_r + \bar{\mathbf{r}} \tag{22}$$

III. METHODS

A mathematical head model was constructed to both create synthetic EEG data and to evaluate the effectiveness of the proposed method. Matlab 7 (Mathworks Inc.) and EEGLab 4.515 (Makeig et al., 1997; Delorme and Makeig, 2004) were used to do all modelling, calculations, and plotting. BERG head model parameters (Berg and Scherg, 1994) and artwork for the model were derived from the BrainStorm software package (Baillet et al., 2000) for Matlab. The BERG parameters used in the three-layer head model are listed in Table 1. The head model was calibrated with a volumetric grid/voxel resolution of 0.5 cm^3 and implemented using the equations provided in the previous sections. There were a total of 5439 voxels used to define the volume of the head model in this study. Localization was not constrained from occurring in the ventricles or other physiologically improbable areas, following the philosophy of minimal assumptions in the localization process.

	Center	**Radii**	**sigma**	**Mu**	**lamda**
Layer1	0.0083	0.0899	0.3300	0.5732	0.5195
Layer2	0.0006	0.0949	0.0042	0.0394	0.0275
Layer3	0.0489	0.1025	0.3300	0.9464	0.1441

Table 1. Parameters used for construction of the head model calculated using the BrainStorm software package. 'Center' is the center of the head. 'Radii' is the radii of the sphere. 'Sigma' is conductivity. 'Mu' defines the BERG eccentricity factors. 'Lamda' defines the BERG magnitude factors.

CREATION OF SIMULATED EEG

We defined three physical source characteristic scenarios by strategically assigning source properties. The first scenario's single-voxel source is placed in the central region of the right hemisphere, distal from all other sources, providing the simplest case for source separation and volume estimation. This is labelled as source (1). This thus

created the case where topographical comparisons of source may not provide a good measure of the difference between individual sources. The second scenario examined difficult source separation with a high likelihood of volume overlap when source separation is imperfect. This entailed a group of single-voxel sources, proximally placed in the right temporal pole. These are labelled as sources (2) through (4). Each source was assigned the same orientation, differing from that of source (1). The third scenario examined the volume estimation for a trapezoidal multi-voxel source. This 26-voxel source was placed in the left orbito-frontal region, distally from other sources. All voxels comprising this source were assigned the same orientation, differing from all other sources. Figure 2 illustrates the source locations and orientations on a head model used

The topographical projections of each model source were calculated to create simulated scalp-EEG data and to later compare ICA-derived topographies of each source to their original counterparts. These were calculated by projecting each modelled volume source onto a model scalp, as described in the forward solution of Equation 6, for a given dipole orientation.

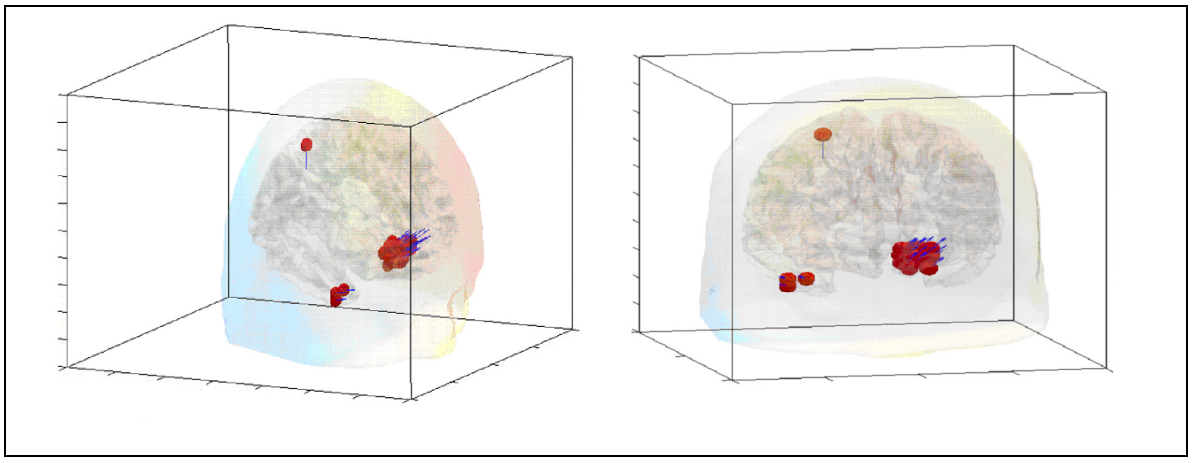

Figure 2. Two views of the head model with simulated sources placed. Arrows at each source voxel indicate positive source dipole direction. Three functionally distinct, single-voxel sources are proximally spaced in the right anterior temporal pole. A single 26-voxel source is modelled in the left orbital frontal pole. A single-voxel source located in the right parietal region models a distally spaced source. The scalp is shown with superimposed projected field polarities originating from the model sources. From the

location and orientation of the placed sources in this depiction and the time-domain activities of each model source the synthetic EEG mixture was created.

The time-domain activities of simulated EEG data were created by combining the dipole projected topographies with synthetic waveforms and additive uncorrelated sensor noise. Distinct waveforms were assigned to each source for easy visual identification in plots. Sources (1) through (5) were assigned the waveform activities of a ramp, a sinusoid, a random uniformly distributed waveform, a square wave, and a waveform with a random super-Gaussian distribution, respectively. All neural sources were set to have zero mean and unit standard deviation in each trial. Each source waveform was projected to the scalp-domain using the topographies calculated via model dipoles in the previous step. The topographically projected activities were summed to create 124 channels, 875 samples/trial, and 29 trials of simulated EEG data with source activities repeating in every trial. Random, uncorrelated sensor noise was added to each trial of simulated EEG after mixing simulated neural sources. Sensor noise amplitude was set to 28 dB below the average source volume levels.

Electrode artefacts were added to the simulated EEG to investigate possible characteristic volumetric spectra that might differ from simulated neural sources. Electrode artefacts having an amplitude approximately 60 dB greater than the simulated neural sources were modelled at one electrode at a location near the apex of the scalp. The artefact was a spike event occurring in every trial at a random latency. A block diagram illustrating the construction of the simulation data is given in Figure 3.

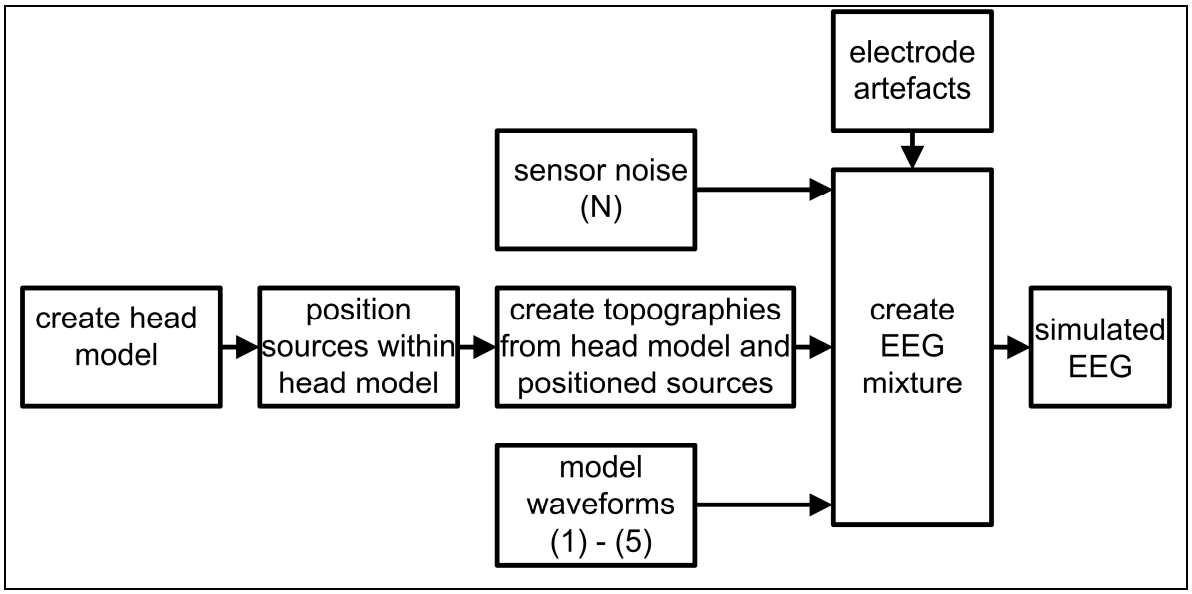

Figure 3. Illustration of the construction of simulated data.

EVALUATION OF THE PROPOSED METHOD

Waveforms and Topographies

Multiple waveforms and topographies were calculated from the EEG mixture using ICA. The extended (Lee et al., 1999) runica algorithm (Makeig et al., 1997) available in the EEGLab 4.515 analysis package (Delorme and Makeig, 2004) was used to separate the simulated EEG into parts. An initial PCA step to reduce the rank of the data from 124 to 8 was used to facilitate convergence of the runica algorithm. This intentional over-estimate of the number of sources comprising the data simulated real analysis situations when the actual number of sources is not known. (It has been recommended to maximally separate the data using all available degrees of freedom (Makeig et al., 1997) thus it is appropriate to simulate an over-estimate of rank.) Both the original model source waveforms and those waveforms recovered using the proposed method were mean-subtracted and normalized to unit standard deviation. As well, the original and recovered topographies were mean subtracted and normalized to have unit norm. The waveforms and topographies were plotted for visual comparison.

Source Location Estimates

In order to calculate differences between the actual model and estimated centers of mass for each of the single-voxel sources (1) through (4), from the synthetic EEG, the difference between the x, y, z coordinates as in Equation 23 was calculated. The actual model centers of mass and estimated centers of mass are x_0, y_0, z_0 and x_1, y_1, z_1, respectively.

$$\textit{error} = \sqrt{(x_0 - x_1)^2 + (y_0 - y_1)^2 + (z_0 - z_1)^2} \tag{23}$$

The error associated with the center of mass of source 5 (the volume source comprised of 26 voxels) was not calculated because its center of mass is not on the head model grid. As designed, the volume source was originally comprised of 27 voxels arranged as 3x3x3, placed on the edge of the white-matter frame. Modular volumes represent active grey matter while the white matter framework provides a physical frame of reference so that the resolved volumes can be named anatomically. One of the voxels however was truncated from the model volume during processing for being too close to the edge of the head model, thus leaving only 26 voxels for evaluation. Fortunately, this does provide the model with the case when the center of mass of a source is not precisely on the grid.

Source center of mass estimates were plotted on the head models of Figure 7. They are indicated as the peaks of the volumetric spectra. Associated errors were tabulated.

Modular Source Volume Estimates

Modular Source volumes were estimated using the thresholding method described in the previous section. We assumed a threshold of 5 standard deviations above the mean (STDM) as an appropriate confidence interval for making source volume plots base on previous experimentation with different sources during the development of the volume estimation algorithm. To relate the thresholded source volume plots to a continuous

measure of volume estimate, the modular volumes of each source with respect to multiple threshold levels from 3 to 6 STDM were calculated (Figure 10). The source volume estimate error was calculated as the difference between the number of voxels comprising the model versus the number of voxels comprising the estimated source as in Equation 24,

$$error = | v_1 - v_0 | \tag{24}$$

where volumes $\boldsymbol{v_0}$ and $\boldsymbol{v_1}$ are the actual volume and the estimated volume, respectively. The original and recovered source volumes with associated error are listed in Table 2.

Overlap

Each raw volumetric spectrum was mean-subtracted and normalized for unit norm in Euclidian space according to Equation 25,

$$\hat{\mathbf{r}} = \frac{\mathbf{r} - \bar{\mathbf{r}}}{\sqrt{(\mathbf{r}_1 - \bar{\mathbf{r}})^2 + (\mathbf{r}_2 - \bar{\mathbf{r}})^2 + .. + (\mathbf{r}_P - \bar{\mathbf{r}})^2}} \tag{25}$$

where $\bar{\mathbf{r}}$ is the mean of all $\mathbf{r}_i$ elements of $\mathbf{r}$. Each $\mathbf{r}$ has 1 x $\boldsymbol{P}$ elements. The resulting zero-mean normalized volumetric spectrum is designated as $\hat{\mathbf{r}}$.

The overlap was calculated between pairs of the zero-mean, normalized volumetric spectra pertaining to the recovered topographies as in Equation 26,

$$S = | \hat{\mathbf{r}}_i \hat{\mathbf{r}}_j^{\,T} | \tag{26}$$

where $\mathbf{r}_i$ and $\mathbf{r}_j$ are the zero mean, normalized volumetric spectra compared. This volume overlap, $\boldsymbol{S}$ is a measure of the similarity between the volumetric spectra. Zero overlap of two vectors $\boldsymbol{u}$ and $\boldsymbol{v}$ is evidenced by a value of 0. A value of 1 indicates maximum volume overlap of $\boldsymbol{u}$ and $\boldsymbol{v}$. The results were tabulated for later inspection.

Volumetric and Topographical Error

To check the correctness of the volume projection component of the algorithm highlighted in Figure 1, the pair-wise overlap of the raw volumetric spectra for each of the original model topographies used to create the simulated EEG were tabulated and compared. This was done in a similar manner to that of the recovered volumetric spectra, using Equations 25 and 26. This also created an instance of idealized volumetric spectra (with errors only relating to mean subtraction of the topographies) by which the recovered volumetric spectra of the ICA-derived topographies were compared, also using Equations 25 and 26. Similarly, a comparison was made between the original model topographies and the recovered topographies.

Peaks of the Volumetric Spectrum

Spectral peak characteristics of all ICA-derived components were tabulated and compared to identify a possible volume-domain characteristic that can be used to distinguish between EEG components relating to neural sources, components relating to electrode artefact, and components resulting from ICA rank estimate error.

IV. RESULTS

The resulting decomposition contains 5 components pertaining to simulated neural sources, 1 component relating to electrode artefact, and 2 components resulting from the intentional rank estimation error. Sources resulting from the rank estimate error are herein referred to as ‘rank error’ components.

WAVEFORMS AND TOPOGRAPHIES

The topographies and waveforms of EEG components (1) through (5) recovered using ICA are plotted in Figure 4 with the model topographies and waveforms used to construct the stimulation data. Plots show the trial-averaged waveform. Visual comparison of the recovered sources (1) to (5) reveals that unmixing and trial averaging produces little distortion. Proximal temporal source waveforms for (2), (3), and (4) demonstrate separation of activities with most visible distortion for (4). The distal source waveform for (1) and the multi-voxel source waveform for (5) also have little distortion. There is no apparent distortion when comparing topographies.

The electrode artefact (6), and associated waveform extracted from the EEG, is given in Figure 5. Plots show the trial-averaged waveform. The position of the focal point in the topography of (6) corresponds to the single electrode at which artefacts were simulated. The corresponding waveform reflects the average spike activity temporally distributed over the entire epoch of the averaged data.

Component topographies and waveforms related to rank estimate error (7) and (8) are given in Figure 6. Artefacts (7) and (8), resulting from the attempt to separate the simulated EEG into more parts than actually comprise the data, have topographies that resemble combinations of simulated sources. The waveforms corresponding to these components do not clearly represent any one source. Plots show the trial-averaged waveform.

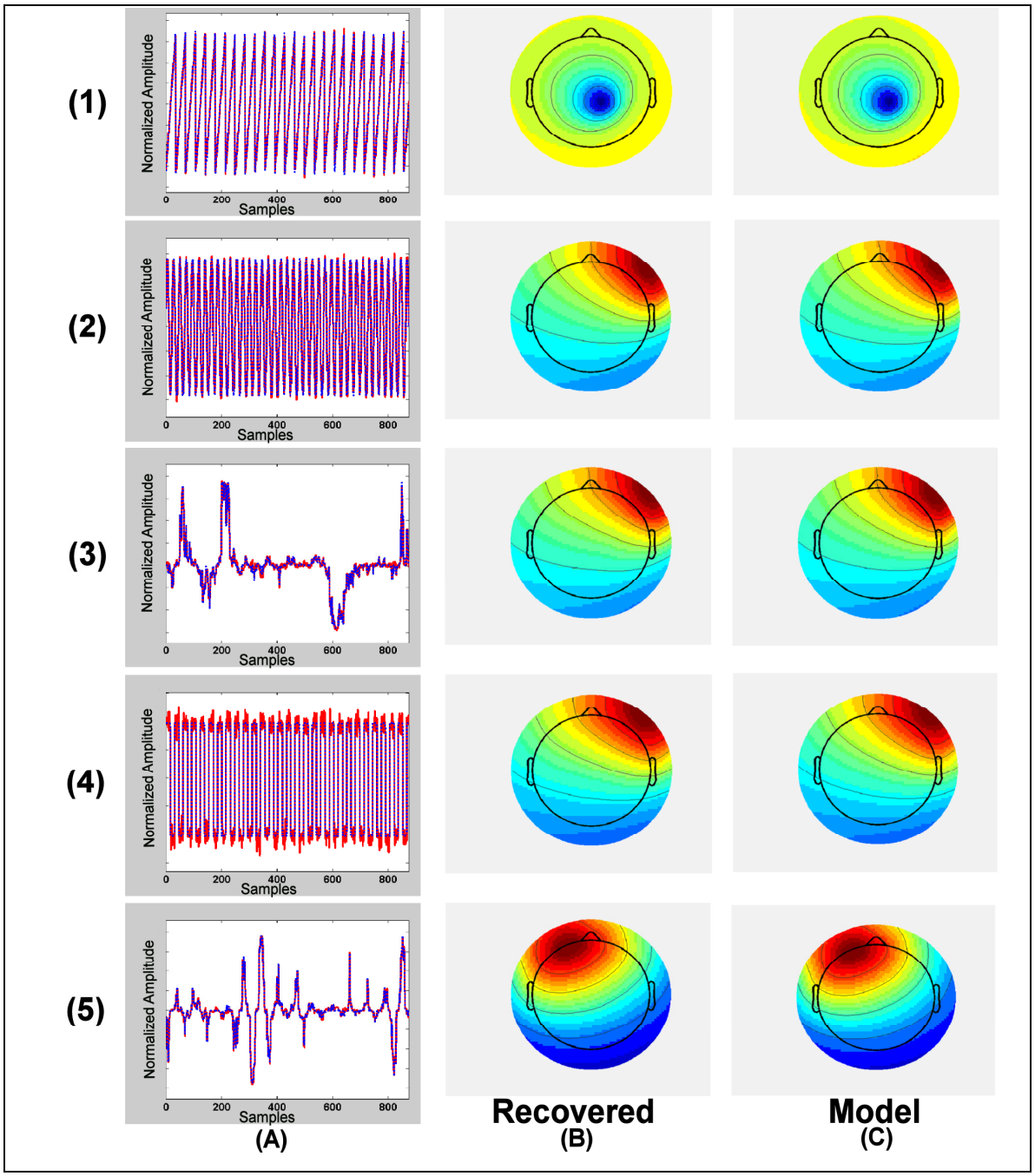

Figure 4. Original and recovered topographies and sources (1) to (5) are presented. Original model waveforms (blue) and recovered waveforms (red) associated with each topography are given in column (A). In cases where only a single waveform appears to exist, the original and recovered waveforms are overlapped. Recovered topographies are given in column (B) while original model topographies are given in column (C). Positive (red,+) and negative (blue,-) polarities are indicated on the topographies.

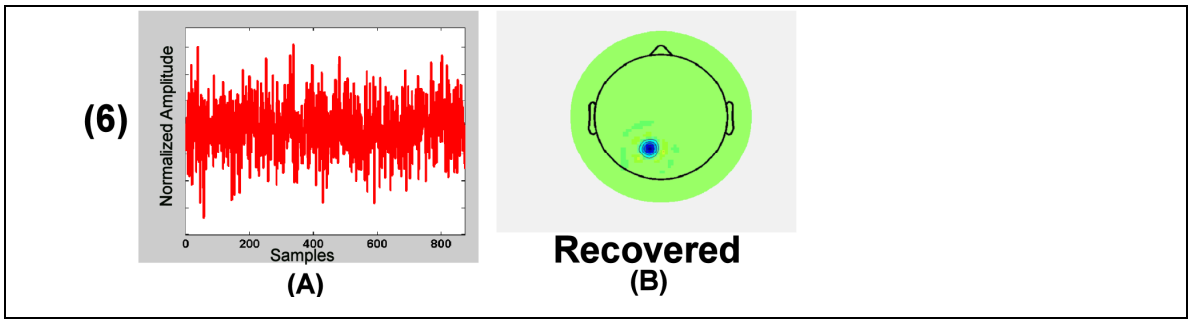

Figure 5. Extracted electrode artefact component (6) added to the EEG. The recovered waveform is given in column (A). The recovered topography is given in column (B). Negative (blue) and neutral (green) polarities are indicated on the topographies.

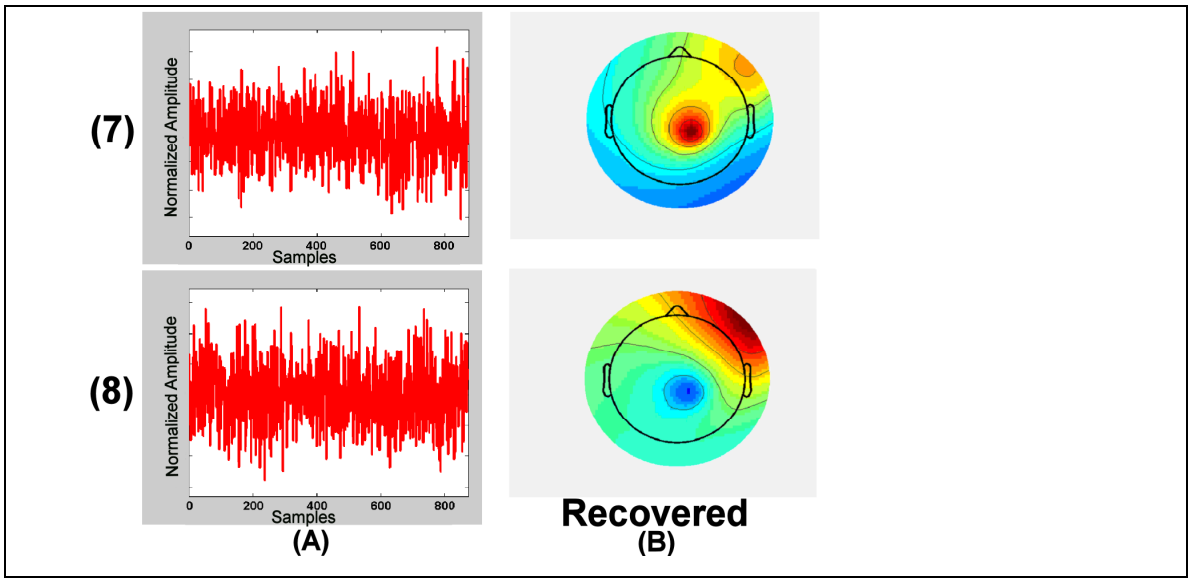

Figure 6. Extracted ICA rank error components (7) and (8). Recovered topographies are given in column (B). Positive (red) and negative (blue) polarities are indicated on the topographies. Recovered waveforms are given in column (A).

SOURCE VOLUME AND LOCATION ESTIMATES

There was no volume estimate error for the distally spaced source. For proximally spaced single-voxel sources and for the multi-voxel source, only small volume estimate

errors were present. There were no center of mass errors for the sources examined. The results of the source location and volume estimate for a 5 STDM threshold are summarized in Table 3 and illustrated in Figures 7, 8, and 9. The volumetric spectrum is given in column (A) of each figure. The locations and volumes with respect to the model head are given in columns (B) and (C) of each figure. Source centers are indicated by the peak of the volumetric spectrum, as shown by the single red sphere in the head model plots. Where applicable, column (D) gives a magnified depiction of the estimated volumes.

A volume was estimated for the electrode artefact, component (6). This volume yields a peculiar spectral fall-off compared to the simulated neural sources making it distinct from the non-artefact sources. It has a characteristically blunt spectral peak and gradual fall-off from the peak. The volumetric spectra of the rank error components (7) and (8) are also blunt like the electrode artefact (indicated by the spectrum of Figure 9a), however all coefficients were less than the threshold of 5 STDM.

	Source Volume (voxels)	**Recovered Estimate of Volume (voxels)**	**Volume Error**	**Location Error**
(1) Distally spaced	1	1	0	0
(2) Proximally spaced	1	2	1	0
(3) Proximally spaced	1	5	4	0
(4) Proximally spaced	1	8	7	0
(5) Multi-voxel	26	18	8	--

Table 2. Source location and volume estimates at a 5 STDM threshold for each type of simulated neural source. Units are given as number of voxels. (The double dash indicates that a comparison was not made.)

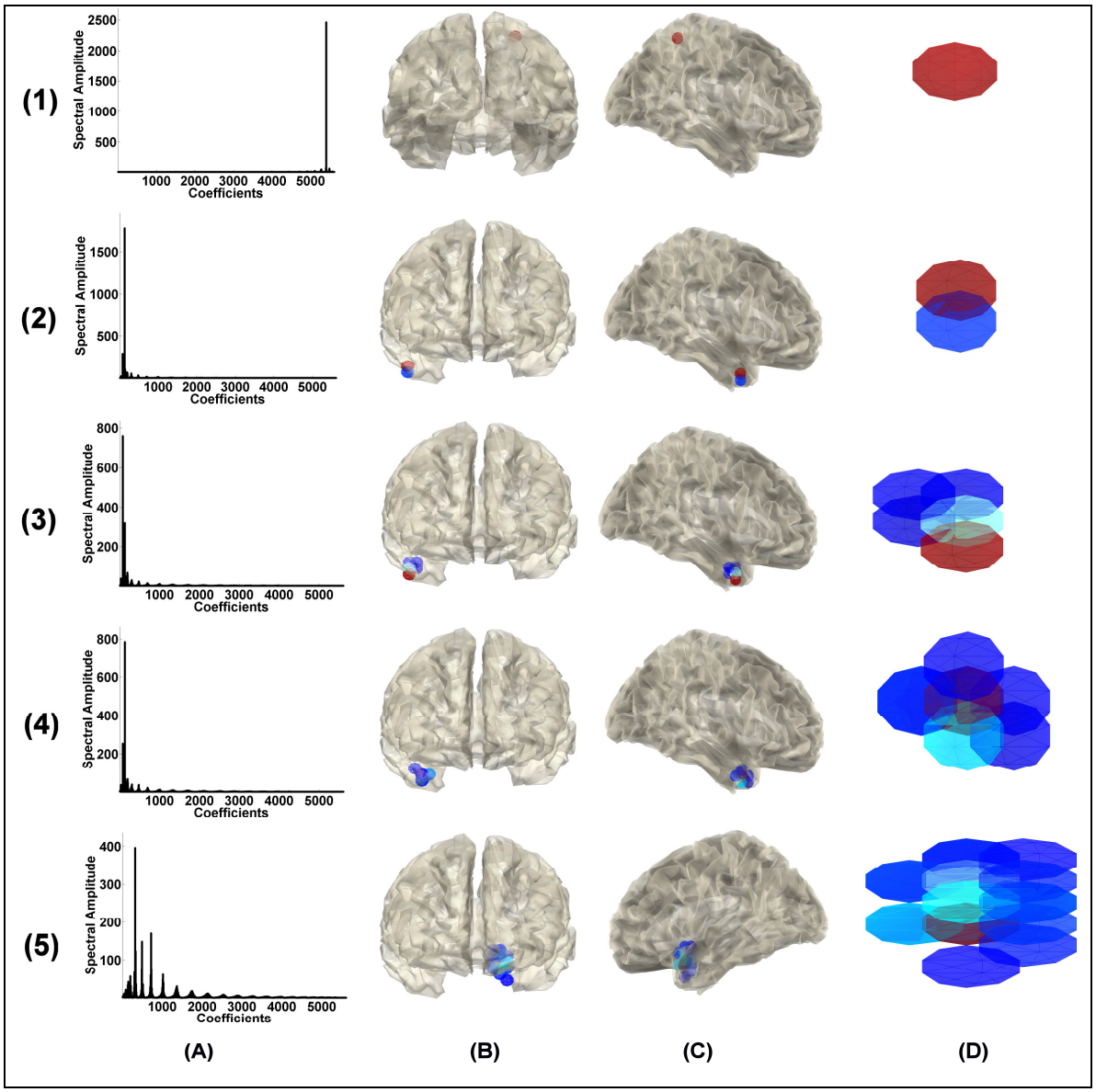

Figure 7. Localization and volume estimate results for simulated neural sources (1) to (5). (A) volumetric spectra. On the vertical axis, spectral amplitude indicates the values of the coefficients of the volumetric spectrum. Each coefficient defining the three-dimensional volume is plotted as a vector of values on the horizontal axis; (B,C) estimated volumes in relation to the head model; (D) magnified side-view of volume estimates. Fall-off from the spectral peak is reflected in the color of the spheres, ranging from dark red (corresponding to the peak of the volumetric spectrum) to dark blue (corresponding to the minimum of the volumetric spectrum).

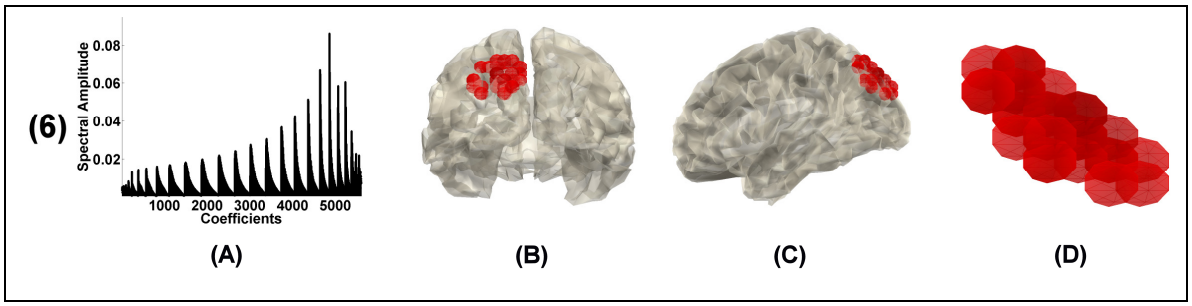

Figure 8. Localization and volume estimate results for the electrode artefact, component (6). (A) volumetric spectra. On the vertical axis, spectral amplitude indicates the values of the coefficients of the volumetric spectrum. Each coefficient defining the three-dimensional volume is plotted as a vector of values on the horizontal axis; (B,C) estimated volumes in relation to the head model; (D) magnified volume estimates. Fall-off of coefficient values from the PSV is reflected in the color of the spheres, ranging from dark red (corresponding to the peak of the volumetric spectrum) to dark blue (corresponding to the minimum of the volumetric spectrum). In this case, only red spheres are present as the spectrum does not have a sharp fall-off, indicating that there is very little difference between signal as a resolvable modular volume and the noise in the volumetric spectrum.

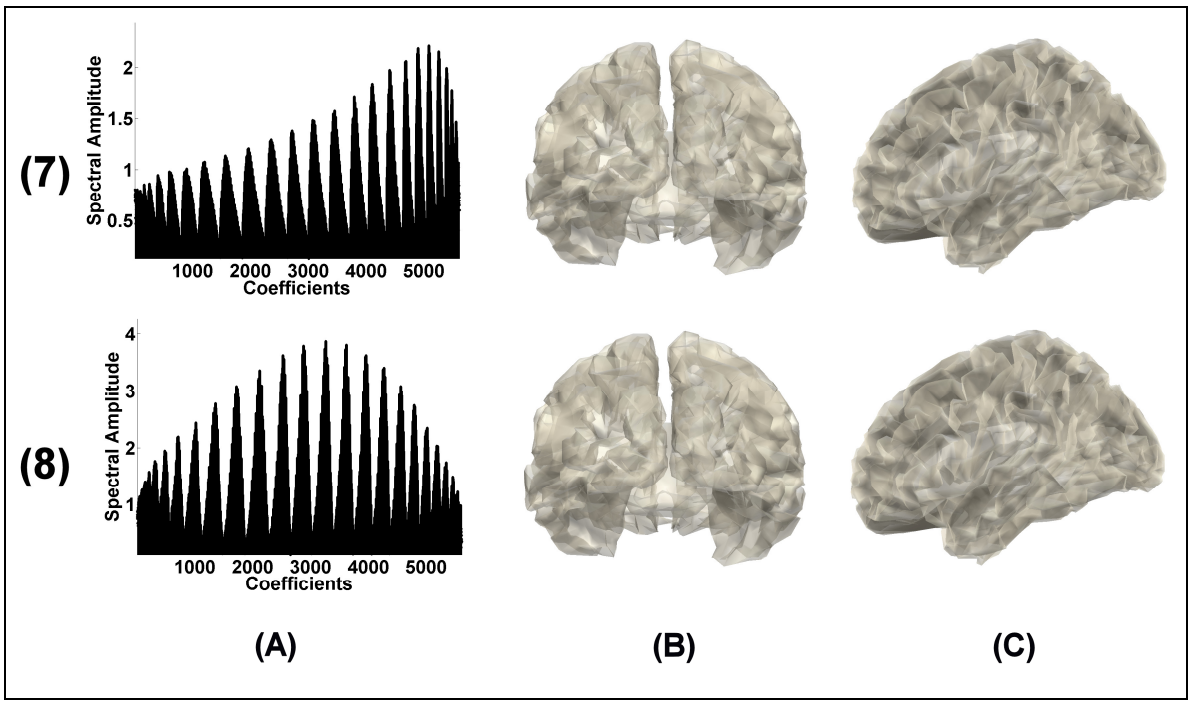

Figure 9. Localization and volume estimate results for rank-error components (7) and (8). (A) volumetric spectra. On the vertical axis, spectral amplitude indicates the values of the coefficients of the volumetric spectrum. Each coefficient defining the three-dimensional volume is plotted as a vector of values on the horizontal axis; (B,C) estimated volumes in relation to the head model. Absence of spheres indicates all spectrum coefficients were below the 5 STDM threshold.

The volume estimates at thresholds increasing from 3 to 6 STDM are plotted in Figure 10. This volume-STDM plot shows that for different STDM thresholds there is an adjustment in the modular volumes estimated. There is a distinct difference between the curves associated with the rank error components (7) and (8), and the simulated neural components (1) through (5). The curve relating to the electrode artefact (6) has characteristics of both the neural components and the rank error components, but is different from neural source components in that the volume estimates are relatively stable over the 3 to 6 STDM threshold interval examined.

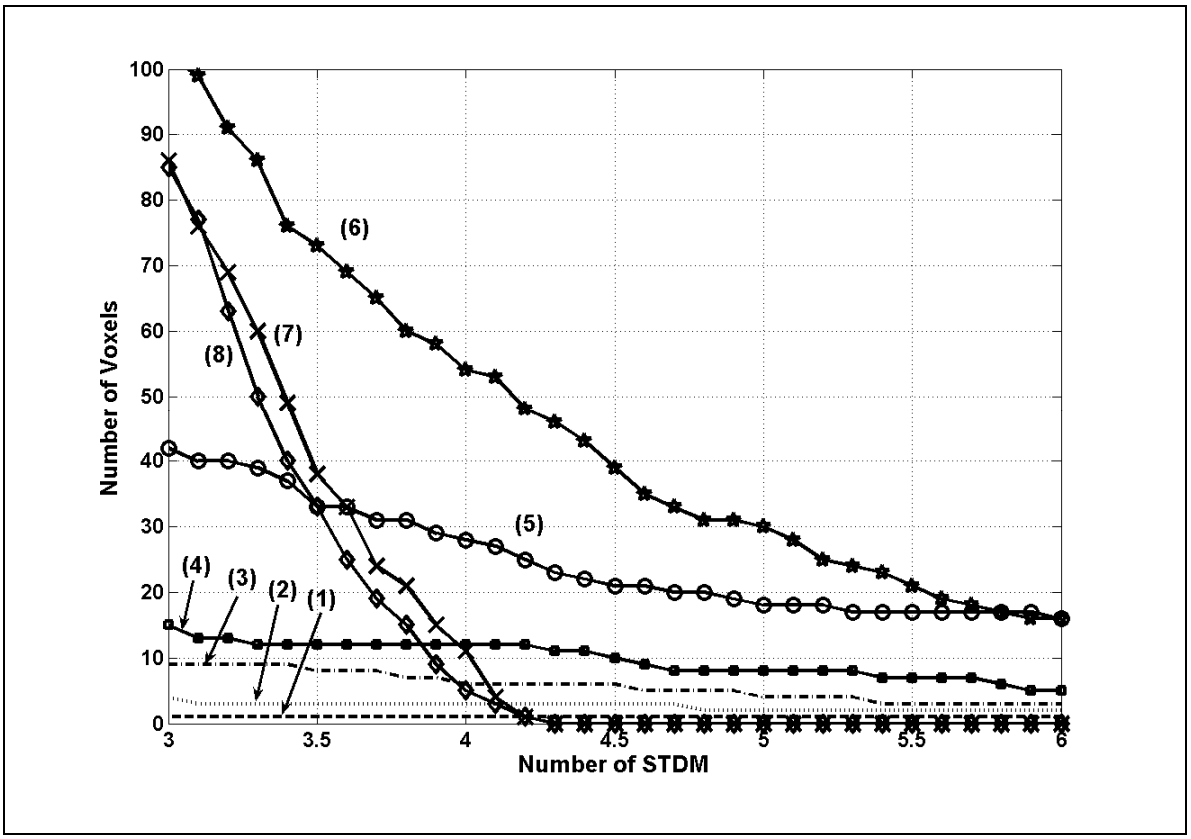

Figure 10. Estimated source volumes for 3 STDM to 6 STDM. The recovered EEG components (1) through (8) are indicated on the plot. Components (1) – (5) are simulated neural sources, (6) is an electrode artefact, and (7) and (8) are rank-error components.

OVERLAP

Overlap of the volumetric spectra pertaining to the spectra estimated from the ICA-derived topographies and the spectra pertaining to the actual model topographies are given in Table 3. With regards to the recovered spectra, there is a notable overlap between sources (2) and (3), and between the electrode artefact (6), and the rank error artefacts (7) and (8). However, there is approximately zero overlap between volumes for the original model spectra. An overlap of 0.540 was calculated for the pair-wise comparison of recovered sources (2) - (3). The pair-wise comparisons for recovered sources (2) - (4), and (3) - (4) gave an overlap of 0.0663 and 0.121, respectively. For the distally spaced sources (1) - (5), the maximum overlaps were 0.00722 and 0.00722,

respectively (the overlap with each other). The overlaps of the volumetric spectra calculated from the model topographies were all less than 0.00346.

	(2)	**(3)**	**(4)**	**(5)**	**(6)**	**(7)**	**(8)**
(1)	[0.00143] {0.000178}	[0.00242] {0.000178}	[0.00316] {0.000178}	[0.00722] {0.00346}	[0.0148]	[0.0757]	[0.00590]
(2)	--	**[0.540]** {0.000141}	[0.0663] {0.000176}	[0.00460] {0.00297}	[0.0322]	[0.00911]	[0.0384]
(3)	--	--	[0.121] {0.000176}	[0.00559] {0.00307}	[0.0548]	[0.0107]	[0.0688]
(4)	--	--	--	[0.00228] {0.00249}	[0.0705]	[0.00427]	[0.0994]
(5)	--	--	--	--	[0.114]	[0.0761]	[0.000614]
(6)	--	--	--	--	--	**[0.361]**	**[0.416]**
(7)	--	--	--	--	--	--	[0.0127]

Table 3. Distance between volumetric spectra calculated for topographies. Distances pertaining to volumetric spectra of recovered topographies are given in [ ], while distances pertaining to the volumetric spectra of model topographies used to create the simulated EEG are given in { }. Maximal difference is indicated by 0, minimal distance is indicated by 1. Values greater than 0.3 have been highlighted to emphasise values of low overlap from high overlap. Numbers across the top of the table in parenthesis indicate component number. (The double dash indicates that the corresponding comparison is in the upper half of the table. e.g, 2 vs. 3 = 3 vs. 2)

VOLUMETRIC AND TOPOGRAPHICAL ERROR

Table 4 compares both actual and estimated topographies and volumetric spectra using the metrics defined by Equations 25 and 26. The greatest difference in volumetric

spectra is with the multi-voxel source (5), followed by the proximally spaced single voxel sources. This is also true for the topographies. There is not however, a consistent trend between topographical error and error of the volumetric spectra. Thus the size of error in one domain can not imply the size of error in the other domain.

	Mod. Vs Rec. (1)	Mod. Vs Rec. (2)	Mod. Vs Rec. (3)	Mod. vs Rec. (4)	Mod. vs Rec. (5)
Topography	0.9999	0.9995	0.9994	0.9996	--
Volume	0.9968	0.9793	0.8990	0.8797	0.8664

Table 4. The similarity between model vs recovered topographies and model vs recovered raw volumetric spectra. Maximum similarity is indicated by 1. Minimum similarity is indicated by 0. Mod. = Model; Rec. = Recovered. Numbers in parenthesis across the top of the table indicate component number. (The double dash indicates a comparison that was not made.)

PEAKS OF THE VOLUMETRIC SPECTRUM

There is large variation in the maxima of the volumetric spectra across recovered components. The peaks are listed in Table 5 for each component of the EEG. The peaks of the recovered neural sources vary between 2,463 and 369.5. The peak for the artefact electrode is 0.08614 and for those components relating to the rank error, the peaks range from 2.212 to 3.868. There is at minimum two orders of magnitude difference between the recovered neural sources and the artefacts. The peaks of the volumetric spectra computed directly from model topographies range from 36,540,000 to 18,950,000. These peaks are extremely large and tend to increase towards infinity (as machine representation) because they indicate a near perfect voxel specificity of the topographies. In examining real data, such large numbers are unlikely to occur as an EEG-derived topography will contain at least some noise and will not necessarily have a volume that is defined and perfectly centered within a single 0.5 cm head model voxel.

	(1)	(2)	(3)	(4)	(5)	(6)	(7)	(8)
Peak Rec.	2463	1777	761.0	786.0	369.5	0.08614	2.212	3.868
Peak Mod.	36540000	19390000	20030000	18950000	--	--	--	--

Table 5. Peaks of the volumetric spectra for each of the model and ICA-derived topographies. Peak Mod. = Peak of the model spectra; Peak Rec. = Peak of the recovered spectra. Numbers in parenthesis across the top of the table indicate component number.

V. DISCUSSION

The primary objective of this paper is to propose and demonstrate a routine to map ICA component topographies to the volume domain without constraining the representation to a single voxel. We have denoted the representation of a scalp-domain topography in the volume-domain as the volumetric spectrum. In addition, we examine the feasibility of using volume-domain mapping of topographies to estimate modular brain source volumes and the volume overlap. In doing so, we found differences in the magnitude of the peaks of the volumetric spectra for three classes of components of the simulated EEG (neural brain source, electrode artefact, and rank error artefact) that might provide a means to differentiate brain and artefact EEG components.

Combining ICA and LCMV Beamform methods to estimate source volumes by the described method provides a novel technical contribution to the field of neuroscience. The LCMV Beamformer alone is only effective at separating EEG for special circumstances. Mathematically, it is limited in flexibility to isolate a large number of sources as the degrees of freedom for source separation in the volume domain are reduced to 1/3 the number of electrodes. It also becomes increasingly difficult to separate sources using the LCMV Beamformer when their relative proximal spacing is reduced (Van Veen et al., 1997). The standard LCMV Beamformer also requires a

baseline EEG estimate to correct for biases in the native volumetric spectrum. ICA in contrast, has some important source separation advantages. In addition to having as many degrees of freedom as there are electrodes, ICA can separate sources that are not well represented in the volume domain, or are proximally spaced inside the head volume. As well, by appropriately combining the LCMV Beamformer and ICA methods, the need for baseline EEG data to compensate for head model bias is avoided.

A further advantage of the proposed method over dipole fitting is demonstrated by the extra information available in the volume domain. Volume domain representation of sources provides for an objective measure of source overlap and an estimate as to the source volume yielded by the ICA unmixing process. In contrast to dipole modelling methods, these volume solutions are not constrained to be a single dipole. This source volume projection relates to the actual volume of the source and provides a measure of error or impreciseness of the source estimation. Estimation error is then evaluated as a meaningful 'blur' of volume representation rather than the conventional 'variance accounted for' by dipole fitting methods. Thus, in real applications, we have both the modular volume-domain specificity defined by volume edge boundaries and a continuous measure of the volume-domain overlap of brain activity components of an ICA decomposition of EEG.

WAVEFORM AND TOPOGRAPHIES

Three classes of EEG components were examined in our simulation. Synthetic EEG was created and subsequently decomposed into eight components. Simulated neural sources, an electrode artefact, and components related to the intentional over-estimation of the number of sources comprising the EEG. The distally spaced source provided an example to show the best possible separation and volume localization result. The proximally spaced single-voxel sources, provided for an evaluation of ICA separability and volume projection blurring for closely spaced statistically independent sources. The multi-voxel source allowed for evaluation of how the signal and noise in the volumetric spectrum

intersect. Those EEG components relating to electrode artefact and rank estimation error artefact allowed us to view how these are represented by the volume-domain projection.

Inspection of simulated neural sources showed that they were recovered by ICA with little distortion overall. The time-domain activities of the active sources were visually compared to those source waveforms recovered using ICA and were found to have only minor distortion. The mathematical comparison of model and recovered topographies in Table 4 demonstrated only very small differences.

The recovery of the waveforms of proximally spaced sources demonstrates that closely spaced statistically independent sources can be separated by ICA in ideal simulation conditions. This is usually a difficult task, where small errors lead to blending of sources such that they can not be individually discerned. We tested to see if proximally spaced sources, having similar topographies, could be discerned as individual volumes. The source waveforms were successfully separated, and the respective topographies were very similar (Figure 7; Table 4), demonstrating separability at 0.5 cm spacing.

The intentional rank estimate error forced the extraction of 2 more components than actually comprise the data. They were found to have topographical characteristics similar to bona fide sources. These were perhaps generated from partial correlations between the multiple simulated sources, source orientations, and noise. However, they were easily distinguished from simulated neural sources by their low volumetric spectrum peaks.

SOURCE LOCATION AND VOLUME ESTIMATES

The proposed method accurately located both proximally spaced, and distally spaced simulated sources. The center of mass error was equal to 0 cm on a grid spacing of 0.5 cm for each of the simulated neural sources examined. The recovery of the centers of mass of proximally spaced sources demonstrates that closely spaced uncorrelated sources can be separated by ICA and localized using our Beamforming methodology.

The plots of the volume - STDM relationship of each component in Figure 10 suggest that the next addition to this algorithm should be an 'optimal' thresholding method. Thus, the volume estimation 'errors' of Table 2 and Figure 7 are not errors per se- rather, they reflect the statistical threshold level selected. Implementation of such an optimal threshold method is left for future work.

OVERLAP

There is overlap of the volumetric spectra for the recovered ICA-derived components but not for the original model source volumetric spectra. This pertains mainly to the recovered volumetric spectra of the proximally placed sources. The overlaps of distally spaced sources are an order of magnitude smaller. Since the volumetric spectra of both sets of topographies are calculated by the same method, this observation suggests that the overlap results from inaccuracies in the ICA-derived topographies. This provides some validation of the assumption that a given topography calculated via ICA might be appropriately modelled with a noise-free term $\mathbf{A}_j^{\mathbf{s}}$ and a noise term $\mathbf{A}_j^{\mathbf{n}}$.

VOLUMETRIC AND TOPOGRAPHICAL ERROR

The comparisons given in Table 4 between the volumetric spectra of the original model sources and the recovered components revealed larger differences than comparisons of the corresponding topographies themselves. This is an advantageous (and expected) result as it demonstrates that the volume domain provides a better comparison of anatomical characteristics of sources. This finding fits with our suggestion that ICA components are well modelled as the sum of a noise-free neural source topography and noise source topography, or the sum of a noise-free neural source volumetric spectrum and a noise volumetric spectrum.

PEAKS OF THE VOLUMETRIC SPECTRUM

A low volumetric spectrum maximum may indicate that an EEG component does not relate to a focal, modular volume. Van Veen et al. (1997) compared the volumetric spectra and source separation properties of the LCMV Beamformer for model brain sources of varying separability characteristics. When sources that are not well separated do not resolve to focal, modular regions within the head model, the resulting peaks of the volumetric spectrum are lower than if sources are well separated and do pertain to focal regions within the model head. This characteristic has presented itself in this study for those topographies that do not originate from a single specific region inside the head model. Also affecting the peak value of the volumetric spectrum is the normalization of the topographies as in Equation 18. They are scaled such to have unit norm in Euclidean space. The degree to which the electrodes reinforce one another as to the projection of variance thus has an effect on this scaling of the topography and thus the volumetric spectrum. This might be the reason why the electrode artefact has such a small peak spectral value.

SUMMARY

The findings of this study indicate that neuroscientists can use volume-domain information for their interpretation of ICA-derived EEG source activities. Volume-domain projection of topographies provide for a possible new method to distinguish bona fide brain sources from artefacts, the degree of separation of sources, and a new graphical representation of brain source volumes.

Acknowledgements:
Funding for this study was provided in part by the Natural Sciences and Engineering Research Council of Canada.

VI. CONCLUSIONS

Our method provides a way to link the time and topography domains of ICA components to a physical volume representation. While our method does require a more robust threshold selection process, it does provide information leading to a bona fide estimate of these brain volume structures (e.g. Brodmann areas) that are responsible for source signals.

In creating this tool, we have overcome some of the characteristic weaknesses of the standard LCMV Beamformer, namely, limits to the degrees of freedom by which to separate EEG sources, challenges in separating proximally located sources, and the necessity of an EEG baseline to compensate for head model bias.

There are many of areas for future work examining and expanding on this algorithm. Using model data, the relation between errors in the volumetric spectrum and errors of the waveform estimate for a variety of sources should be investigated. In addition, this method should be demonstrated using actual scalp-EEG data. Finally, to maximize the utility of this algorithm, it is necessary to make a provision for definitive, robust source volume estimates.

VIII. REFERENCES

Baillet S, Mosher JC, Leahy R. BrainStorm beta release: a Matlab software package for MEG signal processing and source localization and visualization. Proceedings of the 16th Annual Meeting of the Organization for Human Brain Mapping, San Antonio, Texas, 2000.

Bell A, Sejnowski TJ. An information-maximization approach to blind separation and blind deconvolution. Neural Computing, 1995;7:1129-1159.

Berg P, Scherg M. A fast method for forward computation of multiple-shell spherical head models. Electroencephalography and Clinical Neurophysiology, 1994;90:58-64.

Delorme A, Makeig S. EEGLAB: an open source toolbox for analysis of single-trial EEG dynamics. Journal of Neuroscience Methods, 2004;134:9-21

De Lucia M, Fritschy J, Dayan P, Holder D. Detection of spikes in EEG recordings using features derived from ICA. Clinical Neurophysiology, 2006;117(1):139-140.

Ghahremani D, Makeig S, Jung T-P, Bell AJ, Sejnowski TJ. Independent Component Analysis of Simulated EEG Using a Three-Shell Spherical Head Model. Technical Repoft INC-9601, Institute for Neural Computation, University of California San Diego. La Jolla CA, 1996.

Hyvärinen A, J Karhunen, E. Oja. Independent Component Analysis (2001) John Wiley & Sons, New York, NY.

Hyvärinen, A, Oja E. A fast fixed-point algorithm for independent component analysis. Neural Computation, 1997; 9(7):1483-1492.

Hyvärinen A, Oja E. A fast and Robust Fixed-Point Algorithm for Independent Component Analysis. IEEE Transactions on Neural Networks, 1999;10(3):626-634.

Hyvärinen A, Oja E. Independent component analysis: algorithms and applications. Neural Networks, 2000;13(4-5):411-430.

Jentzsch I. Independent Component Analysis Separates Sequence-Sensitive ERP Components. International Journal of Bifurcation and Chaos, 2004;14(2):667-678.

Kobayashi K, Akiyama T, Nakahori T, Yoshinaga H, Gotman J. Systematic source estimation of spikes by a combination of independent component analysis and RAP-MUSIC. I: Principles and simulation study. Journal of Clinical Neurophysiology, 2002;113(5):713-724.

Koles ZJ, Soong ACK. EEG source localization: implementing the spatio-temporal decomposition approach. Electroencephalography and Clinical Neurophysiology, 1998;107:343-352.

Leal AJR, Dias AI, Vieira JP. Analysis of the EEG dynamics of epileptic activity in gelastic seizures using decomposition in independent components. Clinical Neurophysiology, 2006;117(7):1595-1601.

Lee T-W, Girolami M, Bell AJ, Sejnowski TJ. A unifying information-theoretic framework for independent component analysis. Computers and Mathematics with Applications, 2000;39:1-21.

Lee T-W, Girolami M, Sejnowski T. Independent component analysis using extended infomax algorithm for mixed sub-Gaussian and super-Gaussian sources. Neural Comput., 1999;11(2):609-633.

Makeig S, Bell A, Jung T, Sejnowski T. Independent component analysis of electroencephalographic data. In: Touretzky, D., Mozer, M., & Hasselmo, M. (Eds.), Advances in Neural Info. Proc. Sys., 1996;8:145-151.

Makeig S, Delorme A, Westerfield M, Jung TP, Townsend J, Courchesne E, Sejnowski TJ. Electroencephalographic Brain Dynamics Following Manually Responded Visual Targets. Public Library of Science Biology, 2004;2(6);747-762.

Makeig S, Jung TP, Bell A, Ghahremani D, Sejnowski TJ. Blind separation of auditory event-related brain responses into independent components. Proc. Natl. Acad. Sci. USA, 1997;94:10979-10984.

Makeig S, Jung TP, Ghahremani D, Sejnowski TJ. Independent Component Analysis of Simulated ERP Data. In: Integrated Human Brain Science: Theory, Method, Applications (Music), T. Nakada, ed., 2000.

Michel MC, Murray MM, Lantz G, Gonzalez S, Spinelli L, de Peralta RG, Invited Review: EEG source imaging. Clinical Neurophysiology, 2004;115:2195-2222.

Mosher JC, Leahy RM. EEG and MEG Source Localization using Recursively Applied (RAP) MUSIC. Proceedings Thirtieth Annual Asilomar Conference on Signals, Systems, and Computers, Pacific Grove, CA, Nov 3-6, 1996

Onton J, Delorme A, Makeig S. Frontal midline EEG dynamics during working memory. NeuroImage, 2005;17(2):341-356.

Schmidt RO. Multiple Emitter Location and Signal Parameter Estimation. IEEE Transactions on antennas and propagation, 1986;AP-34(3).

Stone JV. Independent component analysis: an introduction. Trends in Cognitive Sciences, 2002;6(2): 59-64.

Tikhonov AN. Solution of incorrectly formulated problems and the regularization method. Soviet Doklady 1963; 4, pp. 1035-1038.

Jung T-P, Makeig S, Westerfield M, Townsend J, Courchesne E, Sejnowski TJ. Analysis and visualization of single-trial event-related potentials. Human Brain Mapping, 2001;14(3):166-85.

Urrestarazu E, LeVan P, Gotman J. Independent component analysis identifies ictal bitemporal activity in intracranial recordings at the time of unilateral discharges. Clinical Neurophysiology, 2006;117(3):549-561.

Van Veen BD, van Drongelen W, Yuchtman M, Suziki A. Localization of Brain Electrical Activity via Linearly Constrained Minimum Variance Spatial Filtering. IEEE Transactions on Biomedical Engineering, 1997;44:867-880.

Yao D. A method to standardize a reference of scalp EEG recordings to a point at infinity. Physiological Measurement, 2001;22:693-711.

Zeman PM, Mahajan SV, Sorensen PL, Driessen PF, Skelton RW, Livingston NJ. Beamform Volume Projection of ICA Components of Scalp EEG: Volume-Domain Uniqueness of Components. (for publication) 2007c.

Zeman PM, Mahajan SV, Livingstone SA, Livingston NJ, Skelton RW. Spectral Shaping to Relax ICA Assumptions to Facilitate Decomposition of EEG. (for publication). 2008e.

Chapter 4: Beamform Volume Projection of ICA Components of Scalp EEG: Volume Domain Uniqueness of Components

The following manuscript demonstrates the method of mapping scalp surface electric fields of components of real EEG data to volume-domain representations. It is demonstrated that the surface potential at the scalp can be mapped to a representation in which components have 3D volume and occupy space. Estimation of modular brain volumes from the ICA decomposition of EEG is also demonstrated. It is shown that the volume-domain representation of these components can be used to obtain an objective measure of how well separated any two components of the decomposition are; in this case, separation refers to how well separated they are as source volumes. Two components of an ICA decomposition of EEG data that ostensibly relate to activities of the brain are considered separate if they relate to unique brain volumes within the head. This measure of separation is a continuous measure that varies between 0, indicating no overlap and thus maximum possible separation, to 1, indicating perfect overlap of components and therefore the poorest possible separation.

A measure of the overlap or anatomical uniqueness of components is important if the waveform activities of these components are to be compared. For example, if a researcher wishes to measure the coordinated relationship between two areas of the brain, (identified by ICA as separate components), it should be first demonstrated that the components relate to unique areas of the brain. The measure of volume overlap objectively establishes that two component waveforms to be compared relate to different brain volumes. Once the anatomical uniqueness of components is established, then any measure of correlated source activity varying over time becomes meaningful because there is some certainty that the detailed characteristics of the component waveform originate from a unique origin. If a significant correlation of activities is found between components that have been verified as pertaining to unique brain volumes, it is probable

that the two brain areas are somehow linked together via anatomical or functional connections.

Article Type: Research Article
Article Title: Beamform Volume Projection of ICA Components of Scalp EEG: Volume-Domain Uniqueness of Components

Philip M. Zeman[1,2,3], Sunny V. Mahajan[1,2], Patricia L. Sorensen[4], Peter F. Driessen[2], Ronald W. Skelton[3], Nigel J. Livingston[1]

[1] CanAssist, University of Victoria, BC, Canada
[2] Department of Electrical and Computer Engineering, University of Victoria, BC, Canada
[3] Department of Psychology, University of Victoria, BC, Canada
[4] Department of Neuroscience, Canadian Centre for Behavioural Neuroscience,

Correspondence may be addressed to Philip M. Zeman:
(voice) +1-250-589-4234 / (fax) +1-250-721-6611 / pzeman@alumni.uvic.ca

Abstract

Objectives:

Our primary objective is to demonstrate the method of volume estimation of independent component analysis (ICA)- derived scalp topographies (Zeman et a., 2008b) using real EEG data. Secondly, we demonstrate how the measure of volume overlap of components provides an objective and anatomically meaningful metric of the physical volume separation of each component.

Methods:

EEG data were collected from 31 participants while they navigated a virtual computer environment. The data for all participants and conditions were concatenated and then separated into components using ICA. The brain volumes for a selected set of components were calculated. The volume overlap of components and the distance between component centers of mass were calculated and examined in conjunction with topographical characteristics to determine the volume separation of each component.

Results:

Component volumes occupied brain regions involved in spatial navigation, working memory, and object recognition. The collective characteristics of distance between centers of mass and dipole characteristics of topographies indicate that, of the 9 components examined, all pertain to unique parts of the brain. The metric of volume overlap, however, indicates that there is a possible partial volume overlap for 2 pairs of components. This indicates that these components may not be fully associated with separate anatomical brain areas.

Conclusions:

We conclude that our methodology successfully estimates the volumes of ICA-derived EEG components and that the separation of brain activities can be evaluated by a physical volume-domain measure.

Keywords: EEG; ICA; LCMV beamforming; volumetric localization; dipole fitting; spatial navigation

I. INTRODUCTION

Using an adaptation of the Linearly Constrained Minimum Variance (LCMV) Beamformer, Zeman et al. (2008b), described a methodology for projecting ICA-derived topographies, calculated from scalp EEG data, to a volumetric representation. They demonstrated that the modular volumes of synthetic sources can be reasonably estimated under simulation conditions. In addition, they showed that these source volume representations provide a meaningful measure of spatial overlap of EEG components separated using independent component analysis (ICA).

In this paper, we demonstrate the same method using real scalp-acquired EEG data. We describe how the measure of spatial overlap provides a measure of physical separation and how, by combining volume characteristics with topographical characteristics, we can associate components of the EEG with specific anatomical brain regions. We provide evidence by way of real data, that neuroscientists using EEG methods can now represent brain sources as modular sources volumes rather than dipolar point sources. In addition, we show that the volume overlap metric provided by these methods is useful in demonstrating that a pair of source waveforms do indeed, arise from separate physical brain volumes. Such a metric is particularly useful when the activities of two sources are to be compared in a measure of cooperation between areas of the brain.

There is no guarantee that all the components calculated via ICA (here were specifically refer to the runica algorithm of Makeig et al.. (1997)) correspond to anatomically unique parts of the brain. When ICA methods are used to separate EEG data into components, separation is usually done using only characteristics of the EEG data time- or frequency-domain activities (Makeig et al., 1997). In some cases, components calculated might arise from poor separation of brain sources or an artefact of the ICA decomposition process itself. Often, activities originating from a single region of the brain are inappropriately split by ICA, and thus, multiple similar sources are created, each having slightly different topographies and waveform characteristics but with similar centers of

mass. This problem may also arise if two adjacent brain sources are poorly resolved in the separation process. While the brain location centers of mass implicated by these components may differ, the brain location volumes implicated by these components may overlap. By ICA definition, there can be no two components with exactly the same time-domain activities. However, a volume overlap of components is still possible. Thus, if a volume overlap is found for a pair of EEG components, there is a question as to which of the pair of waveform activities originates from the brain volume.

Thus, there is a need for a method that provides an efficient, non-blind, and physically justified metric to determine which components of an ICA decomposition of EEG data originate from unique brain volumes and which components relate to common brain volumes. The volume estimation algorithm of Zeman et al., (2008b) may offer such a solution by providing a modular source volume estimate and volume overlap estimate for each ICA-derived component. The modular source volume estimate facilitates interpretation of the source volume by providing a refined estimate of distinct boundaries while the continuous volume overlap estimate provides a measure of the physical distinction between components without removing noise-related blurring that affects both volume-domain and time-domain source properties. In other recent work using this method we clearly identified the modular volumes of the ocular orbital muscles of the eyes (Zeman et al., 2008e). Similarly, we have also used the method to estimate brain volumes associated with the cortical ventral visual pathway for object recognition (Zeman et al., 2008g).

In order to demonstrate modular volume estimation and volume overlap estimation of brain activity components using real EEG data, we utilized EEG data obtained in a larger study of spatial navigation and Foetal Alcohol Spectrum Disorder (FASD). In that study, EEG data were collected while multiple participants undertook the Virtual Morris Water Task (vMWT). That task is thought to elicit activity from areas involved with spatial navigation (Hamilton et al., 2003), working memory, and object recognition. Thus, in evaluating the volume estimation algorithm, we hypothesized that we would find the locations and volumes of components of the EEG data to be in agreement with research

identifying brain structures associated with spatial navigation in a virtual environment. Our objective is to expressly demonstrate the volume estimation algorithm with as little discussion of the ICA methodology and behavioural analysis as possible.

II. METHODS

Matlab 7 (Mathworks Inc.) and EEGLab 4.515 (Makeig et al., 1997; Delorme and Makeig, 2004) were used to do all modelling, calculations, and plotting. BERG head model parameters (Berg and Scherg, 1994) and artwork for the model were derived from the BrainStorm software package (Baillet et al., 2000) for Matlab.

DATA COLLECTION PARADIGM

Approval for this study was granted by the ethics committee of the University of Lethbridge. Participants in the study belonged to one of three groups: university students (11 persons), persons with an FASD rating based on neuropsychological scoring (10 persons), and a socially matched FASD control group (10 persons). All three groups were pooled to comprise a dataset of 31 female participants.

The 1st-person perspective virtual Morris Water Task paradigm of (Sorensen et al., 2006) was used to elicit and capture specific brain activities. This EEG collection paradigm is similar to the behavioural paradigm used by Hamilton et al., (2003). Participants were seated approximately 180 cm from a 40 cm CRT computer screen. The paradigm uses two different behavioural conditions corresponding to two types of trials, cue and place. A different strategy is required to successfully complete each type of trial. The two strategies to complete the task were described to each participant. For each of the behavioural conditions examined, participants were given practice trials until it was clear they understood how to complete the task. During the place condition, the two platforms were visually identical; navigation was possible via wall-mounted pictures. For the first presentation (trial one), the participants were asked to look around the room and then

pick one of the two platforms and "swim" towards it. In cases where they moved to the incorrect platform, they were asked to then swim to the second platform. For the second, third and fourth trials of each block, the subject had to remember the location of the correct platform. For the cue condition, the platforms displayed visually distinctive color patterns. Participants were instructed to attend to the color of the platform during these trials. For the first trial, the participants were required to look at the platforms, pick one and swim towards it. If it was the incorrect platform, they were to swim to the second platform. For the second, third and fourth trials of each block, the participants had to remember the color pattern of the correct platform.

The virtual environment consisted of a round pool placed in a square room. A unique image, framed as a picture, was placed on each of the four walls. The two visible square platforms were placed in different quadrants of the pool. To navigate in the virtual pool, participants pressed the left/right arrow keys on a keyboard. For each trial, participants began in a random starting location along the pool wall. When the participant reached the incorrect platform, forward motion would continue and the participant would appear to "swim through the platform". When the participant reached the correct platform, forward motion would stop and the phrase "Platform Found" was presented on the screen. Different sets of wall-mounted pictures (place condition) and platform colors (cue condition) were presented for each block of trails. Each participant completed 20 blocks of each condition. Each block consisted of four trials during which the platform locations remained constant. The distal cues on the four walls remained constant during each block. Place and cue blocks alternated throughout the session. Prior to the commencement of each block, the participants viewed a blank screen with a fixation point, '+' in the center of the screen, for 2000 ms. They then viewed a pre-trial signal, "Place" or "Cue" for 1000 ms to indicate which navigation strategy should be used to complete the impending block of trials. Between trials within each block, participants viewed a blank screen with a fixation point, '+' in the center of the screen, for 2000 ms.

DATA COLLECTION AND PREPROCESSING

Data were recorded, stored, and then pre-processed in preparation for ICA decomposition and source volume estimation. Data were collected using a 128-channel Geodesics dense-array sensor net and Net Station acquisition software (Electrical Geodesics, Inc., Eugene, Oregon). Data were band-pass filtered (0.1 Hz to 100 Hz) and digitally recorded at a sampling rate of 250 samples/second. The data were average referenced by subtracting the mean calculated across channels from each channel for each time sample (Yao, 2001). While this method of average referencing is not ideal for beamform applications (Van Veen, et al., 1997) and does introduce small errors (Yao, 2001; Zeman et al., 2008b), it is the most common method of average referencing scalp EEG data. The data were segmented into epochs from –1000 ms to 2500 ms (with the moment of task commencement at 0 ms). Of the total number of EEG channels, 112 were free of consistent artefact and were used in subsequent analysis. The same channels were used for all participants. The first trial from each block was omitted from data analysis as the participants found the correct platform by chance. Because of artefacts introduced by movement, only 29 artefact-free trials per condition could be obtained from some of the FASD participants. Thus, to balance the representation of each participant in the data, 29 non-artefact trials per participant for each of the 2 conditions were used in further analysis.

The remaining EEG data of each participant were ‘cleaned’ using an ICA-based artefact removal procedure. Briefly, the datasets of both the cue and place conditions were concatenated for ICA decomposition. These data were then separated into 112 components (from 112 channels) using the runica (Makeig et al., 1997) EEGLab 4.515 (Delorme and Makeig, 2004) function with the ‘logistic’ parameter (Lee et al., 1999) specified. Electrode artefact components were identified by visual inspection of the ICA-derived scalp topographies. Those components with topographies indicating activity at singular electrodes were identified as artefact. The separated data were then re-assembled, omitting those components identified as electrode artefacts.

DATA ANAYSIS

To provide enough data for a strong representation of brain activity, components for volume estimation were calculated from a single ICA decomposition of a grand EEG dataset. Each participant contributed a dataset of 29 trials, with 875 samples/trial, for each of the 2 behavioural conditions. To reduce the memory requirements to process the data, the sampling rate was reduced. The data of each trial were band-pass filtered from 8 Hz to 30 Hz using a 60-point zero-phase FIR filter and then down-sampled to 125 samples/second. Each of the datasets were concatenated to provide for a single grand dataset of 112 channels with 785726 samples (i.e. 29 trials x 437 samples/trial x 31 subjects x 2 conditions). The runica algorithm was used to compute component activities and topographies. The 'logistic' parameter was used for the EEG data decomposition. To compensate for the rank reduction of the data via the previous artefact removal step, we reduced the rank of the data to 70 components using the 'PCA' parameter. While the concatenation of datasets from multiple subjects does weaken the assumption of spatial stationarity, our experience is that the effect of this is more than offset by the overall increase in the quantity of data.

Of the 70 components returned by runica, 9 components were selected to demonstrate the volume estimation methodology. The section criterion was of source 'goodness', based on the dipolar characteristics of source topographies (Onton and Makeig, 2006). A dipolar topography has ideally two foci and a smooth transition of variance away from each of the foci. A topography may also be considered as dipolar with one foci and the requisite smooth transition away from the foci, presuming that the orientation of the dipole places the second foci in the ventral direction were no electrodes are placed. The selected source topographies were prepared for projection to the volume domain by subtracting the mean from each topography (as was previously done in the step of average referencing the data) and were normalized using the Euclidean norm. This process is described in detail by Zeman et al., (2008b).

The raw volumetric spectra and the volumetric spectra for multiple thresholds were calculated using the volume estimation algorithm. This algorithm utilizes a combination of the LCMV Beamformer (Van Veen et al., 1997) and statistical thresholding of an estimated volumetric spectrum to define modular source volumes from the continuous volumetric spectrum.

The volumetric spectra were first calculated for each topography. This was done using the algorithm described in (Zeman et al., 2008b). This algorithm utilizes the LCMV beamformer (Van Veen et al., 1997) to project the variance of ICA-derived scalp topographies into a continuous representation of variance in head model volume. An idealized LCMV Beamformer input is created using topographies calculated via an ICA decomposition of EEG data. Idealized data created from each topography, were then individually projected into the volume domain using a bias-corrected version of the LCMV Beamformer. This provides for a spectrum of volume domain coefficients representing projected variance at all points in the head volume.

We then calculated modular volumes to depict the volumes of sources recovered in the ICA decomposition of EEG data. To do so, an estimate of the volume domain noise was used to define the edges of the volume-projected source. To calculate this noise estimate, it is assumed that the volumetric spectrum is largely representative of noise and that the volume of the source is represented by relatively few coefficients. The brain source volume is represented by outliers in the distribution of noise and the edges of the volume are identified by a threshold calculated as some number of standard deviations above the mean noise estimate (STDM). From the thresholded spectra, the modular volumes for each selected component are defined. Using synthetic data, Zeman et al., (2008b) found that thresholds between 3 and 5 standard deviations above the mean (STDM) provided meaningful results. For this study, those voxels within 4 and 5 STDM are defined by boundaries indicated by 3D concentric shells encapsulating each region.

To view the relationship between the threshold selected and the calculated source volume, the modular volumes for multiple thresholds was calculated. A summary of the volume estimates corresponding to a threshold range of 2 STDM to 6 STDM for each of the components examined was plotted.

To examine differences in the overlap estimate for the raw and the thresholded spectra of the modular volumes, the pair-wise volume overlap (PVO) was calculated for both cases. This was done using Equations 1 and 2 for both the raw spectra (Table 1) and for the spectra thresholded at 4 STDM (Table 2). First, each volumetric spectrum was mean subtracted and normalized using Equation 1,

$$\hat{\mathbf{r}} = \frac{\mathbf{r} - \bar{\mathbf{r}}}{\sqrt{(\mathbf{r}_1 - \bar{\mathbf{r}})^2 + (\mathbf{r}_1 - \bar{\mathbf{r}})^2 + \ldots + (\mathbf{r}_1 - \bar{\mathbf{r}}_P)^2}} \quad (1)$$

where **r** is a ***1*** x ***P*** vector containing the volumetric spectrum coefficients r_1, r_2, to r_P, $\bar{\mathbf{r}}$ is the mean, and $\hat{\mathbf{r}}$ is the zero-mean, normalized spectrum.

The PVO was then calculated as a pair-wise scalar product as in Equation 2,

$$S_{ij} = |(\hat{\mathbf{r}}_i \hat{\mathbf{r}}_j^{\,T})| \text{ for all } i \neq j \quad (2)$$

where S_{ij} is the overlap for an arbitrary pair of zero-mean and normalized volumetric spectra $\hat{\mathbf{r}}_i$ and $\hat{\mathbf{r}}_j$.

To calculate differences in the centers of mass between components, the following steps where used. First, the center of mass of each source was found as the head volume index location of the peak coefficient of each volumetric spectrum (Van Veen et al., 1997; Michel et al., 2004). Second, the distance between pairs of source centers d_{ij} was calculated for all pairs of components using Equation 3,

$$d_{ij} = \sqrt{(x_i - x_j)^2 + (y_i - y_j)^2 + (z_i - z_j)^2} \quad (3)$$

where x_i, y_i, z_i and x_j, y_j, z_j are the centers of mass of a pair of sources. The results were tabulated with corresponding measures of volume overlap for comparison.

III. RESULTS

ICA decomposition of the EEG data yielded 70 components. Of these, the topographies of 9 components selected for volume estimation are plotted in Figure 1 and labelled as (1) through (9).

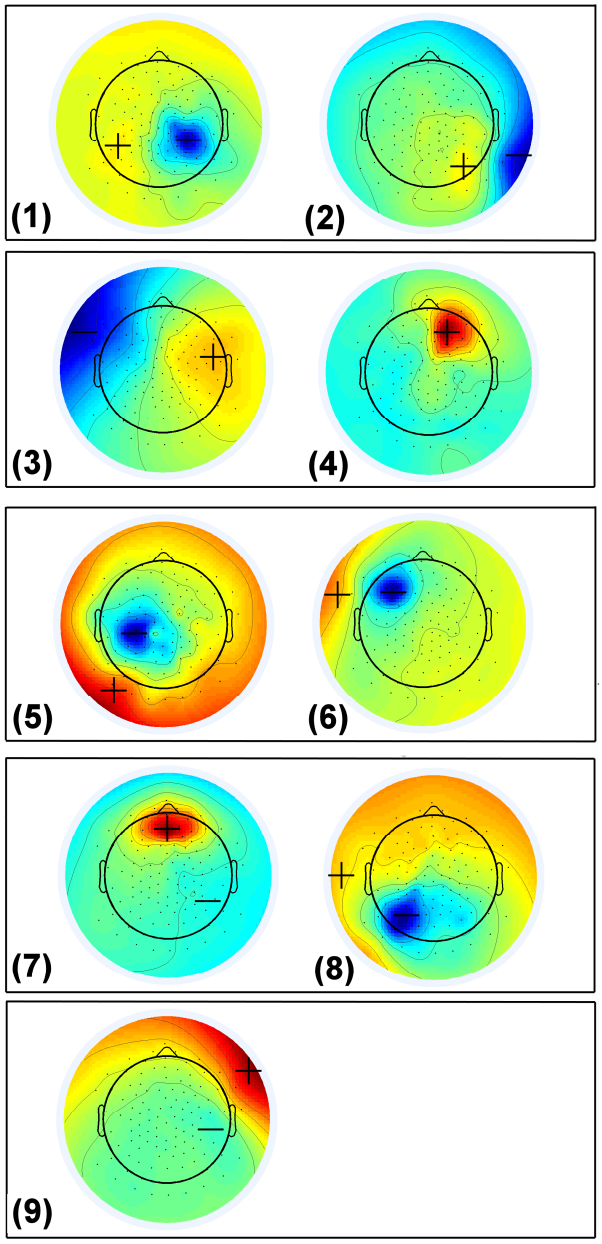

Figure 1. Topographies calculated via ICA of scalp acquired EEG data. Positive field regions are represented by (+) while negative field regions are represented by (-). The field topology outside the head drawing depicts how the scalp field wraps around the sides of the head.

Source volumes were found to reside in multiple areas of the brain and are depicted in Figure 2. Two perspectives of each source volume provide axes for viewing volume size, shape, and location. Visual inspection reveals that the estimated source volumes are

approximately located in the: (1) right parietal cortex, (2) right inferior posterior temporal cortex (or ventrotemporal cortex), (3) left medial orbitofrontal cortex , (4) right lateral superior frontal sulcus (or middle frontal gyrus), (5) left inferior posterior parietal cortex (or left angular gyrus), (6) left dorsolateral prefrontal cortex, (7) right medial superior frontal gyrus, (8) left posterior superior temporal gyrus, and (9) the right temporal pole.

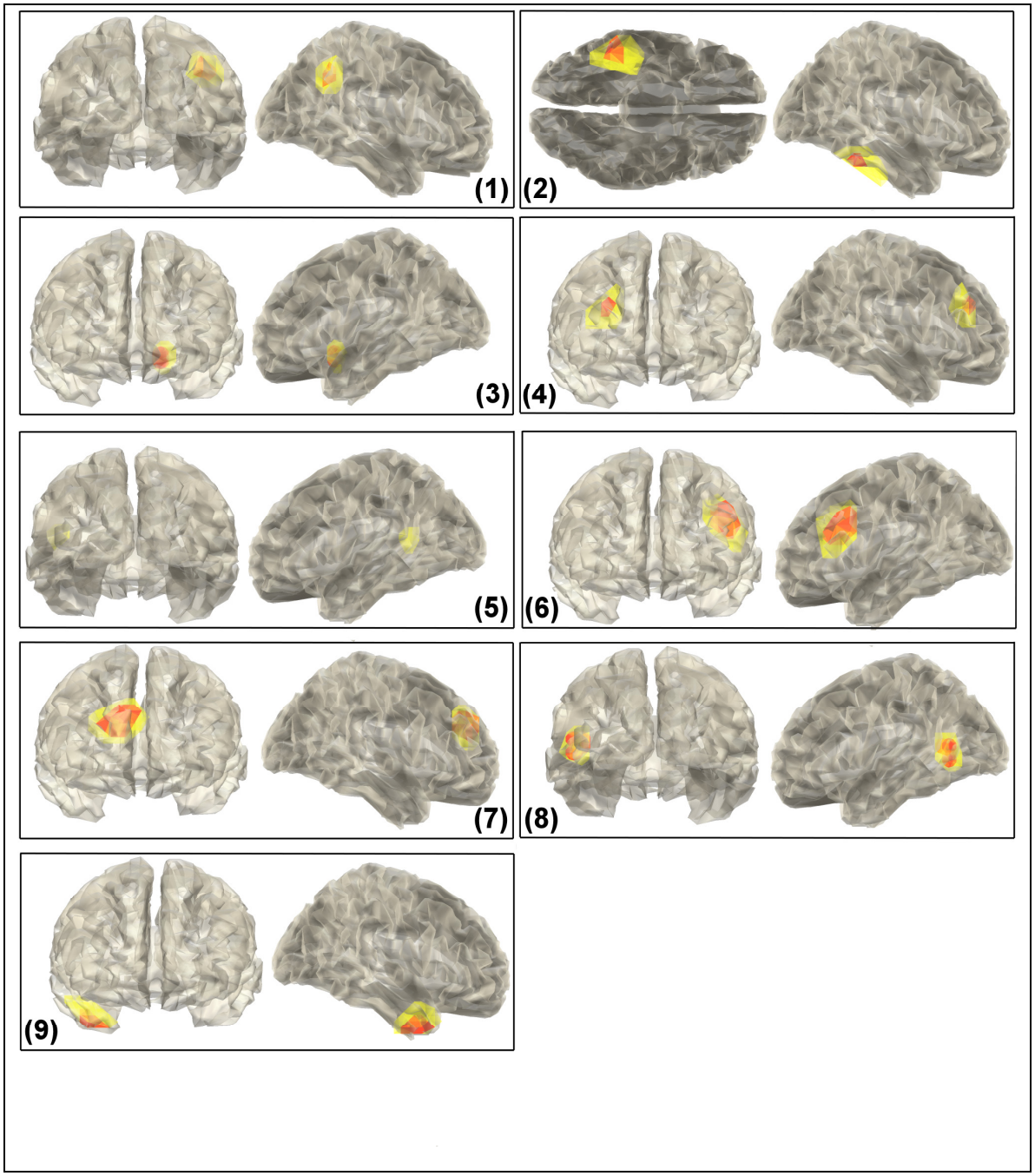

Figure 2. Source localization and volume estimation results for brain sources (1) through (9) projected into a white-matter frame. The two views that best illustrate the source volume within the model head are given. STDM thresholds are indicated as colored shells; 4 STDM is indicated by regions of yellow; 5 STDM is indicated by regions of red. The white matter frame is a component of the BrainStorm software package (Baillet et al., 2000).

A plot illustrating the number of voxels occupied by each source at various STDM thresholds is provided in Figure 3. Notably, all sources have similar characteristic curves relating the number of voxels as a function of STDM. Generally, the curves have a steep negative slope between 2 and 3.5 STDM that decreases when values are greater than 3.5 STDM.

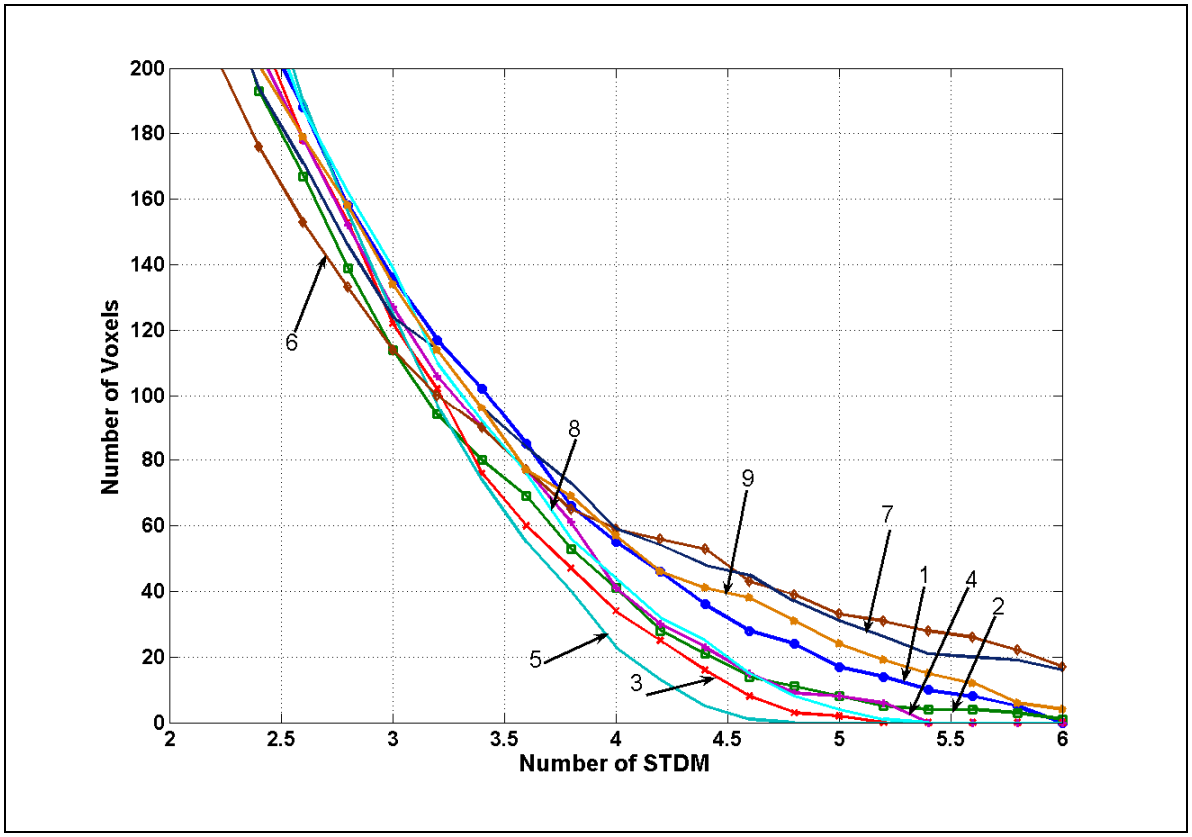

Figure 3. Source volume estimates for multiple STDM thresholds plotted as the volume estimate (number of voxels) versus the threshold used (number of STDM). Each of the 9 brain sources examined is labelled using arrows as 1 through 9.

The PVO of raw volumetric spectra and the absolute distance between the centers of mass of each source is given Table 1. The notably large PVOs are 0.881, 0.935, and 0.553 for source pairs (4)-(7), (5)-(8), and (2)-(9), respectively. The distance between centers of mass for these components (below each PVO given in Table 1), however, illustrates that these pairs of sources do not have the same centers of mass. The distances measured between source centers of these components are not precisely zero. Notably, source pair (5)-(8) has a source center separation of only 1.12 cm while source pairs (4)-(7) and (2)-(9) have a separation of 2.12 and 4.95 cm respectively.

	(2)	**(3)**	**(4)**	**(5)**	**(6)**	**(7)**	**(8)**	**(9)**
(1)	0.202 6.53	0.428 10.1	0.272 9.11	0.196 9.71	0.390 12.1	0.311 9.97	0.0693 9.87	0.271 9.86
(2)	-- --	0.0235 8.57	0.0471 10.2	0.236 11.0	0.391 13.4	0.167 11.4	0.105 10.9	***0.553*** **4.95**
(3)	-- --	-- --	0.152 7.37	0.0313 7.78	0.297 5.89	0.141 6.80	0.176 8.38	0.356 6.78
(4)	-- --	-- --	-- --	0.464 12.4	0.0277 8.63	***0.881*** **2.12**	0.460 13.2	0.341 8.56
(5)	-- --	-- --	-- --	-- --	0.0246 7.57	0.404 11.6	***0.935*** **1.12**	0.330 12.5
(6)	-- --	-- --	-- --	-- --	-- --	0.131 6.82	0.0847 8.63	0.135 12.36
(7)	-- --	-- --	-- --	-- --	-- --	-- --	0.421 12.5	0.199 9.66
(8)	-- --	-- --	-- --	-- --	-- --	-- --	-- --	0.342 12.7

Table 1. Raw source volume overlap (top row) and distance between centers of mass (bottom row). Values greater than 0.5 are given in bold italics. Distance units are centimetres. Distances less than 5 centimetres are given in standard bold.

The PVO for a threshold of 4 STDM (corresponding to the yellow shells of Figure 2) are given in Table 2. Notably, when noise in the volumetric spectrum is removed via thresholding, the overlap is still evident between source pairs (4)-(7) and (5)-(8), while

there is no overlap between (2)-(9). In fact, the overlap between (2)-(9) for this 4 STDM threshold is less than the overlaps for (7)-(9) and (6)-(9) when no threshold is used.

	(2)	**(3)**	**(4)**	**(5)**	**(6)**	**(7)**	**(8)**	**(9)**
(1)	0.00877	0.00799	0.00866	0.00657	0.0104	0.0105	0.00919	0.103
(2)	--	0.00690	0.00748	0.00567	0.00899	0.00903	0.00794	***0.00893***
(3)	--	--	0.00681	0.00516	0.00818	0.00822	0.00723	0.00813
(4)	--	--	--	0.00560	0.00887	***0.297***	0.00784	0.00882
(5)	--	--	--	--	0.00672	0.00676	***0.337***	0.00668
(6)	--	--	--	--	--	0.0107	0.00941	0.0106
(7)	--	--	--	--	--	--	0.00947	0.0106
(8)	--	--	--	--	--	--	--	0.00936

Table 2. The volume overlap of pairs of sources thresholded at 4 STDM. Numbers in bold italics correspond to comparisons highlighted in Table 1.

IV. DISCUSSION

The methods presented in this paper show that volume-projection of ICA source topographies provides a means to describe the physical characteristics of separated sources. By use of these methods, it is possible to represent neural sources comprising the EEG sources as modular anatomical volumes in a model cortex. This is in contrast to current methods that represent EEG sources as model dipoles defining singular points in space. Further, the volume overlap measures described provide an objective measure of the anatomical separation of sources when it is required to demonstrate physical, anatomical separation of brain sources.

We localized and estimated the modular volumes and pair-wise volume overlap (PVO) of a set of ICA components using real scalp-acquired EEG data collected during the spatial navigation task. The components identified by ICA represent characteristics of the data for the frequency band 8 to 30 Hz. Some of the components of the decomposition demonstrated dipolar topographies with characteristics appropriate to describe modular brain sources. A subset of these was projected to the volume domain where the modular brain volumes and volume overlaps were determined.

SOURCE VOLUMES AND OVERLAP

The brain volumes identified in Figure 2 from the EEG data are consistent with what is known of spatial navigation, working memory, and object recognition. Structures including the temporal pole, ventrotemporal cortex, inferior parietal cortex, hippocampus (and parahippocampal structures), anterior cingulate, and orbitofrontal cortex, have been implicated as important for spatial navigation (Hamilton et al., 2003; Spiers and Maquire, 2006) while the dorsolateral prefrontal frontal cortex, the posterior parietal cortex, and ventrotemporal cortex is important for working memory tasks (Collette and Van der Linden, 2002) and visual identification and awareness of objects (Wilenius-Emet et al., 2004).

The curves relating brain volume to a range of selected thresholds illustrate that the volume roll-off characteristic is similar for each of the component volumes. The results of Figure 3 show that a small change in the threshold level between 2 and 3.5 STDM, leads to a large change to the source volume estimate. This change however is less pronounced between 3.5 and 6 STDM. A threshold varied between 3.5 and 5 STDM has little impact on the modular volume estimate (Figure 2). This result is similar to that of the volume brain source modelled in prior work (Zeman et al., 2008b). An alternative to selecting a threshold by an a priori determined STDM is to select a threshold by identifying the 'knee' of the curve relating number of voxels to threshold level. The knee of such characteristic curves reflects a change in the relationship between the axis quantities (Antoniou and Lu, 2007) and is commonly used as a means to separate signal from noise in singular-value or eigen-value decompositions (Haykin, 2002). Thus, for source (5), an appropriate knee threshold might be 4.1 STDM, while for source (3), a 3.6 STDM threshold is appropriate. In both cases, the threshold selection process is justified and the estimated modular volumes are similar.

Our approach provides an empirical method that shows whether EEG sources do, or do not originate from overlapping brain volumes. The raw volumetric spectra in Table 1 suggest there is a possible overlap between source pairs (4)-(7), (5)-(8), and (2)-(9).

Overlap calculated using raw volumetric spectra includes the noise of the volumetric spectrum and the noise contained in the ICA-derived topographies (as described by Zeman et al., 2008b). Having removed the noise for a threshold of 4 STDM (Table 2), there is no-longer overlap for source pair (2)-(9). This difference suggests that overlap for source pair (2)-(9) arises from the noise floor of the volumetric spectrum and not from the source volumes themselves. The measure of distance between source centers supports this inference; the distance separating pair (2)-(9) is 4.95 cm while (4)-(7) and (5)-(8), are only separated by distances of 2.12 and 1.12 cm, respectively. Taken together, the results of the raw volume overlap estimate, the 4 STDM volume overlap estimate, and the estimated distance between source centers strongly suggest an overlap for sources (4)-(7) and (5)-(8) but not for sources (2)-(9).

The dipolar characteristics of source topographies provide source orientation detail to aid in determining the anatomical uniqueness of sources. The modular volume of source (4) appears to have a well-defined edge at the superior frontal sulcus, and, from combined volume location and topographical characteristics, that it has characteristics analogous to a distally oriented dipole sheet located on the middle frontal gyrus. Interestingly, source (7), proximally located next to source (4), has a volume and topography that suggests it may be analogously represented by a dipole sheet on the middle edge of the superior frontal gyrus. Thus, according to the topographical characteristics, source pair (4)-(7) may be unique. They are closely, proximally spaced, and having differing dipolar orientations. A similar argument can be made for source pair (5)-(8). Thus, in this case, the dipolar source characteristics weigh against the evidence that sources originate from common volumes.

Taken together, these results suggest that all components examined with the exception of component pairs (5)-(8) and (4)-(7) are well separated and describe unique brain volumes. Since source pairs (5)-(8) and (4)-(7) have unique orientations, and by ICA definition, unique time-domain activities. The overlap suggests that while they may be unique sources, they are poorly separated by volume. It suggests that caution should be exercised when examining the time-domain activities of these sources as some unknown

portion of their activities may arise from poor source separation. The direct relationship between the measure of volume overlap and of any volume conduction appearing in the time-domain activities of the ICA waveforms has not been demonstrated and is a subject requiring further research.

Acknowledgements:
Funding for this study was provided in part by the Natural Sciences and Engineering Research Council of Canada. We thank the students at the University of Lethbridge and the University of Lethbridge Department of Psychology for making these electroencephalographic data available.

V. CONCLUSIONS

The method provides for volume estimation of ICA-derived EEG components. In doing so, it provides additional descriptive information allowing for informed interpretation of ICA decompositions of EEG data. For the first time, it is possible to describe the separation of ICA brain sources by a truly anatomical measure. Future work should examine more robust estimates of the intersection of the noise floor and the edge of the localized volume. As well, the direct relationship between the component volume overlap and time-domain separation of proximally spaced components should be explored.

VI. REFERENCES

Antoniou A, Lu W-S. Practical Optimization: Algorithms and Engineering Applications, 1st ed. New York: Springer Science and Business Media, 2007.

Baillet S, Mosher JC, Leahy R. BrainStorm beta release: a Matlab software package for MEG signal processing and source localization and visualization. Proceedings of the 16th Annual Meeting of the Organization for Human Brain Mapping, San Antonio, Texas, 2000.

Berg P, Scherg M. A fast method for forward computation of multiple-shell spherical head models. Electroencephalography and Clinical Neurophysiology, 1994;90:58-64.

Collette F, Van der Linden M. Brain imaging of the central executive component of working memory. Neuroscience and Biobehavioral Reviews, 2002;26:105-125.

Contreras-Vidal JL, Kerick SE. Independent component analysis of dynamic brain responses during visuomotor adaptation. NeuroImage, 2004;21(3):936-945.

Delorme A, Makeig S. EEGLAB: an open source toolbox for analysis of single-trial EEG dynamics including independent component analysis. Journal of Neuroscience Methods, 2004;134:9-21.

Delorme A, Serby H, Makeig S. EEGLab Tutorial: VI. Independent Component Clustering. Retrieved Oct. 11, 2006 from <http:\\www.sccn.ucsd.edu/eeglab/clusttut/clustertut.html>.

Hamilton DA, Kodituwakku P, Sutherland RJ, Savage DD. Children with Fetal Alcohol Syndrome are impaired at place learning but not cue-navigation in a virtual Morris water task. Behavioural Brain Research, 2003;143:85-94.

Haykin S. Adaptive Filter Theory, 4th ed. New Jersey: Prentice Hall, 2002.

Lee T-W, Girolami M, Sejnowski T. Independent component analysis using extended infomax algorithm for mixed sub-Gaussian and super-Gaussian sources. Neural Computation, 1999;11(2):609-633.

Makeig S, Delorme A, Westerfield M, Jung TP, Townsend J, Courchesne E, Sejnowski TJ. Electroencephalographic Brain Dynamics Following Manually Responded Visual Targets. Public Library of Science Biology, 2004;2(6);747-762.

Makeig S, Jung TP, Bell A, Ghahremani D, Sejnowski TJ. Blind separation of auditory event-related brain responses into independent components. Proc. Natl. Acad. Sci. USA, 1997;94:10979-10984.

Michel MC, Murray MM, Lantz G, Gonzalez S, Spinelli L, de Peralta RG, Invited Review: EEG source imaging. Clinical Neurophysiology, 2004;115:2195-2222.

Onton J, Delorme A, Makeig S. Frontal midline EEG dynamics during working memory. NeuroImage, 2005;27:341-356.

Spiers HJ, Maguire EA. Thoughts, behaviour, and brain dynamics during navigation in the real world. Neuroimage, 2006;31:1826-1840.

Sorensen PL, Zeman PM, Sutherland RJ. Differing patterns of synchronous cortical activity during a virtual spatial navigation task. Canadian Society for Brain, Behaviour and Cognitive Science, 16th Annual Meeting. Paper presentation, 2006.

Van Veen BD, van Drongelen W, Yuchtman M, Suziki A. Localization of Brain Electrical Activity via Linearly Constrained Minimum Variance Spatial Filtering. IEEE Transactions on Biomedical Engineering, 1997;44:867-880.

Wilenius-Emet M, Revonsuo A, Ojanen V. An electrophysiological correlate of human visual awareness. Neuroscience Letters, 2004;354:38-41.

Yao D. A method to standardize a reference of scalp EEG recordings to a point at infinity. Physiological Measurement, 2001;22:693-711.

Zeman PM, Mahajan SV, Livingstone SA, Driessen PF, Skelton RW, Livingston NJ. Beamform Volume Projection of EEG ICA Topographies. (for publication) 2008b.

Chapter 5: Volume Domain Validation of ICA-Derived EEG Sources

The following manuscript describes a method to validate components of an ICA decomposition of EEG data. This validation method attempts to identify which components of such a decomposition of EEG are representations of brain activities originating from physically modular areas of the brain. It identifies their relative goodness as representing such types of sources, providing a degree of confidence as to how well unmixed a particular component is from other interferers and noise sources in the EEG data. It also provides a logical a priori criteria by which to accept or reject components of the EEG data returned by ICA mining of EEG data. Validating components of an EEG decomposition by this method helps avoid 'fishing' for results in the data because only if a component is accepted by specific a priori determined criteria can it be used to draw concussions about the activity of the brain. Those components that do not satisfy the validation criteria can be objectively omitted from further analysis.

Once this validation methodology has been described and demonstrated using synthetic EEG data, real EEG data collected from a single study participant is decomposed into parts using ICA. The EEG components resulting from this ICA decomposition are then each examined by the validation methodology to determine how effective the method is on real EEG.

Current standard EEG analysis methods determine the validity of components found in a given single-participant experiment by comparing results across experiments and datasets. The availability of this method allows for analysis of EEG data without the necessity to use multiple datasets, subjects, and experiments to derive information from the EEG via the standard method of hypothesis testing. Since by this proposed method components are validate from the data directly, results derived from each individual dataset are sufficient to draw conclusions.

This validation method also provides a means to compare the accuracy of estimates of bona fide brain sources for different source separation methods. Comparison of source separation methods is a difficult task because generally, the correct source waveform by which to compare source estimates is not known. This validation method provides a means to compare algorithms by the relative estimated source volume characteristics of components. A comparison of two different source separation algorithms is made in Chapter 6 where brain activity estimates of a standard ICA method (runica) are compared to those of a new method of data mining.

Article Type: Research Article
Article Title: Volume Domain Validation of ICA-Derived EEG Sources

Philip M. Zeman[1,2,3], Sunny V. Mahajan[1,2], Sharon A. Livingstone[3], Peter F. Driessen[2], Ronald W. Skelton[3], Nigel J. Livingston[1]

[1] CanAssist, University of Victoria, BC, Canada
[2] Department of Electrical and Computer Engineering, University of Victoria, BC, Canada
[3] Department of Psychology, University of Victoria, BC, Canada

Correspondence may be addressed to Philip M. Zeman:
(voice) +1-250-589-4234 / (fax) +1-250-721-6611 / pzeman@alumni.uvic.ca

Abstract

Objectives:

To determine whether the volume-domain characteristics of a *runica* (Makeig et al., 1997) independent component analysis (ICA) decomposition of EEG data can be used to differentiate components relating to brain activity from artefacts. To show ICA convergence characteristics provide confidence in component estimates.

Methods:

Synthetic EEG data containing brain and noise sources were created. The mixture was separated using the runica, ICA algorithm. For each progressive iteration of reduced statistical dependence calculated via runica, scalp variance from component topographies was projected to the volume domain (Zeman et al., 2008b). Using these projections, the peak spectral value, average volume overlap and median volume overlap between estimated component volumes, and the distance travelled by component centers of mass were calculated. ICA components were then ranked using these measures calculated for the final iteration. This was repeated using real EEG data.

Results:

Ranking components according to these measures differentiated synthetic brain activity components from artefacts. Good volume representation was indicated by large peak spectral value while minimal volume overlap and component uniqueness was indicated by low median and average volume overlap. Progressive iterations improved these measures beyond the initial PCA step of runica. The distance travelled by components at each iteration indicated which components had late-converging or non-convergent centers of mass. Analysis of real EEG data yielded comparable results.

Conclusions:

Volume-domain characteristics of components can be used to differentiate artefacts from sources originating from inside the head.

Keywords: EEG; ICA; LCMV beamforming; ICA source validation; data mining; blind source separation.

I. INTRODUCTION

Recently, independent component analysis (ICA) has been used to identify source of neural activity in scalp-acquired EEG data. Studies by Makeig et al. (1996), Jung et al. (2001), Onton et al. (2005) and others (Contreras-Vidal and Kerick, 2004; Makeig et al., 2004) have popularized this approach using the EEGLab toolkit (Delorme and Makeig, 2004) and the runica implementation (Makeig et al., 1997) of the Infomax ICA (Bell and Sejnowski, 1995) algorithm. Each component of the EEG data found by ICA is comprised of a time-varying waveform activity and corresponding scalp topography. Unless otherwise restricted by data dimension reduction methods (Delorme and Makeig, 2004), each ICA decomposition yields as many components as there are electrodes. Generally, a subset of the components of an ICA decomposition pertain to activities of the brain while other components pertain to artefacts.

Although studies have successfully employed ICA, there remains some scepticism regarding its applicability to EEG analysis. We surmise that this partially stems from the absence of a mechanism within the ICA methodology to determine the neuroanatomical and physiological quality of components. Natively, ICA methods use a measure of maximum information to separate the EEG mixture into maximally statistically independent, non-Gaussian components. Brain activities, however, are not necessarily statistically independent, and generally, only a subset of the brain activity components found in a given decomposition of EEG can be related to specific anatomical areas of the brain. Simply, independence is an approximation and does not provide sufficient evidence to support the assumption that the components found are quality estimates of bona fide brain sources. Thus, there is no guarantee that the activities separated from the mixture will pertain to activities originating from specific areas of the brain.

An automated methodology that provides the function of source validation is of particular value when a large number of components result from a decomposition of EEG. Some procedure of selecting possible brain sources from the larger set of components is necessary; especially in such cases when it is not appropriate for a researcher to manually

select their 'favourite' components from a decomposition to draw conclusions about the brain. For purposes of statistical analysis, a clear objective means of component selection is generally preferred and for purposes of exploratory analysis, automated processes can be of considerable aid to the researcher.

Along with the activities of a modular region of brain, a typical ICA decomposition of EEG contains obscure, non-separable background brain activities, line-noise, muscle and eye-movement artefacts. It is worth pointing out an important physical attribute of the sources comprising EEG; brain activities arise from inside the head, while noise activities arise from both inside and outside the head.

The ICA methodology itself may also create artificial 'brain source –like' components from the EEG that are combinations of various noise sources and/or brain activities when the number of components comprising the data has been overestimated. Such components result when a dataset is rank deficient, meaning, that there are more channels than separable sources in the data. Components of this class are herein referred to as 'rank estimate artefacts'. This situation might be avoided using a dimension reduction technique such as Principal Component Analysis (PCA), however the number of sources is usually not known (McCarthy and Wood, 1985) and one can be not certain of the number of dimensions to retain. The problem is that such components can easily be mistaken as bona fide components of the dataset because they can have smooth, dipolar, topographical characteristics (Zeman et al., 2008b; Onton and Makeig, 2006) arising out of random combinations of contributors to the dataset. A methodology that can identify these components from an ICA decomposition is therefore of value.

In this paper we describe a validation methodology that identifies artefacts found in the ICA decomposition from possible brain activity sources by ranking components of the EEG according to their multiple volume-domain attributes. The particular brain activity sources we are interested in identifying are those that can easily be related to anatomy for interpretation; those that relate to physically modular and distinct areas of the brain. We expect that as the time-domain activities of components calculated during the iteration

process of the runica software converge towards a final solution of maximized independence, concomitantly, the volume-domain characteristics of distinct brain activity source components will converge towards values consistent with physical 3-dimensional brain source volumes; these source volumes will be spatially distinct and non-overlapping. Further, components that are well represented in the data are expected to have volume characteristics that converge quickly while those components that lack adequate representation in the data or are components relating to rank estimate artefacts will have volume-domain characteristics that converge slowly or not at all. Our proposed validation process examines both the characteristics of convergence and the final values to which the values to which volume-domain characteristics converge. To distinguish brain activity components from artefacts, components are scored using volume-domain characteristics of their anatomical representation and then sorted according to their scores. We expect that this method of scoring and ranking components by their volume-domain characteristics will provide a means to determine their relative component quality or *goodness,* providing the basis for identifying brain sources from artefacts. In the current study, our validation technique is developed and examined using both synthetic EEG data via a simulated decomposition of EEG data and a decomposition of EEG data collected from a participant of an independent cognitive study.

II. BACKGROUND AND THEORY

Identification of good brain activity components from artefact components has been approached using multiple methods. Perhaps the simplest method is that of examining the percent of the total variance accounted for by each component waveform. By this method, it is assumed that those components with the greatest variance relate to brain activity and the paradigm in which the EEG data were collected while those components accounting for only a small percentage of the total variance relate to artefacts or are activities that are not related to the behavioural paradigm. This however is not necessarily an appropriate measure because often artefacts account for greater variance in the data than brain activities.

Components arising from EEG data decompositions that might represent bona fide brain activities can also be identified via characteristics of their topographies (Jung et al., 2001; Makeig et al., 2004; Onton et al., 2005). Identification of stereotypical artefacts such as eye-blink, eye-movement, and line-noise from the set of components found in an ICA decomposition is a relatively easy task; these artefacts have consistent topographical or time-frequency waveform characteristics (Onton and Makeig, 2007) and prior knowledge and experience is all that is needed to identify them. Such analysis is particularly useful in experiments where only single datasets are analyzed because topographical analysis does not necessarily require validation across datasets gathered from other study participants. For this procedure however, it is advantageous to have expert experience for identifying canonical artefacts and brain activity topographies. Dipole modelling has provided an extension of topographical evaluation of components by mapping the topographical characteristics of components to the volume domain. Through this dipole modelling process, volume domain characteristics such as position of source centers and the 'topographical variance accounted for' by the dipole models have been used to determine the goodness of components. Removal of unusual or uncharacterized artefacts, however, remains an issue (Delorme et al., 2006) and no amount of expertise can provide an objective decision for whether to include or exclude marginal brain activity related components in further analysis steps.

Supplemental to classifying components by known topographical and/or waveform properties is a process of blind clustering of component properties across multiple subjects or multiple data recording sessions (Delorme et al., 2006). It is used as an automated way to separate those components that might be paradigm-related brain activities from artefacts by comparing the decomposition results of multiple datasets. By this method, poorly separated brain activities, inconsistent background brain activities, or rank estimate artefacts can be identified. By using the clustering methodology, it is assumed that components common across a group of study participants (that are not stereotypical artefacts) must be brain sources related to the stimuli and behaviour for each recording session. The comparison across datasets is generally done on multiple

component properties such as by topography, time-frequency waveform, and the location of model dipoles.

Although blind clustering can be useful in some situations, it is not appropriate when separating brain activity components from artefacts in novel experiments because complexities of clustering might lead to incorrect conclusions. For example, there is no assurance that 'experimental effects' discovered will not have arisen from the clustering itself. Delorme et al. (2006) noted that "claims to discovery of physiological facts from component clustering should be accompanied by thoughtful caveat and, preferably, by results of statistical testing against a stable null hypothesis." Thus, blind clustering is not necessarily suitable if the EEG data are exploratory, or if the data were collected in a novel experiment where a stable a priori null hypothesis can not be established.

The goodness of components might also be determined by projecting the variance of topographies derived from an ICA decomposition of EEG to equivalent volumetric representations of variance. This is the basis for the validation methodology proposed in this paper. The method to project topographical variance of individual topographies calculated via and ICA decomposition of EEG data to a model head volume was introduced by Zeman et al. (2008b). In their study, they demonstrated that along with localization of brain source centers of mass, the physical 3-dimensional volume of brain sources can also be estimated in ideal circumstances.

Their volume-domain projection methodology is comprised of the following steps. First, an EEG dataset is decomposed into parts via ICA to yield a set of topographies corresponding to components of the decomposition. The topographies calculated are then used to create data that are idealized for the volume projection algorithm. First, the mean of the electrodes weights defining each topography is subtracted from each topography. The zero-mean topography is then scaled to have unit Euclidian norm. Using the zero-mean and normalized topography, an idealized synthetic source signal is created and idealized uncorrelated noise is added to the idealized signal to create idealized data. These steps assure that an inverse covariance matrix can be calculated from the data.

This process is much like Tikhonov regularization of data (Tikhonov, 1963) for ill-posed problems. A covariance matrix and its inverse is then calculated from the idealized data. This inverse covariance matrix is used in conjunction with the least-constrained minimum variance (LCMV) beamform (Van Veen et al., 1997) algorithm to determine the equivalent relative variances at all locations (or voxels) inside a volume head model. In this case, a BERG (Berg and Scherg, 1994) head model is used. Once the topographical variance is projected into the head volume via the LCMV beamformer, the equivalent volume projected variance must be corrected for distortion caused by non-uniform electrode spacing. This bias correction is done by dividing the projected topographical variance of the idealized data by the uncorrelated noise used to create the idealized EEG data. The result is a bias-corrected projection of topographical variance into a volume domain representation. When no topographical 'signal' is present, the volume-domain representation of variance is equal at all locations in the head. In contrast, when a signal is present, the volume domain variance reflects characteristics of the topography. The bias corrected volume projected variance is called the volumetric spectrum representing the volumetric variance at all voxels inside the head model. This process is thoroughly described in (Zeman et al., 2008b).

Multiple volume-domain characteristics can be derived from the volumetric spectrum of each component. For example, the position-index of the maximum value of the volumetric spectrum in the head model indicates which voxel in the head model has the greatest variance and is thus, considered to be the location of the center of mass of the source corresponding to the topography (Van Veen et al., 1997, Michel et al., 2004). This maximum value is referred to as the peak spectral value and has been demonstrated to be large for sources that are well represented in the volume (having a focal source origin towards a single-voxel representation) and reduced when a component is poorly represented (Zeman et al., 2008b). The peak spectral value is a function of two properties: the normalized variance of the scalp topography and the voxel specificity of the volume-domain representation. The peak spectral value represents how well the electrodes weights, comprising the corresponding topography, together, map variance to a single voxel in the volume-domain projection. This value is reduced if two spatially

distinct brain sources are poorly separated or a single distinct brain source is wide by volume, compared to the case where only one spatially distinct single-voxel brain source is present (Zeman et al., 2008b; Van Veen et al., 1997). Characteristics of the roll-off from the peak spectral value also provide important information about the source. When sources are poorly separated, the volume-projected variance around the center of mass rolls-off from the peak more gradually (Van Veen et al., 1997); essentially the topographical variance is scattered over more head model voxels. Hence, as well as providing a measure of the spatial distinctness of sources, the volume domain representation also provides a means to estimate the physical 3-dimensional space that a source might occupy in the head (Zeman et al., 2008b). The availability of an indicator of the physical space occupied by each component provides a means to calculate the physical overlap of sources.

III. METHODS

Our validation method relies on the following volume-domain characteristics calculated using the volume-projection methodology (Zeman et al., 2008b): the peak spectral value, average volume overlap, median volume overlap, and the distance travelled by component centers of mass for each iterative step of the runica algorithm.

For the current analysis, we first determined if the algorithm would perform as expected on idealized data as it is an assumption that clear convergence of volume-domain properties will result over iterations of the runica algorithm; it isn't appropriate in this first step to complicate the analysis by modelling source activities that are not separable by ICA. This part of the study examined the convergence of volume-domain characteristics of simplified synthetic data to determine whether maximization of statistical independence among idealized brain source time-domain activities relates to improved voxel specificity of their volume representation, decreased volume overlap, and consistent, timely convergence of the centers of mass of these components and in contrast, that canonical artefacts do not share these characteristics. Using the volume-domain characteristics calculated on the final iterative step of the runica algorithm, in

conjunction with the total distance travelled by the centers of mass of components over all iterations of the algorithm, the components were ranked and classified to determine if canonical artefacts can be separated from idealized brain sources.

Once the logical convergence of volume-domain characteristics for modular brain volumes was successfully demonstrated on idealized data, the algorithm was examined using real EEG data in the second part of this study. In the second part, real EEG data were examined to determine if the proposed validation methodology can be applied to data that are more typical of real EEG data having high noise levels, varied strengths of source representation in the data, sources do not perfectly satisfy the assumption of spatial modularity, and sources that do not perfectly satisfy ICA assumptions of non-Gaussianity and statistical independence.

The head model artwork and mathematical head model parameters used for this study was derived from the open-source BrainStorm software package (Baillet et al., 2000; (Berg and Scherg, 1994). A total of 5439 voxels define the three-shell BERG head model with a voxel grid spacing of 0.5 cm There was no constraint placed on the projection of variance other than that variance can only be represented within the confines of the model head volume. Matlab 7 (Mathworks Inc.) and EEGLab 4.515 (Delorme and Makeig, 2004) with the runica source separation algorithm were used to do all modelling, calculations, and plotting.

SIMULATED EEG

Synthetic scalp-EEG data were generated solely for the purpose of determining if, during the iterative steps of the runica algorithm, the volume-domain characteristics of sources would converge to logical values. Hence, a set of 'toy' signals were used to create this EEG because the properties of these signals are known, they are easy to identify, and generally found in other research evaluating signal processing algorithms. The synthetic EEG data were created as the sum of the topographical projection of multiple volume-modelled brain activity sources and additive sensor noise sources. These data were comprised of 6 parts, modelling one distally-placed brain source, multiple proximally-

spaced brain sources, one brain source of large volume, and one electrode artefact. The distally-placed brain source was assigned a unit voxel and was placed in the central cortical region of the right hemisphere to evaluate the simplest source separation case to identify the best possible volume-domain convergence characteristics. The three proximally-spaced sources were situated in the right temporal pole, each occupying a unit voxel to evaluate the convergence characteristics of volume-domain source properties for closely-spaced sources. These sources were assigned common orientations, unique to the orientation of the distally-placed source. A multi-voxel source occupying a volume of 26 voxels was situated in the left ventral pre-frontal region to evaluate the volume-domain convergence characteristics of non-focal (and more realistic) source volumes. All voxels comprising this source were assigned the same orientation, differing from the orientations of all previously placed sources. Each of these five brain sources were assigned visually unique waveform activities: a sinusoid, a ramp, a square wave, a super-Gaussian distribution, and a uniformly distributed waveform. All waveforms had a mean of zero and a standard deviation of one. The scalp topography of each source was calculated by projecting each volume-domain source to the scalp-domain. Using these topographical projections, the activities of each source were summed to create 124 channels, 875 samples/trial, and 29 trials of simulated EEG data with source activities repeating in each trial. Random white Gaussian uncorrelated sensor noise, 28 dB below the average simulated neural source volume level, was added to every trial of simulated EEG after mixing simulated neural sources at the scalp. An electrode artefact 60 dB greater than simulated neural sources was modelled as a random spike event in each trial occurring near the apex of the scalp.

The synthetic EEG, consisting of a mixture of simulated neural activities and simulated artefacts was then subjected to our proposed method for separating signals from artefacts. First, components of the EEG were identified using runica, then the characteristics of convergences of the components were examined in the volume-domain, and finally, the components were ranked based on their volume-domain characteristics.

Decomposition of Synthetic EEG

The runica implementation of the Infomax algorithm (available with the EEGLab 4.515 toolbox for Matlab) was used to separate the synthetic EEG mixture into components. Two non-standard parameters of the runica software were specified. The 'extended' ICA parameter was used to specify 20 training blocks. The 'PCA' (Principal Component Analysis) parameter was specified to reduce the data from 124 to 8 dimensions before performing ICA. While there were only 6 parts comprising the EEG, we purposefully 'over-estimated' this number to generate 2 extra 'rank estimate artefact' components. This was done to view the convergence characteristics of such components and to determine if the proposed methodology would classify such components as artefacts.

The component topographies, calculated at each runica iteration, were stored to allow for volume-domain analysis of each component for each step of minimization. The topographies corresponding to the PCA starting point of the runica minimization process were designated as the result of iteration 1. Topographies calculated in subsequent iterations were stored consecutively increasing from iteration number 2.

Volume Domain Convergence

The volumetric spectra were calculated from the topographies determined at each iteration step of the runica algorithm. Then, for each volumetric spectrum, the peak spectral value (PSV), average volume overlap (AVO), median volume overlap (MVO), and the location of the centers of mass were calculated. From the center of mass locations, the distance travelled (DT) between iterations was calculated.

Peak Spectra Values

The PSV was determined as the maximum value of the volumetric spectrum. It was noted for each component and each iteration step of the runica algorithm. The average and median PSVs were calculated across all components of the decomposition for each iteration of the algorithm.

Volume Overlap Characteristics

The volume overlap of components evaluating how the coefficients of pairs of volumetric spectra vary together was calculated. This was calculated via Equation 1,

$$S_{ij} = \left| \frac{(\mathbf{r}_i - \bar{\mathbf{r}}_i)(\mathbf{r}_j - \bar{\mathbf{r}}_j)^T}{\left\|(\mathbf{r}_i - \bar{\mathbf{r}}_i)\right\|\left\|(\mathbf{r}_j - \bar{\mathbf{r}}_j)\right\|} \right| \quad \textbf{for all } i \neq j \tag{1}$$

where vectors $\mathbf{r}_i$ and $\mathbf{r}_j$ are the volumetric spectra and $\bar{\mathbf{r}}_i$ and $\bar{\mathbf{r}}_j$ are their respective means. Each vector has 1 x P elements, where P is the number of spectral coefficients representing the variance in the head volume. The overlap ranges between 0 and 1 indicating no overlap and maximum overlap, respectively. This calculation essentially makes the comparison of two volumetric spectra as comparing the surfaces of two hyper-surfaces.

The AVO was calculated as the sum across S_j for all $i \neq j$, while holding j constant and then divided by the number of values in the summation. This was repeated for each component j and iteration of runica. Similarly, the MVO was calculated as the median of S_j for all $i \neq j$ while holding j constant and then repeated for each j component and iteration of runica. By these measures the volumetric uniqueness of each component is estimated.

The average AVO and median AVO was calculated across the set of j components for each iteration.

Center of Mass Distance Travelled

For each component at each iteration, the location of each center of mass and DT was calculated. The three-dimensional x-y-z position of the voxel with the largest value (the voxel corresponding to the PSV), the PSV, for each component was determined. Using

the position of the previous step and the position of the current step, the distance travelled, $\boldsymbol{\delta}$ for each iteration $\boldsymbol{k}$ was calculated as in Equation 2,

$$\delta_k = \sqrt{(x_k - x_{k-1})^2 + (y_k - y_{k-1})^2 + (z_k - z_{k-1})^2} \quad (2)$$

where $\boldsymbol{k}$ varies from 2 to the total number of iterations. For iteration number 1, $\boldsymbol{\delta_i}$ is defined to be zero.

Component Ranking and Automated Validation

The components were ranked using the MVO, AVO, and PSV calculated for the last iteration. To provide a summary of the DT, the TDT was calculated as the sum of all $\boldsymbol{\delta_k}$, defined in Equation 2 and was included in the ranking.

REAL EEG DATA

Data Collection and Pre-Processing

Data collected for a separate study of Fetal Alcohol Spectrum Disorder (FASD) (Sorensen et al., 2006) were acquired to demonstrate the validation methodology on real EEG data and to relate these results to the results calculated using synthetic data. The data of one female participant was selected at random from the data of the socially-matched control group of the larger FASD study to analyze in the current study.
Data were collected while the participant navigated a 1st person computer-based virtual arena maze in a paradigm similar to that described by Hamilton et al. (2003). Details of this specific paradigm are described by Sorensen et al. (2006). Participation in the paradigm required the participant to locate the 'correct' platform of 2 visible platforms in each trial using either a 'cue' or 'place' cognitive strategy. The cue strategy required the participant to identify the correct platform by the color of the platform and then move to it using left/right keyboard arrow key presses. The place strategy required participants to identify the correct platform based on configural information of multiple pictures located

on the walls of the arena maze and then once identified, move to it. Each trial was completed when the participant reached the correct visible platform.

These data were sampled using a 128-channel Geodesics sensor net and Net Station acquisition software (Electrical Geodesics, Inc., Eugene, Oregon), with a 500 Hz sample rate. A hardware filter with a high pass cut-off frequency of 0.1 Hz and a low pass cut-off frequency of 200 Hz was used to reduce aliasing related to digital sampling and to remove very low frequency activities.

The EEG data were de-referenced by calculating the average across channels for each individual time sample and subtracting this value from each channel (Yao, 2001). Data trials were extracted from the recorded continuous EEG data to provide analysis around the onset of the task. Trials were segmented as -1000 to 2500 ms such that the onset of the task was at 0 ms. After segmentation, trials were visually inspected for artefacts. Those trials contaminated with non-stereotypical artefacts resulting in excessively noisy data were discarded. Trials containing stereotypical eye-movements and eye-blink artefacts were retained. After trial inspection and rejection, 45 cue trials and 47 place trials remained for further analysis. Next, consistently noisy channels were removed. This left 112 channels of data from the original 128 channels to be used for further analysis. Each trial of data individually was then digitally band-pass filtered 3 to 80 Hz, using a zero-phase linear filter, and down-sampled to 250 samples per second.

Decomposition

The data were decomposed into parts using runica available with the EEGLab 4.515 toolkit for Matlab as was done previously for the analysis of synthetic EEG data. The PCA runica parameter was used to decrease the dimension of the data to 30 dimensions from 112 to reduce the noise in the dataset and to provide a suitable number of dimensions for detailed analysis in this study. (Results calculated from 112 dimensions would not be easily represented in the plots.) Similarly as for the analysis of the synthetic data, component topographies were calculated at each iterative step of the

runica algorithm and were stored for volume-domain analysis of each component. Topographies corresponding to the PCA starting point of the runica minimization process were designated as the result of iteration 1. Topographies resulting from subsequent iterations were stored consecutively increasing from iteration number 2. Topographies resulting from the final iteration of the runica decomposition were plotted.

Volume Domain Characteristics

The components derived from the ICA decomposition were validated similarly as was done previously in the analysis of the synthetic EEG data. The PSV and DT were calculated the same way as was done for the synthetic data. The PSV was derived as the peak of the volumetric spectrum for each iterative step of the runica algorithm and the DT was calculated using Equation 2 as the difference between centers of mass of components between iterative steps of the algorithm. Calculation of the AVO and MVO was done two different ways. First, the MVO and AVO were calculated the same was as was done for the synthetic EEG data (as the dot product in Equation 1 where the mean was subtracted from vectors $\mathbf{r}_i$ and $\mathbf{r}_j$ and the zero-mean vectors were normalized using the Euclidian norm). A second method of measuring overlap was introduced to address instabilities associated with the first overlap estimation method. For this second method of measuring overlap, the means were not subtracted from vector s $\mathbf{r}_i$ and $\mathbf{r}_j$ prior to scaling to it unit Euclidian norm. This is illustrated in Equation 3,

$$\boldsymbol{S}'_{ij} = \left| \frac{(\mathbf{r}_i)(\mathbf{r}_j)^T}{\|(\mathbf{r}_i)\|\|(\mathbf{r}_j)\|} \right| \quad \textbf{for all } \boldsymbol{i} \neq \boldsymbol{j} \tag{3}$$

where the pair-wise overlap is designated as $\boldsymbol{S'_{ij}}$. In this case, the two spectra are compared as one would compare the direction of two vectors, where, in the previous case, the spectra were compared as the covariance of two surfaces. Similarly as for the synthetic data examined previously using Equation 1, a result of 0 indicates that the two spectra compared have no volume-domain overlap while a 1 indicates they have perfect volume-domain overlap.

The summary measures of overlap for each component were calculated as before using the synthetic EEG data however this time they were calculated using the pair-wise overlap S'_{ij}. These summary measures were designated as AVO′ and MVO′, for the average and the median, respectively. The AVO' was calculated as the sum across S'_{ij} for all $i \neq j$, while holding j constant and then divided by the number of values in the summation and was repeated for each component j and iteration of runica. Similarly, the MVO' was calculated as the median of S_{ij} for all $i \neq j$ while holding j constant and then repeated for each j component and iteration of runica. The average AVO' and median AVO' were calculated across the set of j components for each iteration. By these measures we attempted to describe the volumetric uniqueness of each component.

The PSV and DT were plotted along with the AVO, MVO, AVO′ and MVO′ for each component at each iteration of the runica algorithm. To summarize trends of these measures during iterations of runica, the means and medians of these values were also calculated and plotted similarly as was done for the synthetic data.

The distance travelled by the center of mass of each component at each iterative step of the runica algorithm was calculated using Equation 2, in the same way as was done for the synthetic data. From the DT for each component, the TDT was calculated as was done previously. These values were plotted for inspection.

Expert Validation

The results of the proposed evaluation methodology were compared with expert evaluation of components of the EEG decomposition based on their topographical characteristics. A lab member not associated with this research but who analyzes EEG data on other projects was asked to tag each topography given in Figure 5 with a 'B' if the topography suggests the component is a good estimate of brain activity originating from a modular area of the brain, a 'b' if the component represents poorly separated brain activity originating from multiple areas, a '-' of the component represents an artefact or

is very badly separated brain activity, or an ‘E’ if the component relates to eye-movement or eye-blink. If there was uncertainty in determining whether a topography related to an artefact or brain activity, the lab member tagged the topography with a ‘u’. These results were summarized in a table.

Automated Validation

Automatic scoring and classification of each of the components was examined similarly as was done for the synthetic data. The PSV, MVO′, AVO′, values calculated for each component for the final runica iteration were sorted and plotted. The TDT was calculated over all iterations using Equation 2 as the sum of the distance travelled by a given component center of mass over the iteration process. The TDT scores were sorted and plotted. The scores for the final PSV, MVO′, AVO′ and the TDT were sorted in order from worst to best and tabulated. An attempt was made to identify the knee of the curve on each of these sorted plots to identify a separating point between good components and artefacts. The results of validation by the MVO’ and PSV measures were tabulated for comparison with the results of expert validation.

IV. RESULTS

SIMULATED EEG

The runica algorithm converged after 316 iterations, yielding multiple components from the synthetic EEG mixture. The decomposition resulted in five components corresponding to the five simulated brain sources, one component relating to the electrode artefact, and two components resulting from the rank estimation error. Five of the 8 recovered components were identified as the 5 synthetic sources used to create the EEG data and have been numbered: 1, 2, 3, 5 and 6. The topographies and waveforms of these components, calculated for the last iterative step of the runica algorithm, closely matched the synthetic waveforms used in the construction of the data (not shown). By visual inspection of the scalp topographies of recovered components, the electrode

artefact was identified and labelled as component number 4. The recovery of these components demonstrated the successful separation of them from the EEG mixture as was intended by design of the data. Visual inspection of the resulting topographies also revealed two rank estimation error artefacts; these were labelled as component numbers 7 and 8. The topographies of component numbers 7 and 8 appeared to be a mixture of the other sources comprising the data (not shown).

The volume-domain results corresponding to the calculated EEG components are plotted in Figures 1 to 4. The PSVs of each component corresponding to iterative step of the runica algorithm are plotted in Figure 1a. The average and median PSV are given in Figure 1b. The AVO and MVO are plotted in Figures 2a and 2b, respectively. The average AVO and median AVO are plotted in Figure 2c. The DT for each iteration is given in Figure 3. The final PSV and TDT are plotted as Figures 4a and 4b while the final MVO and AVO are plotted as Figures 4c and 4d.

Volume Domain Convergence

Peak Spectral Coefficient Values

By the final iteration of the runica process of estimating maximally statistically independent components via the time-domain activities of the EEG mixture, the PSV of each of the 8 individual components had converged (see Figure 1a). The final PSVs of the brain activity components (1, 2, 3, 5, and 6) are generally much larger than those for the electrode artefact (4) and rank estimate artefacts (7 and 8). The PSV convergence of the multi-voxel component (component 3), is notably smoother than the other components suggesting some fundamental difference between source types. This smoothness is an indication that ICA is sensitive to the voxel specificity of a brain source, since by design, the 26 voxel source is much wider and occupies more voxels than the single voxel sources. The PSVs of all components clearly exceeded the initial value (calculated in the PCA step) over multiple iterations with the exception of the electrode artefact, component (4).

The average and median PSV curves summarize the overall PSV convergence characteristics of all 8 components (see Figure 1b). Both the average and median values are low for the first iteration and increase and stabilize at a higher value. Notably, the average shows a greater overshoot and instability than the median for early iterations as the average estimate reflects components (namely components 1 and 2) that have very large spectral peaks and some initial instability. The overshoot of component 2 plotted in Figure 1a is clearly reflected in the average plotted in Figure 1b. Comparing Figure 1a with 1b, it is clear that the bona fide components provide the greatest PSV contribution that accounts for the overall average and median PSV improvement.

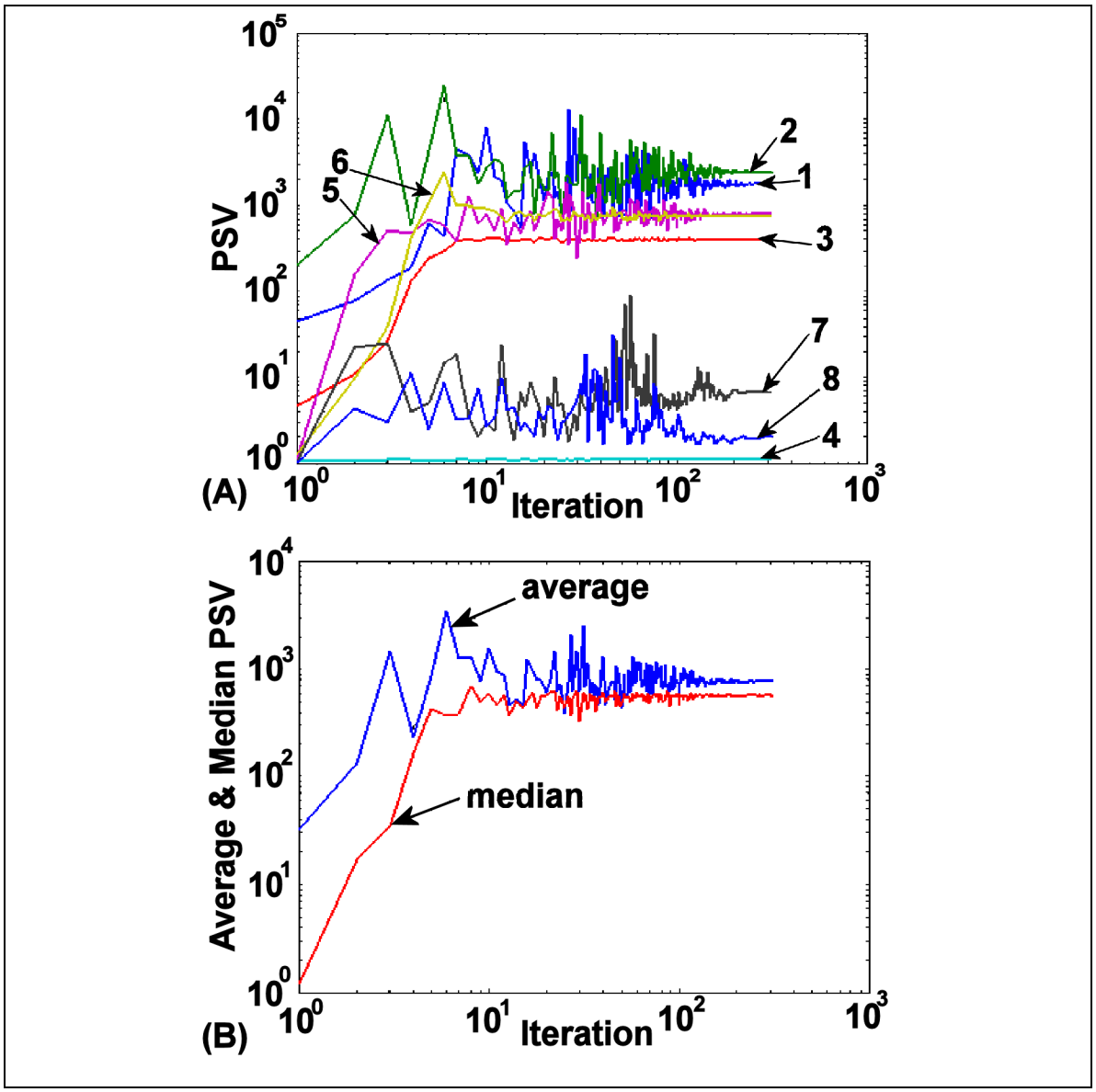

Figure 1. The convergence characteristics of the peak spectral value (PSV) over iterations calculated from synthetic EEG data; (A) for each component at each iteration; (B) for the average and median calculated across components for each iteration. Components identified by ICA are labelled (1) through (8). The horizontal and vertical axes are log-log scale to emphasise early changes in the PSV. The vertical axes are unitless; the volumetric spectrum from which the PSV is derived is calculated using a ratio of variances (Zeman et al., 2008b).

Volume Overlap Characteristics

An illustration of the concept of pair-wise volume overlap is given in Figure 2 showing why this metric is a continuous measure of volumetric similarity. The coefficients describing the projected volume-domain variance for components 5 and 6 (from topographies derived from the final iteration of the runica algorithm) have been plotted on the same figure to compare the relative values of the coefficients. Each coefficient represents the projected volume-domain variance (or spectral amplitude) at a unique location inside the head model. The volume overlap is a summary measure of how the values of coefficients differ at each grid location in the head model. The coefficients are ordered on a 1-dimensional axis according to the index position in the head model. If the two spectra in the figure were both identical, the volume overlap would be exactly 1. This would indicate perfect overlap of the volumetric spectra and that both volumetric spectra pertain to exactly the same brain volume.

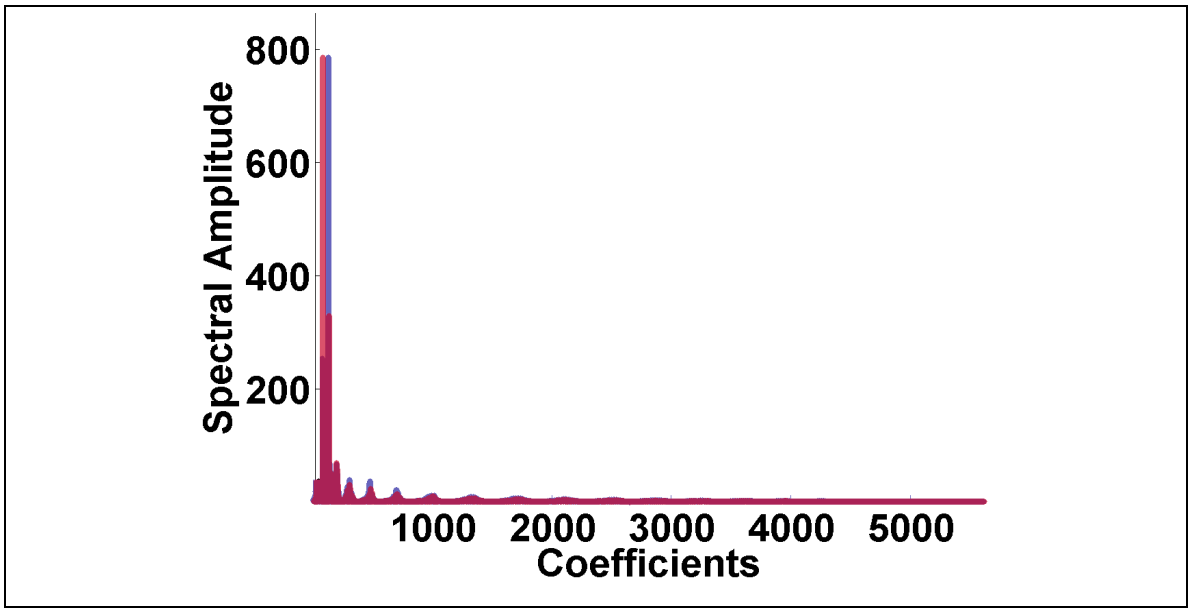

Figure 2. The volumetric spectra of components 3 (light-red) and 4 (light-blue) superimposed to illustrate the concept of pair-wise overlap. Overlapped portion is dark red. Vertical axis: Coefficient value; Horizontal axis: Coefficient index. The more similar the spectra, the greater the calculated overlap ranging between 1 (maximum overlap) and 0 (minimum overlap).

The changes in the AVO and MVO over iterations reveal that the estimated overlap as a covariance of spectral coefficients of volume pairs decreases over runica iterations. The AVO and MVO of each component for each iterative step of the runica algorithm is given in Figure 3a and 3b, respectively. At the second iteration, the AVO of 4 of the 8 components (numbers 1, 6, 7, and 8) dramatically increase and then decrease to values less than the first iteration indicating an initial momentary instability but overall improvement in this volume overlap estimate. The AVO of the remaining components (2, 3, 4, and 5) decrease from the first iteration to the second and generally continue to improve thereafter. The MVO reveals a similar pattern for all components; after the second iteration the MVO for each component decreases. This general decrease shows multiple local peaks and irregularities to approximately 200 iterations at which point the AVO and MVO stabilize.

The average and median AVO for all 8 components are given in Figure 3c. As with the AVO and MVO for each component separately, the average and median AVO show the initial increase in the estimate of volume overlap on iteration number 2 and that these values decrease quickly towards convergence at a low estimate of overlap. This indicates that when the values converge, the sources are unique by modular volume and therefore well separated. During convergence, however, local peaks and irregularities continue for about 200 iterations and then stabilize. The final average and median AVO are lower than those values calculated for the first iteration, indicating that ICA separation of these sources reduced the effective volume overlap of components.

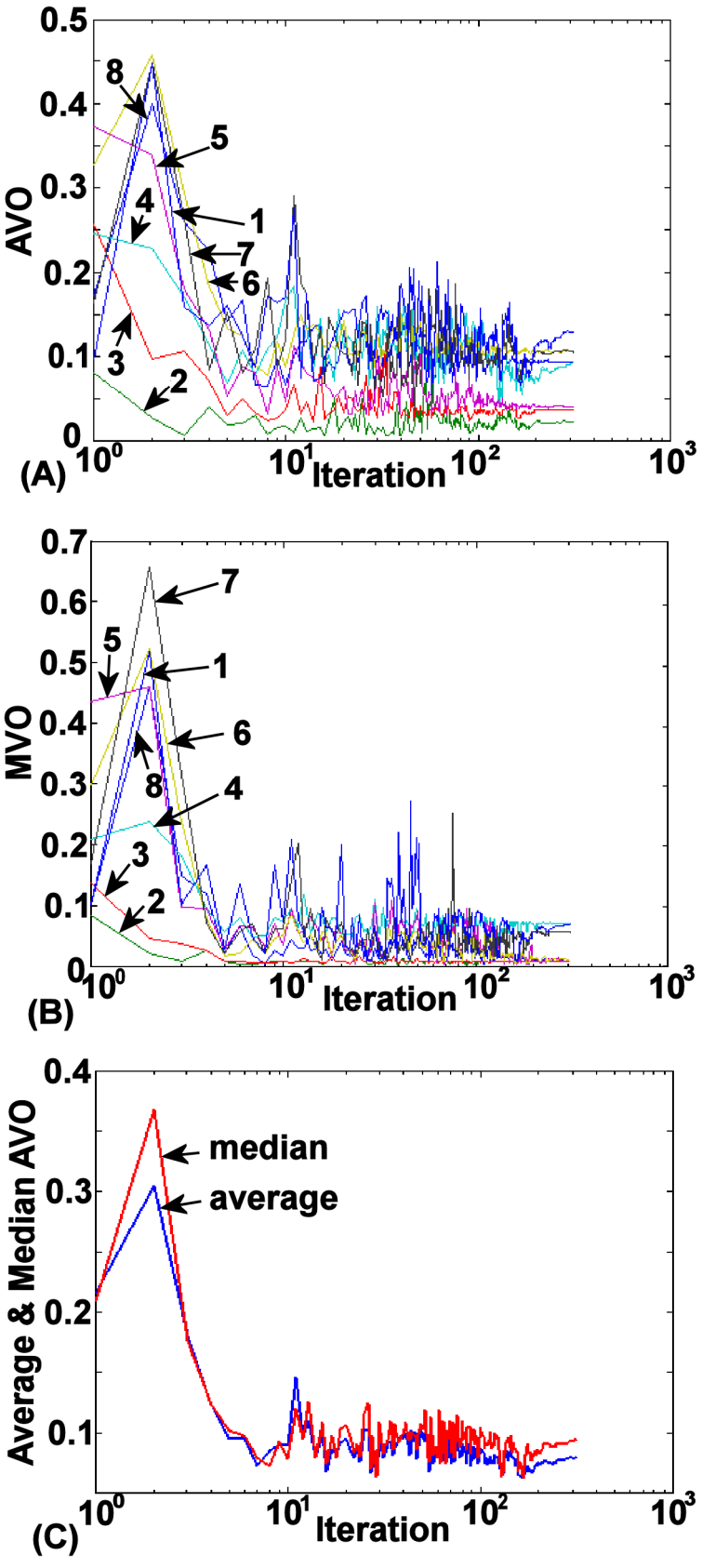
AVO
Iteration
(A)
MVO
Iteration
(B)
Average & Median AVO
median
average
Iteration
(C)

Figure 3. The convergence characteristics of the average volume overlap (AVO) and the median volume overlap (MVO) over iterations calculated from synthetic EEG data; (A) the AVO for each component; (B) the MVO for each component; (C) for the average and median AVO calculated across components for each iteration. Components identified by ICA are labelled (1) through (8). Plots are log-log scale to emphasise early changes in the MVO and AVO. The vertical axes are unitless as values are derived as dot products of volumetric spectra (Zeman et a., 2008b).

Center of Mass Distance Travelled

Figure 4 illustrates the instability of the rank estimate error components (components 7 and 8). The main plot of the figure illustrates the distance travelled by the centers of mass of the rank error components for each runica iteration. The continuous movement of the center of mass of these components beyond the 200th iteration , and up to approximately iteration 300, is indicated by the arrow (g) in the figure. For comparison, the distance travelled for each iteration of the more stable bona fide components in the data are indicated by arrow (a) showing convergence before the 15th iteration. Notably, the centers of mass of these components never travel more than 2 cm on an iteration and are represented only in the bottom left-hand corner of the figure. On a single iteration, the rank estimate error artefacts, however, moved distances greater than 7 cm -- greater than half the width of the brain. The inset of Figure 4 provides a 3-dimensional depiction of the travel of the centers of the mass of the rank-error estimate components, displaying their spatial variation (indicated by arrow (c)). This 'spider web' of lines showing the path of the centers of mass between iterations clearly shows the unreliability of these components. Their centers of mass do not simply reverberate around a single location, but travel around most of the right hemisphere. The centers of mass of bona fide components (1, 2, 3, 4, 5, and 6) clearly have different characteristics of travel. They move a very short distance (as indicated by the main figure window) and are thus minimally represented in the 3-dimensional plot of the figure inset. The summary statistic, TDT captures the extent of travel of these components for the entire minimization process.

The starting location of each center of mass is indicated as a '+' in the inset of Figure 4. The final locations are indicated in the figure inset as (b) for the three proximal simulated brain sources (f) for the single 26 voxel brain source, (d) for the distal brain source. The electrode artefact component (4) did not travel after the first PCA iteration and has zero travel distance, indicated in the figure inset as (e).

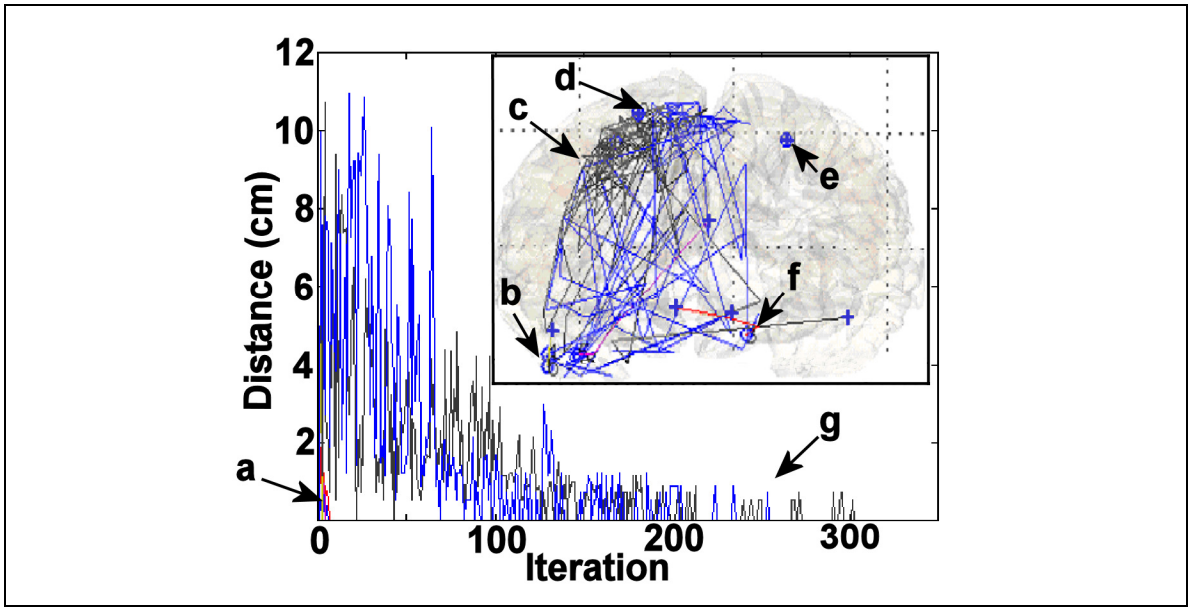

Figure 4. Movement of component centers of mass for each iteration of the runica maximization of statistical independence revealing major differences between components of source activities versus components resulting from rank estimation error (calculated from synthetic EEG data). Main Figure: Distance travelled (DT) is the difference in location of centres of mass from one iteration to the next. The distances travelled for the rank estimation error components (7) and (8) are large and carry through past iteration 200. These are given in blue (component 7) and black (component 8). The late center of mass changes for these components is indicated by label (g). The source activity components (1, 2, 3, 4, 5, and 6) travel short distances and convergence before iteration 15 as indicated by label (a) and are barely visible on the figure. They are indicated by a minute red and yellow lines in the plot left bottom corner of the plot. Inset: A Frontal view of 3D model brain. Path of travel is indicated with start position (+) and end position (O). Components are labelled as (b) proximal brain activity

components (1, 5, and 6); (f) multi-voxel brain activity component (3); (d) central distal brain activity component (2); (e) electrode artefact component (4); (c) web of path of travel indicated by connecting lines for components (7) and (8). Most connecting lines visible in the figure result from movement of (7) and (8) labelled in blue and black, respectively.

Component Ranking By Volume Characteristics

Each of the 8 components are ranked in Figure 5 on the basis of their final PSV, AVO, MVO, and TDT scores to illustrate how relative scoring by each measure separates artefacts from the simulated brain sources. For each figure, the values have been sorted and plotted from left to right such that the worst components are on the left side and the best components are on the right side of each plot. Where possible for each measure, a line dividing brain activity components from artefacts indicates that the measure separated artefacts (or a class of artefact) from other components. The ranked PSVs are given in Figure 5a, with a separation of the 'rank estimate artefacts' (7) and (8) and the electrode artefact (4) from the simulated neural components. Similarly in Figure 5c, the MVO clearly separates artefact components (7), (8), and (4) from the simulated neural components. Figure 5b illustrates clear separation of the 'rank estimate artefacts (7) and (8) from the other components using the measure of TDT. Lastly, Figure 5d shows that artefact and simulated neural source components were not separated using the AVO.

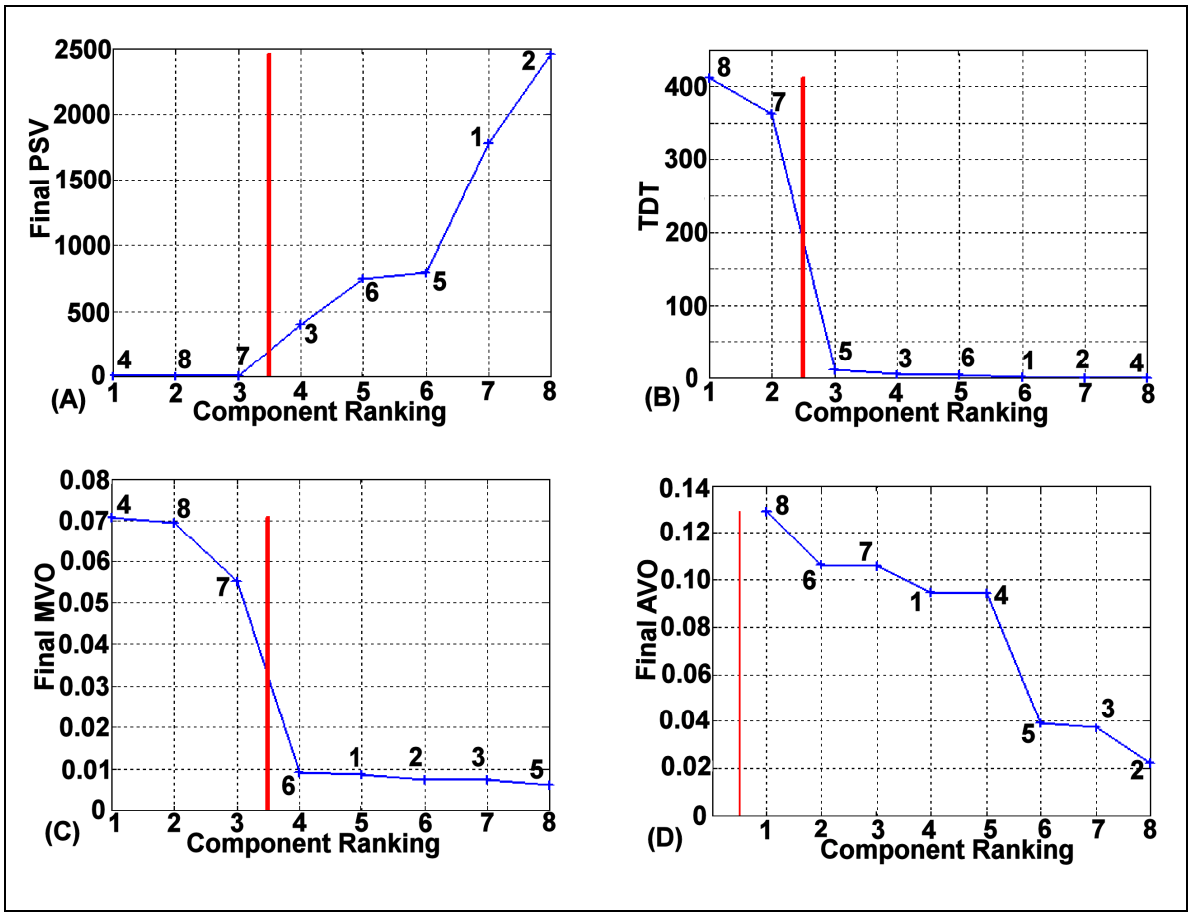

Figure 5. Ranking results for components calculated from synthetic EEG data. (A) peak spectral value (PSV); (B) total distance travelled (TDT); (C) median volume overlap (MVO); (D) average volume overlap (AVO). Component numbers are indicated on the plots next to each rank position point (+). Wherever possible, a vertical line was placed in each figure where natural features in the data separate artefacts from brain activities. The plots shows that those components that score well on all three measures of MVO, PSV, and TDT are 'good' modular brain sources.

REAL EEG DATA

The runica decomposition and following component validation process followed steps similar to the analysis of the synthetic EEG data. The runica decomposition of real EEG data automatically converged and exited after 488 iterations yielding 30 components with corresponding waveforms and topographies. The topographies of components calculated for the final iteration are plotted in Figure 6 for visual inspection. A subset of these

components likely corresponds to good representations of brain activities originating from modular areas of the brain while others are artefact, non-modular brain activities that do not pertain to a specific area of the brain, or are poorly separated brain activities.

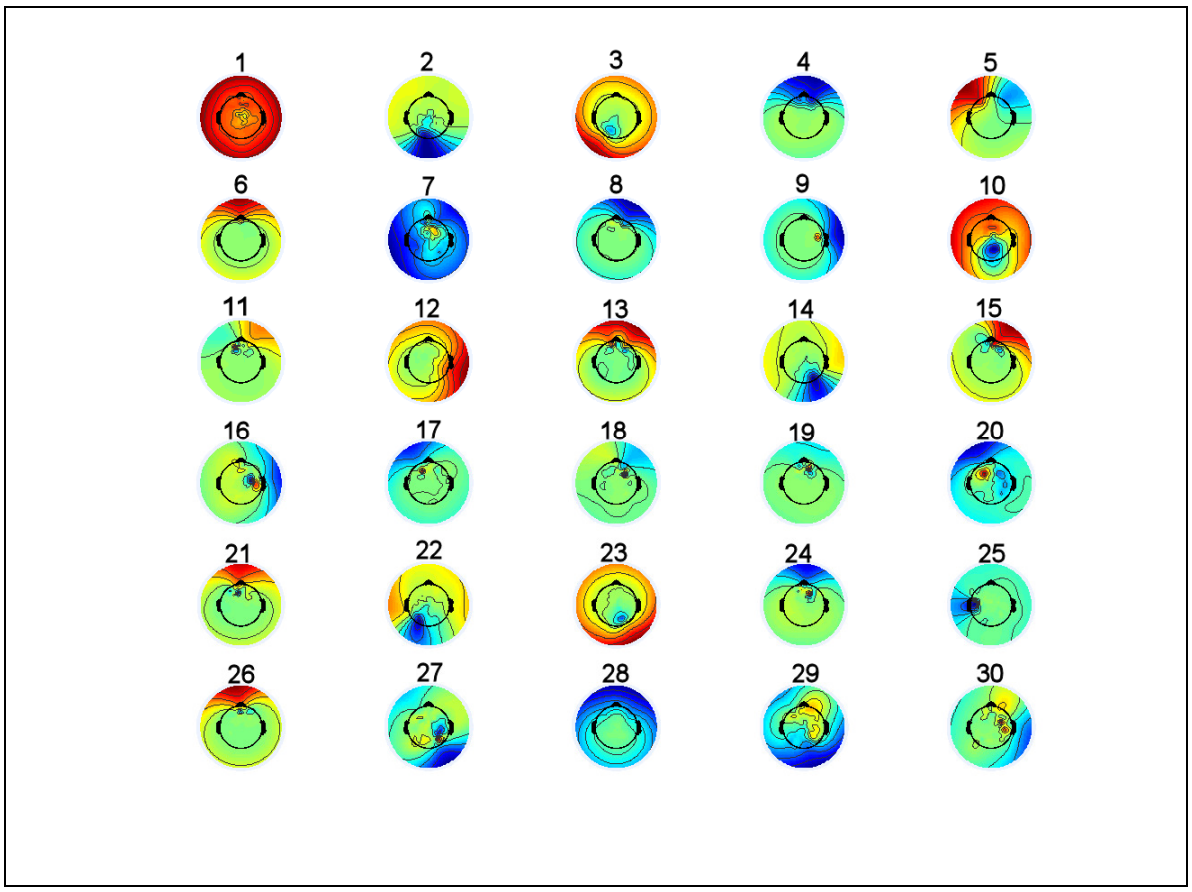

Figure 6. Topographies of components calculated from real EEG data that were returned by runica source separation. Each topography has been assigned a unique number identifier. Scalp intensities vary from negative values (blue) through to positive values (red).

Volume Domain Convergence

The average and median PSV convergence curves plotted in Figure 7a show that, runica processing of real EEG data, generally improves the volume-domain specificity of components. Essentially, over sequential steps of the runica iterative process, the volume representations of components become more focal towards a single voxel, and specific to

a particular region of the head. By iteration 100, the median PSV plateaus; subsequent iterations actually decreases the median value slightly suggesting possible overtraining of the ICA weight separation matrix and iteration of the runica algorithm on noise. The average PSV from iteration 100 to 488 is visually flat. The median and average PSV of components clearly exceeded the initial value (calculated in the PCA step) over multiple iterations. The offset difference between the median and the average (the average has a large positive offset compared to the median) suggests that the PSV improved by a large amount for a small number of components while for most components, the PSV improved only by a small amount, decreased, or did not change.

The changes in the average and median AVO and MVO given in Figure 7b suggest that the measure of volume overlap by how the coefficients of the covary as a surface using the current AVO and MVO measures is unstable for real data. This instability is evident as an initial spike for both the MVO and the AVO corresponding to early iterations (similar to the case for the synthetic data), however after the spike the measures only decrease by a small amount and then slowly increase as iterations continue. After iteration 100 (for which the PSV converged), the average and median MVO and AVO begins to diverge and increase; the average and median measures do not converge for the real data as it did for the synthetic data.

The changes in the average and median AVO′ and MVO′ (which make volume overlap comparisons analogous to comparing the direction of vectors) of Figure 7c reveal that this measure of estimated overlap generally decreases over runica iterations and is a stable measure. By iteration 100 these plots appear to be nearly converged on minimum values. The median and average plot of the MVO′ demonstrates a slight increase between iteration 100 and 488 suggesting possible overtraining.

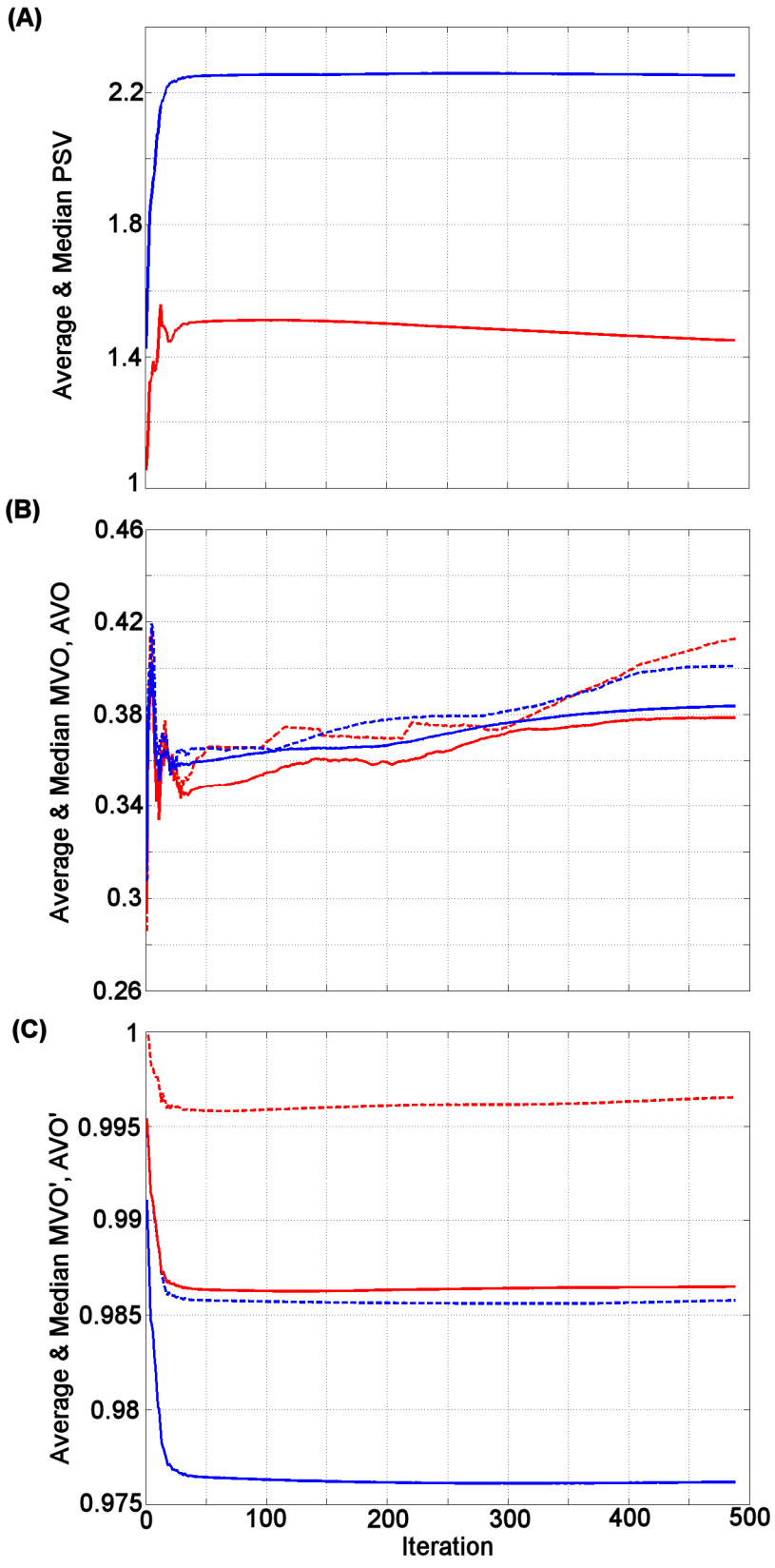
(A)
Average & Median PSV
2.2
1.8
1.4
1
(B)
Average & Median MVO, AVO
0.46
0.42
0.38
0.34
0.3
0.26
(C)
Average & Median MVO', AVO'
1
0.995
0.99
0.985
0.98
0.975
0
100
200
300
400
500
Iteration

Figure 7. The convergence characteristics of the average volume overlap (AVO), median volume overlap (MVO) and the peak spectral value (PSV) of components over iterations calculated for real EEG data; (A) the average and median PSV calculated across all components of the decomposition; (B) the average MVO and AVO, and the median MVO and AVO calculated across all components of the decomposition. The vertical axes are unitless as values are (A) derived as a ratio of variances and (B) derived as dot products of volumetric spectra.

Examining the AVO and MVO of individual components in relation to the average plot of Figure 7b reveals that the AVO' and MVO measure is indeed unstable for real data (results not shown). Many of the individual components have AVO and MVO values that change from decreasing to increasing after iteration 50 while others change between decreasing to increasing multiple times prior to completion of the runica algorithm indicating that these measure are not a good property to describe the volume overlap and volume uniqueness characteristics of an individual component.

Examining the PSV, AVO′, MVO′ and DT for components individually (Figure 8) shows improved volume-domain characteristics over the runica estimation process for a select subset of components. Notably for approximately 15 components, the PSV (Figure 8a) increased as expected while the MVO′ and AVO′ (Figures 8d and 8d, respectively) decreased as expected. Interestingly, the MVO' of all of the components started at approximately 1 indicating that after the PCA step of the runica algorithm, there was considerable overlap among all components of the decomposition. By iteration 100 of the runica process most components appear to have converged according to the PSV, MVO′, and AVO′ plots; this is with the exception of component 20 which appears to be approaching convergence. Up to iteration 100, these volume-domain characteristics have improved for at least 15 components. After approximately iteration 100, the PSV, MVO′, and AVO′ of a subset of these components experience small reductions in improvement suggesting over-learning. The DT for each iteration illustrated in Figure 8c shows that the centers of mass of most components converged prior to iteration 50. However, the

centers of mass for 8 components continued to make small movements (steps less than 3 cm) between iteration 100 and iteration 450. These later movements occurred for component numbers 10, 17, 20, 29, 7, 13, 21, and 11.

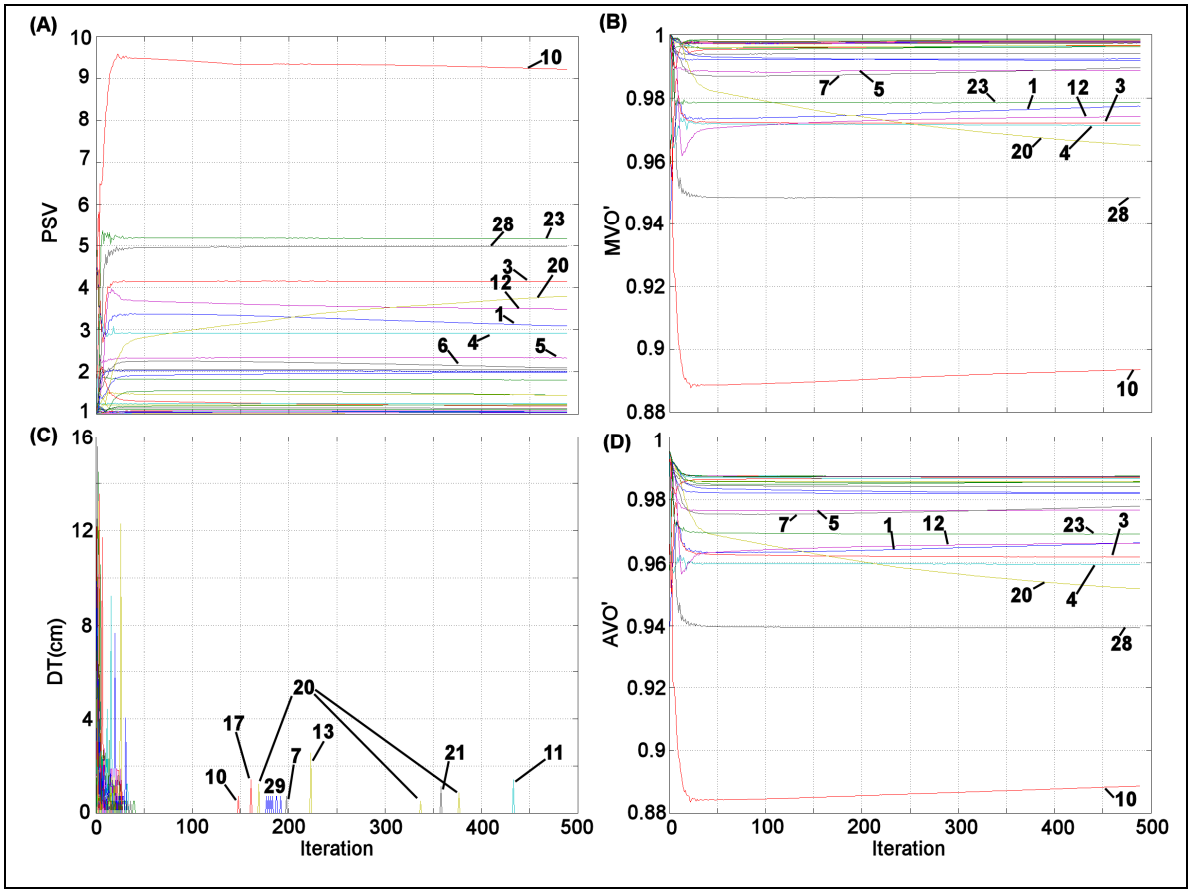

Figure 8. The convergence characteristics of each component indicated by the (A) peak spectral value (PSV); (B) the median volume overlap (MVO); (C) the total distance travelled by the center of mass in centimetres (TDT); (D) the average volume overlap (AVO). The vertical axes for (A, B, and D) are unitless; the volumetric spectrum from which the PSV is derived is calculated using a ratio of variances and the median and average volume overlaps are dot products of volumetric spectra. In plot (C) those components with late iterations are indicated in the figure. In plots (A, B, and D) only those components with final values that are visually distinguishable have been labelled. (See Table 1 for the final values of all components.)

Component Ranking By Volume Characteristics

Each of the 30 components are ranked in Figure 9 on the basis of their final PSV (Figure 9a), AVO′ (Figure 9b), MOV′ (also Figure 9b), along with the TDT (Figure 9c) over iterations of runica to determine which of these components could be representative of modular brain sources. In each figure, the sorted values are plotted from left to right such that the worst components are on the left and the best components are on the right. Where appropriate, a vertical line indicating the knee of the curve has been placed to divide the left and right plot areas. The relative PSV scores of Figure 9a suggest that components 10, 23, 28, 3, 20, 12, 1, 4, 5, 7, 14, 22, 29, 2, 27, and 16 might be components originating from the head that could represent brain activities of varying qualities. The remaining components 15, 13, 19, 11, 18, 8, 24, 26, 9, 21, 17, 30, 6, 25 are allocated as artefacts. The relative MVO′ and AVO′ scores plotted in Figure 9b are very similar each other and their ranking also have some similarity to the ranked PSV scores. The MVO′ and AVO′ scores suggest that components 2, 14, 22, 29, 7, 5, 23 ,1 ,12 ,3 ,4 ,20 ,28 ,10 are possibly components that originate from inside the head and have varying degrees of 3-dimenstional volume overlap. The MVO′ and AVO′ scores indicate that components 30, 9, 18, 24, 15, 19, 13, 8, 11, 26, 6, 21, 17, 27, 16, and 25 are artefacts. The TDT plot of Figure 9b does not have a characteristic curve from which a knee can be selected to separate possible artefacts from sources originating from inside the head. Instead it provides a relative ranking of the stability of each of the components where components 17, 18, 15, 1, 7, 19, 5, 3, 25, 27, 10, 9, 8, 26, 23, 2, and 6 are most stable and components 20, 24, 30, 29, 16, 13, 11, 14, 28, 12, 4, 21, and 22 are less stable. Taken together, the AVO′, MVO′ and PSV plots indicate that approximately half of the components of the decomposition can automatically be regarded as artefacts and can thus be automatically rejected from further analysis.

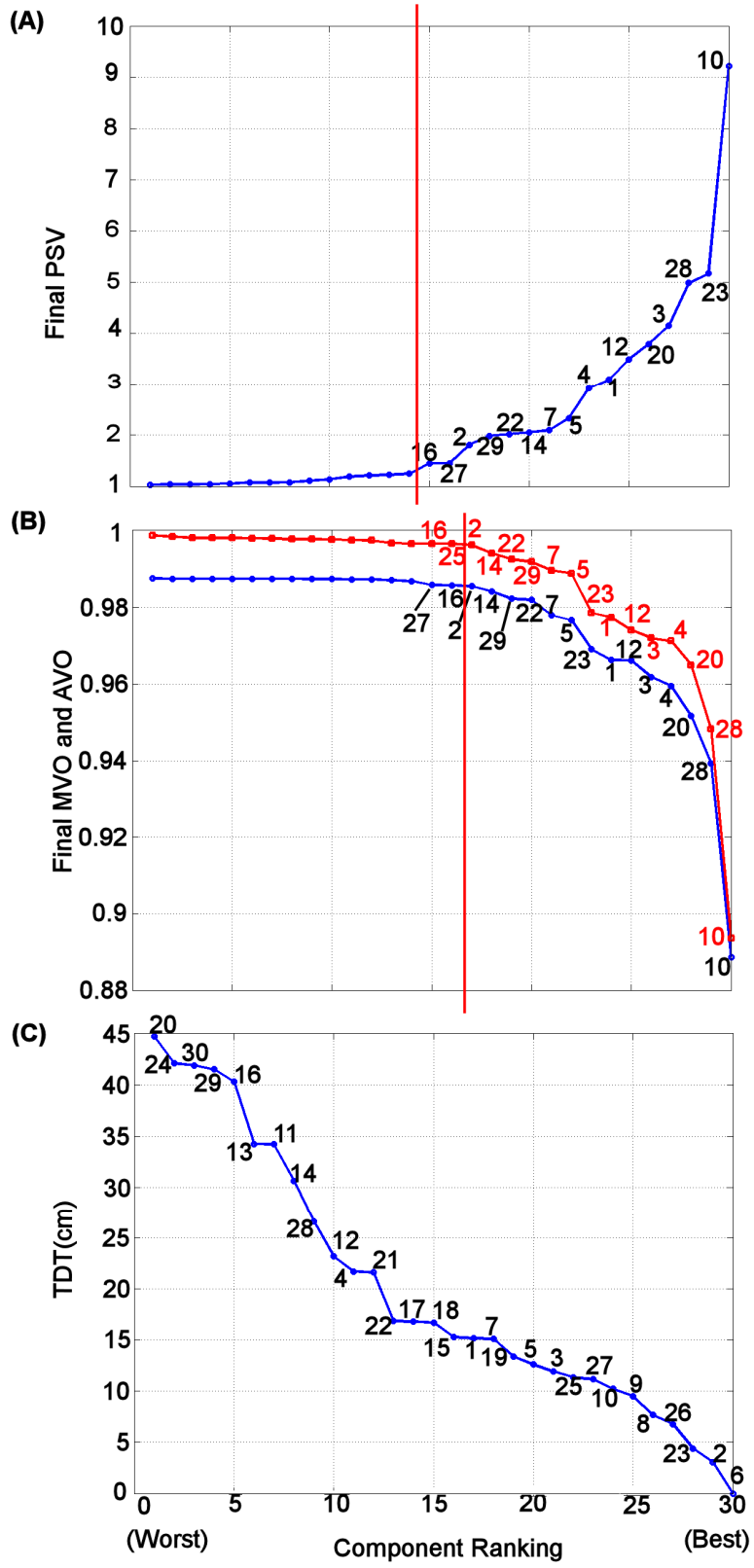
(A)
Final PSV
(B)
Final MVO and AVO
(C)
TDT(cm)
(Worst)
Component Ranking
(Best)

Figure 9. Ranking results for components calculated from real EEG data. (A) peak spectral value (PSV); (B) median and average volume overlap (MVO and AVO); (C) total distance travelled (TDT). Component numbers are indicated on the plots next to each rank position point. A vertical line was placed in (A) and (B) to indicate the knee of the curve. (No knee is evident for (C).)

The ranked scores for the PSV, MVO′, AVO′, and TDT are given in Table 1 such that the best components according to each measure are on the right side of the table while the worst components according to each measure are on the left side of the table.

PSV	15,13,19,11,18,8,24,26,9,21,17,30,6,25,16,27,2,29,22,14,7,5,4,1,12,20,3,28,23,10
MVO	30,9,18,24,15,19,13,8,11,26,6,21,17,27,16,25,2,14,22,29,7,5,23,1,12,3,4,20,28,10
AVO	9,18,15,24,26,11,19,13,8,6,21,30,17,25,27,16,2,14,29,22,7,5,23,1,12,3,4,20,28,10
TDT	20,24,30,29,16,13,11,14,28,12,4,21,22,17,18,15,1,7,19,5,3,25,27,10,9,8,26,23,2,6

Table 1. Component scores for PSV, MVO, AVO, and TDT sorted from worst to best from left to right. For PSV, the largest PSV corresponds to the component on the right side of the table while the lowest PSV corresponds to the component on the left side of the table. For MVO and AVO, the largest value corresponds to the component on the left side of the table while the right side of the table contains the component corresponding to the smallest value. The component with the largest TDT is given on the left side of the table while the right side of the table contains the component with the smallest TDT.

Expert Validation vs. Volume-Domain Validation

The results of expert validation of components by visual inspection of their topographies of Figure 6 are tabulated in Table 2. Components are allocated as either ‘E’ for eye-artefact, ‘B’ for good brain activity that might originate from a single modular brain location, ‘b’ for a poorly separated brain activity, and ‘-’ indicating that the component is clearly an artefact. Components that are ambiguous are tagged with a ‘u’.

Also provided in Table 2 are the ranking of components by the PSV and MVO′ scoring process is given in Table 1 to compare the automated and expert ranking results. The

comparisons shows that the MVO′ and the PSV are complimentary; if either of the MVO′ or the PSV find a component as an artefact, then that component should be allocated as such. Those components listed as artefacts by the proposed validation method are in agreement with the expert analysis with the exception of components 7 and 27. Comparing the expert allocation of artefacts as eye-artefacts with the proposed validation method indicates that the validation method does not identify eye-movement or blink contamination of the EEG as artefact.

cnum	**1**	**2**	**3**	**4**	**5**	**6**	**7**	**8**	**9**	**10**	**11**	**12**	**13**	**14**	**15**
expert	B	B	B	E	E	-	-	-	-	B	-	B	-	B	-
PSV	H	h	H	H	H	-	H	-	-	H	-	H	-	h	-
MVO	V	v	V	V	V	-	V	-	-	V	-	V	-	v	-
Cnum	**16**	**17**	**18**	**19**	**20**	**21**	**22**	**23**	**24**	**25**	**26**	**27**	**28**	**29**	**30**
expert	-	-	-	-	b	-	B	B	-	-	-	B	E	b	-
PSV	h	-	-	-	H	-	h	H	-	-	-	H	H	h	-
MVO	-	-	-	-	V	-	v	V	-	-	-	-	V	v	-

Table 2. Rating of components calculated from the real EEG dataset for the PSV, MVO, and by expert evaluation. ‘cnum’ indicates the component number corresponding to Figure 5. The rating types for expert validation are: ‘B’ = good distinct modular brain activity; ‘b’ = poorly separated brain activity; ‘-‘ = artefact or very badly separated brain activity; ‘E’ = eye-movement or blink related component; ‘u’ indicates the expert was uncertain. The rating types for validation by PSV are: ‘H’ = good head model representation and voxel specificity; ‘h’ = moderate head model representation and voxel specificity; ‘-‘ = poor head model representation and voxel specificity indicating an artefact. The rating types for validation by MVO are: ‘V’ = good volume uniqueness (minimum overlap); ‘v’ = moderate volume uniqueness (moderate overlap); ‘-‘ = poor volume uniqueness indicating an artefact.

V. DISCUSSION

The major contribution of this paper is in providing a method to distinguish ICA components that relate to possible brain activities originating from within the head from those relating to noise and artefact. This was accomplished using both simulated EEG

and real EEG data. We simulated EEG recorded from 124 electrodes in standard positions on a head as would be generated by 5 neural sources of activity in the head, combined with artefact contribution at the scalp to determine the ideal estimated volume-domain characteristics of physically distinct, modular brain sources versus those of a canonical artefact. Typically in EEG analysis, the number of sources is unknown (McCarthy and Wood, 1985) therefore our simulation also mimicked this scenario searching for more sources than actually existed in the data using ICA. We then examined our proposed method for determining the goodness of estimated brain sources by evaluating how volume-domain characteristics of sources converge to stable values during runica iterations and how the final values found by ICA differ between types of components. By sorting and ranking these characteristics, we were able to clearly distinguish the simulated neural sources from artefacts.

The validation methodology was then applied to real EEG data to examine the usefulness of volume-domain characteristics for separating artefacts from good component representations of brain sources in a real scenario. In doing so, an additional measure of volume overlap for separating artefacts from brain sources was introduced. The volume domain measures were then used to determine which components of the decomposition of real EEG data related to possible brain sources or artefacts, providing the function of component validation. The validation results calculated on the real EEG data using the proposed algorithm were then compared to manual expert validation results and results were found to be comparable. The validation methodology distinguished artefacts from those components that were good representations of brain activity, with one exception; the proposed algorithm did not identify occular components as artefacts. The automated algorithm however was helpful in objectively determining which components where marginal estimates of brain activity and which of these estimates of brain activity should be allocated as noise.

CONVERGENCE CHARACTERISTICS

Peak Spectral Values

The convergence curves for the average and median PSV showed that runica iterations improved separation of simulated brain sources and artefacts beyond the first PCA iteration. They both increased from their starting values and converged at values larger than their starting point. A similar result was found for the real EEG data where the average and median PSV curves increased and converged at values greater than their initial values. Thus, the average and median PSV calculated across components for each iteration is a good indicator of the progression of the runica algorithm in identifying sources originating from focal areas of the head.

When examining the synthetic data, the median PSV provided a better measure of the trend of convergence of volume representation than the average PSV. The average PSV was greatly influenced by the PSV of the single-voxel simulated brain sources (components 1 and 2). This is likely because the PSVs of these components are much larger than those of the other components and only a small number of components were examined. These components have high voxel specificity; whereas, the multi-voxel brain volume has a broader volume definition. In this case, the median measure provides a better summary statistic of all components than the average, as it is less influenced by a small number of components. The average and median PSV curves for the real EEG data are similar to the synthetic data. Together these results suggest the PSV is a good measure of performance of the source separation algorithm.

The simulation results demonstrate that source estimation improvement of modular brain sources provided by iterative steps of the runica algorithm is evident by volume-domain improvement in the PSV. Evaluation of the PSV of each individual component showed that the convergence curve of the PSV for artefacts is characteristically different than that for brain activity components. The consistently very low convergence curve of the electrode artefact PSV (component 4) indicates that it is very poorly represented by

volume nor is not well represented as a scalp topography defined by multiple electrode weights with unit Euclidean norm. Normalization of topographies in this way is a required step of the volume projection algorithm use (Zeman et al., 2008b). For this case, the runica algorithm provides little refinement beyond its initial separation from other components. The PSV of components relating to rank estimate artefacts indicate that they may be characterized as having slightly better volume-domain or topographical characteristics than electrode artefacts, but lower than the bona fide brain sources. The simulation results indicate that PSVs curves, calculated for real EEG data, to which brain activity components converge should be greater than for electrode artefacts and rank estimate error artefacts. This was confirmed by the results of the PSV curves calculated using the real EEG data. Generally, the PSV of those components that were eventually identified as good brain activity components increased over iteration steps of the runica algorithm.

Volume Overlap Characteristics

Measuring the volume overlap by the dot product of the normalized volumetric spectra as in Equations 2 and 3 in this way is not a measure of how a pair of 3-dimensionl volumes with clear edges and boundaries overlap. It is a continuous measure of the similarity of the projected variances that includes a decreasing level of source-related variance as the distance from the center of mass increases. Eventually the source-related variance meets the noise floor of the volume projection. Thus, the measure is sensitive to the variance at all locations in the head. In this way, a continuous measure of overlap, the MVO, AVO, or MVO' and AVO' can be obtained that is independent of any statistical noise thresholding.

Generally, iterative steps of the runica algorithm decreased the volume overlap of components in the simulation as measured by the MVO and AVO calculated as a measure of how the projected voxel variances co-vary. The average and median AVO showed that runica iterations improved separation over the initial PCA iteration, decreasing overlap to a stable value. Both the average AVO and the median AVO

indicate that there is greater overlap for the 1st iteration (PCA step) than for the final ICA result. For the 2nd iteration (1st ICA step) however there is a momentary increase in source overlap. This might be related to large changes in the rank estimate artefact components relating to noise. After approximately 100 iterations, the volume overlap is less than that at the first iteration however the overlap between iterations 100 and 200 increases, again, possibly due to the instability of 'rank estimate artefact' components (7and 8).

The AVO and MVO measures of individual components for the simulation show characteristic differences between simulated artefacts and modelled brain activity components, primarily, around and including, the final runica iteration. In contrast to the PSV measure, where the convergence curves of brain components and artefacts differ, there is no clear, consistent difference in the early convergence characteristics of the MVO across components. This is likely because the MVO and AVO for a given component are sensitive to changes in all other components of the decomposition, including artefacts. The results demonstrate however, that for converged values, the final value of the MVO differentiates between the simulated neural sources and the artefacts.

This properties of the MVO and AVO were different for real EEG data compared to the simulated data. The average and median AVO and MVO demonstrated substantial instability and only began to converge very late in the runica source separation process indicating that this measure of overlap using the MVO and AVO is unstable. We believe this is largely a result of characteristics of the noise in real EEG data that were not adequately modelled in the simulation; namely, that there are at least as many artefact components in the real EEG as there are modular brain source components and our prior work shows that pair-wise volume overlaps involving artefact components are much larger than well-resolved brain activity components (Zeman et al., 2008b). Since the AVO and MVO are calculated across components of the decomposition, all artefact components affect it. The average volume overlap (AVO) or median volume overlap (MVO) is calculated across the set of pair-wise relationships of the components of the decomposition (see Equation 1). Changes in the convergence curve of the average and

median AVO and MVO after iteration 300 could be the result of changes in the noise components of the decomposition. Because of this instability and sensitivity to noise, a modified version of overlap, the MVO' and AVO', was introduced.

The measures of average and median MVO' and AVO' calculated for real EEG data show that the overall during the runica source separation process, the overlap of components decreased. The result that these values also converged early and remained stable demonstrates that they are a better measure of volume overlap than the original measures used in the simulation. The result that the overlaps of the volumetric spectra decreased for a subset of components suggests that only a subset of components were separated into parts that have non-overlapping volumes during the runica source separation process and that these components probably relate to activities originating from within distinct modular areas of the brain.

The clear difference between the MVO calculated for the synthetic EEG data and the MVO' calculated using the new estimation of overlap for the real EEG data is that in the overlap numbers for the new MVO' are much larger than the old overlap numbers for the MVO. During our experimentation using simulated data, we evaluated both methods of estimating component overlap and found them to be similar except for this apparent 'offset' of values. We found that even for the model data, estimating the MVO as the Euclidean norm dot product of two vectors yielded larger numbers than when the mean is subtracted before calculating the norm of each vector and the subsequent dot product. The reason for this 'offset' is simple. The numbers of the MVO' are high (suggesting a small difference between compared vectors and therefore large overlap) because most of the coefficients are small-valued and relate to noise if a source has a focal volume and is represented by a small number of coefficients. However, as long as the projected variance increases for a small number of coefficients at a specific unique location while the other coefficients at all other locations remain small and random, the vector will continue to orient to a unique location and thus be increasingly unique when compared to the vectors describing other components.

Using the PSV and the MVO' together provides a complimentary approach to validating components. While the MVO' and the PSV appear to provide the same information, they do not, and having both PSV and the MVO' to characterize components is better than having only the PSV. The PSV is a result of both the voxel specificity of each component and the scaling of the topography used by the volume projection algorithm. The MVO' provides a way to evaluate the voxel specificity of a component with respect to other components independent of the scaling of the topography because the coefficients of the spectra are re-scaled in Equation 3. We view this scaling of the topography in the volume projection algorithm as a step that weakens the PSV as a validation criterion.

The MVO' has a relation to the PSV as is evident by their plots of Figure 7 and as the voxel specificity of the component improves (as measured by the PSV), the MVO' also increases. The PSV however does not provide information of a component in relation to the other components; the MVO' does provide this additional information. Our other experimentation comparing the MVO' to the PSV (data not provided) has revealed that there is a correlation measured across components that are good activity estimates (are above the knee of the PSV and MVO' curves). However, for poor brain activity estimates and artefacts, the PSV and MVO are uncorrelated.

Center of Mass Distance Travelled

The simulation results show that the DT is different for simulated bona fide sources versus rank estimate artefacts and suggest that this measure might be useful in identifying the number of sources in real EEG data or identifying weakly defined our poorly separated sources. However, these types of components were not directly assessed in the simulation. The result that the electrode artefact, which was defined in the data as being spatially stationary and having a large proportion of the total variance, did not travel during iterations of runica enforces the idea that DT can be used to identify only weakly defined components (not necessarily artefacts of non-biological origin).

The result that the simulated centers of mass of brain activity components converged earlier than their corresponding PSVs has one very important implication. That is, for brain activity components, the early center of mass convergence and later PSV convergence indicate that further refinement occurs after the center of mass has been found. Thus, the center of mass, if not stabilized early, indicates that the volume representation of the component is not stable.

The center of mass convergence results found via analysis of real EEG data were similar to the simulated data in that in both cases, the centers of mass of components had their greatest movements during the early stages of the source separation process. Also similar was that there were a small number of sources in the real EEG data that had centers of mass that moved after 100 iterations when most other centers of mass had converged.

The convergence result of the PSV and MVO' for the real EEG data that these volume domain measures of improvement ceased to improve indicate that iteration should be the final estimation step for this data. The runica algorithm however did not exit until iteration 488. The runica algorithm uses a measure of change of the weight matrix to a value of 10E-6 which is a heuristic to indicate that any increase in the statistical independence among components is marginal. It is conceivable that while the runica algorithm was no longer improving the volume domain properties of sources, it was adding noise to the brain source estimates to continue to increase their statistical independence. One might conclude then that when the PSV and MVO' cease to improve after some number of iterations, the runica algorithm should exist and the results of the current iteration should be retained as the final solution of the source estimates. This particular research question has been left for future investigation.

COMPONENT RANKING BY VOLUME CHARACTERISTICS

The component ranking simulation results suggest hat brain activity components can be identified from artefacts for real EEG data using the PSV, MVO, and TDT measures.

The ranking of components by PSV for the final iteration showed which components were best represented in the volume domain according to their relative voxel specificity and the Euclidean norm characteristics of the topography. Ranking components of the simulation according to MVO scores provided a means to evaluate the volume overlap of components. In this simulation, this measure clearly separated the artefact components from simulated brain activity components. Differing from the PSV and MVO, the TDT is a measure that can potentially identify weak components such as the rank estimate error components that do not converge early in the source separation process.

Ranking components of the ICA decomposition of real EEG by their PSV, TDT and MVO′, provided a means to separate artefacts from possible brain activity components. Automatic identification of artefacts via the validation algorithm was largely facilitated by component PSV and MVO′ scores and was largely in agreement with expert artefact identification. The result that the automated algorithm classified eye-artefacts as good components makes sense because eye-movement activities originate from inside the skull. Fortunately, such artefacts are stereotypical and they can usually be easily identified by visual inspection. Unlike the simulation results, the TDT for the real EEG data did not identify any 'rank error artefacts', however it did provide an objective measure of the stability of the center of mass of EEG components providing a metric of reliability for the component.

This automated ranking process is particularly useful for those components that are marginal such as components 16, 20, or 29 and an objective criterion is needed to determine if they should be included in further analysis and considered for drawing conclusions about brain activity. It is also helpful when non-experts or new researchers are analyzing EEG data to help them decided which components are artefacts (such as the muscle artefact of component 25) and which might pertain to actual brain activities.

Acknowledgements:
Funding for this study was provided, in part, by the Natural Sciences and Engineering Research Council of Canada, CanAssist, and the University of Victoria.

SUMMARY

Taken together, the convergence curves and the final converged results of the volume domain measures PSV, MVO′, and TDT provide objective measures by which to validate components of a decomposition of EEG to identify artefacts from possible brain activities. We suggest that the logical convergence curves of these measures provide intuitive confidence in the relative goodness of the estimate of individual components.

Our validation methodology provides a novel technical contribution to the problem of ICA source validation, differing from the established methods of validation by relative component variances and validation by component clustering. We are not aware of other methods of validation that utilize these multiple volume-domain characteristics. In providing these measures to rank components, our proposed method offers a semi-blind means of scoring the relative qualities of brain activity estimates and separating artefacts from possible brain activity components.

VI. CONCLUSIONS

Volume domain characteristics of an ICA decomposition of EEG can be used to differentiate artefacts from those that might be brain activities. Volume domain characteristics of convergence provide confidence in the quality of source estimation. Future work is required to test the proposed method on more detailed EEG models and more real scalp-EEG datasets.

VII. REFERENCES

Baillet S, Mosher JC, Leahy R. BrainStorm beta release: a Matlab software package for MEG signal processing and source localization and visualization. Proceedings of the 16th

Annual Meeting of the Organization for Human Brain Mapping, San Antonio, Texas, 2000.

Bell A, Sejnowski TJ. An information-maximization approach to blind separation and blind deconvolution. Neural Comp, 1995;7:1129-1159.

Berg P, Scherg M. A fast method for forward computation of multiple-shell spherical head models. Electroencephalography and Clinical Neurophysiology, 1994;90:58-64.

Contreras-Vidal JL, Kerick SE. Independent component analysis of dynamic brain responses during visuomotor adaptation. NeuroImage, 2004; Mar. 21(3):936-945.

Delorme A, Makeig S. EEGLAB: an open source toolbox for analysis of single-trial EEG dynamics including independent component analysis. Journal of Neuroscience Methods, 2004;134:9-21.

Delorme A, Serby H, Makeig S. EEGLab Tutorial: VI. Independent Component Clustering. Retrieved October 11, 2006 from <http:\\www.sccn.ucsd.edu/eeglab/clusttut/clustertut.html>.

Hamilton DA, Kodituwakku P, Sutherland RJ, Savage DD. Children with Fetal Alcohol Syndrome are impaired at place learning but not cued-navigation in a virtual Morris water task. Behavioural Brain Research 2003, 143:85-94.

Hyvärinen A, Karhunen J, Oja E. Independent Component Analysis. New York: John Wiley & Sons, 2001.

Jung TP, Makeit S, Mckeown MJ, Bell AJ, Lee TW, Sejnowski TJ. Imaging Brain Dynamics Using Independent Component Analysis. Proceedings of the IEEE, v89, no7, 2001.

Jung TP, Makeig S, Westerfield M, Townsend J, Courchesne E, Sejnowki TJ. Analysis and visualization of single-trial event-related potentials. Human Brain Mapping, 2001;14(3):166-85.

Makeig S, Bell A, Jung T, Sejnowski, T. Independent component analysis of electroencephalographic data. In: Touretzky D, Mozer M, Hasselmo M (Eds). Advances in Neural Information Processing Systems. MIT Press, 1996;8:145-151.

Makeig S, Delorme A, Westerfield M, Jung TP, Townsend J, Courchesne E, Sejnowski TJ. Electroencephalographic Brain Dynamics Following Manually Responded Visual Targets. PLoS Biology, 2004;2(6):0747-0762.

Makeig S, Jung TP, Ghahremani D, Bell AJ, Sejnowski TJ. Blind separation of auditory event-related brain responses into independent components. Proc Natl Acad Sci USA 1997;94:10979-10984.

Makeig S, Jung T-P, Ghahremani D, Sejnowski TJ. Independent Component Analysis of Simulated ERP Data. In: Nakada T (Ed). Integrated Human Brain Science: Theory, Method, Applications (Music). Elsevier, 2000.

McCarthy G, Wood CC. Scalp distributions of event-related potentials: an ambiguity associated with analysis of variance models. Electroenceph. Clin. Neurophysiol., 1985;62: 203-208.

Michel MC, Murray MM, Lantz G, Gonzalez S, Spinelli L, de Peralta RG, Invited Review: EEG source imaging. Clinical Neurophysiology, 2004;115:2195-2222.

Onton J, Delorme A, Makeig S. Frontal midline EEG dynamics during working memory. NeuroImage, 2005;17(2):341-356.

Onton J, Makeig S. Information-based modeling of event-related brain dynamics. In: Neuper C, Klimesch W, editors. Event-Related Dynamics of Brain Oscillations. Progress in Brain Research vol.159. Amsterdam: Elsevier, 2007.

Sorensen PL, Zeman PM, Sutherland RJ. Differing patterns of synchronous cortical activity during a virtual spatial navigation task. Canadian Society for Brain, Behaviour and Cognitive Science, 16th Annual Meeting. Paper presentation. 2006.

Tikhonov AN. Solution of incorrectly formulated problems and the regularization method. Soviet Doklady 1963; 4, pp. 1035-1038.

Van Veen BD, van Drongelen W, Yuchtman M, Suziki A. Localization of Brain Electrical Activity via Linearly Constrained Minimum Variance Spatial Filtering. IEEE Transactions on Biomedical Engineering, 1997;44:867-880.

Yao D. A method to standardize a reference of scalp EEG recordings to a point at infinity. Physiological Measurement, 2001;22:693-711.

Zeman PM, Mahajan SV, Livingstone SA, Driessen PF, Skelton RW, Livingston NJ. Beamform Volume Projection of EEG ICA Topographies. (for publication) 2008b.

Zeman PM, Mahajan SV, Sorensen PL, Driessen PF, Skelton RW, Livingston NJ. Beamform Volume Projection of ICA Components of Scalp EEG: Volume-Domain Uniqueness of Components. (for publication) 2007c.

Chapter 6: Spectral Shaping to Relax ICA Assumptions to Facilitate Decomposition of EEG

The following manuscript builds on the work of Section II, Chapter 2, showing that the activities of the brain do not necessarily fit the assumptions of ICA and that ICA does not necessarily identify the bona fide activities of distinct areas of the brain. A set of tools for extracting more information from components of the EEG has been developed in Chapters 3 to 5. In Chapter 5, a specific methodology is given for measuring the quality of components as describing particular volumes of the brain. Thus, it is now possible to identify the voxel specificity of components, determine the extent of anatomical volumetric separation of pairs of components, and how well components are represented in the data above the EEG noise floor. The tools provide a means to identify the actual modular volumes of components for the purpose of identifying the anatomical region that the components activity waveform represents.

Article Type: Research Article

Article Title: Spectral Shaping to Relax ICA Assumptions to Facilitate Decomposition of EEG

Philip M. Zeman[1,2,3], Sunny V. Mahajan[1,2], Sharon A. Livingstone[3], Peter F. Driessen[2], Nigel J. Livingston[1], Ronald W. Skelton[3]

[1] CanAssist, University of Victoria, BC, Canada

[2] Department of Electrical and Computer Engineering, University of Victoria, BC, Canada

[3] Department of Psychology, University of Victoria, BC, Canada

Correspondence may be addressed to Philip M. Zeman:
(voice) +1-250-589-4234 / (fax) +1-250-721-6611 / pzeman@alumni.uvic.ca

Abstract

Objectives:

To demonstrate statistics of scalp-EEG differ across the EEG frequency spectrum. To demonstrate that shaping of the EEG frequency spectrum prior to standard ICA decomposition improves estimates of source activities, separating the EEG into more anatomically specific parts.

Methods:

In the first step, the Band-Selective ICA (BSICA) algorithm of Zhang and Chan, (2006) in conjunction with the runica ICA algorithm (Makeig et al., 1997) were used to calculate a frequency spectrum shaping filter that emphasizes frequencies of statistical independence. Second, this filter was used to shape the frequency spectrum of EEG data prior to using runica, a second time, to calculate new spatial source separation filters. Third, these spatial source separation filters were used to decompose unshaped EEG data into its component parts. Fourth, components calculated by these steps were compared to components obtained by standard application of runica. Differences between the results were identified by examining characteristics of component topography, modelled physical brain volume overlap (Zeman et al., 2008b), and pair-wise time-domain correlation of activities as a function of frequency.

Results:

The spectral shaping method separated bilateral activities of the EEG into two distinct, anatomically correct components that standard ICA methods did not and visibly improved the topographical representation of two other contributors to the EEG. Spectral shaping brought about statistically significant changes to the pair-wise correlation of brain activity components (as compared to the standard runica method) as a function of frequency for the frequency bands 2-18 Hz (increased correlation) and 20-38 Hz (decreased correlation), assigning the greatest correlation to the low frequencies of the brain activity frequency spectrum. Shaping also significantly decreased the pair-wise correlation of brain activity component activities in the 40-76 Hz frequency band to appropriately assign the lowest level of correlated activity of the EEG spectrum to the frequency band thought to contain non-brain activity related noise. Shaping provided no significant changes to the physically modelled overlap of estimated brain volumes.

Conclusions:

The statistics of the scalp EEG differ according to the frequency band examined. Further, the proposed spectral shaping method preserved the real correlative structure of brain source activities and separated the contributors to the EEG into more anatomically specific parts better than the standard method.

Keywords: EEG; ICA; data mining; blind source separation; runica; band-selective ICA.

(I) INTRODUCTION

Recent developments in the analysis of scalp acquired EEG, in the context of cognitive neuroscience, have provided for new methods by which to separate EEG data into components. Usually, each component is described by a topographical depiction of the scalp surface electric field and a time-varying waveform that indicates how the scalp field fluctuates in intensity over time. Generally, the objective in cognitive neuroscience is to discover multiple components from within the EEG data that each represent the activities of a unique brain area. It is however difficult to make such discoveries; a current neuroscience research problem is in determining how to appropriately separation of the EEG into components. To do so requires finding suitable criteria by which to separate the EEG into the activities of its individual contributors.

There are multiple criteria by which EEG data can be separated into component parts for analysis. Two well-known methods that use related separation criteria are principal component analysis (PCA), and independent component analysis (ICA). The first, PCA, separates EEG data into uncorrelated components (Spencer et al., 1999; Donchin and Heffley, 1979) by the separation criteria of linear independence of Eigen vectors defining the data. The measure of correlation that describes the relationship between parts of the data is a second order statistic. The second, more recently developed method, ICA, separates EEG data into components of maximal statistical independence (Hyvärinen and Oja, 1997; Contreras-Vidal and Kerick, 2004; Makeig et al., 1996; Makeig et al., 2004; Onton et al., 2005; Jung et al., 2001) using various measures of independence and common information (Hyvärinen et al., 2001; Lee et al., 1999; Dyrholm et al., 2007; Anenüller et al., 2003). Statistical independence, as a separation criterion, extends the measure of correlation as it describes the relationship between parts of the data using statistics that are second order and higher.

Generally, when analyzing EEG data, the separation criteria of uncorrelatedness and independence of the PCA and ICA source separation procedures, respectively, are applied across all frequencies contained in the data. The action of doing so treats all

frequencies equally (assuming they have equal variance) for determining how to separate the EEG into components; it is assumed that all frequencies have the same statistics. For example, an estimate of correlation of two processes, **x** and **y,** is defined by a single parameter **Cxy**, and is not calculated as a function of frequency. It is important to recognize that the variance of activities across the frequency spectrum is not uniform as the low frequencies have the greatest variance.

Current understanding of the operation and function of the brain indicates that brain activities at different frequencies measured from either the cortical surface or the surface of the scalp are indicative of different physiological processes and human behaviour (Başar, 2005; Silberstein et al., 2005; Roelfsema et al., 1997). In addition, a given region of the brain contains neurons of many types with a variety of local connections with near-by neurons and long-distance connections to other neurons in distant, distinct areas of the brain. Assuming that the oscillatory activities measured from the brain have some relation to the interconnectivity of neurons, long and short distant connections will have different oscillatory properties and these properties may differ across the frequency spectrum. This is a theory originally proposed by Nunez, (1989). Plausibly then, the measured activities at different frequencies have different statistical properties. Taken together, this suggests that a given area of the brain might participate in multiple concurrent operations such as local processing of information and simultaneous transfer of information to other parts of the brain. It is thus possible that distinct, anatomically modular brain areas have activities that are most correlated in one or more frequency bands and are least correlated and/or statistically independent in some other band of frequencies.

Measuring the time-varying correlation of activities between distinct areas of the brain is of interest. It has been suggested that correlated activities measured between distinct brain areas indicates transfer of information between these areas of the brain (Roelfsema et al., 1997). Thus, it is important in studies that examine the coordination and transfer of information among different parts of the brain to preserve the natural time-varying correlative structure of brain source estimates.

Methods employing separation criteria that account for varied statistics across frequency bands might yield more anatomically and physiologically accurate components than those methods employing the separation criteria of standard PCA and ICA methods. Brain activities that are both statistically independent and originate from distinct areas of the brain and not directly involved with the long-distance transfer of information between distinct areas of the brain would facilitate the identification of distinct modular brain sources. Source separation matrices used by PCA and ICA could be constructed based on these 'local brain' frequencies to improve the identification of bona fide brain sources contributing to the EEG.

When the characteristics of brain source activities do not fit the source separation criteria employed by standard PCA and ICA, errors in estimating the activities of distinct brain contributors to the EEG typically present themselves in two ways. The first is the allocation of anatomically (spatially) distinct sources as a single component by the source separation algorithm. This occurs when the activities of two anatomically distinct brain areas are strongly correlated in some band of frequencies, either transiently or over extended intervals of time. By the standard PCA and ICA separation criteria these two distinct contributors to the EEG appear to be one. Herein, this type of error is referred to as *failed separation distortion*. Failed separation distortion is typically seen with the activities originating from bilaterally symmetric brain areas because such areas often operate in synchrony. The second type of estimation error presentation is the distortion of bona fide source activities by standard PCA and ICA to make them as uncorrelated or statistically independent from the activities of other sources as possible. Typically, the activities of two distinct brain areas may be weakly correlated or otherwise not exactly statistically independent, in which case, they are appropriately identified as separate parts, however, the estimates of their actual activities are distorted by the separation criteria. Herein, this is referred to as *forced independence distortion*. Forced independence distortion is the inclusion of random noise or parts of other component activities from the EEG mixture in the source estimate.

To reduce both of these types of estimation errors caused by correlated source activities, the sub-band decomposition (SDICA) mathematical model (Cichocki and Georgiey, 2003; Tanaka and Cichocki, 2004; Cichocki and Zurada, 2004) originally developed for the separation of audio-class signals is utilized by our proposed source separation algorithm to relax the strict assumptions of ICA. The SDICA mathematical model assumes that wide-band source activities are generally dependent but some narrow-band subcomponents of the source activities are independent. An algorithm and software implementation employing the principles of SDICA called Band-Selective ICA (BSICA) (Zhang and Chan, 2006) adaptively identifies those frequencies that provide for greater overall independence among components. Zhang and Chan (2006) demonstrated that, when BSICA is used as a post-processing step, it improves separation of audio-class signals that have been pre-processed using the FastICA source separation algorithm (Hyvärinen, 1999).

We propose a new source separation algorithm, called Spectral Shaping ICA, to improve upon EEG source estimation by standard ICA methods. This new algorithm is essentially a combination of the BSICA and runica algorithms and is designed to address both the failure to identify separate sources, and the distortion related to forced independence. The algorithm attempts to identify all distinct modular brain contributors to the EEG while at the same time preserving the naturally occurring correlations between the activities of these distinct areas of the brain. Following the SDICA model, this algorithm assumes that each contributor to the EEG has some activity in some frequency band that is independent from the activities of other contributors and can be used to identify the brain source as a unique physical entity contributing activity to the EEG mixture. Hence, the strict requirement that sources comprising the EEG mixture be statistically independent is relaxed so that frequency bands of dependence and correlated activities can exist. In this paper we compare our proposed *spectral shaping* method with the established *standard* ICA method, runica.

This paper is organized as follows. First, our method of evaluating the proposed source separation algorithm and the expectation of this evaluation are described. Second, a

background of the standard runica ICA source separation is given so that the proposed algorithm can later be related to the standard algorithm. Third, a detailed description of the proposed spectral shaping algorithm is provided. Following this, a procedure for comparing the EEG decomposition results of the spectral shaping method to the standard method is described and the results of this procedure are subsequently provided. Finally, a discussion of the results and concluding remarks are given. A block diagram depicting the methods used to evaluate the proposed algorithm is given in Appendix A.

MEASURING IMPROVEMENT

In order to determine if our method improves the estimate of source activities contributing to the EEG, components of the EEG calculated using each method are compared 3 ways. These include (1) their topographical characteristics, (2) time-frequency characteristics, and (3) the characteristics of their modelled physical volume-domain representation.

The topographical characteristic will be used as a primary 'first-pass' method of component evaluation to identify differences, similarities, and improvements of the spectral shaping method over the standard method. Generally, the component topographies that are desirable for cognitive neuroscience research are those described as dipolar, with few loci of scalp intensity and smooth transitions of intensity between these loci. Such topographies are desirable because they can be represented by some number of modelled source dipoles to relate the scalp EEG to brain anatomy. In the ideal case, these topographies can be accurately modelled by a single dipole, implicating that the component represents the activities of a single location in the brain.

While this method does provide an intuitive insight into the complexity of the source structure underlying the scalp field, it is subjective because multiple dipoles at different locations in the head can also produce smooth and simple scalp fields. Because of these differences between decomposition methods will also be quantified by comparing the pair-wise correlative structure of brain activity related components of the EEG as a

function of frequency. This can be done via analysis of the activities of each component calculated using each decomposition method. Differences between decomposition methods will also be quantified by evaluating volume domain differences between similar components calculated using each decomposition method. Our prior work has demonstrated that it is possible to estimate the brain source volume overlap via projection of component scalp topographies into a model head volume (Zeman et a., 2008b).

Improvements offered by the spectral shaping method over the standard method are expected to present in multiple ways. We expect to find that the activities of brain sources estimated via the spectral shaping method have a pair-wise correlative relationship as a function of frequency that has more correlative activities in the lower frequency part of the scalp EEG spectrum than the high frequency part of the scalp EEG spectrum; large correlation values for the paired activities of different brain sources should exist predominantly in the brain activity frequency band of the scalp acquired EEG (< 50 Hz). This same relation determined for brain sources estimated using the standard method should be comparatively flat across frequencies demonstrating that the steps of standard ICA do in fact, distort the naturally occurring correlative structure of the data. Second, we expect that the volume overlap of separate components that represent modular 3-dimensional brain areas will be appropriate to the physical constraints of brain anatomy; that is, each component will pertain to a unique area of the brain. Since noise interference is always present, and a canonical average head model will be used in the evaluation of overlap, there will never be exactly zero overlap, thus, components relating to specific brain areas that are calculated via the spectral shaping method should have reduced volume overlap compared to the standard method.

SOURCE SEPARATION BACKGROUND

The EEG mixture is modelled using the linear source mixture representation given in Equation 1,

$$\mathbf{x} = \mathbf{A}\mathbf{s} \tag{1}$$

where $\mathbf{x} = [x_1(t), x_2(t), \ldots x_M(t)]^T$ is recorded EEG data from M channels, and $\mathbf{s} = [s_1(t), s_2(t), \ldots s_J(t)]^T$ represents J source activities comprising the mixture. Each **s** is a component of the observed EEG data **x**. The matrix **A** defines the physical spatial characteristics of how the sources were mixed to form the EEG data at each electrode. It describes the spatial scalp variance of the ICA component topography electrode weights.

Generally **A** and **s** are not known and we are required to solve for them having only, **x,** the observed EEG mixture of activities.

Each column of **A** describes the electric field projected to the scalp as measured from discrete spatial samples via electrodes and is generally referred to as the topography of the component. We denote this as $\mathbf{A}_j$ where the index j refers to a specific component of the EEG decomposition and column of the mixing matrix. Each column of the mixing matrix $\mathbf{A}_j$ holds the relative weighting of electrodes that describe the topographical variance of the electric field at the scalp.

Some assumptions are required to unmix the observed data and find the component source activities and their corresponding electric field scalp topographies. Foremost, it is assumed that the source activities are non-Gaussian and statistically independent. It is also generally assumed that the number of sources J is less than or equal to the number of EEG channels M, otherwise the data is over-determined. For simplicity, the remainder of this description assumes that $M = J$. Further, it is assumed that each channel of data defining **x** has a mean of zero. This zero-mean criterion is easily satisfied by subtracting the mean of each channel of recorded EEG from each sample in that channel before commencing with ICA.

The ICA algorithm, runica, finds an estimate of **s**, denoted as $\hat{\mathbf{s}}$ using Equation 2,

$$\hat{\mathbf{s}} = \mathbf{WPx} \tag{2}$$

where **P** is called the sphering matrix and **W** is called the ICA weight matrix. The sphering matrix provides orthogonalization and normalization of **x**. It is this sphering matrix that is used to identify uncorrelated source activities. The weight matrix provides a rotation of the orthogonalized and normalized **x**. It is this weight matrix that identifies statistically independent source activities.

The sphering matrix **P**, is solved as in Equation 3,

$$\mathbf{P} = \mathbf{C}^{-1/2}(\mathbf{x}) \tag{3}$$

where $\mathbf{C}^{-1/2}(\mathbf{x})$ is the matrix square-root of the inverse of the covariance estimate of the data **x**.

Using **x** and **P**, the runica algorithm iterates, selecting random samples of sphered data, to find a **W** such that the individual source activity estimates (calculated via Equation 2) stored in the rows of $\hat{\mathbf{s}}$ are as statistically independent as possible.

Together, the matrices **W** and **P** describe how to spatially unmix the sources comprising the EEG mixture. From the weight matrix **W** and the sphering matrix **P**, the matrix **A**, that mixed the source activities is estimated as $\hat{\mathbf{A}}$ using Equation 4.

$$\hat{\mathbf{A}} = (\mathbf{WP})^{-1} \tag{4}$$

A notable feature of the runica algorithm is that it samples the sphered data in blocks and does sample randomization. This is done in multiple iterations until there is little to no improvement on the calculated weight matrix. This characteristic provides a frequency invariant estimate of the statistical independence of the sources **s**.

In contrast to the runica algorithm, the BSICA algorithm estimates sources $\hat{\mathbf{s}}$ and a mixing matrix $\hat{\mathbf{A}}$ by searching for a weight matrix **W** that maximizes the independence

of sources, while also adaptively searching for time-domain coefficients **h** of a time-domain filter that further maximizes the independence of the estimated source activities. This time-domain filter **h** is used by BSICA to emphasize the activities of the sphered version of **x** for frequency bands that have the greatest independence. Details of the BSICA method are provided in (Zhang and Chan, 2006). Unlike runica, BSICA does not randomize samples of **x** while calculating **h** and **W** and thus does not have the property of frequency invariance that runica has; there is no sample randomization. Here we denote the mixing matrix found by BSICA as $\mathbf{W}^h$. Thus, the estimated source activities $\hat{\mathbf{s}}$ are calculated using $\mathbf{W}^h$ as in Equation 5.

$$\hat{\mathbf{s}} = \mathbf{W}^h\mathbf{P}\mathbf{x} \tag{5}$$

Similarly as in Equation 4 for runica, the mixing matrix estimate $\hat{\mathbf{A}}$ for BSICA is calculated from the weight and sphering matrices. This time however, a modified weight matrix is used as in Equation 6.

$$\hat{\mathbf{A}} = (\mathbf{W}^h\mathbf{P})^{-1} \tag{6}$$

PROPOSED SOURCE SEPARATION METHOD

The spectral shaping method exploits the complementary properties of runica and BSICA (Figure 1). It adaptively calculates and utilizes a shaping filter to emphasize frequencies of independence from the EEG data via BSICA post-processing of an initial runica source separation procedure. Next, the EEG data **x** are filtered or *shaped* using the calculated shaping filter and then used to define sphering and weight matrices via a second usage of runica. The sphering and weight matrices calculated in this way are denoted as $\mathbf{P}^h$ and $\mathbf{W}^h$, respectively. By using $\mathbf{P}^h$ and $\mathbf{W}^h$ to separate the EEG data **x**, source distortion is expected to be reduced. The calculation of estimates of source activities $\hat{\mathbf{s}}$ by our method is given in Equation 7,

$$\hat{\mathbf{s}} = \mathbf{W}^{\mathbf{h}}\mathbf{P}^{\mathbf{h}}\mathbf{x} \tag{7}$$

where **x** is the non-shaped EEG data with the mean of each channel removed.

Similarly as in Equations 4 and 6, the estimate of the mixing matrix, $\hat{\mathbf{A}}$ is calculated as in Equation 8, however, in this case, both the weight and sphering matrices are modified by the shaping filter.

$$\hat{\mathbf{A}} = (\mathbf{W}^{\mathbf{h}}\mathbf{P}^{\mathbf{h}})^{-1} \tag{8}$$

Our method differs from the BSICA in two main ways. The fundamental difference between BSICA and our method is that our method finds both the sphering and the weight matrices using shaped data (with frequencies of independence emphasized), whereas BSICA only adaptively calculates the weight matrix based on adaptive time-domain filtering. The validity of calculation of the sphereing matrix using data shaped by a filter that emphasizes frequencies of independence is based on the statistical property variables that are statistically independent are also uncorrelated. Hence, if the EEG at these particular frequencies results from separate process or 'random variables' that are statistically independent then they are also uncorrelated. Both runic and BSICA make iterative estimates of the ICA unmixing matrix and the sphering matrix provides the starting point for estimating the unmixing matrix. Our method has a starting point for the ICA rotation of the data that is different than that of the BSICA algorithm and this difference is provided by the new matrix $\mathbf{P}^{\mathrm{h}}$. The second difference is that our method incorporates the procedure of random data sampling via the runica algorithm, which our experimentation with runica suggests is a key component to that algorithms success.

The spectral shaping methodology has 4 main processing steps, presented as 4 main processing blocks in Figure 1. Block (a) provides training of the shaping filter and consists of two parts. First, runica is used to calculate a preliminary weight matrix **W** and a sphering matrix **P** from the zero-mean EEG data, **x**. These spatial unmixing matrices **W** and **P** are inputs to the BSICA block. The BSICA algorithm is used to calculate filter

coefficients, **h**. The coefficients of **h** emphasize frequencies of statistical independence and in doing so, attenuate those frequencies of dependence. Block (b) separates the brain activities from the EEG mixture, calculating new spatial unmixing matrices $\mathbf{P}^h$ and $\mathbf{W}^h$. Using **h** to shape the spectra of **x**, (denoted in the figure as 'SS') the dataset $\mathbf{x}^h$ is created and statistical independence is maximized by runica on $\mathbf{x}^h$. This creates the new sphering matrix $\mathbf{P}^h$ and weight matrix $\mathbf{W}^h$. To calculate estimated source activities $\hat{\mathbf{s}}$, the matrices $\mathbf{P}^h$ and $\mathbf{W}^h$ are combined with the unshaped EEG data **x** in block (c). Finally, in block (d), the matrix of estimated brain source topographies, $\hat{\mathbf{A}}$ is generated from $\mathbf{P}^h$ and $\mathbf{W}^h$.

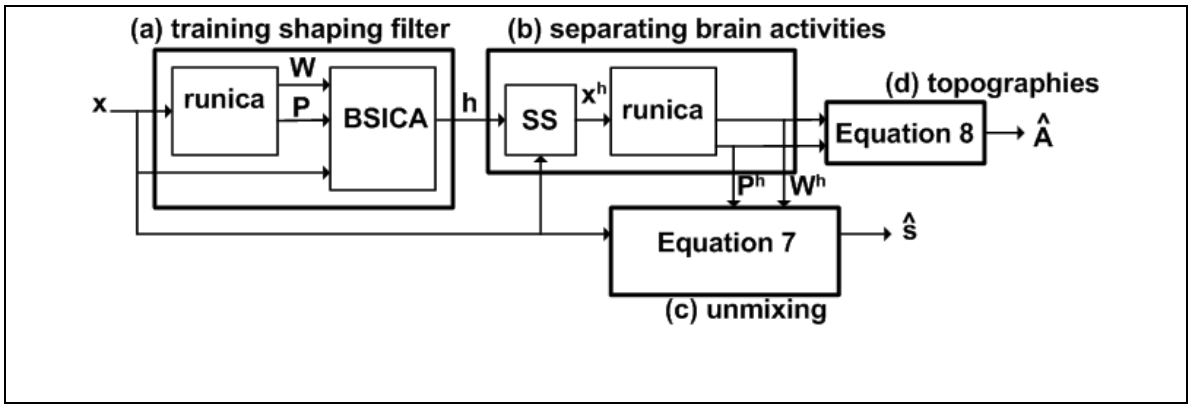

Figure 1. Block diagram of our proposed method. Mathematical symbols are discussed in the main text. 'runica' denotes use of the runica algorithm. BSICA denotes use of the BSICA algorithm. 'SS' denotes shaping of the EEG frequency spectrum using the calculated filter coefficients. 'MS' demotes mean subtraction of the data of each channel and is part of the ICA evaluation of statistics that are second order and higher. Block (a): training of the spectral shaping filter; Block (b): calculation of the separation matrices for the brain activity; Block (c): calculation of estimated source activities; Block (d): calculation of topographies of components of the EEG.

(II) METHODS

Data Collection and Preparation

Data were acquired from a larger study of foetal alcohol spectrum disorder (FASD) (Sorensen et al., 2006). EEG data collected from one female participant was selected at random from the socially-matched control group of the larger study and were used in this study.

These acquired data were acquired using a 128-channel Geodesics sensor net and Net Station acquisition software (Electrical Geodesics, Inc., Eugene, Oregon), with a 500 Hz sample rate. A hardware filter with a high pass cut-off frequency of 0.1 Hz and a low pass cut-off frequency of 200 Hz was used to eliminate aliasing related to digital sampling and to remove very low frequency activities. Data were recorded while the participant executed a virtual spatial navigation task similar to that described by Hamilton et al. (2003). Details of this specific task and data collection paradigm are described by Sorensen et al. (2006). The paradigm required the participant to navigate a 1st person computer-based virtual arena maze using one of two behavioural strategies. Two types of trials were presented that were each optimized for one of these two strategies. Trials optimized for each strategy were presented to the study participant in blocks of 10 trials. The participant was asked to locate the 'correct' platform of 2 visible platforms in each trial of the experiment using either an allocentric or egocentric cognitive strategy. For cue trials, the participant was required to employ an egocentric strategy while for place trials, an allocentric strategy was required. The cue strategy required participants to identify the correct platform by the color of the platform and then move to it using left or right arrow keyboard presses. The allocentric strategy required participants to identify the correct platform based on configural information of multiple pictures located on the walls of the arena maze and then once identified, move to it. Each trial was completed when the participant reached the correct visible platform. On the first trial of each block, if the participant failed to reach the correct platform, the participant was given instructions for how to complete the trial and was directed towards the correct platform. When the correct platform was reached at the completion of each trial, the participant was notified that the trial was completed successfully. Following the completion of each behavioural trial, a blank screen with a short inter-trial interval was presented; this was followed by the start of the next trial.

The EEG data were de-referenced by calculating the average across channels for each individual time sample and subtracting this value from each channel, a procedure known as average referencing (Yao, 2001). Data segments were extracted from the recorded continuous EEG data to provide analysis around the onset of the task. The data were segmented as -1000 to 2500 ms such that the onset of the task was at 0 ms. The segmented trials were then visually inspected for artefacts. Based on visual inspection of channel data, channels that were consistently noisy across many trials were removed leaving data from 112 channels to be used for further analysis. Those trial segments contaminated with non-stereotypical artefacts were discarded. Also discarded from further analysis was the first trial of each behavioural block. Trial segments containing stereotypical eye-movements, eye-blink artefacts and electrode artefacts were retained, leaving 45 cue trials and 47 place trials for further analysis. Each trial of data was digitally band-pass filtered 3 to 80 Hz, using a zero-phase linear filter, and then down-sampled to 250 samples per second. Since in this study only characteristics of the decomposition are of interest, the cue and place conditions were treated equally, in terms of signal processing, to form a 92 trial dataset.

Decompositions

The prepared EEG data were first separated into components via the standard runica decomposition method. In doing so, the data were reduced to 30 principal dimensions by specifying the 'PCA' parameter of the runica software, to yield estimated source activities, $\hat{\mathbf{s}}$ and the estimated mixing matrix, $\hat{\mathbf{A}}$. The individual source activity estimates $\mathbf{s}_j$ for each j component were stored for later analysis and the estimated topographies $\hat{\mathbf{A}}_j$ corresponding to each j component plotted and also stored for later analysis.

After decomposition of the prepared EEG data using the standard runica method, the proposed spectral shaping method, following the description in Figure 1, was used. First, the runica algorithm was used in conjunction with the BSICA algorithm to calculate a

shaping filter **h**. Then the shaping filter was used to shape the prepared EEG data and this shaped data was used with runica a second time to construct new spatial separation matrices $\mathbf{P}^h$ and $\mathbf{W}^h$. These new separation matrices were used to separate the prepared, unshaped EEG data into source waveform estimates $\hat{\mathbf{s}}$ and calculate the mixing matrix $\hat{\mathbf{A}}$. For steps using runica, the PCA parameter was specified to reduce the data to 30 principal dimensions.

Adjustments were made to the BSICA algorithm to work with EEG data and our implementation. The adjustments were as follows. Instead of convolving data with the adaptive filter coefficients using the Matlab 'conv' command as is default in the BSICA software, the Matlab 'filtfilt' command was used. This reduced the execution time of the software and ensured that the filtered results would have zero phase distortion. Data blocks for BSICA were assigned such that each block contained 875 consecutive data samples (i.e., whole trials of sampled data without randomization of samples) of EEG data thus preserving the time-domain characteristics of the data. The learning rates for **W** (internal to the BSICA algorithm) and **h** were set low (to 0.001 and 0.015, respectively), to minimize the effects of outlier noise on filter calculations. It was specified that the BSICA algorithm use 13 coefficients to define the shaping filter, **h** to reduce the chances of over fitting the data.

On completion of the spectral shaping source separation algorithm, the waveforms for each *j* component $\hat{\mathbf{s}}_j$ and the topographies of each component $\hat{\mathbf{A}}_j$ were stored for later analysis. For inspection, each of the topographies $\hat{\mathbf{A}}_j$ were plotted. To identify which frequency bands were identified as having the most statistical independence and were thus emphasized, the shaping filter coefficients **h**, calculated during the BSICA step of the spectral shaping algorithm were used to plot the magnitude spectrum of the shaping filter.

The volumetric spectrum $\mathbf{r}_j$ of each *j* component for each decomposition method was calculated from each component topography as the first step for doing volume-domain

analysis of component quality. The volumetric spectrum (Zeman et al., 2008b) is a volume-domain representation of the topographical scalp field. It is calculated via a process of projecting the topographical characteristics of a component into a mathematically defined head model. This process maps the spatial scalp variance described by the ICA component topography electrode weights $\hat{\mathbf{A}}_j$ to an optimal volume representation using a closed-form mathematical solution (Van Veen et al., 1997). A three-shell head model comprised of 5439 voxels that describe the variance at every location in the model head was created using the BrainStorm software package (Baillet et al., 2000). Each voxel was defined as cube with the length of each side of the cube equal to 5 mm. The relative levels of projected variance at each of these voxels, when arranged as a 1 x 5439 vector, defines the volumetric spectrum $\mathbf{r}_j$.

Following decomposition of the data using the standard and shaped decomposition methods and the volume projection of component topographies, each component was assessed according to three properties to compare decomposition methods. These comparisons were made using each component's scalp topography, pair-wise correlation of waveform activity, and volume-domain overlap with other components of the decomposition determined from the volumetric spectra calculated previously.

Component Assessment

Scoring and Matching

Before the difference between the decomposition methods could be assessed, it was necessary to identify the artefact components from the set of all components calculated for each of the decomposition methods. To identify which components were artefacts and which might relate to activities originating from inside the head, each of the components were scored according to the peak value of their corresponding volumetric spectrum. In previous work it was shown that the largest coefficient of the volumetric spectrum, the Peak Spectral Value (PSV) (maximum value of $\mathbf{r}_j$), can be used to identify

noise components from a decomposition of EEG using ICA (Zeman et al., 2008d). To do this in the current study, the PSVs of the components for each decomposition method were sorted in descending order to determine a minimum threshold. Those components with a PSV greater than this threshold were retained for further analysis while those below the threshold were discarded as artefact. This threshold was determined as the PSV corresponding to the knee of the curve (data not provided) formed by the sorted PSV scores. Those components below the knee and implicated as artefact were removed from the analysis.

Components that were common to both decomposition methods and determined as 'dipolar' based on visual inspection of their topographical characteristics were cross-labelled and noted for making comparisons between the standard and spectral shaping decomposition methods. A component was identified as dipolar if its topography exhibited paired foci; one positive region of intensity and one negative region of intensity. A component was also considered to be dipolar if the topography exhibited a single positive or a single negative region of intensity. The components of this set are hereon referred to as the *common dipolar components*. Those components with dipolar topographies that were unique to one or the other decomposition methods were classified as *unique dipolar components* and were noted for later analysis to identify their physical origin. Those components with non-dipolar topographies that were unique to each decomposition method but were not identified as artefact by the PSV thresholding method were omitted from further analysis.

Decomposition Algorithm Assessment by Common Components

The characteristics of the common dipolar components calculated via the two decomposition methods were compared using multiple characteristics to determine if the spectrally shaped decomposition method provides an improvement over the standard method. These characteristics were: topographical properties of components, the pair-wise correlative structure of component waveforms, and the modelled volume-domain overlap of component source anatomy.

Topographies of Common Components

The topographies of the cross-labelled components were visually inspected and compared to identify subtle differences in the dipolar quality of components between decomposition methods. The cross-labelled component pairs with the greatest visible topographical differences between decomposition methods were noted.

Pair-Wise Correlation Spectra of Common Components

The pair-wise correlative structure of component activities as a function of frequency was examined to identify differences between decomposition methods. Each common dipolar component waveform activity s_j was band-pass filtered using a 3 Hz wide frequency window defined by a 120 point FIR filter for each trial separately. This 3 Hz window was shifted in steps of 2 Hz (from 2-100 Hz) to isolate activities in each frequency band. The activities isolated by this filtering process were denoted as $\mathbf{s}_j(f)$, where j is the component index and f indicates the center of the frequency bin of the band-pass filter. These band-pass filtered activities were then Hanning windowed to reduce spectral leakage in subsequent analysis steps, yielding $\hat{\mathbf{s}}_j(f)$ as in Equation 9,

$$\hat{\mathbf{s}}_i(f) = \boldsymbol{\omega}\, \mathbf{s}_i(f) \tag{9}$$

where $\boldsymbol{\omega}$ defines the Hanning window. From the Hanning windowed waveforms, the pair-wise correlative structure $\mathbf{C}_{ij}(f)$ of pairs of i,j components as a function of frequency for each trial separately, was calculated using the cross correlation relation in Equation 10,

$$\mathbf{C}_{ij}(f) = \frac{\sum_k \{[\hat{\mathbf{s}}_i(f) - \bar{\hat{\mathbf{s}}}_i(f)][\hat{\mathbf{s}}_j(f) - \bar{\hat{\mathbf{s}}}_j(f)]\}}{\sqrt{\sum_k [\hat{\mathbf{s}}_i(f) - \bar{\hat{\mathbf{s}}}_i(f)]^2}\sqrt{\sum_k [\hat{\mathbf{s}}_j(f) - \bar{\hat{\mathbf{s}}}_j(f)]^2}} \quad \textbf{for all } i \neq j \tag{10}$$

where $\bar{\hat{\mathbf{s}}}(f)$ is the mean of $\hat{\mathbf{s}}(f)$. The variable *k* is an index for the summation in the equation that varies from 1 to *K*, where *K* is the number of samples (875) in each trial of data.

The trials of each $\mathbf{C}_{ij}(f)$ were then averaged to yield a summary pair-wise correlation result $\bar{\mathbf{C}}_{ij}(f)$ for each component pair.

These summary average pair-wise correlation results for each component pair for each decomposition method were plotted. (Plots of six representative spectra are provided.) Consistency of the correlation estimate across trials for each component pair was determined via random estimates of the mean from the set of trials available. This consistency is indicated on the plots by errors bars calculated as 1 standard deviation of the mean of 2000 blocks of 20 randomly selected trials from the 92 trial dataset for each component pair, separately for each decomposition method.

Grand Average Pair-Wise Correlation Spectra of Common Components

Grand-average pair-wise correlation spectra were calculated to provide a summary of the correlative properties as a function of frequency for each decomposition method. This was calculated as the absolute value of the summary $\bar{\mathbf{C}}_{ij}(f)$ of each component pair, averaged across all component pairs, for each decomposition method separately.

Statistical testing of the pair-wise correlation spectra between the two decomposition methods was used to determine if spectral shaping provided for significant changes to decomposition results. The statistics were calculated for two sets of intervals, with each set of intervals selected to examine different characteristics of the EEG data.

For the first set of intervals, the EEG spectrum was divided into a low frequency interval and high frequency interval to compare the non-brain activity part of the scalp EEG frequency spectrum (>50 Hz) (Delorme and Makeig, 2006) to the part of the scalp EEG spectrum known to contain brain activities.

To compare the correlation values between decomposition methods for each frequency interval, the average pair-wise correlation value for each frequency interval was calculated. To do so, the pair-wise correlation frequency bins in that interval were averaged. The bin average $\overline{C}_{ij}(f_A \ldots f_B)$, of each component pair i,j for each frequency interval $f_A..f_B$ was calculated as in Equation 11,

$$\overline{C}_{ij}(f_A \ldots f_B) = \frac{1}{N}\sum_{g} C_{ij}(f_g) \tag{11}$$

where N is the number of bin intervals (number of steps of 2 Hz) in the summation and f_g indicates the center frequency of the frequency bin. The index g varies from the lowest frequency of the interval, f_A to the highest frequency of the interval, f_B. The results of this evaluation were plotted. Using the measures of the interval, statistics evaluating the pair-wise correlation structure of the EEG using the waveforms of cross-labelled components were calculated. Pair-wise comparisons were made using 2-tailed t-tests ($p<0.05$, uncorrected for multiple tests) to provide a measure of difference between the proposed and standard decomposition methods.

The second set of intervals was selected using characteristics of the grand average pair-wise correlation plots as a guide. This set of intervals was selected by dividing the brain activity band of the EEG spectrum into low and high frequency brain activity bands. These intervals were examined to determine effects of the spectral shaping method that were specific to the estimated brain activities contained in the EEG. The highest frequency in the brain activity band was determined as the frequency where the grand-average pair-wise correlation spectra decreased to the noise floor.

Volume-Domain Overlap of Common Components

In our prior work (Zeman et al., 2008b) we described a procedure to measure volume-domain source overlap. We were able to show that overlap was greater for modelled artefacts or poorly separated brain sources comprising the EEG than for well-separated model brain sources. To measure overlap in the current study, a volume overlap score for each component pair was calculated using the volumetric spectrum of each component $\mathbf{r}_j$ calculated earlier. Hereon this is referred to as the pair-wise volume overlap (PVO). A PVO of 1 indicates that the component pair being evaluated overlap maximally while a PVO of 0 indicates no overlap. Calculated PVOs will always be greater than zero because this measure of the volume overlap uses the continuous spread of variance of the volumetric spectrum of each component. That is, there are no strict volume edges defined, but rather a gradual roll-off of variance from the peak variance at the center of the component volume into the noise floor. Nevertheless, the smaller the PVO, the better the source separation.

The PVO of component pairs was calculated for each of the two decomposition methods. The pair-wise overlap S_{ij} for two components i and j, was calculated from the mean-subtracted and normalized (Euclidean norm) volumetric spectra as in Equation 12,

$$\boldsymbol{S}_{ij} = \frac{(\boldsymbol{r}_i - \bar{\boldsymbol{r}}_i)(\boldsymbol{r}_j - \bar{\boldsymbol{r}}_j)^T}{|(\boldsymbol{r}_i - \bar{\boldsymbol{r}}_i)||(\boldsymbol{r}_i - \bar{\boldsymbol{r}}_i)|} \tag{12}$$

where $\boldsymbol{r}_i$ and $\boldsymbol{r}_j$ are the volumetric spectra of components i and j and $\bar{\boldsymbol{r}}_i$ and $\bar{\boldsymbol{r}}_j$ are their corresponding mean values.

The results were tabulated for each component pair and for each decomposition method separately to show changes for each component pair.

The average PVO for each decomposition method was calculated across the individual PVOs of each decomposition method to identify any average improvement offered by the spectral shaping method. This average PVO was plotted for inspection. A t-test ($p<0.05$) was used to provide a measure of the difference between the distribution of the PVOs of the standard and the distribution of PVOs of the shaped decomposition method to determine if there was any overall significant change in the volume overlap of brain activity components.

Decomposition Algorithm Assessment by Unique Components

Those components that were identified as unique because they did not have topographical matches for both the shaped and standard decomposition methods were evaluated 2 ways. First, the modular 3-dimensional volumes of these components were estimated to account for the component by physiology as an unbiased reference. Second, the pair-wise correlations of their waveform activities were examined to determine if these components were a logical result of the spectral shaping algorithm.

Modular Volume Depiction of Unique Components

The modular 3-dimensional volumes of the unique components identified using the shaped decomposition were estimated to determine their plausible anatomical origin. To estimate these modular volumes, the volumetric spectra $\mathbf{r}_j$ of each unique component were thresholded to define edges of their corresponding component volume. An estimate of the noise level in the volumetric spectrum of each component is used to calculate this threshold. For details see Zeman et al. (2008b). The calculated modular volumes were plotted for interpretation with respect to a white matter cortex for confidence intervals of 4 and 5 standard deviations above the mean noise level in the volumetric spectrum $\mathbf{r}_j$. Modular volumes represent active grey matter while the white matter framework provides a physical frame of reference so that the resolved volumes can be named anatomically.

Pair-wise Cross-Correlation Spectra of Unique Components

The pair-wise cross-correlation spectra were calculated and plotted for the unique dipolar components of the shaped decomposition. These spectra were calculated as described previously using Equations 9 and 10. Consistency of the correlation estimate across segmented trials for each component pair was determined via random estimates of the mean from the set of trials available. Error bars on the plot were calculated as the standard deviation of the mean of 2000 random samples of 20 trials from the 92 trial dataset.

(III) RESULTS

Decompositions

Decompositions of EEG data by each method yielded 30 components with corresponding waveforms and topographies. Subsequent projection of topographical variance to the volume domain via the volume-projection algorithm yielded a volumetric spectrum corresponding to each component.

Shaping Filter

The magnitude characteristics of the shaping filter (Figure 2), calculated as part of the spectral shaping decomposition method, illustrate that statistical independence varies over frequency bands. The peaks and notches of the magnitude frequency spectrum are defined by coefficients of the shaping filter that were calculated by the procedure of Figure 1, block (a). The notable peaks and notches are for the frequency bands around 11, 27, 42, and 73 Hz. The filter de-emphasizes 11 Hz, emphasizes the frequency band 27-42 Hz, and greatly emphasizes the frequencies around 73 Hz (approximately 62-85 Hz). Other variations in the spectrum are characteristic of smooth transitions of overshoot or undershoot between points of emphasis and de-emphasis related to the

number of coefficients defining the shaping filter. It illustrates that frequencies of brain activity in the band 27-42 Hz are more independent than the frequency band around 11 Hz. It also shows that activities outside the EEG brain activity frequency band (> 50 Hz) (Delorme and Makeig, 2006) are more independent than the activities inside the brain activity frequency band.

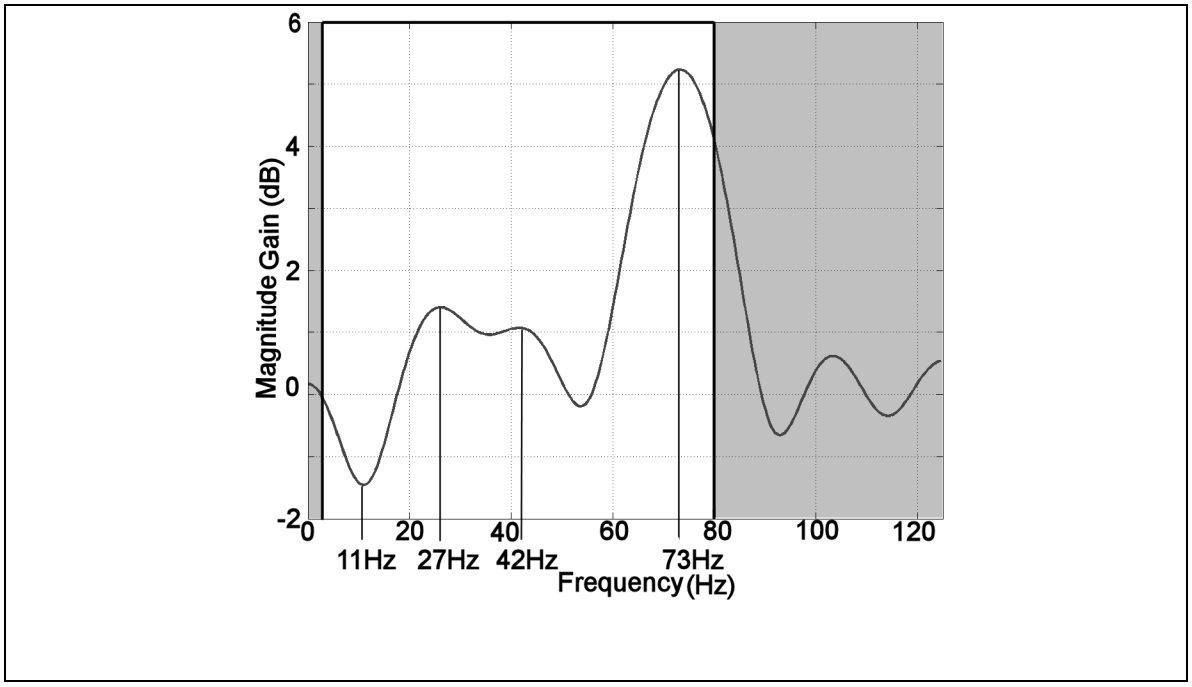

Figure 2. Magnitude frequency spectrum of the shaping filter created via automatic detection of frequencies of independence. Peaks in the magnitude spectrum emphasize frequencies of independence while troughs de-emphasize frequencies of dependence. The idealized magnitude characteristics of the band-pass filter used to prepare the EEG data is indicated by the shaded region in the figure.

Component Assessment

Scoring, Matching, and Assessing Topographies

Components have been numbered 1 through 30 according to their descending PSV scores, separately, for each decomposition method. When sorted by their PSV scores, most noise-related components were separated from possible brain-related activities. The

topographies of components above the threshold used to separate artefacts from possible brain activity sources are plotted in Figure 3. EEG components topographies calculated using the standard method are given in Figure 3a while those calculated using the shaped method are given in Figure 3b.

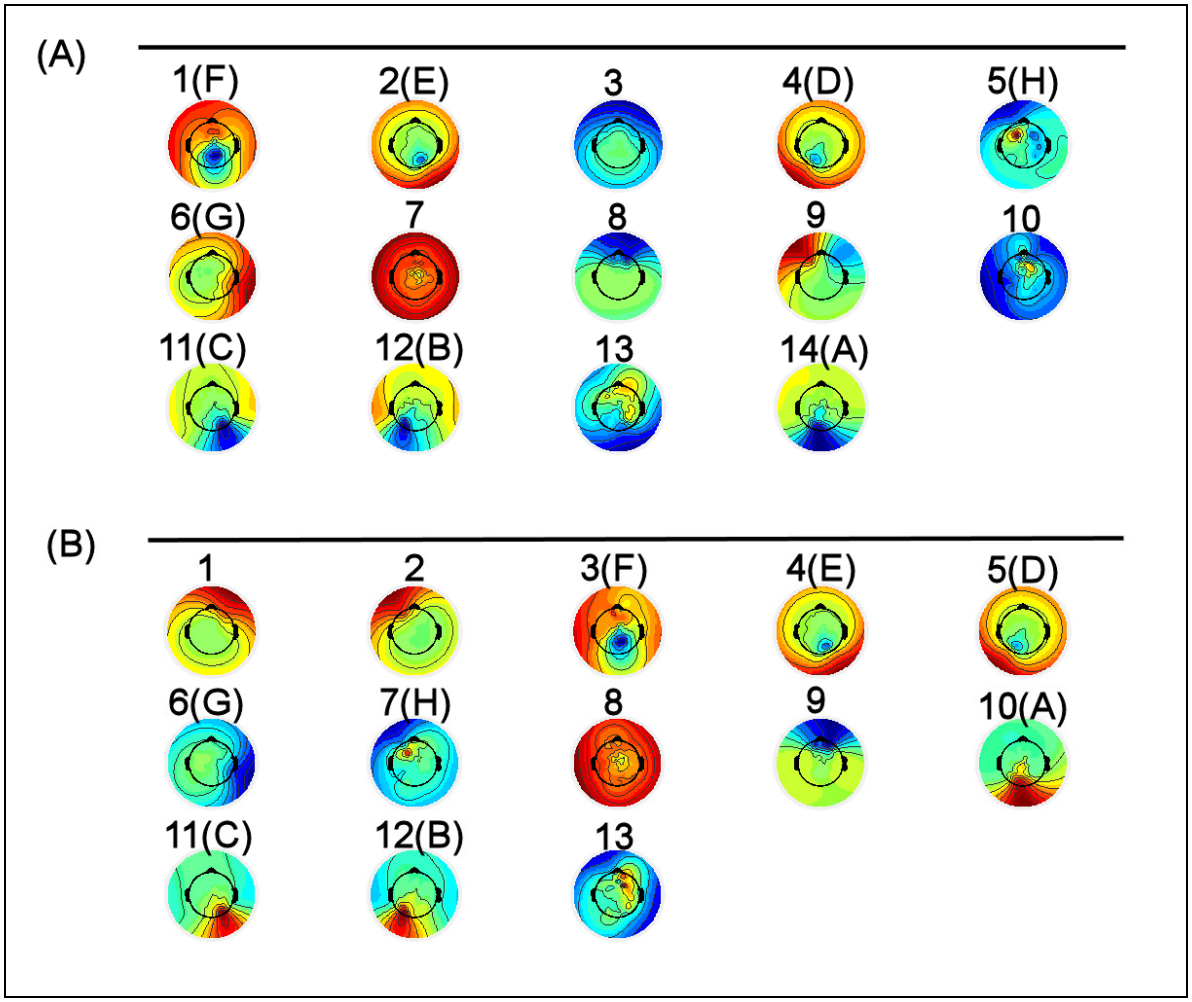

Figure 3. Topographies corresponding to EEG components calculated. (A) standard; (B) shaping. Topographies are sorted in descending order according to PSV rank. Only those components greater than the cut-off threshold are shown. Components are cross-labelled by letter to retain their PSV sorted rank and component matching for standard and shaped components/topographies. Colors of maximum red or blue intensity indicate positive or negative maxima, respectively. Green indicates neural or zero. Component topographies have a sign ambiguity when they are evaluated independently of their waveform activity

(Zeman et al., 2007; Makeig et al., 2004). In the current figure, relative polarities as positive or negative are not important when making comparisons between topographies.

By comparing components according to their topographies across decomposition methods, a set of 8 common dipolar components was identified and cross-labelled as (A) to (H) (Figure 3) to be used to compare decomposition characteristics of the two methods. Component 8 of the standard method and component 9 of the shaped method, although they match across decomposition methods and they fit our criteria of a dipolar component, were not cross-labelled and included in the methods comparison.

Decomposition Algorithm Assessment by Common Components

Visible differences (Figure 3) between the topographies $\mathbf{A}_j$ of the cross-labelled components suggest improvement was provided by the spectral shaping method over the standard method. Topographies F and H, calculated using the spectral shaping method, are visibly smoother and more dipolar (using the definition given in the introduction of this paper) for the spectral shaping method than those calculated via the standard method. This is most clearly visible for component H where better separation of a left hemisphere contributor from possibly 2 right hemisphere contributors to the EEG is evident.

Three noise components from the standard method and two components omitted from the spectral shaping method that were not eliminated via the PSV threshold were eliminated because they did not meet the dipolar criteria. These were components 7 from the standard decomposition method and 8 from the spectra shaping decomposition method and components 10 and 13 from the standard decomposition method with topographies that are similar to component 13 from the spectral shaping decomposition method.

Two unique components calculated by each decomposition method did not have matching topographies between decompositions but did have dipolar topographies and warranted further investigation. Similarities of location of topographical foci (neglecting

polarity of the foci) for the topographies of components 3 and 9 of the standard decomposition and 1 and 2 calculated using the spectral shaping decomposition method suggest that these components from the two decompositions are related. Components 3 and 9 of the standard decomposition could thus be describing common origins of activities. Component 3 of the standard decomposition is characteristic of an in-phase, anterior bilateral source pair and appears to be related to the bilateral pair of components 1 and 2 of the spectral shaping decomposition. Component 3 might also be and in-phase version of the out-of-phase component 9 of the standard decomposition. This speculation is supported by the absence of components similar to component 3 and 9 from the spectral shaping decomposition and the presence of components 1 and 2.

Pair-Wise Correlation Spectra of Common Components

The pair-wise correlation spectra for a subset of the component pairs is provided in Figure 4. The pair-wise correlation spectra of components of Figure 4 calculated using the standard method is generally flat compared to those of the shaped method suggesting an important change in the time-domain activities of estimated sources. Generally, the pair-wise correlation is larger at low frequencies and smaller at high frequencies for the shaped method than for the standard method. (Except for the pair given in Figure 4c.) Error bars in the figure illustrate the consistency of the pair-wise correlation spectra across the 96 trials of data in the frequency band 2-80 Hz for both the shaped and standard methods. For the 80-100 Hz frequency band, however, the error bars indicate that pair-wise correlations are not consistent. The inconsistency in this band is expected as it is outside the frequency range (2-80 Hz) of the band-pass filter used in preparing the EEG data for analysis.

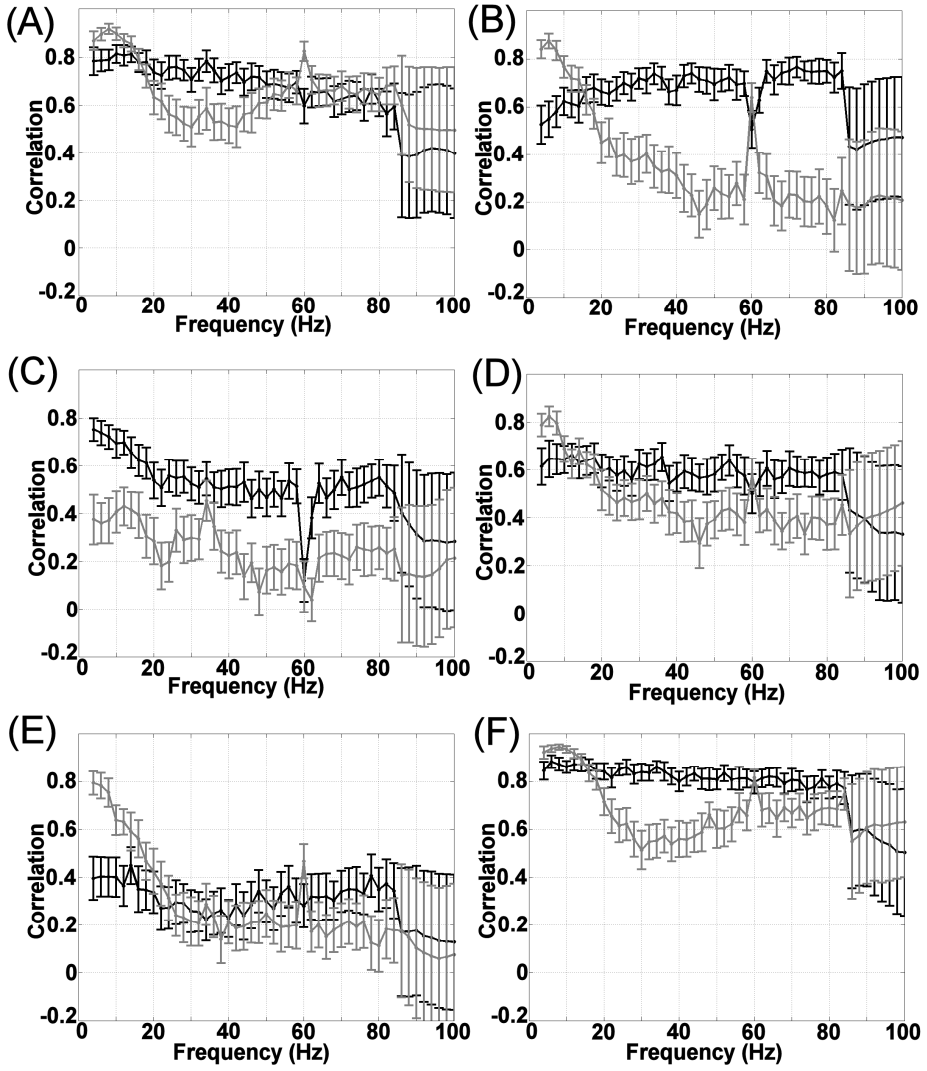

Figure 4. Pair-wise correlation as a function of frequency for a sample of 8 of the 28 pair-wise correlation spectra for the shaped and standard decompositions. Gray plotted lines are shaped component results. Error bars on each plot are the standard deviation of the mean of 2000 random samples of 20 trials from the 92 trial dataset for a given component pair. These results were plotted. Black plotted lines are the standard component results. Component pairs are (A) B and D; (B) A and F; (C) G and H; (D) A and E; (E) E and H; (F) E and C.

Grand-Average Pair-Wise Correlation Spectra of Common Components

The grand-average pair-wise correlation spectrum of components obtained using the spectral shaping method has a greater range of correlation than that of the standard method. This difference is illustrated in Figure 5. This range of correlation of components activities calculated using the spectral shaping method has a shape more similar to the power spectrum of scalp EEG than that of the standard method, with maximum correlation at low frequencies (< 20 Hz) and minimum correlation at high frequencies. There is a peak correlation of 0.65 at 6 Hz, with a gradual decrease in correlation to approximately 0.3 at 36 Hz. The correlation spectrum is relatively flat at approximately 0.3 in the interval 36-85 Hz (excluding a peak at 60 Hz). In contrast, the average pair-wise correlation spectrum for the standard decomposition is relatively flat with correlation equal to 0.4 between 20 and 85 Hz. However, it has a peak correlation of 0.5 between 2 and 20 Hz. For the spectral shaping method and the standard method, the correlation is low (consistently < 0.3) for frequencies greater than 85 Hz.

The grand-average pair-wise correlation spectra of the shaped method indicate that there are distinct regions where correlation of brain activities exists and where correlation does not. It demonstrates that areas of the brain have varied levels of correlated activities in the frequency band 2-38 Hz, whereas at frequencies higher than 38 Hz, there is little to no correlation relating to brain activity. Frequencies greater than 38 Hz illustrate the noise floor indicating uncorrelated activity. There is a clear average difference between correlation activities of the band 2-20 Hz and 20-40 Hz.

A 60 Hz peak that is likely AC power noise in the grand-average pair-wise correlation spectra illustrates that the spectral shaping method does not suppress the correlated 60 Hz noise activity present in each component. Conversely, for the standard decomposition there is a notch in the correlation structure at 60 Hz. This AC power noise is ever present in the environment and its visibility in this result is not unreasonable.

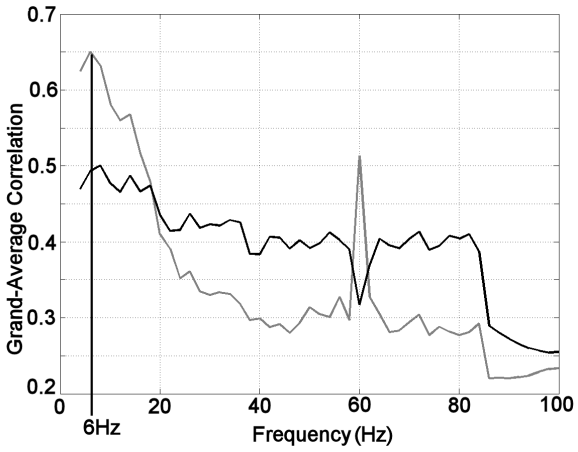

Figure 5. The average pair-wise correlation spectra for the standard (black) and shaped (grey) decomposition methods.

The plots of Figure 6 show the average pair-wise correlation level calculated across components of each decomposition method. Significant differences between decomposition methods for the pair-wise correlation spectra of the high EEG frequency band are indicated by the plots of Figure 6a that compare the brain (2-38 Hz) and non-brain (40-76 Hz) frequency intervals. The average correlation level of the shaped spectrum is significantly lower than that of the standard spectrum ($p=0.0201$) for the high frequency band (40-76 Hz). For the low frequency EEG band (2-38 Hz), there is no significant difference ($p=0.933$) between the average correlation level for the two decomposition methods. This indicates that the activities in the high frequency EEG band (denoted in the figure as 'HighEEG' in Figure 5) are uncorrelated.

The plots of Figure 6b, illustrating differences between the decomposition methods, show that on average, the standard decomposition method obscures the correlative relationships between activities of different parts of the brain and that the shaped method preserves them. The shaped method provides a statistically significant increase ($p=0.0232$) in the pair-wise correlation of the low frequency brain activity band (denoted in the figure as

'LowBrain') (2-18 Hz) and a significant decrease ($p = 0.0159$) in the high frequency brain activity band (denoted in the figure as 'HighBrain') (20-38 Hz) compared to the standard method. This result indicates that the low frequency brain activity band has higher correlation for the shaped method than the standard method while for the high frequency brain activity frequency band the shaped method has lower correlation than the standard method.

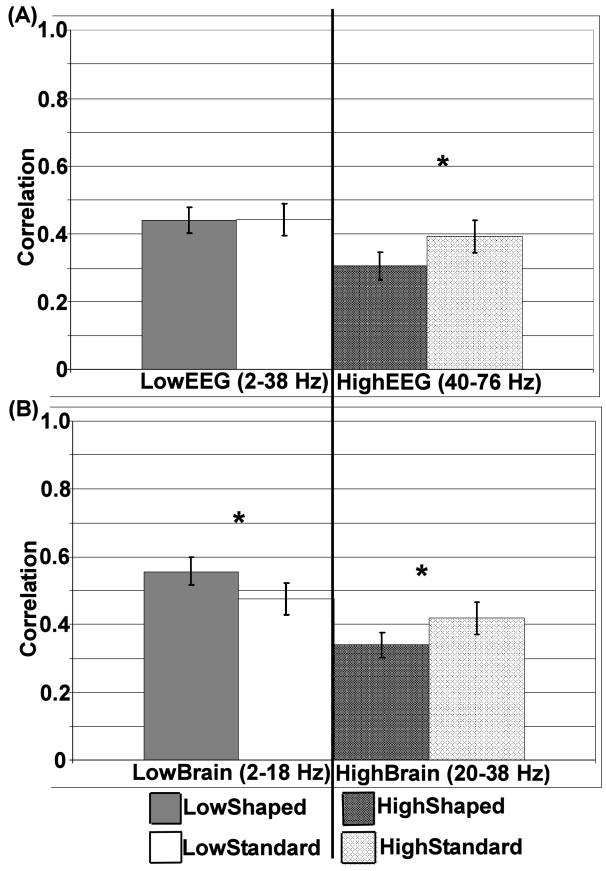

Figure 6. The summarized pair-wise correlation of components for various frequency bands comparing the shaped and standard methods. Error bars indicate standard error. Statistically significant differences are indicated as (*). (A) comparison of shaped and standard methods for the EEG frequency spectrum divided into two bands, LowEEG (2-38 Hz) and HighEEG (40-76 Hz). The difference between the methods for the HighEEG

band is significant (p=0.0201) for $p < 0.05$. (B) comparison of the shaped and standard methods for the brain activity portion of the EEG spectrum. There is a significant difference ($p = 0.0232$) for LowBrain frequency band (2-18 Hz) and a significant difference (p=0.0159) for HighBrain frequency band (20-38 Hz) for $p < 0.05$.

Volume-Domain Overlap of Common Components

Figure 7 shows that the spectral shaping method has a lower average PVO than the standard method. However, a t-test examining the difference between methods yielded a non-significant difference (p=0.56) in the pair-wise volume overlap properties indicating that this decrease was not significant and that there is no substantive difference in the volume representations of components.

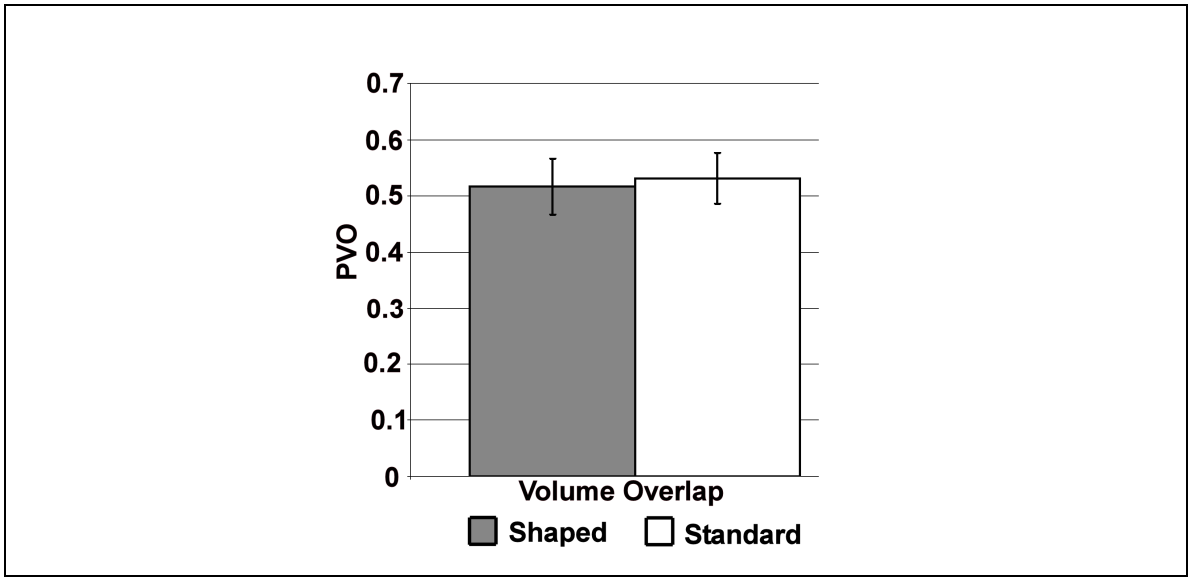

Figure 7. Comparison of the pair-wise volume overlap (PVO), ranging from 0 to 1 for components common to both the shaped and standard decomposition methods showing that there is on average no statistically significant difference. A value of 0 indicates no overlap while a value of 1 indicates maximum possible overlap. Error bars are the standard error.

The individual PVOs of each component for each decomposition method are given in Table 1, along with the difference calculated between the decomposition methods. In 16

of the 28 pair-wise comparisons (57% of the comparisons), the PVO was lower for the spectral shaping method than for the standard method. The greatest PVO decrease resulting from spectral shaping was seen for component pairs: H-A, H-B, H-D, H-E, H-F while the greatest PVO increase was seen for component pairs: A-G, C-G, E-G, H-G.

Component Pair	Shaped Method	Standard Method	Shaped - Standard
A-G	0.351	0.181	0.171
A-H	0.256	0.558	**-0.301**
B-C	0.451	0.494	**-0.0433**
B-D	0.791	0.802	**-0.0106**
B-E	0.45	0.471	**-0.021**
B-F	0.454	0.465	**-0.0107**
B-G	0.0828	0.0251	0.0578
B-H	0.00301	0.449	**-0.446**
C-D	0.554	0.582	**-0.0279**
C-E	0.868	0.872	**-0.00324**
C-F	0.712	0.688	0.024
C-G	0.764	0.62	0.144
C-H	0.465	0.553	**-0.0875**
D-E	0.694	0.705	**-0.0109**
D-F	0.559	0.494	0.0652
D-G	0.0475	0.0499	**-0.00242**
D-H	0.198	0.472	**-0.274**
E-F	0.656	0.575	0.0814
E-G	0.4	0.249	0.151
E-H	0.368	0.488	**-0.12**
F-G	0.421	0.351	0.0703
F-H	0.342	0.434	**-0.0916**
G-H	0.494	0.307	0.187
A-G	0.517	0.532	-0.0154
A-H	0.351	0.181	0.171
B-C	0.256	0.558	**-0.301**
B-D	0.451	0.494	**-0.0433**
B-E	0.791	0.802	**-0.0106**

Table 1. The pair-wise volume overlap (PVO) of the set of cross-labelled components common to both the standard and the spectral shaping decomposition methods. Table entries where the shaped decomposition method is less than that of the standard decomposition method are given in bold.

Decomposition Algorithm Assessment by Unique Components

Modular Volume Depiction of Unique Components

The plot of Figure 8a shows that components 1 and 2 of the shaped decomposition method pertain to a pair of bilateral modular volumes. These comprise a bilateral source pair located in the orbital regions of the skull beneath the left and right poles of the frontal lobe of the cerebral cortex. Visual comparison of calculated modular volumes of these components with fMRI results examining activities of the orbital muscles of a different study (Law et al., 1998) provides corroboration that these two components represent the activities of the orbital muscles of the right and left eyes, respectively. This result shows that the spectral shaping method correctly identified these sources contributing to the EEG as two distinct entities. The standard decomposition method does not yield similar components topographies that can be localized as similar source volumes and thus it does not appropriately separate the ocular muscles activities contributing to the EEG. The ocular movement activities contributing to the EEG were, in fact, separated into an 'in-phase' component and an opposite-phase component as visible by their topographies (see components 3 and 9 of the standard decomposition in Figure 3a).

Pair-wise Cross-Correlation Spectra of Unique Components

The pair-wise cross correlation of components 1 and 2 of the shaped decomposition illustrated in Figure 8b shows a distinct notch in the pair-wise correlation at 34 Hz. There is also a peak in the correlative structure at 60 Hz and a general increase in pair-wise correlation from 2-8 Hz. Excluding the 34 Hz frequency band, the correlation is approximately flat between 8 and 84 Hz with an average correlation of approximately 0.46. This result shows that the spectral shaping method can successfully separate the activities of two components that have a relatively high correlation at most frequencies except for a single narrow frequency band.

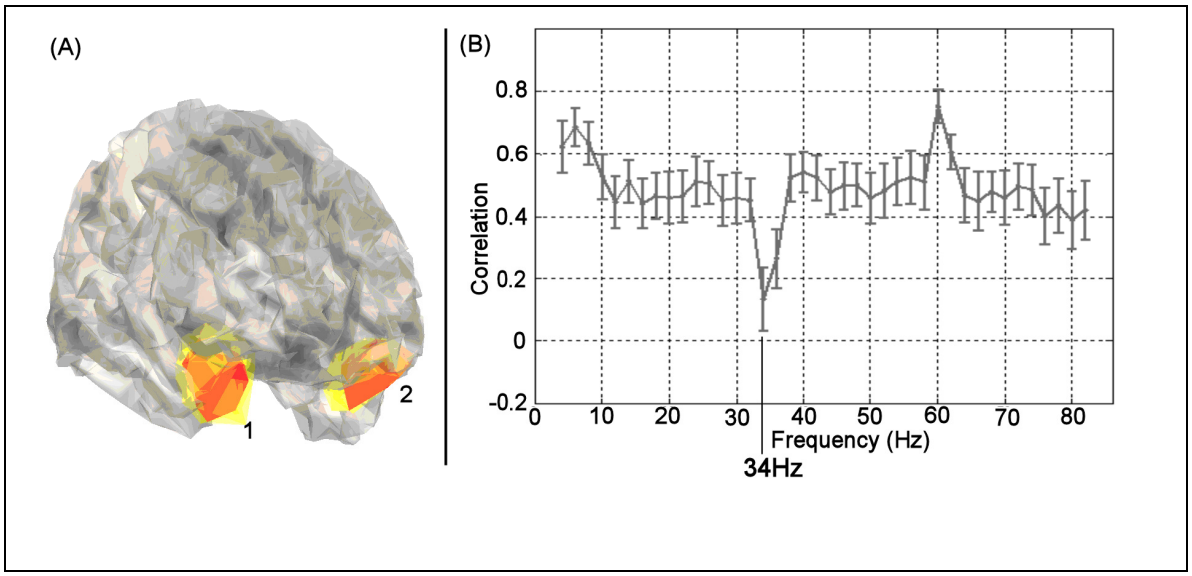

Figure 8. Results of the new components of the shaped decomposition. (A) The volumes of components 1 and 2 for 4 (yellow) and 5 (red) standard deviations above the volume noise estimate (Zeman et al., 2008b). (B) The pair-wise correlation as a function of frequency for components (1 and 2). Error bars are the standard deviation of random samples of the mean.

IV. DISCUSSION

The discussion is divided into three parts. First, the implications of results presented earlier in the paper are interpreted, and where appropriate, are related to other work. Subsequent to this, the main findings are summarized. Finally, the paper is concluded with a statement of how the methods and results have addressed our main objectives.

This study has demonstrated that the statistics across the EEG frequency spectrum vary according to frequency band. This study has also demonstrated that emphasizing frequencies of independence of the EEG data prior to calculating the ICA source separation matrices can improve ICA estimates of contributors to the EEG. Furthermore, this study has demonstrated that the separation of highly correlated sources comprising

the EEG is possible. These findings were demonstrated using real EEG data collected from study participants while they were engaged in a computer-based virtual spatial navigation task. The Band-Selective ICA (BSICA) algorithm (Zhang and Chan, 2006) in combination with the runica algorithm (Makeig et al., 1997) were used to calculate a frequency spectrum shaping filter to emphasize frequencies of statistical independence in the EEG data. Subsequently, this shaping filter was used to shape the frequency spectrum of the EEG data before applying the runica algorithm a second time to calculate spatial source separation filters. These spatial separation filters were then used to separate the original unshaped EEG into the estimates of individual source contributors to the EEG data. The source estimates obtained via spectral shaping were compared to results obtained using standard application of runica. Differences in the estimates of brain activity using the spectral shaping method versus the standard method were evaluated according to characteristics of component scalp topography, volume-domain overlap, and pair-wise correlation of component time-domain activities at steps in frequency.

The statistical property that a variable is required to be uncorrelated if it is statistically independent (Hyvärinen et al., 2001) makes it appropriate to use the shaping filter calculated to identify frequencies of independence, to identify frequencies of uncorrelatednesss. For this reason, it is appropriate to shape the EEG spectrum prior to calculating the sphering matrix **P** to reduce the negative effects of correlated source activities on source separation. Thus, when the algorithm identifies the frequencies of independence it is also identifying frequencies of uncorrelatedness. The converse however is not true. Frequencies that are not emphasized by the shaping filter are not necessarily correlated.

Preserving the correlative relationship among source activities is useful for those neuroscience studies that wish to examine the transfer of information throughout the brain or the coordinated relationships among areas of the brain. For example, in a study using implanted cortical electrodes, Roelfsema at al. (1997) demonstrated correlated

activities between multiple areas of the brain of cats. From these correlated activities, they inferred that these brain areas were operating together to facilitate behaviour.

SHAPING FILTER

From the magnitude spectrum of the spectral shaping filter that was calculated to emphasize frequencies of independence, it is clear that the level of statistical independence among sources varies according to EEG frequency band considered. The result that the magnitude spectrum of the shaping filter indicated that there is greater independence for frequencies greater than 50 Hz than for frequencies lower than 50 Hz is sensible, since much of the variance of brain activity found in scalp-recorded EEG data is below 50 Hz; activities comprising the EEG that have frequencies greater than 50 Hz are likely to be either external interference or weak brain activity. The varied levels of independence for the brain activity frequency band (frequencies less than 50 Hz) illustrated by the magnitude spectrum of the shaping filter indicates the activities of the brain have varied statistical characteristics depending on the frequency band examined; it is evident that brain activities in the current dataset for the frequency band of 18-50 Hz are more independent (at zero lag) than those less than 18 Hz.

ASSESSING TOPOGRAPHIES

The result that there were subtle improvements of the dipolar characteristic of some of the topographies of components found using the spectral shaping method over the standard method qualitatively suggests the spectral shaping method provides better source separation of the EEG than the standard method. These subtle changes however are difficult to quantify and are not sufficient to draw any conclusions regarding improvements provided by shaping of the EEG spectrum. Thus, other component characteristics were examined.

PAIR-WISE CORRELATION SPECTRA OF COMMON COMPONENTS

The result that the correlation spectra of component activities as a function of frequency calculated using the spectral shaping method are more similar to brain activity frequency spectra than the correlation spectra calculated using the standard decomposition method provides important objective evidence that the spectral shaping method preserved correlated activities. This is evident as a trend in the pair-wise correlation plots and is clearly demonstrated by the grand-average plot of the pair-wise correlations; most of the power of the correlation spectrum is located at low frequencies with less power at high frequencies.

VOLUME-DOMAIN OVERLAP OF COMMON COMPONENTS

Small reductions in the volume overlap of most of the components were present for the spectral shaping method compared to the standard method however, this did not result in a significant average difference between decomposition methods. This small reduction in volume overlap for most sources was obscured in the calculated average difference by slight increases in the volume overlap for a small number of components. Following results found in our prior work, a more conclusive difference in the average volume overlap was expected in the current study. In our prior work examining convergence characteristics of volume characteristics of ICA derived sources (Zeman et al., 2008d) we found that over successive iterations of reduction in statistical dependence using the runica algorithm, the MVO reduces and converges for components. There are multiple possible reasons for the non-significant change in the current study. For example, (1) brain source volumes may have been adjusted to their bona fide volume overlap characteristics, (2) the non-significant changes or increases might be related to inaccuracies or limitations of the head model thus demonstrating a limit of the volume estimation method, or (3) the criterion of statistical independence might identify activites that pertain to the centers of mass of very focal brain areas as to region of maximal statistical independence (independent functional units without long-distance interaction

with other brain areas) while in contrast, the spectral shaping method, allowing for some correlated activity, will identify an entire active structure region of the brain.

VOLUME DEPICTION AND CROSS-CORRELATION OF UNIQUE COMPONENTS

The result that localization and volume estimation of the two unique dipolar components relate to the extra-ocular muscles (Law et al., 1998) and that these two volumes are highly correlated at most frequencies except for the narrow band at 34 Hz provides strong evidence that tightly correlated sources can be separated using the shaping methodology. This finding is in agreement with prior literature (Brown and Day, 1997) which shows that the eyes have an acceleration peak around the frequency of 34 Hz. Generally, when a saccade of the eyes takes place, the eyes move together and and in-phase as the eyes move left or right together. During vergence, the eyes act to maintain fixation on an object and thus move inward and down to maintaining fixation on an object stimulus. The decreased correlation at 34 Hz measured over the trials of data might arise by two mechanisms. Eye movements might be uncorrelated during vergence as each eye must adapt to its own unique perturbations to maintain fixation on the object. This drop in the correlation at 34 Hz might also arise as an effect of the size of the correlation analysis window. For example, in part of the analysis window, the eyes may move in phase, left and right, for saccadic movement and in another part of the same analysis window, the eyes move in the opposite phase during moments of vergence. Thus the window may contain both negative and positive correlations, resulting in a decreased total correlation for the analysis window.

The result that the left and right occulo-motor components can now be appropriately separated from the EEG mixture provides for an important possibility for neuroscience research. Because the exact phase and frequency of bursts of information that the eyes provide the brain between movements of the eyes is now known from the time-domain activities of the ocular components, these bursts can potentially be traced throughout the brain. In addition, the ability to determine periods of vergence from the eye movement

activities in the EEG at 34 Hz provides a possible reference signal to determine when the study participant is fixating on a stimulus versus when they are simply moving their eyes with no specific point of fixation and interest.

SUMMARY AND CONCLUSIONS

Our results suggest that the changes provided by the spectral shaping method over the standard method were in the direction of improved activity estimates. Significant changes in the time-structure of component activities were accompanied by small non-significant changes to the volume-domain characteristics of components. The significant changes in the pair-wise correlative structure were in the direction to make the activities more 'brain-like' indicating that the spectral shaping method can reduce estimate error we have called forced independence distortion.

Further, the proposed spectral shaping method was able to split a bilateral pair of components that had highly correlated activities at most frequencies except for a narrow band of frequencies for which they were uncorrelated. These bilateral components were not appropriately represented via decomposition of the EEG data using the standard method and thus the spectral shaping method can address estimation error due to failed separation distortion.

In sum, the strict requirement that sources comprising the EEG mixture be statistically independent is relaxed so that frequency bands of dependence and correlated activities can exist. This study has demonstrated that the statistics across the scalp-EEG frequency spectrum are variable and that by shaping of the EEG frequency spectrum prior to standard ICA decomposition the estimates of source activities can be improved.

Acknowledgements:
Funding for this study was provided in part by the Natural Sciences and Engineering Research Council of Canada and by the Alberta Heritage Foundation. Thank-you also to

Sunny Mahajan who's role in the development of the volume estimation methods made this study possible.

V. CONCLUSIONS

The analysis presented in this study indicates that spectral shaping enables separation of components not separable by standard ICA methods. This method more effectively estimates modular source activities than established methods.

VIII. REFERENCES

Amari S, Cichocki A. A New Learning Algorithm for Blind Signal Separation. In: Advances in Neural Information Processing Systems 8, Editors D. Touretzky, M. Mozer, and M. Hasselmo, pp757-763, MIT Press, Cambridge MA, 1996

Anenüller J, Sejnowski TJ, Makeig S. Complex independent component analysis of frequency-domain electroencephalographic data. Neural Networks 2003;16(9):1311-1323.

Baillet S, Mosher JC, Leahy R. BrainStorm beta release: a Matlab software package for MEG signal processing and source localization and visualization. Proceedings of the 16th Annual Meeting of the Organization for Human Brain Mapping, San Antonio, Texas, 2000.

Başar, E. Memory as the "whole brain work": a large-scale model based on "oscillations in super-synergy". International Journal of Psychophysiology 2005;58:199-226.

Bell A, Sejnowski TJ. An information-maximization approach to blind separation and blind deconvolution. Neural Comp 1995;7:1129-1159.

Brown P, Day BL. Eye acceleration during large horizontal saccades in man. Experimental Brain Research 1997; 113:153-157.

Contreras-Vidal JL, Kerick SE. Independent component analysis of dynamic brain responses during visuomotor adaptation. NeuroImage 2004; Mar. 21(3):936-945.

Delorme A, Makeig S. EEGLAB: an open source toolbox for analysis of single-trial EEG dynamics including independent component analysis. J. Neuroscience Methods 2004;134:9-21.

Delorme A, Serby H, Makeig S. EEGLab Tutorial: VI. Independent Component Clustering. Retrieved October 11, 2006 from <http:\\www.sccn.ucsd.edu/eeglab/clusttut/clustertut.html>.

Dien J, Wayne K, George RM. Evaluation of PCA and ICA of Simulated ERPs: Promax vs. Infomax Rotations. Human Brain Mapping, 2007;28:742-763.

Donchin E, Heffley E, Multivariate analysis of event-related potential data: A tutorial review. In D. Otto (Ed.) Multidisciplinary perspectives in event-related potential research (EPA 600/977-043) pp.55-572. Washington, DC. US Government Printing Office.

Dyrholm M, Makeig S, Hansen LK. Model Selection for Convolutive ICA with an Application to Spatiotemporal analysis of EEG. Neural Computation 2007;19(4):934-955.

Hamilton DA, Kodituwakku P, Sutherland RJ, Savage DD. Children with Fetal Alcohol Syndrome are impaired at place learning but not cued-navigation in a virtual Morris water task. Behavioural Brain Research 2003, 143:85-94.

Hyvärinen A. Fast and Robust Fixed-Point Algorithms for Independent Component Analysis. IEEE Transactions on Neural Networks. 1999;10(3):626-734.

Hyvärinen A, Karhunen J, Oja E. Independent Component Analysis. New York: John Wiley & Sons, 2001.

Hyvärinen A, Oja E. A fast fixed-point algorithm for independent component analysis. Neural Computation 1997;9(7):1483-1492.

Jung TP, Makeig S, Westerfield M, Townsend J, Courchesne E, Sejnowki TJ. Analysis and visualization of single-trial event-related potentials. Human Brain Mapping 2001; Nov. 14(3):166-85

Kosslyn SM, Pascual-Leone A, Felician O, Camposano S, Keenan JP, Thompson WL, Ganis G, Sukel KE, Alpert NM. The Role of Area 17 in Visual Imagery: Convergent Evidence from PET and rTMS. Science 2 1999, vol 284 no 5411, 167-170.

Law I, Svarer C, Rostrup E, Paulson O. Parieto-occipital cortex activation during self-generated eye movements in the dark. Brain 1998:121;2189-2200.

Lee T-W, Girolami M, Sejnowski T. Independent component analysis using extended infomax algorithm for mixed sub-Gaussian and super-Gaussian sources. Neural Comput., 1999;11(2):609-633.

Makeig S, Bell A, Jung T, Sejnowski, T. Independent component analysis of electroencephalographic data. In: Touretzky D, Mozer M, Hasselmo M (Eds). Advances in Neural Information Processing Systems. MIT Press, 1996;8:145-151.

Makeig S, Delorme A, Westerfield M, Jung TP, Townsend J, Courchesne E, Sejinowski TJ. Electroencephalographic Brain Dynamics Following Manually Responded Visual Targets. PloS Biology 2004;Jun.2(6):0747-0762

Makeig S, Jung TP, Ghahremani D, Bell AJ, Sejnowski TJ. Blind separation of auditory event-related brain responses into independent components. Proc Natl Acad Sci USA 1997;94:10979-10984.

Makeig S, Jung T-P, Ghahremani D, Sejnowski TJ. Independent Component Analysis of Simulated ERP Data. In: Nakada T (Ed). Integrated Human Brain Science: Theory, Method, Applications (Music). Elsevier, 2000.

Menendez RGP, Andino SG. Comparison of Algorithms for the Localization of Focal Sources: Evaluation with Data and Analysis of Experimental Data. V4 n?. International Journal of Bioelectromagnetism

Nishitani N, Schürmann M, Amunts K, Hari R. Broca's Region: From Action to Language. Physiology 2005. 20:60-69.

Nunez PL. Generation of Human EEG by a Combination of Long and Short Range Neocortical Interactions. Brain Topography 1989;1(3):199-215.

Onton J, Delorme A, Makeig S. Frontal midline EEG dynamics during working memory. NeuroImage 2005; Aug 15;17(2):341-356.

Parra L, Sajda P. Converging Evidence of Linear Independent Components in EEG, Proc 1st Int'l IEEE EMBS Conf. Neural Eng 2003;525-528.

Roelfsema, PR, Engel AK, Konig P, Singer W. Visuomotor integration is associated with zero time-lag synchronization among cortical areas. Nature 1997; 385:157-161.

Silberstein P, Pogosyan A, Kuhn AA, Hotton G, Tisch S, Kupsch A, Dowsey-Limousin P, Hariz MI, Brown P. Cortico-cortical coupling in Parkinson's disease and its modulation by therapy. Brain 2005,128:1277-1291.

Sorensen PL, Zeman PM, Sutherland RJ. Differing patterns of synchronous cortical activity during a virtual spatial navigation task. Canadian Society for Brain, Behaviour and Cognitive Science, 16th Annual Meeting. Paper presentation. 2006.

Spencer KM, Dien J, Donchin E. A componential analysis of the ERP elicited by novel events using a dense electrode array. Phychophysiology 1999;36:409-414.

Yao D. A method to standardize a reference of scalp EEG recordings to a point at infinity. Physiological Measurement 2001;22:693-711.

Zhang K, Chan L-W. An Adaptive Method for SubBand Decomposition ICA. Communicated by Hyvarinen, A. Neural Computation 2006:18;191-223.

Zeman PM, Till BC, Livingston NJ, Tanaka JW, Driessen PF. Independent component analysis and clustering improve signal-to-noise ratio for statistical analysis of event-related potentials. Clinical Neurophysiology 2007; 118(12):2591-2604.

Zeman PM, Sorensen PL, Livingstone SA, Skelton RW, Livingston NJ. Understanding and Improving ICA Source Separation of EEG Data. (for publication) 2008a.

Zeman PM, Mahajan SV, Livingstone SA, Driessen PF, Skelton RW, Livingston NJ. Beamform Volume Projection of EEG ICA Topographies. (for publication) 2008b.

Zeman PM, Mahajan SV, Sorensen PL, Driessen PF, Skelton RW, Livingston NJ. Beamform Volume Projection of ICA Components of Scalp EEG: Volume-Domain Uniqueness of Components. (for publication) 2007c.

Zeman PM, Mahajan SV, Livingstone SA, Driessen PF, Skelton RW, Livingston NJ. Volume Domain Validation of ICA-Derived EEG Sources. (for publication) 2008d.

APPENDIX A- BLOCK DIAGRAM OF ANALYSIS METHODOLOGY

A block diagram illustrating the procedure used to evaluate the performance of the proposed algorithm against the standard method is given in Figure A1.

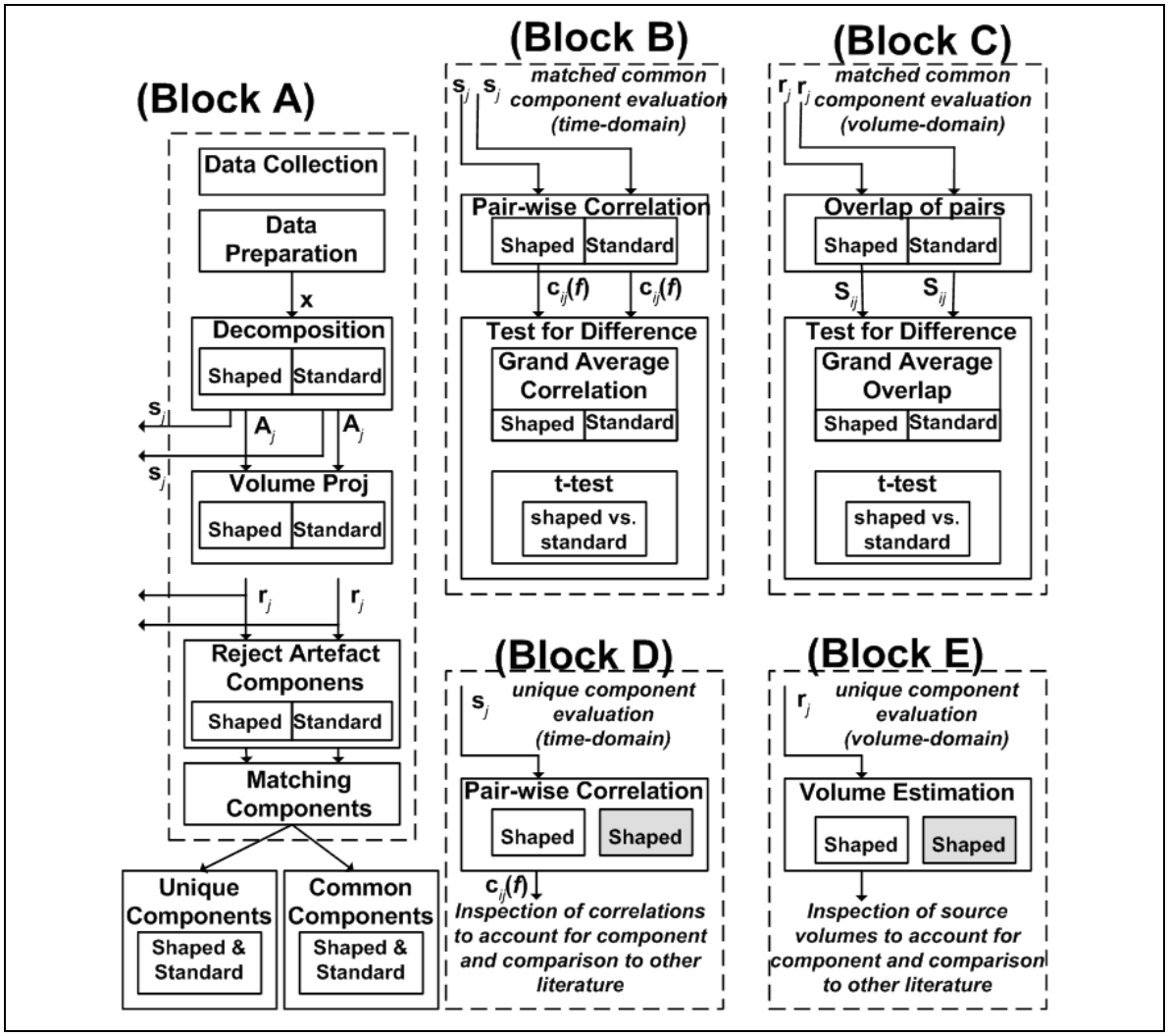

Figure A1. Block diagram of the analysis steps used to compare the decomposition results of the spectral shaping method against results obtained using the standard separation method, runica. (Block A) EEG decomposition via both the shaped and standard methods and matching of components with similar topographies between

decompositions; (Block B) evaluation of the components with topographies that are similar between both decompositions by time-domain metrics; (Block C) evaluation of the components with topographies that are similar between both decompositions by volume-domain metrics; (Block D) evaluation of unique components of the shaped decomposition by time-domain metrics; (Block E) evaluation of the unique components of the shaped decomposition by volume-domain metrics.

Section IV: The novelty, utility, and context of the methodological advancements

The previous section described new methods for obtaining more information about the brain activities hidden in the scalp EEG. In Chapter 3, a method of projecting the topographies of ICA components into a volume-domain representation was proposed. This volume projection algorithm facilitated the estimation of the modular volume of brain-related components of the EEG (provided that these components are appropriately separated and thus have single centers of mass), and measures of the volume-domain overlap of these components. In Chapter 4, the estimation of modular component volumes and estimation of volume-domain overlap of components using real EEG data was examined. Using the collective results of the two prior chapters, Chapter 5 demonstrated that the volume-domain overlap of components, the peak value of the volumetric spectrum, and the convergence characteristic of the movement of the center of mass of each component can be used to evaluate how well components represent physically modular brain sources. Finally, in Chapter 6, we examined a new method for mining the EEG data to obtain more accurate estimates of bona fide brain sources volumes and source activities. The new method incorporates the concept of notch filtering introduced in Chapter 2, and expands on it. The results in Chapter 6 show that by shaping the EEG frequency spectrum to emphasize frequencies for which source activities are independent and de-emphasizing frequencies for which source activities are correlated or dependent, source estimation error can be reduced. It was shown that this new method yields components that are better representations of bona fide brain sources than the standard ICA method.

The purpose of the current section is to explain how all of the concepts presented thus far relate and can be combined together to provide a new analytical approach for examining EEG data. It is shown that single subject analysis of EEG data using this complete methodology can in fact be accomplished. Information can be meaningfully extracted from the EEG to describe the coordination of the different areas of the brain and how

they function over time. Results presented in the current section are an elaboration of the data examined in Chapter 6.

Chapter 7: Building a Multi-Component Spatio-Temporal Model of Brain Activity Using Scalp EEG Data

The following manuscript provides results showing the successful use of the combination of the methods developed for transforming the scalp EEG into a meaningful representation of brain activity.

The results provided here show that the power levels for specific brain areas vary over time and that the power levels of these areas are different between behavioural conditions associated with the virtual Morris Water Task paradigm. The time-varying level of correlation between the activities of multiple distinct brain areas is demonstrated. We demonstrate that this time-varying correlation provides a means to show differences in the brain area coordination between behavioural conditions and thus, that the method is sensitive to differences in cognitive brain activity. The new methodology is compared and contrasted with similar new methodologies to demonstrate the uniqueness and benefits of our methodology for analysis of EEG data.

Article Type: Research Article

Article Title: Building a Multi-Component Spatio-Temporal Model Using Scalp-EEG Data

Philip M. Zeman[1,2,3], Sharon A. Livingstone[3], Nigel J. Livingston[1], Ronald W. Skelton[3]

[1] CanAssist, University of Victoria, BC, Canada

[2] Department of Electrical and Computer Engineering, University of Victoria, BC, Canada

[3] Department of Psychology, University of Victoria, BC, Canada

Correspondence may be addressed to Philip M. Zeman:
(voice) +1-250-589-4234 / (fax) +1-250-721-6611 / pzeman@alumni.uvic.ca

ABSTRACT

Recent technological advances in EEG data analysis have addressed some important barriers to obtaining useful information about functional brain activity from scalp recordings. In this paper, an EEG analysis methodology that incorporates these new advances is described and results obtained using this methodology are presented. To demonstrate the advantageous features of this methodology, its characteristics are compared to other closely related experimental methodologies.

The motivation to separate the scalp-EEG into individual activities of distinct areas of the brain is described. This motivation is contrasted with those of other related methods. It is demonstrated that the proposed method can achieve a system-level representation of brain function by showing how the activities of each area of the brain are correlated. The steps of the methodology are described in detail so that other researchers can use this methodology in their work. This method is compared to a closely related experimental method employed by the EEG analysis software package EEGLab (Makeig et al., 1997).

This methodology is described as follows. The data-mining process utilized by our new methodology is intended to more accurately isolate activities comprising the EEG that pertain to modular volumes of the brain; if the activities of distinct areas of the brain are accurately estimated by the source separation process, measures of the time-varying correlation relationship as a function of frequency between components of the EEG can be used to examine coordination and transfer of information between modular areas of the brain. Our methodology also incorporates a new method to represent brain activity components of the EEG as 3D volumes within the head. Lastly, our methodology incorporates a validation system that uses criteria that are independent of the data-mining criteria and are meaningful for evaluation of EEG components as representing activities from modular 3D areas of the brain.

This new methodology provides a means to extract functional information about the brain from scalp-acquired EEG data that differs from closely related experimental methodologies.

1. INTRODUCTION

Current scalp EEG analysis methods can be improved upon to show how different anatomical parts of the brain interact during information processing. Recent methods that have been developed attempt to show what areas of the brain are active (Makeig et al., 1997) for information processing during various behavioural paradigms, however, these methods are not appropriate to show how different areas of the brain coordinate their activities over time. This work proposes and demonstrates EEG analysis results that describe how different parts of the brain coordinate activities over time. This new analysis methodology has been developed from recent technical advancements in EEG analysis.

Three main technical barriers have recently been addressed by the recent work on which the proposed analysis methodology is based. The first barrier addressed is of mining the EEG data to separate partially correlated sources comprising scalp EEG data into component parts. Current Principal Component Analysis (PCA) and Independent Component Analysis (ICA) methods separate scalp-acquired EEG data using criteria of uncorrelatedness and statistical independence. However, these criteria are not necessarily appropriate to identify the actual, bona fide activities, originating from specific volumetric regions of the brain. It has, in fact, been shown that the brain activities that comprise the EEG are not necessarily uncorrelated or statistically independent (Roelfsema et al., 1997; Summerfield and Mangels, 2005; Silberstein et al., 2005). The second barrier relates to realistic anatomical modelling of the volumetric regions from which brain source activities originate. Point source dipole representations that account for EEG scalp potentials have been used in prior work and are only sparsely descriptive of the origin of scalp activities; they provide only a location of center of mass and do not describe the actual volumetric region from which scalp activities originate. Other methods map the scalp field of components of the EEG to the surface of a cortical model; they also do not provide a volume representation of the brain source region. Such a

measure of source volume can be advantageous, particularly when it is important to show that two components of the EEG have been well separated by the data-mining algorithm. The third barrier to development of a completely new EEG analysis methodology is the ambiguity in determining what components of the EEG found during data-mining are artefacts and which are bona fide brain activity sources; current EEG brain source validation methods do not provide a means to clearly determine if a source found via data-mining originates from a functioning volumetric unit of neural tissue in the brain or if it is an artefact. These barriers have all been addressed by work of Zeman et al., 2008b;2008e) and thus have facilitated the development of this analysis methodology.

This new methodology addresses some larger analysis issues that have limited the conclusions that can be drawn from the scalp EEG. Foremost is that current methods require multiple datasets be used to deduce characteristics of brain function. Because of this, only through the analysis of data obtained through multiple data collection sessions from multiple subjects, using statistics to determine what aspects of the EEG are consistent across a participant group, can these activities be linked to specific human behaviour. Further, only by inferring anatomical origins of the EEG scalp field via dipole modelling methods can the EEG be used to link the EEG to the activities of the brain. In contrast, a methodology by which to analyze the EEG data collected from a single persons could provide a means to identify "what happened in the brain" during the data collection paradigm rather than "what happens in the brains of most people" during the paradigm. Second, current standard EEG analysis methods do not examine the EEG and activities of the brain as a dynamically working system. For example, the most common analytical method used by neuroscientists relates isolated activities of the brain to particular human skills and behaviours. This approach has been very helpful in establishing a fundamental understanding of brain function and its relation to behaviour. For example, Brodmann area 17 (primary visual cortex) is used for processing early sensory visual stimuli and without it we can have no conscious experience of vision (Danckert et al., 2003). Similarly, we use the hand area of the motor homunculus (Brodmann area 4) for skilled movement of our hands and fingers (Takada et al., 1998). Study of the brain by this conceptualization however is not ideal as these behaviours

occur via processing that relies not only on their primary neural correlates, but also on the intactness of connections to and from these primary processing areas. This is important because the brain functions via the *interconnectedness* of active areas. Clearly, a more informative perspective on normal and abnormal brain function can be obtained if the brain is analyzed as a system of functionally coordinated areas.

A method that can be used to examine specific *relationships* between individual time-varying activities of parts of the brain will have a considerable impact on both neuroscience and clinical applications. The availability of such a methodology would permit the use of EEG to study individual differences in brain activity, to examine unique brain pathologies, and to measure recovery from brain injuries. This system-level view provides a more complete characterization of pathologies that can disconnect one brain area from another than can the view and analysis of brain areas in isolation. An EEG methodology that focuses on interconnectedness of areas would help clinicians and researchers understand how damage in one part of the brain affects the activities of other parts.

There is evidence that system-level brain function can be successfully examined via measures of the time-varying correlation of activities of separate areas of the brain. For example, using electrodes implanted in multiple areas of the cerebral cortex of cats, Roelfsema et al., (1997) showed that the activities of distinct areas of the cortex are correlated during the stimulus-response portion of their behavioural paradigm, however during the reward phase of their paradigm the correlation of activities of the cortex significantly decreases. These significant correlative relationships found in their study are illustrated in Figure 1. Their study also found significant zero-lag correlation of activities for visual and motor areas of the brain. The greatest correlative relationships were between Brodmann areas 17 bilaterally (low-level visual processing) and area 18 in the right-hemisphere, and between right-hemisphere 17 and 18 and right-hemisphere 21. Correlative relationships were also strong between right-hemisphere area 21 and left-hemisphere area 7. Finally, large correlative relationships were found between left-hemisphere area 7 and left-hemisphere 5lc, left-hemisphere 5lc and left-hemisphere 5mc,

left-hemisphere 5mc and left-hemisphere 4c (skilled use of the forelimb). The authors suggest that the correlated activities are indicators of coordination among brain areas from which the correlated activities are detected.

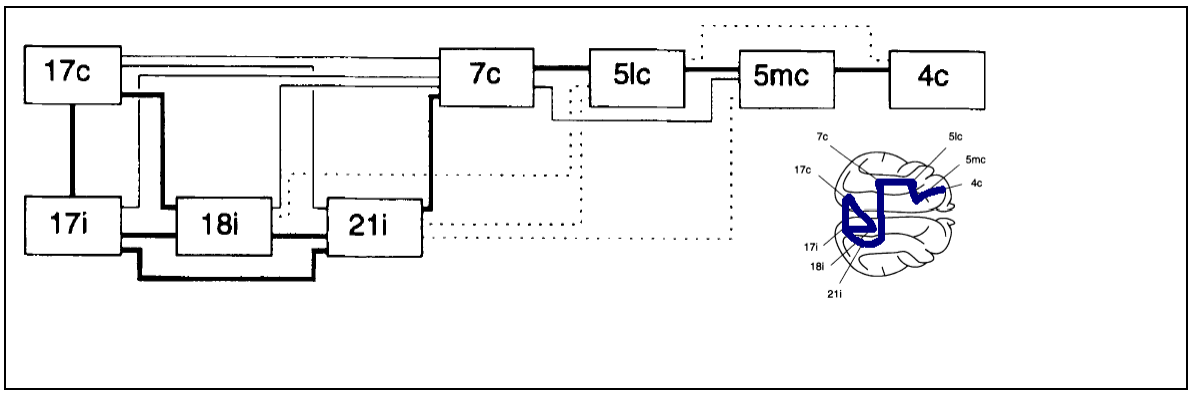

Figure 1. Model of visual-motor processing in the cat, adapted from Roelfsema et al. (1997). Thickness of lines indicates relative synchronization strength among the areas from which recording were obtained during the task, averaged across cats. Thick lines indicate the largest correlation with a correlation rank exceeding 10%; thin lines indicate interactions with a correlation coefficient between 5% and 10%; broken lines indicate interactions with correlation coefficient smaller than 5%. Areas not connected by lines did not exhibit significant synchronization.

The major barrier to using scalp-acquired EEG to study correlation of activities from separate parts of the brain is that these standard measures simply do not directly provide the activities from distinct parts of the brain. The data collected at each scalp electrode is a mixture of activities from many parts of the brain. Therefore, the scalp EEG mixture must be processed before coordination among areas of the brain can be investigated.

Past research has employed various methods to separate the EEG mixture into its constituent parts. However, these methods do not necessarily provide separation of the EEG into the bona fide activities originating from specific areas of the brain; the methods often impose source characteristics that are not exactly appropriate. Source activity characteristics have been restricted to either being uncorrelated or statistically

independent. This is like using a square cookie-cutter to make round cookies. We all know that a round cookie cutter would be more effective, but we've restricted ourselves to the only tool available, a square cookie cutter. In order to estimate coordination (via measure of correlation of brain activities) between areas of the brain using the EEG, it is necessary that the unmixed components of the EEG represent the bona fide activities and thus a new data-mining algorithm is required.

If the component parts of the EEG are incorrectly identified, attempts to localize their brain source origins will not necessarily be successful. Fundamentally, calculating the origins of some unknown number of sources that together project a complex electric field to the scalp is not possible; there is no unique solution when the number of sources is unknown. There is however, a single unique solution for a component of the EEG if there is assurance that the component represents only one source and that the source has a modular physical volume and a single center of mass. Thus, a data-mining algorithm applied to the scalp EEG must separate the EEG mixture into parts, such that each part has these characteristics. The robustness of source location modelling is limited by current data-mining methods; they do not directly mine the EEG data to provide accurate estimates of bona fide brain source activities originating from physically modular areas of the brain with single centers of mass.

Validation of components has been attempted using multiple properties. For example, dipole modelling methods are used to account for the scalp field variance of individual components of the EEG as originating from a location or locations in the brain. Often, most of the variance of the EEG component topography is accounted for by a single dipole. Unfortunately, the EEG unmixing process does not directly search for components that have scalp variance that can be represented by a single dipole or that have single centers of mass. The scalp field may actually represent the combination of multiple dipoles in different locations of the brain or multiple centers of mass. Prior methods have also used the percentage variance explained by components of the data to infer that the component is good. For example, if 99% of the scalp variance is accounted for by a single dipole, the source model might be considered good. Unfortunately, it is

possible that this dipole model might still not accurately indicate the real brain source origins of the scalp variance. There actually might be two anatomical sources, spaced bilaterally and modelling these sources by two equivalent dipoles in the head might only account for 95% of the scalp variance. Further, this measure of 'variance accounted for' does not directly evaluate the component as representing activities originating from a modular volume of the brain.

Variance of the time waveform of the data has also been used to differentiate brain sources from artefacts in the validation process. However, by this measure artefacts can easily contribute as much or more variance as brain activities.

Clustering methods have also been used to validate components. They are used to determine which components obtained through multiple separate decompositions of data from multiple study participants are common across decompositions. It is assumed that those components common to all (or most) participant decompositions are related to brain activity and the behavioural paradigm for which the data were collected. Unfortunately, this method is not appropriate for data obtained from a single participant in a single EEG recording session.

In order to validate the EEG components derived from a single person from a single data recording session, the validation method should have some specific characteristics. First, there should be an agreed upon value or validation criteria that the result found via data mining must satisfy before the result is accepted. Second, the validation method must evaluate the properties of the component that are important and relevant to the use of the result. For example, since our objective is to compare the activities of modular areas of the brain, the physical modularity and physical separation of components should be evaluated. Third, the validation process must have criteria that are independent of the data mining process so that the validation process does not simply confirm the metrics used by the data-mining algorithm. For example, if statistical independence is used as source separation criteria during data-mining, it should not also be used as criteria during validation of data-mining results.

New technological advances have provided a compendium of methods that when used together allow for analysis and interpretation of EEG collected from single participants. These include (1) data mining with specific criteria to identify source contributions to the EEG that allow for partial correlations of source activities (Zeman et al., 2008e), (2) estimate brain source volumes (Zeman et al., 2008b,c), (3) validate these sources by their volume-domain characteristics and separate them from artefacts (Zeman et al., 2008d), and (4) estimate coordination among areas of the brain as visible by measures of zero-lag pair-wise correlation (Zeman et al., 2008e). Together, these methods provide a semi-automated approach to constructing a system-level representation of brain function from scalp-acquired EEG data. We have named the complete methodology Multi-Component Spatio-Temporal Modelling using EEG data (MCSTM-EEG).

2. DATA REPRESENTATION USING MCSTM-EEG

Our methodology considers that an important aspect of brain function can be represented as a system of processing nodes and time-varying communication links between them. The methodology transforms aspects of the EEG data into nodal brain volumes and the functional links between these volumes. These links are inferred from estimates of zero-lag correlation of activities of brain-related components of the EEG. The nodes are representative of macroscopic functional areas of processing within the brain. These areas are defined as modular volumes of neural tissue, or as regions inclusive of a particular gyrus or sulcus on the cerebral cortex. Links between nodes correspond to pathways for coordination and information transfer. These links may exist as multiple types of anatomically or physiologically structured pathways such as cortico-cortical fibre paths via fascicles and major white matter projections, intralaminar cortico-cortical projections, thalamocortical projections, or cortico-transthalamo-cortical pathways (Shepherd, 2004). Together, modular nodes (areas, or regions) and the links between them define networks of brain activity.

The set of diagrams provided in the current section give a representation of the outcome of analysis using our methodology. Figures 2 to 4 arise from data collected, analyzed, and described in our prior work (Zeman et al., 2008e). These plots were not previously presented but are provided here to illustrate the capabilities of our proposed method. The results show that we can indeed represent brain activity as functional nodes, with individual activities and correlated relationships. Importantly, these figures provide an easily interpretable and meaningful representation of brain activity at the system-level. These are not plots of uncorrelated or statistically independent components of the EEG, but rather they are plots of the estimated bona fide activities of specific brain volumes and their corresponding time-domain activation relationships.

The full description of the data collection, and behavioural analysis pertaining to these data appears elsewhere (Sorensen et al., 2006; Zeman et al., 2008e). The data presented in the current study were obtained from a single female participant from the control group of a larger study of foetal alcohol syndrome. The objective of the original study was to reveal differences between the EEG of control participants and participants with foetal alcohol spectrum disorder (FASD) related to spatial navigation ability. A computer-based virtual Morris Water Task (vMWT) behavioural paradigm was used to elicit the behaviour and brain activities associated with spatial navigation. Participants navigated the vMWT from the first person perspective and travelled to target locations (or platforms) in the virtual environment. The study examined two behavioural conditions, labelled ‘cue’ and ‘place’. In the cue condition, participants were required to identify the correct platform location based on its color and move to it using the arrow keys on the keyboard. For the place condition, the platforms were both the same color and participants navigated to the correct platform location using configural information from multiple distinct pictures on the walls of the maze.

Figure 2 illustrates multiple views of a set of 8 source volumes. These volumes represent the complete set of brain areas that were active during the data recording while the participant navigated the vMWT. The brain volumes resolved from these data are presented with respect to a canonical representation of the white matter of the brain.

Modeled active brain volumes represent grey matter volumes while the white matter framework provides a physical frame of reference so that the resolved volumes can be named anatomically. A close-up of the brain volumes of the ventral visual pathway is labelled in Figure 2d. The relative locations of these volumes on the white matter cortex suggests they occupy the inferior portions of Brodmann areas 17, 18, and 19, bilaterally, and area 20 on the right side of the brain. A volume is also represented in the dorsolateral region of the left hemisphere frontal lobe, possibly the hand area of the motor homunculus. There is also a volume near the midline posterior to the cingulate cortex of the right hemisphere, possibly Brodmann area 30 or 31. The appearance of these areas in the data indicates that the participant was actively using their ventral visual pathways during the task. This finding is consistent with the maze navigation behaviour of the paradigm as there is a requirement for visual discrimination and identification of features in the vMWT. The source separation and volume estimation methodology appear to have provided anatomically meaningful results.

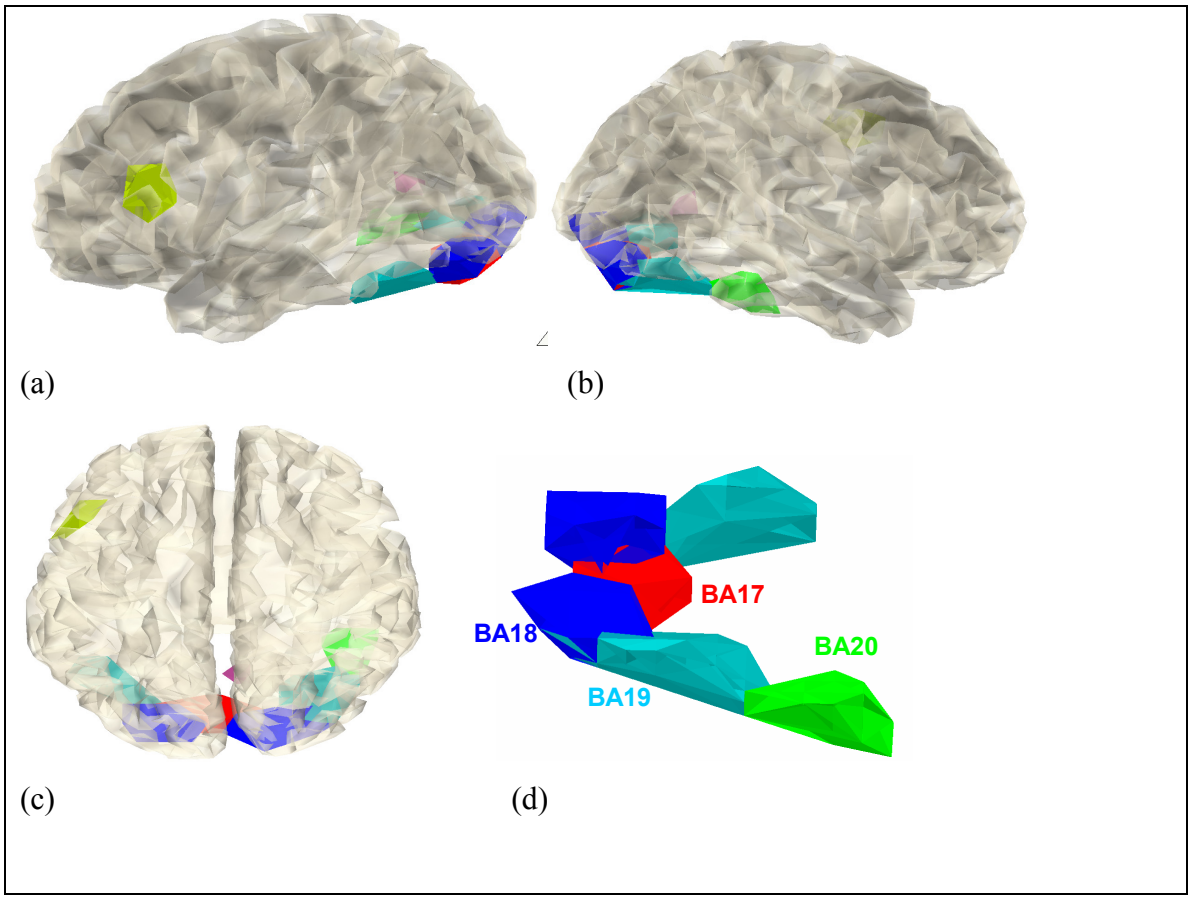

Figure 2. Active modular brain volumes calculated from the EEG data depicted on a white matter head model from the place/cue dataset for the data and processing described by Zeman et al., (2008e). These data were collected from the single subject recording session, described in the main text. Volume edges are defined at 4 standard deviations above the mean noise level (STDM) originating in each ICA topography projected into the head model volume. The STDM and volume estimation methodology is described by Zeman et al. (2008b). Two lateral perspectives (a and b) and a posterior view (c) are provided. View (d) is a close-up of active regions of the dorsal visual pathways from (a, b, c). Colors used indicate symmetry across the midline. The brain model grid spacing is 0.5 cm.

The volumes identified that define the ventral visual pathways appear to reflect the cyto-architectonics of the cortex. Having done so has allowed the labelling of each volume by

a different Brodmann number. Each part of the visual pathway is known to provide a different type of function in processing visual information, and because the data-mining algorithm identified them as separate parts, it is apparent that the relationship between activities of these parts changes over the duration of the task. These parts differ by cellular characteristics and thus likely have different electro- capacitive and conductive properties. It is reasonable to conclude that these properties facilitate the source separation algorithm to identify them as separate components. (In fact, this is shown by differences in the brain sources waveform activities compared in the power plot of Figure 3 shown later.)

Information describing which areas of the brain are active, when they are active during the task, and under what behavioural conditions they are active is provided via time-varying power levels that correspond to each of the resolved brain volumes. For example, the plots of Figure 3 provide the trial-average time-varying power-levels of brain volumes identified in the left and right ventral visual pathways. These have been calculated from the source time-varying waveforms corresponding to each brain area. To do so, the time-domain samples of each waveform of each trial and condition were squared to calculate instantaneous power. The power waveforms were then ensemble averaged to provide a generalized representation of the stimulus-locked power levels of each brain volume corresponding to each brain area for each behavioural condition. It is not possible to make comparisons of the power levels between components because each component is not necessarily scaled by the same amount by the separation filter. However, it is possible to make power level comparisons among behavioural conditions as the same scaling values are used for the data from both conditions. Waveform shapes, however, can be compared for all cases and the changes in the power levels of these areas over time are meaningful.

The plots given in Figure 3 reveal differences in the trial-averaged activation power levels for the cue and place behavioural conditions. The Left hemisphere activities for cue and place are given in Figure 3a and 3c respectively (left side of the plot) while the right hemisphere activities for cue and place are given in Figure 3b and 3c respectively

(right side of plot). The colors used in these plots correspond to the colors of Figure 2 that illustrate each modelled brain volume. One notable difference between the activation power levels for cue and place occurs in the left hemisphere in Brodmann area 18 where the trial-average stimulus-locked activation level varies in amplitude with respect to time in a different way for each condition. Another notable difference is that for the cue condition, there is greater average power originating from Brodmann area 20 than for the place condition for the right hemisphere after approximately 75 ms after trial onset and persists after 100 ms. As well, there are differences for the earlier visual areas (Brodmann areas 17 and 18) at approximately 100 ms for the left hemisphere.

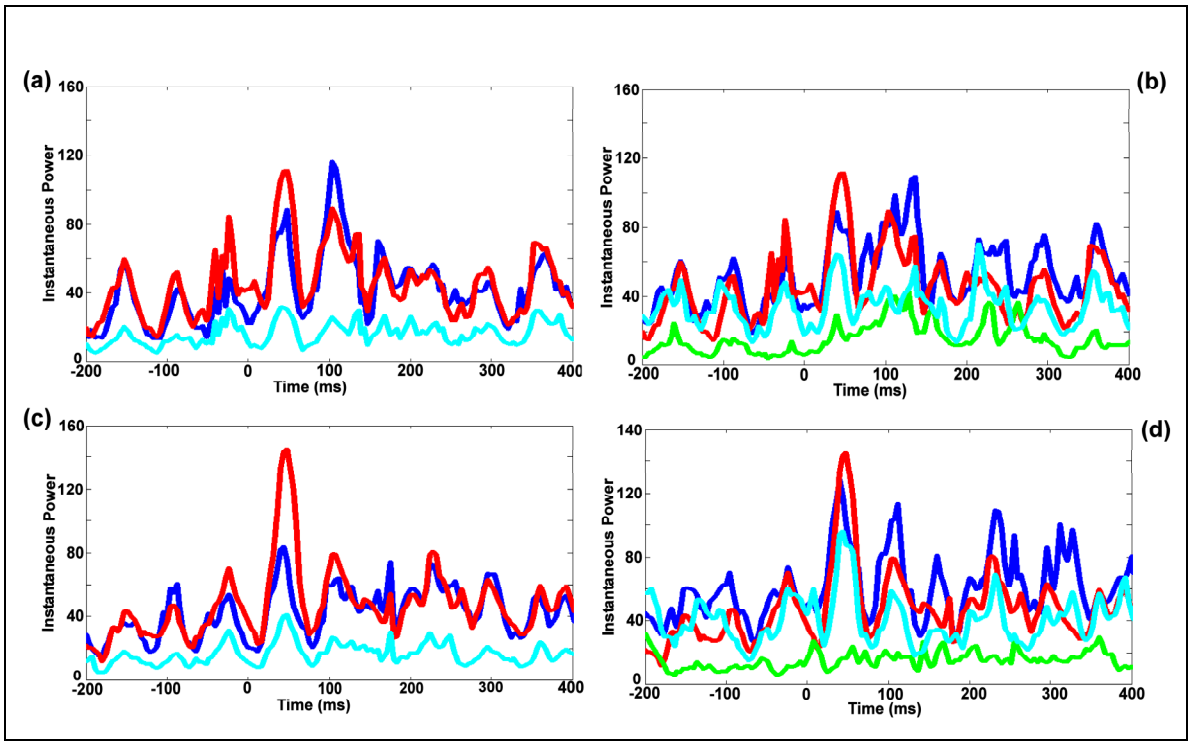

Figure 3. Ensemble averaged instantaneous power as a function of time for activities of the brain volumes of Figure 2d band pass filtered 3 to 40 Hz. Plots (a,c) are left hemisphere and (b,d) are right hemisphere. Plots (a,b) correspond to the cue condition. Plots (c,d) correspond to the place condition. The colors of the lines in this figure match the volume colors in the volume estimation illustrations. Red=Area 17, Blue = Area 18, Turquoise = Area 19, Green = Area 20. Instantaneous power was calculated as the square of each time sample for each individual trial. The power activities calculated for each individual trial were then ensemble averaged to obtain the current figures. This

shows the stimulus locked power fluctuation of multiple visual areas of the brain in relation to the start of the trial.

Our prior research provides additional evidence that the data-mining algorithm facilitates measurement of frequency specific correlated activities (Zeman et al., 2008e). In that study, important brain activity frequencies for examining the transfer of visual information were identified. Specifically, it was demonstrated that the activities of the left and right extra-ocular muscle groups, when appropriately separated from the EEG, exhibit large power levels in the frequency band 34-36 Hz with uncorrelated activities (average correlation < 0.2) in the same frequency band. It was concluded that this particular frequency band corresponds vergence movements of the eyes. Vergence occurs when the eyes move to focus visual information of interest on the fovea of the retina. This extra-ocular muscle activity provides both the precise frequency of vergence and the individual phases of the left and right eye movements. This frequency band, then, can be used to search for particular types of brain activities in the EEG relating to visual information processing in various parts of the brain. Given that the frequency and phase of vergence is known, related activities can be traced throughout the brain revealing brain activities for interpreting visual information associated with objects of cognitive interest.

Figure 4 shows time-varying pair-wise zero-lag correlations for two separate brain volumes and for the two behavioural conditions (place and cue) for the frequency band of ocular vergence. To create these representations, the activities of each source waveform for each trial of data for both behavioural conditions were band-pass filtered from 34 to 36 Hz. Once the activities in the frequency band of vergence were isolated, the time-varying correlation was calculated for each trial and each pair of components. The calculation of time-varying correlation used a 500 ms sliding window with 50% overlap. Prior to calculating correlation values for each window, each portion of the waveform was Hanning windowed to reduce edge effects on the correlation estimate. This created correlation values at steps in time for each trial and for each behavioural condition. These values were ensemble averaged for each of the cue and place conditions to create

an average correlation estimate. Finally, the absolute values of these average correlation values were calculated. Error bars describing the variability of the correlation estimate across trials were calculated as the mean of random samples of the trials for each condition. There were 2000 draws of 20 random samples from the set of trials for each condition to generate this statistic.

The average stimulus-locked correlation estimates show clear differences between the behavioural conditions as a function of time. Figure 4a represents the time-varying relationship between visual Brodmann area 18 of the right hemisphere and part of the motor homunculus of inferior Brodmann area 4 of the left hemisphere. Figure 4b represents the time-varying relationship of Brodmann area 18 of the left and right hemispheres. These values are given for each of the two behavioural conditions, place (plotted in red) and cue (plotted in blue). Divergence in the error bars of two compared conditions or two intervals of time suggests that the link and level of cooperation for these conditions or time intervals differ. Thus, for this particular study participant, there is a relationship between the dorsolateral region of the left hemisphere frontal lobe and the visual area of the right hemisphere that differs between behavioural conditions shortly after the trial onset. As well, there is a clear weakening of the correlative relationship of activities between the two visual Brodmann areas 18 bilaterally after the trial onset.

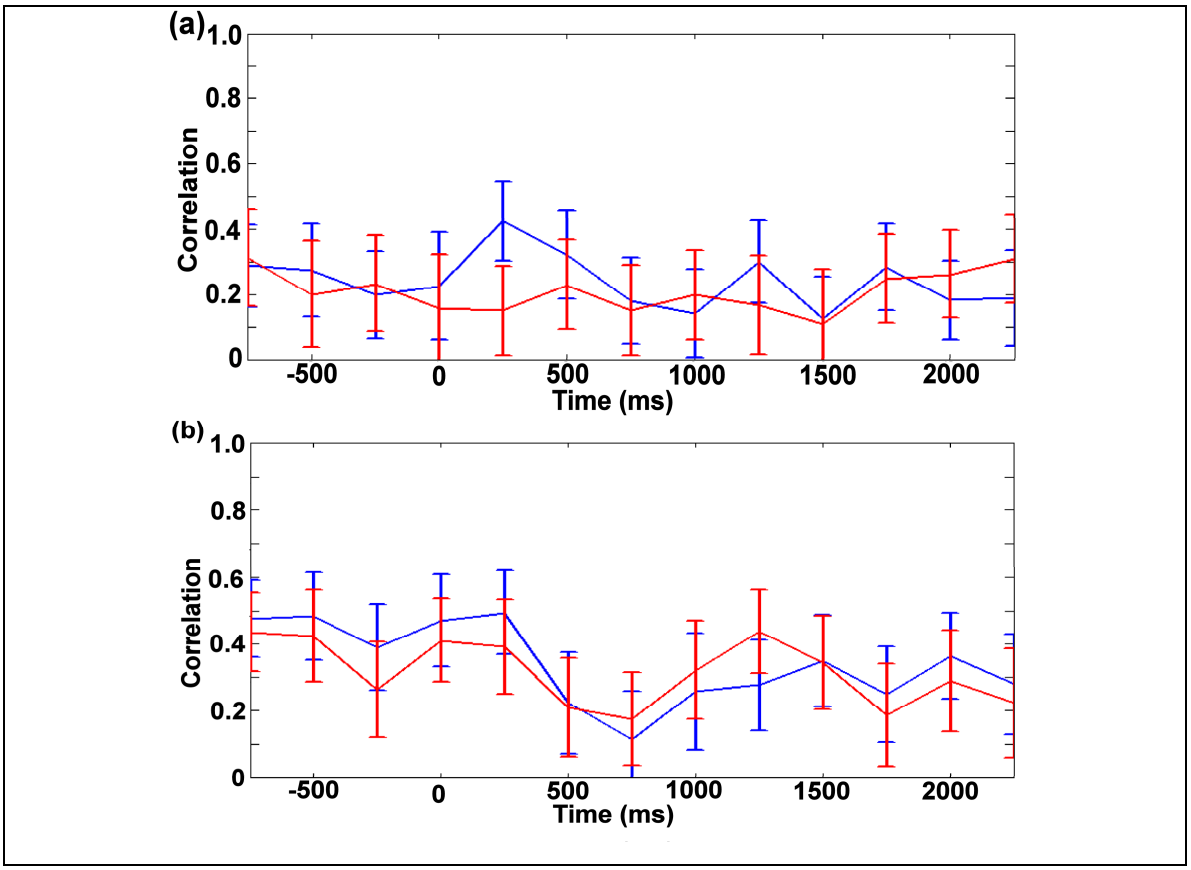

Figure 4. Two examples of the time-varying pair-wise zero-lag correlations in the frequency band 34 to 36 Hz relating to a subset of the brain volumes illustrated in Figure 2 (Blue = cue condition, Red = place condition). (a) The case that there is a difference in correlation between two behavioural conditions. There is a difference between cue and place for the interval around 250 ms for correlation between hand area (H) dorsolateral region of the left hemisphere frontal lobe and Brodmann area 18 of the right hemisphere. (b) The case that there is a large change in the time-domain correlation between two brain areas over time. There is a difference between the windows centered at 250 ms and 500 ms for both the cue and place conditions. The correlation for this case was calculated between the two ventral Brodmann areas 18 of the left and right hemispheres. Pair-wise correlation is measured in intervals of time, using 500 ms windows with 50% overlap. Plotted points in the figure indicate the center of each window. Error bars represent the standard deviation of the mean of 2000 random samples of 20 trials from the trials of each condition.

3. RELATED METHODOLOGIES

As described earlier, the proposed MCST-EEG methodology is a result of recent advancements in EEG analysis. This includes a new data-mining algorithm used to identify bona fide brain activity components (Zeman et al., 2008e), a new brain volume estimation method for realistic anatomical representation of brain activity component of the EEG (Zeman et al., 2008b), and a new validation method to identify 'good' brain activity components from artefacts (zeman et al., 2008d). The data mining method is fundamentally based on the Infomax ICA source separation method (Bell and Sejnowski, 1995) and a combination of the runica (Makeig et al., 1997) and BSICA (Zhang and Chan, 2006) algorithms. Further, the validation and volume estimation method are fundamentally based on the least-constrained minimum variance (LCMV) beamforming algorithm (Van Veen et al., 1997).

Although our methodology is based on previous work, it differs from these closely related methods on three main points: (1) data mining methodology and source separation purpose and criteria, (2) 3-dimensional volumetric representation of brain sources, and (3) source validation methodology and criteria. These differences define and differentiate our methodology from other work for analyzing brain activity using the scalp EEG.

Differing from other methods, our data-mining methodology is specifically designed to explore the time-varying correlative relationship among brain source activities comprising the EEG mixture. Attempts have been made to use ICA to identify time-domain relationships between components via measures of correlation or coherence (Onton et al., 2005; Makeig et al., 2004). Such investigations identify the residual relationship among components after statistical independence among components has been maximized and do not necessarily provide results describing brain function. However**,** our method attempts to preserve the correlative relationships of EEG sources during the data-mining process while still identifying individual physical contributors to the EEG mixture. To separate activities while still preserving their natural correlative structure, those frequencies of brain activity having the least statistical dependence and

that are not likely involved in coordination among distinct parts of the brain are identified. Those frequencies of independence identified are emphasised to increase their influence during calculation of the PCA-sphering and ICA-rotation steps of the Infomax ICA (REF) procedure (Zeman et al., 2008e).

Standard PCA methods are not designed to preserve the bona fide natural correlative relationships that exist among brain source activities. PCA has been used extensively in prior work to separate data into uncorrelated parts. The fundamental assumption of PCA is that the parts comprising the mixture are uncorrelated and thus application to EEG splits it into uncorrelated parts. Using this method identifies only uncorrelated factors of the EEG mixture; uncorrelated parts are identified even if the parts comprising the data are not uncorrelated. However, usually a small number of these uncorrelated factors can be related to specific anatomical parts of the brain via source localization. While some PCA factors might have a close resemblance to brain activities by time-frequency characteristics and by anatomically reasonable foci of origin, this does not necessarily mean that they accurately represent brain activities.

The Infomax ICA process (on which our algorithm is based) builds on the initial PCA step that makes the data uncorrelated and provides an additional rotation to the data to make them as statistically independent as possible. This is an important and useful step in adjusting the data because statistical independence is a stricter criterion by which to split data into groups (Bell and Sejnowski, 1995). For example, it is possible for two parts to be uncorrelated but not statistically independent; however, if two parts are statistically independent they are guaranteed to be uncorrelated. Uncorrelatedness is based on only the second order statistic of the data, whereas independence includes the statistics of second order and higher. In other words, if two variables or processes are statistically independent, then one process or variable can not be used to predict the other. The ability to make such predictions remains if the two parts are uncorrelated but not statistically independent. Thus, by successfully maximizing the independence among components, no two components identified from the EEG mixture will contain duplicate information.

The EEGLab (Delorme and Makeig, 2004) toolkit provides a methodology to analyze EEG data using ICA. The EEG analysis and decomposition methodology of this toolkit bears the closest resemblance to our proposed methodology. It provides a means to separate the EEG data into a set of components that are as statistically independent as possible (Makeig et al., 2004). The default algorithm provided by the EEGLab toolkit and most widely used in EEG analysis is runica. It is assumed that the non-deterministic qualities of brain activity will satisfy the separation criteria of statistical independence used by runica and thus a subset of the components found by this algorithm will resemble brain activity and will be suitable to relate to brain anatomy via dipole localization. However, as is the case for PCA, a close resemblance of components to plausible brain activities by time-frequency qualities and the ability to model the components by equivalent dipoles does not mean they accurately describe brain activities.

Our methodology relates components of the EEG to brain anatomy as estimated brain volumes rather than by modelling source locations with dipoles. Instead of using dipole fitting as is customary with the EEGLab toolkit, our methodology estimates the volume modularity and volume overlap of components of the EEG to determine a relationship to brain anatomy. Such volumes have physical qualities that distinctly differ from those of model dipoles. For example, model dipoles are point sources and have no size whereas source volumes have centers of mass, occupy 3-dimensional space, and have physical boundaries. These properties provide for the opportunity for two adjacent volumes to physically overlap. These representations can also have varied physical shapes. This has two advantages. First, the volume representation of sources is anatomically meaningful; as was demonstrated earlier, it is possible for a volume representation to implicate an entire Brodmann area as the source of some scalp-projected activity. Second, cortical pathways are visible by volume representation of adjacent active cortical volumes; this cannot be provided by representation of point source dipoles.

Our method employs a unique validation system to identify which components of the data mining decomposition appropriately represent brain sources. The algorithm

determines which components of the decomposition are brain-related and which are not via their aforementioned volume-domain characteristics. These characteristics are used to describe how well each component is represented in a model head volume. This is done by calculating the best LCMV fit of the scalp topography of each EEG component found by the data-mining algorithm to the head model (Van Veen et al., 1997; Zeman et al., 2008b). Those components that score high by these measures are accepted as bona fide brain sources while those that score low are considered to be artefacts or poorly recovered brain sources. By this method, brain sources meeting a priori determined criteria are separated from artefacts.

In contrast to our validation method, the existing EEGLab methodology uses primarily two validation mechanisms. One method assumes that brain activity-related components can be identified from the set of components found in a decomposition of EEG data by sorting them according to their relative waveform variance. Those components that account for the greatest total variance are usually retained as possible sources of interest (as possible brain sources) while those of low variance are assumed to be noise. This however does not directly determine which components are artefact and which are brain-related because the measure of variance of brain activity components is often similar to the artefacts themselves. This arises via the following mechanism. Components related to the paradigm have small amplitudes compared to artefacts and occur in most trials whereas the amplitudes of artefacts are large but do not usually occur in every trial. The statistic of variance that summarizes the entire dataset does not necessarily distinguish them. A different method employs a process of clustering components across multiple data sets (Delorme and Makeig, 2004). The clustering methodology assumes that those components related to the paradigm will appear in all (or most) datasets. The component groups formed by clustering that are populated by components from all (or most) data sets are classified as pertaining to the paradigm. These components will either be related to activities of the brain or will be stereotypical artefacts that are easily identified by topographical characteristics. Components are clustered based on the combined or individual characteristics of component frequency spectra, time-waveform characteristics, and point-source dipole locations.

The volume-domain projection of component topographies provided by our methodology which is not available in EEGLab, provides assurance that components relate to different anatomical brain areas. This facilitates the comparison of the time-domain activities of different parts of the anatomy. This assurance provides evidence that any correlations found between activities are not the result of poor source separation but occur because the activities of two brain areas compared are actually correlated. To make such time activity comparisons, the two components compared should relate to different anatomically brain volumes. We have previously demonstrated how pair-wise overlap of components can be calculated (Zeman et al., 2008b) and used to determine if two components found by data mining relate to the same volume. A case of overlap would indicate poorly separated sources that do not provide a meaningful comparison of time-domain activities. Clearly, studies that use the location of the center of mass as a measure of anatomical difference between sources do not have this objective assurance that the correlation calculated from source time-varying activities are valid and not the result of parasitic volume condition at the scalp.

4. MCST METHODOLOGY

Figure 5 summarizes the steps of our modelling methodology. These steps (or a subset of these steps) have been followed for the analysis in two different studies: Sorensen et al., (2006) and Zeman et al. (2008e). Here we describe each step of the methodology, the purpose of each step, and the relationships between each step in detail so that this methodology can be used by other labs in their future research.

For clarity, each major step (of 11 in total) is labelled as a block from (a) to (k). The first block (a), indicates the design of a paradigm appropriate to study the brain activity and behaviour of interest. In block (b) the EEG data are acquired using a suitable recording system. In block (c), the data are de-referenced so that topographical characteristics and electrode activities can be interpreted for preliminary noise removal in block (d). The noise removal block includes the rejection of unacceptably noisy trials and de-noising of

the EEG to remove non-biological noise via ICA noise removal methods. The EEG data mining block (e) provides separation of biological source activities remaining after removal of non-biological artefacts that are statistically independent of brain activities) into components. The volume projection block (f) maps ICA-derived scalp topographies found in the decomposition into a volume-domain projection of variance inside a head model. A validation process in block (g) is then used to determine which components of the data mining decomposition originate from inside the head. This distinguishes 'good' brain activity components from poorly separated brain activity components or any remaining ubiquitous non-biological noise. After validation, the anatomical volumes corresponding to brain source components are estimated in block (h). Block (i) provides an estimate of the time-varying coordination of the "good" brain source components. Block (j) provides estimates of the time-varying power levels of each brain areas. Finally, using the parameters calculated in each of the previous blocks, a graphical representation of brain function is constructed in block (k).

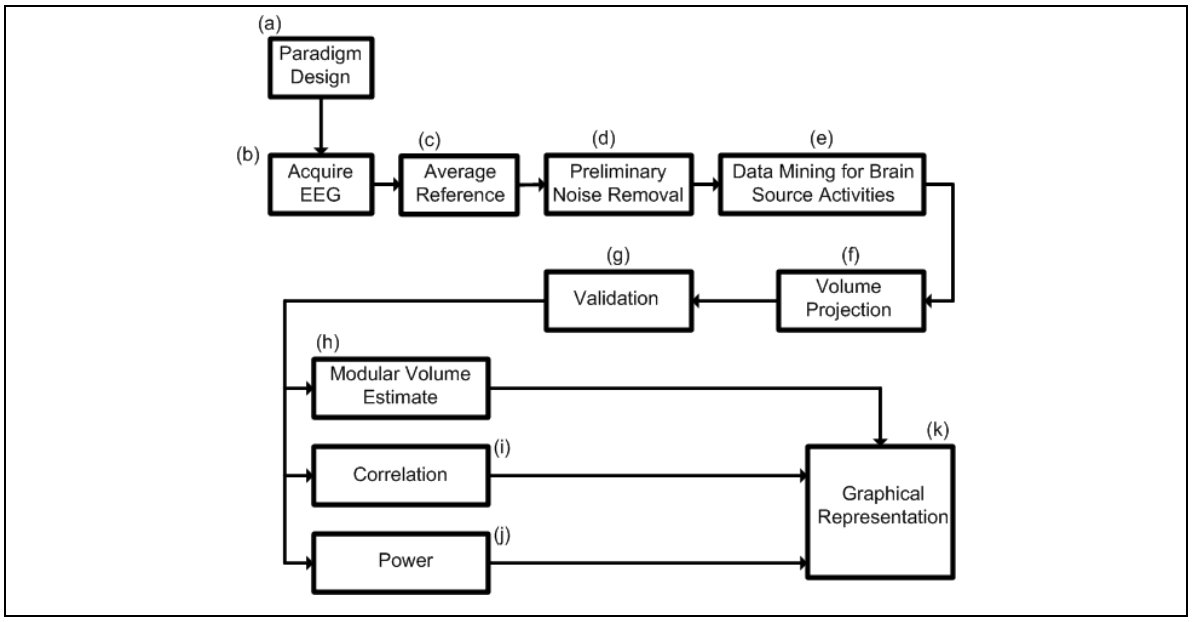

Figure 5. Block diagram illustrating steps of the our proposed MCST processing method.

(a) Paradigm Design

The data collection paradigm that elicits specific brain activity should provide for two specific data characteristics. These characteristics are required to facilitate the data-mining process. First, the paradigm should elicit the activities of multiple areas of the brain, to the limit of having no more brain sources contributing to the EEG than there are recording electrodes. In practice, we recommend there be at least twice as many electrodes as possible brain source contributions to the EEG data to ensure there are enough degrees of freedom by which to separate noise from brain activities. Second, the paradigm should elicit as many different pair-wise functional network links between areas of the brain as possible. This can generally be satisfied if brain activities related to multiple behaviours are captured in the EEG. The EEG data must contain activities from multiple behaviours so that the activities related to functional coupling and decoupling of modular areas of the brain can be recorded. This is similar to the collection of EEG data resulting from multiple behavioural tasks to allow for post-recording decoupling of components as is done for PCA methods (Donchin and Heffley, 1978). However, in this case we are also striving for ethological plausibility in the paradigm and to have as many active brain areas as possible within data-mining constraints. Having a large number of brain sources contributing to the EEG allows for a more detailed model of functional brain activity. In contrast, PCA methods strive for paradigm simplicity and a small number of active brain areas to simplify analysis of the data. For example, the processing results demonstrated earlier in this paper were obtained using data collected while a study participant navigated a computer-based virtual arena maze. The behaviour associated with spatial navigation is thought to result from activity in many parts of the brain and in this case we were able to resolve 8 active brain sources.

(b) De-Referencing the Data

De-referencing makes the data of each recording channel descriptive of the scalp field in the vicinity of the recording channel and independent of the reference electrode. EEG recording hardware typically requires activities at the scalp be acquired as the difference

in the electric field between each recording channel and a common reference channel (or channels) (Electrical Geodesics, Inc., Eugene, Oregon). (The recently developed Biosemi (Biosemi B.V., Amsterdam, Netherlands) Active-II amplifier system does require channel de-referencing as it does not acquire data via differences between recording channels.) Two methods of de-referencing are compatible with our data processing method. The method described by Van Veen et al., (1997) finds and uses a de-referencing matrix transform. The method is ideal for subsequent beamforming localization and volume estimation steps used in our methodology; however it is not a standard method used among EEG researchers. A more general and commonly used method, known as average referencing (Dien 1998; Yao, 2001; Yao et al., 2005), is also suitable. By this method, the average across channels at each time sample is subtracted from each channel. While it is not as precise as the matrix transform method and does introduce some small error in our volume domain projection algorithm, we have shown that interpretable results are attainable (Zeman et al., 2008b) and thus, the averaging method has been used in our investigations of brain activity (Zeman et al., 2008c).

(c) Data Acquisition

The methodology requires some specific hardware characteristics. First, simultaneous sampling of the data at all electrodes with at least 16-bit quantization resolution for digitization of the scalp activity is recommended. This quantization resolution provides the dynamic range needed to simultaneously record both brain activities and common artefacts. These include brain activities, interfering biological generators, and external noise sources. When both brain activities and artefacts are collected with the necessary dynamic amplitude range, artefacts and brain activities are more easily separated. Any clipping during data acquisition will negatively affect the data-mining process. It is also required that the data be sampled at 250 samples per second or greater to obtain clear estimates of the parts comprising the EEG. At minimum, 32 uniformly spaced electrodes placed in standard sensor positions should be used. Work by Sorensen et al. (2006) has used 112 electrodes and work by Zeman et al., (2008) has used 32 electrodes. While the minimum of 32 electrodes has been used successfully, it is not ideal; the potential number

of sources that can be found is decreased when a small number of electrodes are used. Further, fewer electrodes makes the separation of partially correlated brain sources difficult. For this reason, a large number of electrodes is preferred, provided that each electrode does not contribute more noise than useful signal to the data. Having a large number of electrodes also facilitates our volume projection and estimation algorithm. It has been shown that the number of electrodes has a bearing on the success of localization methods. However, the accuracy of localization however also depends greatly on the source localization method used (Michel et al., 2004) and therefore the relationship between source localization accuracy and the number of electrodes is not clear. It has been shown that reasonable localization is possible with 31 electrodes using the EPIFOCUS source estimation and localization algorithm (Grave et al., 2001). Not all source localization algorithms however are equal and localization accuracy varies. Source localization algorithms, on average, have the greatest precision increase when the number of electrodes is increased from 25 to 100 electrodes (Grave et al., 2001). The source localization and volume estimation accuracy of our method for a varied number of electrodes has not yet been examined and has been left for future research.

(d) Gross Noise Removal

A preliminary noise removal step, prior to mining the EEG data for brain sources is used to reduce the effect of non-biological artefacts influencing brain source separation. These non-biological artefacts include those that arise from noisy EEG sensors, trials distorted by cable movement. The noise is reduced via three processing steps. The first step removes noisy electrode channels from the dataset. Consistently noisy channels are identified by viewing the plotted activities of each EEG channel for every trial of data comprising the dataset. This manual inspection has been done in our prior work (Zeman et al., 2008e) however a computer algorithm is appropriate to do this heuristically. For example, an EEG channel should only be eliminated if channel noise events are frequent as there are negative consequences to removing EEG channels from the dataset. There is a compromise between maintaining appropriate spatial sampling required by processing steps involving beamforming (Van Veen et al., 1997; Zeman et al., 2008c) and channel

elimination. Equidistant spatial sampling and symmetric sampling about the midline must be maintained. If one electrode is removed, its contralateral pair should also be removed. Removal of large groups of electrodes in the same scalp area should also be avoided so that uniform spatial sampling can be maintained. The second step is the removal of distorted trials from the dataset. Distorted trials are identified by visually panning through each trial of plotted data. Trials that have large noise events across many channels are removed from the dataset. There is a compromise between eliminating noise and retaining enough data. It is necessary to retain as many trials as possible but also to remove as many noisy trials as possible. The third noise removal step employs standard ICA. Once distorted trials and noisy electrode channels have been removed, standard ICA (runica) is used to remove remaining ubiquitous non-biological noise. Such non-biological noise sources are easily separated from brain activities by standard ICA methods because their time-domain activities generally meet the ICA source separation assumption of being statistically independent of brain activity (Hyvärinen et al., 2001). Overall, this preliminary noise removal process reduces the total variance related to non-biological artefacts in the dataset and thus facilitates the mining of the remaining EEG data for brain activities.

(e) EEG Data Mining

Separation of the individual activities of distinct anatomical contributors to the EEG requires appropriate separation criteria. Such criteria should be appropriate and sensitive to the actual time-domain relationships between different anatomical areas of the brain. The best separation criteria are not necessarily those of standard correlation or statistical independence used by PCA or ICA, respectively. Prior work has shown that different frequencies have different functional meanings in relation to behaviour (Kopp et al., 2004) and that parts of the brain are highly correlated at specific frequencies (Summerfield and Mangels, 2005; Roelfsema et al.1997; Silberstein et al., 2005). Thus standard PCA and ICA methods are not necessarily appropriate to estimate the bona fide activities of parts of the brain.

The data-mining algorithm used in our analysis methodology exploits the varied characteristics of different frequency bands of the EEG to facilitate source separation. Since it has been established in neuroscience literature that the various frequency bands of activity measurable from the scalp have different functional meanings, it is reasonable to conclude that the activities of distinct areas of the brain will be more correlated in some frequency bands than others. It is also probable that these frequencies of correlated activity vary according to the behavioural paradigm in which the data were recorded and have some relation to the specific human behaviour being studied. Our data mining algorithm separates the EEG mixture into parts based on the activities in those frequency bands of least correlation and statistical dependence. Since the frequencies of independence are not known a priori, our algorithm includes the provision to adaptively search for and identify those frequencies of least statistical dependence for each EEG data set. Thus, by this separation criterion we separate the EEG into the activities of physical modular volumes of brain. These characteristics have been demonstrated in Zeman et al. (2008).

Figure 6 provides and illustration of our conceptualization of areas of the brain projecting activities to the scalp. Depicted are two brain volumes having differing relational statistics for different frequency bands. In this example, two active brain volumes contributing to the scalp-recorded EEG are shown. Brain source **A** radiates activities in two frequency bands defined by $\boldsymbol{f_1}$ and $\boldsymbol{f_2}$ of some arbitrary non-overlapping band width. Similarly, brain source **B** radiates activities in the same two frequency bands, $\boldsymbol{f_1}$ and $\boldsymbol{f_2}$. Our model assumes that the relative statistical dependence and correlatedness of frequency bands $\boldsymbol{f_1}$ and $\boldsymbol{f_2}$ differ. Here, η denotes a measure of statistical dependence among brain sources. The dependence between **A** and **B** is η_1 in $\boldsymbol{f_1}$ while for $\boldsymbol{f_2}$, the dependence between **A** and **B** is η_2. Consider that the activities of brain sources **A** and **B** in frequency band $\boldsymbol{f_1}$ are not statistically independent but are in fact, correlated at zero-lag. In contrast, those activities of **A** and **B** in frequency band $\boldsymbol{f_2}$ are uncorrelated and statistically independent at zero-lag. Thus the relative dependence in the time window of analysis of the brain activity is such that $\eta_1 > \eta_2$. These uncorrelated and statistically independent activities in $\boldsymbol{f_1}$ and $\boldsymbol{f_2}$ can be either occurring simultaneously or they can

occur at different moments in time. What is most important is the summary statistic of dependence for the data analysis window. From this arrangement of source activities, the standard PCA and ICA methods will identify one source. Our method however, will identify two sources. A study of brain activity has confirmed that this is an effective criterion for separating brain activities: statistical independence at specific frequencies (Zeman et al., 2008e).

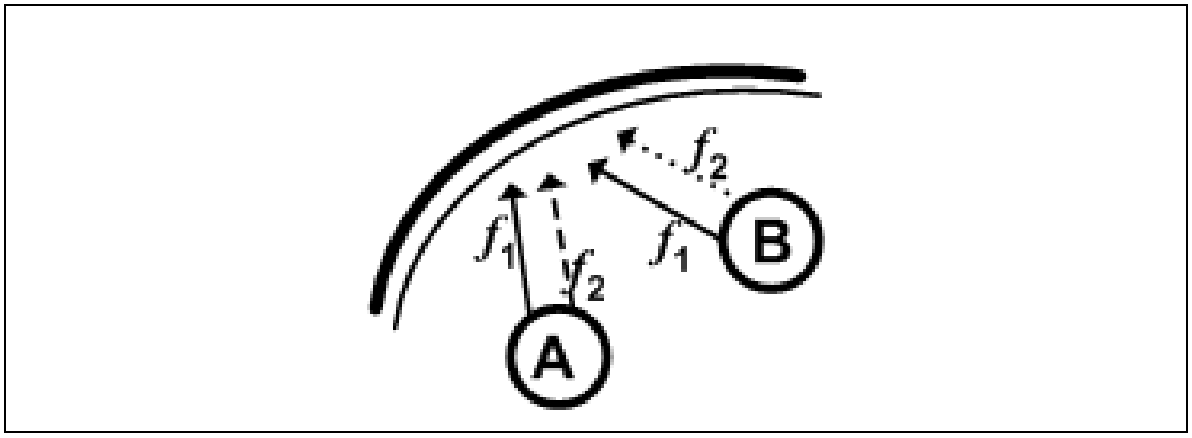

Figure 6. Distinct modular brain sources **A** and **B** projecting activities to the scalp. Activities relating to function of these sources exist in multiple frequency bands defined by f_1 and f_2. In frequency band f_1, brain sources **A** and **B** are correlated and dependent, depicted as solid line arrows projecting to the scalp. Activities in frequency band f_2, originating from brain sources **A** and **B** are uncorrelated and statistically independent, depicted by different lines-types (dashed and dotted).

Separation of the EEG into parts by first identifying and emphasizing frequencies of statistical independence, and then separating the EEG into parts using ICA, provides two improvements over standard ICA methods (Zeman et al., 2008e). First, it reduces source estimation errors occurring when the bona fide source activities are highly correlated. This error presents as the failure to identify two different contributors to the EEG mixture as two different components. The second error occurs when the bona fide source activities have low but significant levels of correlation or have transient moments of

highly correlated activities. This error presents as correct allocation of contributors as separate components, however the bona fide activities themselves are distorted to appear uncorrelated and statistically independent.

(f) Volume Projection

If the data-mining algorithm identifies physically modular brain source contributions to the EEG then finding a correct solution to the inverse problem is feasible. While the inverse problem is known to have an infinite number of solutions there is a caveat to consider. It is the case when it is guaranteed that the scalp field topography to be localized arises from the projection of a simple modular volume inside the head with a single center of mass. The volume should extend outwards in three dimensions from the center of mass; however, the volume need not be spherical. This has been modelled (Zeman et al., 2008b) by placing synthetic sources in a head volume, finding their individual forward scalp projections, and then using each individual scalp projection to separately solve for the original synthetic source location. Thus, a correct closed-form map from a topographical representation to a volume is available, provided the volume is modular. The uncertainty of the inverse problem is therefore related to the certainty that the data mining algorithm has identified and separated a modular brain source from the EEG.

To obtain the volume-domain projection of components, the algorithm of Zeman et al. (2008b) is used. The method uses an adaptation of the LCMV Beamformer (Van Veen et al., 1997). The resulting volume projection is effectively the close form mathematical mapping of the variance of the topographies to variance in a 3D canonical head model. It is a continuous map of the variance onto discrete voxel locations within the head. This volume domain map of variance is called the *volumetric spectrum*. Thus each voxel within the head model holds some amount of projected variance from the topography. A BERG 3-layer model (Berg and Scherg, 1994) is used to define the head volume. This volume projected variance of a brain source topography is large in the region of the source origin and is smaller at voxels not near the source origin. Each of the volume

domain characteristics used in the validation process is calculated from the volumetric spectrum.

(g) Validation

Our methodology utilizes a validation algorithm that uses criteria appropriate to our analysis goal to model the functional interaction of multiples areas of the brain. These criteria are a priori determined and components are required to satisfy these criteria to be used in the construction of the functional representation of brain activity.

The source volume representation of components is an informative representation for validation. It is more informative than scalp surface domain representations, dipolar representations, or cortical surface projection representations because the source volume representation is descriptive of regions in the head. The topographical characteristic of each EEG component is a scalp surface representation and is defined by the electrode weights calculated from the rows of the estimated ICA mixing matrix. This topography is often represented as a spline-interpolated and smoothed graphic instead of as discrete spatial samples provided by the electrode weights. From this depiction, the focal points of the scalp field can be found and these focal points can be compared across multiple components. In contrast to this scalp surface topographical representation, a volume representation has modularity in 3 dimensions; it has mass, occupies space, and has edges or boundaries. Thus, comparisons across components can incorporate characteristics of volume centers of mass, volume boundaries or overlap and hence can establish volume modularity. Knowing the center of mass and the boundary edges of the volume, combined with knowledge of the high-intensity focal points of the scalp field, provides the means to calculate the 3D orientation of the source as a model dipole. Representation as volumes also provides the characteristic of volume shape.

The validation process separates brain sources from non-brain sources and provides a rating of the goodness of the brain sources (Zeman et al., 2008d). This discrimination and rating of source goodness is available via characteristics of the volume-domain

representation of components. These characteristics are determined from the volumetric spectrum of each component. Non-modular sources that contribute to the EEG have volume-domain characteristics that are different from simple modular brain activity contributors to the EEG. These characteristics can be used to distinguish simple modular sources from those which are not. We identify good components by sorting and ranking components according to their volume domain characteristics. These characteristics include the voxel specificity of the component defined as the peak spectral value (PSV), the median volume overlap (MVO) of the component with other components of the decomposition, and characteristics of convergence of the center of mass of each component during the ICA maximization of statistical independence. The convergence of the center of mass is summarized as, the total distance that the center of mass of each source travels in the head volume, over iterations of the algorithm. This is herein referred to as the total distance travelled (TDT). The TDT shows which components are not well represented in the data. The relative goodness of sources as representations of modular areas of the brain that project activities to the scalp is determined by ranking components by each scoring method.

Results are not assumed or contrived by the validation processing. The criteria used to validate components differ from, and are blind to the criteria used in the data mining process. Data mining uses criteria of the time domain characteristics of sources without knowledge of a head model volume. In contrast, the validation step, which occurs only once after completion of the data-mining algorithm, knows only of topographies and the volume head model and makes no assumptions of the time relation of sources. It does not assume any specific frequency characteristics or time-domain characteristics of the brain sources' activities. For example, the validation process does not assume that a source containing a large peak at 10 Hz, is a good representation of brain activity. This is beneficial because artefacts are also known to contribute activities in this frequency band.

Since we use a canonical head model in the validation process, inaccuracies in the head model create a bound on scoring separation of brain activity components and artefacts. This bound however only affects the upper limits of component scoring. In component

scoring, we are interested in the lower boundary between artefacts and good brain sources. As long as the upper bound is high enough to allow for discrimination between good and poor components, the generalities of a canonical head model are not an issue. We have demonstrated that the upper bound is sufficiently high to allow for separation of good brain components from artefact (Zeman et al., 2008f).

In sum, our validation criteria are well aligned with our goal to study anatomically modular brain areas contributing to the EEG. Our validation criteria scores components according to physical properties such as modularity. Physically modular brain representations have some logical characteristics and thus the criteria by which to keep or reject components for further analysis is objective; this is not the same as 'fishing' for results in the data. A priori, it is determined that a component result will not be accepted unless it meets the following validation criteria.

1. Because components must occupy a three-dimensional space, only one time varying activity should originate from each unique brain volume.
2. Components should be unique by volume; no two ICA component waveforms should relate to the same brain volume.
3. A good brain source should have a smooth dipolar representation, relating to a single center of mass when its activities are projected to the scalp surface.
4. Components should be well-represented in the data, having centers of mass that converge early during the data mining process.

(h) Brain Volume Estimates

Modular brain volumes are estimated from the volume-domain projected topographies of each source. This is done using the volume estimation algorithm of Zeman et al., (2008b). Each topography is assumed to contain both the topographical characteristics of the brain source and some amount of non-spatially specific random noise. Both are projected into the volume domain by the volume projection algorithm to obtain the volumetric spectrum of each component. The variance pertaining to voxels of the brain

source is greater than the variance for those voxels that contain only noise. This spatially non-specific random noise is represented in the head model volume as scattered variance. It is further assumed that there are more voxels representing the noise variance (scattered variance) than variance relating to the brain volume. Thus, those voxels with variance that pertains to the brain volume are outliers in the distribution of variance throughout the head model. Modular volumes are calculated by estimating the level of the noise of the distribution in the volume domain and then thresholding the volume domain coefficients. Thus, those voxels that have non-zero variance and remain after thresholding, define a region inside the head model that represents the brain source volume.

In the implementation used in the work referenced in this paper, we use a voxel grid spacing of 0.5 cm with 112 scalp electrodes. Pairing this method with data mining using standard ICA methods, we examined synthetic EEG data and have demonstrated the ability to distinguish between brain sources at the 0.5 cm voxel resolution using 124 electrodes (Zeman et al., 2008b). In our head model implementation, there are a total of 5439 voxels that define the volumetric spectrum of each component. We have found that generally, resolved brain volumes occupy fewer than 500 voxels. Successful use of the method to estimate brain source volumes from real EEG data has been demonstrated for a dataset of 32 electrode channels (Zeman et al., 2008f). The accuracy of localization for 32 electrodes has not been specifically tested using synthetic data.

As in the validation process, there is an upper bound on accuracy imposed by the use of a canonical head model. We however assume that this upper bound is beyond what is required to map a meaningful representation of active brain volumes. In the special case that greater accuracy is required, a custom head model can be used in place of the generalized canonical head model.

(i) Correlation

Once a set of validated brain sources have been identified a system-level analysis of coordinated brain function is possible. Coordination of the activities among brain areas is estimated via correlation of band-passed brain source activities as was similarly done by Roelfsema et al. (1997) using electrodes implanted in the cortex. However, in our case, validated brain source activities are used instead of signals from implanted electrodes. (The results of their study are presented in Figure 1 of the current paper.) By using implanted electrodes, these researchers knew the location of the cortex from which they were measuring and were therefore are able to create a map of correlated activities (or coordination) between various brain areas. However in our case, measures of correlation, indicating coordination, are made using the activities of multiple estimated brain sources. By determining the brain volumes from which these activities originate, a map of the coordinated activities of multiple areas of the brain can be created. The method is described and demonstrated in Zeman et al. (2008e). For the calculation of correlation, it is assumed that brain source waveform feature activities are piece-wise stationary. By this assumption, correlation is calculated using a sliding analysis window that is appropriately sized to capture the frequency band of interest.

(j) Power

The instantaneous time-varying power calculated for each validated brain volume provides a means to determine which part of the brain is active at what time and for which behavioural condition. This is accomplished in three steps. First, the data of each trial are separately band-pass filtered to obtain the activities of interest for power analysis. Once the activities in the frequency band of interest have been isolated, each time-sample of filtered data is squared, separately for each trial. The time-varying power calculated for each trial is then averaged separately for each behavioural condition to obtain a grand-average time-varying power estimate.

(k) Graphical Representation of Data

The data are graphically depicted as a set of volumes and waveforms. The volumes are represented in three dimensions. The canonical white matter frame artwork on which brain volumes are represented was obtained from the BrainStorm software package (Baillet et al., 2000), although any canonical white matter representation may be used. For example, a custom head model and white matter representation might be used to improve volume representation of source activities. Each waveform characterises the time activities that originate from a specific volume. From these waveforms, power levels (as a function of time) and the relational activities of multiple brain areas are calculated and depicted graphically.

5. SUMMARY AND CONCLUSIONS

What is most striking about the results given in this paper is that their representation makes intuitive sense, without much interpretation or inference. During data collection, the participant was actively engaged in a visual task; processing of this data by our methodology showed that activities of the ventral visual pathways are clearly represented in the data and were active during the task. The 'ventral stream' is thought to underlie various aspects of object perception, including identification of physical properties of objects, such as color. The task during which the data were collected required the participant to either discriminate between two platforms of different colors, or identify multiple visual stimuli in the arena maze and use their relative position to distinguish between two platforms of the same color. Further, the participant pressed buttons using their right hand to navigate; data processing revealed that activity of the dorsolateral region of the left hemisphere frontal lobe (possibly the hand area of the motor homunculus) was represented in the EEG.

In addition to the success of our methodology in identifying some expected areas of activity, it is especially important to note that we made no assumptions about what the EEG results should look like; free of bias, the data gave results that made sense.

Using fMRI data, spatial navigation studies often identify activity in medial temporal areas like the parahippocampal gyrus and the hippocampus (for example, Maguire et al., 1998; Spiers and Maguire, 2006). Our methodology did not isolate or model the activities of these areas of the brain. It is probable that these areas were active while the EEG data were collected, but we did not detect any activity. There are three possible explanations for this outcome. First, the activity of these additional areas might have been too weak to reach a threshold to be detected by our methods. Failure to detect some types of activation is a typical characteristic of many imaging methods. For example, consider the case where a patient complains of knee pain and is tested using a structural MRI. The MRI may fail to show any damage, whereas a later surgical intervention may reveal a small fragment of calcified cartilage disrupting the mechanical operation of the knee. A second reason for failure to detect some of the expected activity is that the signal-to-noise ratio could be too low to extract the activities of these other areas from the EEG. This is similar to the first explanation however in this case, assumptions are made about the noise. It is possible that more active areas of the brain could have been identified if the dataset had a lower noise level. A third reason relates to the consistency of the activation of brain areas. Clearly, activities of the visual system and limb motor system should be consistently present in the data; activities of other high-level cortical areas may not occur consistently in every trial or may occur very briefly in every trial because such control could at times be mediated by subcortical systems of the brain. In this way, when compared to activity in visual areas, the activities of spatial areas are not well represented in the data.

In this paper we have described our new methodology for EEG analysis and data representation. This methodology, herein referred to as Multi-Component Spatio-Temporal modelling using EEG data (MCST-EEG), differs from other methodology primarily by its fundamental goals and assumptions. The experienced EEG researcher

will note that brain activities and cortical volumes represented in Figures 2, 3, and 4 are not normally seen from scalp EEG data. We have shown how our method differs from closely related methods on three main points. (1) Our data mining criteria are suited for the identification of brain activity rather than the search for uncorrelated or statistically independent components. (2) Our method of relating the EEG to anatomy attempts to find brain volumes rather than point source dipoles. (3) Components found by the data mining process are validated by multiple characteristics of the volume domain projections of components, rather than qualifying components based only on variance in the data, topographical characteristics, or by clustering across multiple datasets.

Our analysis methodology still requires significant development and refinement. The body of this work, provided in a previous series of papers, represents an effort to demonstrate the feasibility of doing this type of analysis of scalp EEG data. We have not yet exhaustively tested our algorithms or specified bounds of accuracy or fallibility. Future work should test our methodology and further compare it to other similar methods of analysis. We remain optimistic that this methodology will be a useful addition to the practice of EEG analysis.

REFERENCES

Amari S, Cichocki A. A New Learning Algorithm for Blind Signal Separation. In: Advances in Neural Information Processing Systems 8, Editors D. Touretzky, M. Mozer, and M. Hasselmo, pp757-763, MIT Press, Cambridge MA, 1996

Andrew C. Quantification of event-related coherence (ERCoh). In: Pfurtscheller G, Lopes da Silva FH (Eds). Handbook of electroencephalography and clinical neurophysiology. Revised Series, v6. Amsterdam, The Netherlands: Elsevier, 1999:119-137.

Anemueller J, Sejnowski TJ, Makeig S. Complex independent component analysis of frequency domain electroencephalographic data. Neural Network 2003;16:1311-1323.

Baddeley AD, Hitch G. (1974). Working memory. In: Bower GH (Ed). The psychology of learning and motivation: Advances in research and theory, v8. New York: Academic Press, 1974:47-89.

Baddeley A. The episodic buffer: a new component of working memory? Trends in Cognitive Sciences 2000;4(11):417-423.

Baddeley A, Della Salla S. Working memory and executive control. Philosophical Transactions R. Soc. Lond 1996;351:1397-1404.

Baillet S, Mosher JC, Leahy R. BrainStorm beta release: a Matlab software package for MEG signal processing and source localization and visualization. Proceedings of the 16th Annual Meeting of the Organization for Human Brain Mapping, San Antonio, Texas, 2000.

Başar, E. Memory as the "whole brain work": a large-scale model based on "oscillations in super-synergy". International Journal of Psychophysiology 2005;58:199-226.

Bell A, Sejnowski TJ. An information-maximization approach to blind separation and blind deconvolution. Neural Comp 1995;7:1129-1159.

Berg P, Scherg M. A fast method for forward computation of multiple-shell spherical head models. Electroencephalography and Clinical Neurophysiology 1994;90:58-64.

Danckert J, Revol P, Pisella L, Krolak-Salmon P, Vighetto A, Goodale M, Rossetti Y. Measuring unconscious actions in action-blindsight: exploring the kinematics of pointing movements to targets in the blind field of two patients with cortical hemianopia. Neuropsychologia 2003; 41:1068-1081.

Delorme A, Makeig S. EEGLAB: an open source toolbox for analysis of single-trial EEG dynamics including independent component analysis. J. Neuroscience Methods 2004;134:9-21.

Dien J. Issues in the application of the average reference: review, critiques, and recommendations. Behaviour Research Methods, Instruments & Computers 1998;30:34-43.

Donchin E, Heffley EF. Multivariate analysis of event-related potential data: A tutorial review. In Otto DA (Ed), Multidisciplinary Perspectives in Event-related Brain Potential Research. Washington, DC: U.S. Gov Printing Office. Pp. 555-572, 1978.

Grave de Peralta Menendez R, Andino SG, Lantz G, Michel CM, Landis T. Noninvasive Localization of Electromagnetic Epileptic Activity. I. Method Descriptions and Simulations. Brain Topography 2001;14(2):131-137.

Hyvärinen A. Fast and Robust Fixed-Point Algorithms for Independent Component Analysis. IEEE Transactions on Neural Networks. 1999;10(3):626-734.

Hyvärinen A, Karhunen J, Oja E. Independent Component Analysis. New York: John Wiley & Sons, 2001.

Kopp F, Schroger E, Lipka S. Neural networks engaged in short-term memory rehearsal are disrupted by irrelevant speech in human subjects. Neuroscience Letters 2004;354:42-45.

Hyvärinen A, Oja E. A fast fixed-point algorithm for independent component analysis. Neural Computation 1997;9(7):1483-1492.

Maguire EA, Burgess N, Donnett JG, Frackowiak RSJ, Frith CD, O'Keefe J. Knowing Where and Getting There: A Human Navigation Network. Science 1998;280:921-924.

Makeig S, Delorme A, Westerfield M, Jung TP, Townsend J, Courchesne E, Sejinowski TJ. Electroencephalographic Brain Dynamics Following Manually Responded Visual Targets. PloS Biology 2004;2(6):0747-0762.

Makeig S, Jung TP, Ghahremani D, Bell AJ, Sejnowski TJ. Blind separation of auditory event-related brain responses into independent components. Proc Natl Acad Sci USA 1997;94:10979-10984.

Michel CM, Murray, MM, Lantz, G, Gonzalez S, Spinelli L, de Peralta, RG. EEG source imaging. Clinical Neurophysiology 2004;115:2195-2222.

Onton J, Delorme A, Makeig S. Frontal midline EEG dynamics during working memory. NeuroImage 2005;17(2):341-356.

Raghavachari S, Kahana MJ, Rizzuto DS, Caplan JB, Kirschen MP, Bourgeois B, Madsen JR, Lisman JE. Gating of Human Theta Oscillations by a Working Memory Task. The Journal of Neuroscience 2001;21(9):3175-3183.

Roelfsema, PR, Engel AK, Konig P, Singer W. Visuomotor integration is associated with zero time-lag synchronization among cortical areas. Nature 1997; 385:157-161.

Summerfield C, Mangels JA. Functional coupling between frontal and parietal lobes during recognition memory. Brain Imaging 2005;8;16(2):117-122.

Sorensen PL, Zeman PM, Sutherland RJ. Differing patterns of synchronous cortical activity during a virtual spatial navigation task. Canadian Society for Brain, Behaviour and Cognitive Science, 16th Annual Meeting. Paper presentation. 2006.

Spiers HJ, Maguire EA. Thoughts, behaviour, and brain dynamics during navigation in the real world. NeuroImage 2006;31:1826-1840.

Takada M, Tokuno H, Nambu A, Inase M. Corticostriatal projections from the somatic motor areas of the frontal cortex in the macaque monkey: segregation versus overlap of input zones from the primary motor cortex, the supplementary motor area, and the premotor cortex. Experimental Brain Research 1998;120:114-128.

Yao D. A method to standardize a reference of scalp EEG recordings to a point at infinity. Physiological Measurement 2001;22:693-711.

Yao D, Wang L, Oostenveld R, Nielsen KM, Arendt-Nielsen L, Chen ACN. A comparative study of different references for EEG spectral mapping: the issue of the neutral reference and the use of the infinity reference. Physiological Measurement 2005; 26:173-184.

Shepherd GM. The Synaptic Organization of the Brain. 5th ed. Oxford, NY: Oxford University Press, 2004

Van Veen BD, van Drongelen W, Yuchtman M, Suziki A. Localization of Brain Electrical Activity via Linearly Constrained Minimum Variance Spatial Filtering. IEEE Transactions on Biomedical Engineering 1997;44:867-880.

Zeman PM, Sorensen PL, Livingstone SA, Skelton RW, Livingston NJ. Understanding and Improving ICA Source Separation of EEG Data. (for publication) 2008a.

Zeman PM, Mahajan SV, Livingstone SA, Driessen PF, Skelton RW, Livingston NJ. Beamform Volume Projection of EEG ICA Topographies. (for publication) 2008b.

Zeman PM, Mahajan SV, Sorensen PL, Driessen PF, Skelton RW, Livingston NJ. Beamform Volume Projection of ICA Components of Scalp EEG: Volume-Domain Uniqueness of Components. (for publication) 2007c.

Zeman PM, Mahajan SV, Livingstone SA, Driessen PF, Skelton RW, Livingston NJ. Volume Domain Validation of ICA-Derived EEG Sources. (for publication) 2008d.

Zeman PM, Mahajan SV, Livingstone SA, Livingston NJ, Skelton RW. Spectral Shaping to Relax ICA Assumptions to Facilitate Decomposition of EEG. (for publication). 2008e.

Zeman PM, Livingstone SA, Livingston NJ, Skelton RW. Feasibility of System Analysis of Brain Activity for Spatial Navigation using Scalp-EEG. (for publication). 2008g.

Zhang K, Chan L-W. An Adaptive Method for SubBand Decomposition ICA. Communicated by Hyvarinen, A. Neural Computation 2006:18;191-223.

Section V: Application of New Methods

In the previous section we described our complete methodology which utilizes the novel technical contributions discussed in previous sections. Results of the methodology were demonstrated to show that it can provide a meaningful representation of the scalp EEG obtained from a single study participant. In the previous section, the methodology was also compared to other closely related work. In doing so we demonstrated that our method is novel and can be used to investigate brain function more directly than other closely related methods.

In the current section, a new dataset is examined using our proposed methodology.

Chapter 8: Feasibility of System Analysis of Brain Activity for Spatial Navigation Using Scalp-EEG

The following manuscript demonstrates how the methodology developed over the previous chapters can be used to meaningfully analyze the EEG data of a group and to compare the brain activities of individuals to the activities of the group. To do so, EEG data acquired during a spatial navigation study at the University of Victoria are examined.

Article Type: Research Article

Article Title: Feasibility of System Analysis of Brain Activity for Spatial Navigation using Scalp-EEG

Philip M. Zeman[1,2,3], Sharon A. Livingstone[3], Nigel J. Livingston[1], Ronald W. Skelton[3]

[1] CanAssist, University of Victoria, BC, Canada

[2] Department of Electrical and Computer Engineering, University of Victoria, BC, Canada

[3] Department of Psychology, University of Victoria, BC, Canada

Correspondence may be addressed to Philip M. Zeman:
(voice) +1-250-589-4234 / (fax) +1-250-721-6611 / pzeman@alumni.uvic.ca

Keywords: EEG; ICA; Multi-Component Spatio-Temporal modeling; neurodiagnostics; spatial navigation; data mining; virtual Morris Water Task, egocentric navigation; allocentric navigation.

Abstract

Objectives:

To demonstrate the feasibility of using a 32-channel scalp-EEG acquisition system to examine brain function related to spatial navigation using the Multi-Component Spatio-Temporal EEG (MCST-EEG) analysis methodology (Zeman et al., 2008f). To construct a model of the functional relationship of brain areas active in egocentric (cue based) and allocentric (place based) navigation conditions during a virtual Morris Water Task (vMWT). To identify analysis methods that might be used in a larger study to analyze brain activities for neurodiagnostic purposes.

Methods:

EEG data were collected while participants completed trials of a vMWT paradigm that were biased towards allocentric and egocentric navigation strategies. These data were separated into components using the Spectral Shaping ICA (SS-ICA) algorithm (Zeman et al., 2008e), validated using a volume-domain validation algorithm (Zeman et al., 2008c), and localized (Zeman et al., 2008d) to examine brain activities associated with task conditions. The volumetric origins of activities of validated EEG components were estimated and depicted on a canonical cortex (Zeman et al., 2008b). Component activation comparisons were made between navigation conditions for the first second of navigation. Brain-behaviour relationships were identified by calculating correlations of component activation with trial completion latencies, and component activation with explicit knowledge of platform location. Pair-wise zero-lag correlations among component activities were calculated to estimate functional relationships between brain areas. Correlations were also calculated to determine the consistency of pair-wise activation of components across participants.

Results:

The EEG data were separated into 31 components. A subset of these components were linked to specific areas of the brain: the superior medial parietal lobule, primary motor, posterior parietal, anterior parietal, medial anterior parietal areas of the right hemisphere, the dorsal extrastriate visual, and the posterior inferior temporal cortex of the left hemisphere; bilaterally: the dorsolateral prefrontal cortices, superior parietal lobules, ventral extrastriate visual cortices, and primary striate visual cortices. Activities of the

right hemisphere posterior parietal cortex were significantly greater during allocentric trials than egocentric trials. Activation of the ventral extrastriate visual cortices bilaterally and the dorsolateral prefrontal cortex of the right hemisphere were related to increased average time to complete trials optimized for the allocentric navigation condition. No significant correlations of brain area activation with accuracy of explicit knowledge of the platform location were found. A greater number of zero-lag correlations among multiple brain areas were found for the allocentric condition than the egocentric condition.

Conclusions:

It is feasible to use a 32-channel scalp-EEG acquisition system to examine brain function related to spatial navigation using the Multi-Component Spatio-Temporal EEG (MCST-EEG) analysis methodology. The MCST analysis methodology was used to successfully model the functional relationship of brain areas active in egocentric (cue based) and allocentric (place based) navigation conditions during a virtual Morris Water Task (vMWT). Analysis methods were identified that might be used in a larger study to analyze brain activities for neurodiagnostic purposes.

(I) INTRODUCTION

To understand the relationship between behaviour and brain function, it is important to have suitable tools to acquire and analyze brain activity data. For example, recent developments in functional magnetic resonant imaging (fMRI) technology have provided glimpses of brain function as it relates to behaviour. Using fMRI it is possible to measure how activities of specific parts of the brain respond to manipulations in a behavioural paradigm because the method provides anatomically-referenced activations that vary between human behaviours. While fMRI analysis is very useful in this regard, it is also very expensive, making it unavailable to most researchers. Given this barrier of expense, a low cost methodology for examining the functional activities of the brain would be favourable and have a significant impact in the neuroscience community.

PURPOSE OF THIS STUDY

The current study examines the feasibility of describing functional brain activity associated with spatial navigation using a low cost 32-electrode scalp-EEG recording system. This method of data acquisition is paired with the recently developed Multi-Component Spatio-Temporal (MCST) EEG analysis methodology (Zeman et al., 2008f) to construct a data-driven model of the brain activity of spatial navigation. Since the current study is largely one of feasibility, both significant and non-significant trends in the data are identified and described so that results can be anticipated in future work. Moreover, the purpose of this work is to use trends in the data to provide topics for debate and future investigation.

This feasibility study will be followed by a larger study characterizing functional brain activity in healthy adults. The larger study will be used to create a 'normative' sample against which to test data obtained from populations with injuries, and with pathological brain conditions in neurodiagnostic applications.

RELATION OF COGNITIVE FUNCTION, SPATIAL NAVIGATION, AND BRAIN PATHOLOGIES

The behavioural paradigm used in the current study was modeled after the Morris Water Maze (MWM) task (Morris, 1981), originally designed to study spatial navigation behaviour in laboratory animals. The MWM consists of a large, round pool filled with cool, opaque, milky water and requires animals (usually rats) to find and escape onto a fixed-location platform hidden just below the surface of the water. Because a variety of different start positions are used, and because there are no local proximal landmarks that, by themselves, indicate the platform location, optimal performance of the task requires that animals utilize multiple distal cues such as the location of windows, pictures, and bookshelves in the research laboratory environment to navigate within the pool. Prior work has demonstrated that healthy, adult rats learn the location of the hidden platform using these distal cues (over multiple trials) and become able to take direct paths to it from multiple start locations (Morris, 1981).

The study of spatial navigation in humans is more complex than for rats because the navigation environment used to study navigation in rats is not physically suitable for humans. For this reason, a computer-based virtual environment is generally used to mimic the original MWM task, providing human participants a 1st-person perspective view of what an avatar sees inside a circular arena maze; the human navigator is visually provided with a 'rat's-eye' view of the navigation environment. The current study refers to the computer-based task as the virtual Morris Water Task (vMWT). For a detailed description, see Livingstone and Skelton, (2007).

For the vMWT, study participants are required to find a platform hidden at a target location just under the floor of an arena maze with characteristics similar to the water-filled animal maze. The arena is located within a large room with windows through which an outdoor environment consisting of mountains, a lake, and an island can be viewed. When the participant 'walks' across the target location, the platform rises up, becoming visible and indicating the end of the trial. As in the original animal paradigm,

the circular arena itself is featureless except for the arena maze ring defining the edge of the navigation space, requiring the participant to use distal environmental information for navigation. Even when start locations are varied from trial to trial, most healthy participants are able to learn the location of the hidden platform.

Using a computer-based adaptation of the original MWM, a maze created by Livingstone and Skelton (2007) was used by Ross et al., (2006) to show consistent gender differences in navigation performance indicating that, on average, males are able to go to the target platform location more quickly and directly than females. The findings of Ross et al., (2006), support previous findings of Astur et al., (1998) who also used their own adaptation of the MWM in behavioural studies of spatial navigation in humans. Prior research by Sandstrom et al. (1998) found that females tend to rely on distal landmarks when navigating in a vMWT whereas males use a combination of distal landmarks and geometric features for navigation. More recently, Hamilton et al. (2003) have adapted the original MWM to their own computer-based virtual maze and have demonstrated that persons with foetal alcohol syndrome (FAS) tend to select erroneous, indirect headings and stop searching for the platform sooner than controls. Our own recent work (Livingstone and Skelton, 2007) using our maze has demonstrated that individuals with traumatic brain injury (TBI) take longer than controls to reach the location of the platform when only distal information is available, but navigate as well as controls when there is a landmark or 'cue' in close proximity to the platform.

Healthy human navigators are thought to employ two types of cognitive processing during navigation tasks (Nadel and Hardt, 2004; Burgess, 2008). These are known as *allocentric* and *egocentric* and each is associated with the use of differing behavioural strategies when a navigation problem is presented. There is evidence that these two different types of cognitive processing have differing physiological requirements, and utilize differing anatomical substrates of the brain (Iaria et al., 2003; Burgess, 2008). Egocentric strategies are thought to involve the physiology of multiple areas of the brain that define the *egocentric navigation system* while allocentric strategies are though to involve multiple areas of the brain that are a part of the *allocentric navigation system*.

Here, the term *system* refers to all areas of the brain that work together for either type of navigation, including visual processing pathways.

Egocentric strategies or 'response strategies' (Bohbot et al., 2007) involving the egocentric navigation system are sometimes referred to as 'non-spatial' (Iaria et al., 2003). These strategies are employed by the navigator who does not need to know, or ignores, the spatial relationships among distal visual stimuli in the environment because the information of importance for the navigation goal is available from a single cue or landmark viewed from the perspective of the navigator. Similarly, using an egocentric strategy, the navigator can follow a complex path where the final goal is not visible, by sequentially moving towards a series of cues or landmarks that constitute a route to that goal. This type of strategy can be considered one of simple 'stimulus-response' associations such that when the stimulus cue or landmark is visible, the navigator moves directly towards it. Navigation involving stimulus-response associations and egocentric processing is often referred to as 'cue' navigation.

In contrast, allocentric strategies that involve the allocentric navigation system are sometimes referred to as 'spatial' strategies and are considered to be more complex than egocentric strategies. It was proposed (O'Keefe and Nadel, 1978; Nadel and Hardt, 2004) that allocentric navigation requires the formation and use of a 'cognitive map' (Tolman, 1948) of the environment. Creation of a cognitive map is believed to involve the encoding of the static spatial relationships of multiple features in the environment with each other, the position of the navigational goal, and the current position of the navigator. Navigation using the cognitive map therefore must combine previously encoded static spatial relationships, the navigational goal, and the current location of the navigator to generate goal-directed movement. This type of navigation is often referred to as 'place' navigation (Morris et al., 1982; Moffat and Resnick, 2002; Iaria et al., 2003; McGregor et al., 2004).

A navigator that is new to an environment must create a cognitive spatial map before allocentric navigation can take place. Prior research has not examined the behavioural

procedure for constructing a spatial map in detail; here we have deducted a logical process. First, navigation about the environment is required to create the map. Navigation at this stage can be facilitated using inefficient non-allocentric strategies such as an egocentric strategy or a non-allocentric idiosyncratic strategy (Kallai et al., 2005). For example, a navigator might randomly move throughout the navigation space, move in concentric circles of decreasing or increasing radii, or move in a path of some arbitrary geometric pattern (such as a pentagram). Some research has considered this 'spontaneous strategy selection' (Iaria et al., 2003; Bohbot et al., 2004). It is assumed that features in the room that comprise the allocentric information can be used egocentrically during this stage of allocentric learning to guide locomotion. While navigation using the maze using egocentric information may not be efficient, it provides a context in which the navigator may (1) actively make hypotheses about how to navigate the environment or (2) move about the space while passively (without intention) making passive associations; it facilitates trial and error learning. During this navigation, the location of the platform must be found (by chance) in order to facilitate association of the platform and features of the environment. After multiple successful trials navigating to the goal using the inefficient strategy and associating the location of the platform with the (1) strategy just employed to reach it, and (2) the visual feature information viewed from the platform, allocentric relationships become available and a cognitive spatial map is formed. During learning, navigators collect visual information while moving about the space, testing relationships between visual information and platform location to construct a spatial map of allocentric space.

Many factors influence navigation strategy selection and the most efficient strategy for a given navigation problem may not always be employed (Iaria et al., 2003), even after navigators have been given ample time to explore the environment. Strategy selection may be biased in individuals. If allocentric and egocentric information are both reliable, the navigator may use one or both to achieve the goal. Strategy selection may also be biased by recent navigation experience. Our prior research (Skelton et al., manuscript in preparation) found if participants do a cue task prior to being given the choice to navigate by cues or by place information, they are more likely to continue to use cue information.

In contrast, if they do a place task prior to being presented with the option of navigating by place information or cue information, there is approximately a 50% chance they will navigate by place and a 50% chance they will navigate by cue.

Navigation necessitates the ability to recognize and distinguish among features of the environment. Here we specifically consider navigation according to visual feature information. We hypothesize that when an egocentric strategy is employed by the navigator, an object recognition system will be concurrently active. When navigating according to visual information it is necessary to uniquely identify and differentiate among the objects present in the navigation environment. For example, given a scenario where there is a fire hydrant and a sign post are present in a maze, the navigator must (1) be able to distinguish between the two objects in order to (2) chose one of them to orient towards and commence locomotion (navigate egocentrically).

Similarly, we hypothesize that when an allocentric strategy and the allocentric navigation system is employed by the navigator, an object recognition system will also be transiently or concurrently active. This is for the same reason as for the egocentric case, to differentiate between objects in the environment, however this time the object information is used in a different way. In this case, multiple objects are utilized for navigation using an allocentric strategy and thus the direction of orienting and locomotion is determined by the relative angles of the objects from the current viewing angle of the navigator and employment of a cognitive map.

This leads us to the question of the level or depth of processing that might be required for object recognition in each of the egocentric and allocentric cases. Presumably, it is only necessary to differentiate objects by their visual characteristics and it is not necessary that each object be processed to the depth of object naming and object usage. When an object with a name and usage does come into view of the navigator during locomotion, areas of the brain associated with language and usage context might become active, however this presumably is not a necessity for navigation behaviour. Hence, in an analysis of brain activities associated with egocentric and allocentric navigation, it is expected that areas of

the brain important for object recognition and object processing will become active and the depth of processing may vary.

The model of Skelton et al., (manuscript submitted) suggests dynamic use of egocentric navigation systems and object identification systems during allocentric navigation. Their model describes that the navigator will alternate between allocentric and egocentric strategies to facilitate locomotion. They suggest that both systems are active, acquiring and processing information. However, only one system has control over locomotion at a given time.

Studies of navigational behaviour in rats and humans have suggested a central role of the hippocampus in allocentric navigation. Animal lesion studies have identified the hippocampus in relation to successful completion of behavioural trials optimized for allocentric strategies such that rats with lesions to only the hippocampus show increased latencies to complete place trials but are still able to perform simple cue-based tasks (Morris et al., 1982). In human studies of navigation after brain injury there is evidence to show that damage to the medial temporal region of the cortex (hippocampus) is associated with poor performance in tasks optimized for allocentric navigation. For example, temporal lobectomy patients demonstrate an inability to select or use allocentric strategies when performing a virtual radial arm maze task (Bohbot et al., 2004) and patients with focal hippocampal damage (either via anoxia or surgery) perform poorly on trials optimized for allocentric strategies compared to healthy controls (Astur et al., 2002).

Increased latency to complete allocentric mazes has been observed in participants with non-focal traumatic brain injury (TBI). Participants with TBI have longer latencies on trials optimized for allocentric strategies in our virtual MWT paradigm but show no impairment on egocentric versions of the task (Livingstone and Skelton, 2007). Injury related to TBI is generally diffuse and it is difficult to identify loci of dysfunction. However, it is speculated that impaired allocentric navigation in such circumstances is related to the high probability of hippocampal damage (Livingstone and Skelton, 2007;

Bigler, 2001) and/or damage to pathways interconnecting the hippocampus with other areas of the brain.

Research using rat models suggests the hippocampus and the related entorhinal cortex encodes a cognitive map of the environment and the position of the rat in the environment. Evidence suggests the cognitive map is represented by the activities of place cells in the hippocampus (O'keefe and Nadel, 1978; O'keefe and Dostrovsky, 1971), providing an up-to-date representation of allocentric space. These cells fire when a rat is placed in specific locations in the maze environment. Other research has demonstrated that grid cells located in the medial entorhinal cortex of the rat encode and provide representation of an animals own position in the environment (Fyhn et al., 2004). Grid cells are activated in a stereotypical manner across environments, irrespective of the particular landmarks in the environments.

Research using rats has demonstrated that allocentric navigation performance is affected by damage to several brain areas (for reviews see Brandeis et al., 1989; d'Hooge and Deyn, 2001; Nadel, 1991). The hippocampus is connected to multiple areas of the cortex via multiple pathways. The perirhinal and parahippocampal cortices receive sensory information from the visual and somatosensory association cortices, and receive information directly from the poster parietal cortex, and indirectly from the hippocampus. Projections proceed indirectly from the caudal third of the inferior parietal lobule via the inferior longitudinal fasciculus to the parahippocampal gyrus. Projections to the parietal cortex take an indirect path from the hippocampus via the entorhinal cortex to the parietal cortex. The parahippocampal cortex is also reciprocally connected with the prefrontal cortex (Goldman-Rakic et al., 1984).

Research has linked spatial processing ability with hippocampal function and function of the posterior parietal cortex. Lesion studies (Kolb et al., 1983; Kolb and Walkey, 1987; DiMattia and Kesner, 1988) examining allocentric spatial navigation in rats using the MWM task demonstrated injury to the posterior parietal cortex causes error in initial heading, and increased latencies to reach the platform. Similarly, human research has

demonstrated that persons with posterior parietal cortex injury exhibit various forms of spatial disorientation (Husain and Nachev, 2007). The posterior parietal cortex is believed to integrate information from the hippocampus (place cells) and entorhinal cortex (grid cells) with information from the visual cortices (Whitlock et al., 2008). This information is linked to goal-oriented movement through projections from the posterior parietal cortex to anterior areas of the parietal cortex involved with somatosensory processing and motor planning. In relation to navigation, a study by (Nitz, 2006) used rats to show that cells of the posterior parietal cortex encode complete navigational motor sequences or 'navigational epochs'.

The posterior parietal cortex is believed to put visual and other sensory information into register with the different coordinate systems of eye, head, and body axis to support accurate eye, head, limb, and whole body movements to targets (Andersen and Buneo, 2002; Andersen et al., 1987; Taira et al., 1990; Snyder et al., 1998). Visually guided limb movement (reaching or grasping) is generally described as involving a stream of visual information processing guiding motor action that projects from the visual cortices dorsally through parietal to pre-motor and motor areas of the cortex. Information transfer via this stream from the retina passes through the dorsolateral geniculate nucleus of the thalamus (LGNd), the primary visual striate cortex, to the dorsal extrastriate cortex. It continues dorsally through the lateral intraparietal cortex, ventral intraparietal cortex, and posterior parietal cortex. This dorsal stream (illustrated in Figure 1) provides visual input to posterior parietal cortex, critical for spatial perception, enabling representation of objects in space (Ungerleider and Mishkin, 1982).

A related visual processing stream that projects to the posterior parietal cortex utilizes subcortical pathways (Figure 1). This pathway begins at the retina and projects through the superior colliculus and the pulvinar to the cortex, bypassing the primary visual cortex (Goodale 1993). Visual information from the retina reaches the posterior parietal cortex subcortically. This pathway is generally thought to be involved in 'non-conscious' localization of objects and may play a role in a phenomenon called 'blindsight' where persons with cortical lesions preventing them from consciously localizing objects in

space can point to the correct location of stimuli with asked, with greater than chance probability (Danckert et al., 2003).

The ventral visual processing stream, projecting through the temporal lobes, should also be involved in spatial navigation albeit not for localization of objects in space, but for object identification and recognition (Figure 1). This 'ventral stream' provides a major source of visual input to temporal lobe which is critical for processing features of objects (color, and behavioural use) (Ungerleider and Mishkin, 1982; Goodale et al., 1998). Persons with injury to the temporal lobe disrupting this pathway have inability to recognize objects (Farah, 1990). The stream provides a path from the retina, through the dorsolateral geniculate nucleus of the thalamus (LGNd), through the primary visual striate cortex, to the ventral extrastriate visual cortex for medium level visual processing. From there, information passes anteriorly through the posterior inferotemporal cortex, the central inferotemporal cortex, and the anterior inferotemporal cortex.

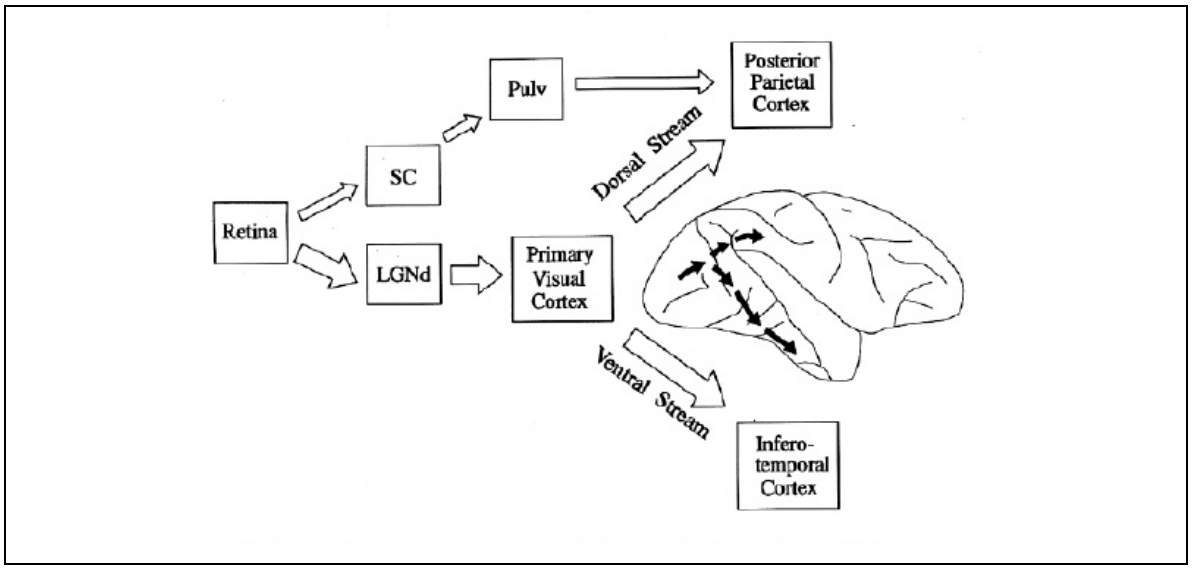

Figure 1. Block diagram of visual information streams from the retina to various locations in the cortex. Adapted from Goodale et al. (1998). Pathway (1) subcortical: retina – superior colliculus (SC) – pulvinar – posterior parietal cortex (PPC); Pathway (2) dorsal stream: retina – dorsolateral geniculate nucleus (LGNd) – primary visual cortex to posterior parietal cortex (PPC); Pathway (3): ventral stream: retina – lateral geniculate nucleus – primary visual cortex to the inferotemporal cortex (IT).

These cortical streams, or pathways, are not segregated to one hemisphere but are generally thought to be present in both hemispheres, however, to different degrees of specialization. Generally, the right hemisphere of the brain is believed responsible for spatial function, but an analogy to language function suggests differential spatial lateralization across the population should be expected. For example, statistics obtained from studies that use either the WADA (Rasmussen and Milner, 1997) or brain stimulation (Ojemann et al. 1989) technique to localize language function prior to brain surgery indicate that language function tends to be lateralized to the left hemisphere (particularly in right handed individuals). It is known that for language functions like speech production, the majority (96%) of right handed individuals are left lateralized for language whereas a smaller number (4%) are right lateralized for language (Rasmussen and Milner, 1997). In left handed individuals the majority (70%) are left lateralized for language, but the remaining 30% are either right lateralized or have bilateral language function. If spatial lateralization is similarly variable in the population but opposite to language function, then we should expect to see evidence of varied lateralization of processing among study participants when analyzing their brain activities associated with spatial navigation tasks. Moreover, this language lateralization analogy suggests that handedness may not be a predictor of spatial function lateralization. The statistic that describes bilateral allocation of language function (some part of the 30% statistic above) may also have a spatial function analogue.

(II) METHODS

DATA COLLECTION AND PREPARATION

Participants

Twelve healthy student participants were recruited to participate in the current study. Of these 12 participants, 11 were right-handed (participant #s 1, 2, 3, 4, 5, 6, 7, 8, 9, 10, 12) and 1 was left handed (participant # 11). Participant numbers 1, 2, 3, 5, 6, 10, and 11

were male. By self report, participants had either normal or corrected-to-normal vision using contact lenses. This research was approved by the University of Victoria Ethics Committee. Participants that were part of the Psychology 100 pool received credit toward their course grade while other participants received a monetary payment of $10 each.

Participants were seated approximately 70 cm from the front of a 17 inch LCD computer screen to accommodate game playing. Participants used a joystick to navigate in the virtual environment; all participants used their right hand to operate the joystick. A chin cup was provided for participants to rest their chin and support their head during the experiment, keeping their head in a stable position. Supporting the head in this way provided the additional property of reducing cable and electrode noise in the EEG normally caused by head movement.

Description of Paradigm and Sequencing of Trials

There is no established time-location for determining when in an EEG recording brain activities associated with spatial navigation that differentiate egocentric and allocentric strategies will appear. The time location of task-relevant brain activities in the EEG however can be anticipated. The paradigm has been designed so that in the first second of each trial, participants are orienting themselves and selecting their destination. It is expected there will be brain activities related to task preparation prior to trial onset and brain activities relating to task execution immediately after trial onset. Our recent work has demonstrated that during the first second of this particular paradigm, there is eye-movement activity which differentiates the behavioural conditions of allocentric and egocentric navigation (Skelton et al., manuscript submitted). In that study, the first second of eye-movement acquired during place trials indicates participants look at allocentric features and then at the maze floor at the location of the hidden platform. Gaze generally remains at the location of the platform on the maze floor until the location has been reached. In contrast, the first second of eye-movement in cue trials generally shows looking at cues at the start of each trial and when the cue of interest is identified,

gaze on the cue is maintained until completion of locomotion when the hidden platform is reached. For both place and cue trials, when a successful navigation strategy has not been adopted, gaze is less predictable.

Our prior work indicates that people look to locations that are appropriate to the cognitive strategy employed. Our prior work also indicates that most participants learn and then maintain a single strategy to complete the navigation task early within each block of 10 trials; participants tend to reach their shortest latencies prior to the second half of the block (trials 6 to 10). Thus we expect that the brain activity of the last half of each block will be related to the spatial navigation strategy employed.

In the current experiment, data were recorded for 4 types of trials, presented in 4 different blocks which are herein refer to as 'visible', 'place', 'cue', and 'ambiguous'. The first block consisted of 4 visible platform trials and was used to determine if participants could use the joystick to navigate the space to a visible platform. This block also provided baseline latencies for participants to navigate from various places in the arena maze to the platform. Second, a set of 3 blocks was presented, each block consisting of 11 trials of the same type, (place, cue or ambiguous). These 3 blocks were sequenced as one of the two following possibilities: (1) cue, ambiguous, place or (2) place, ambiguous, cue (randomized between study participants). In each of the 3 blocks, the first 10 trials required participants to find a hidden platform several start positions presented in pseudo-random order. Trials were completed when the participant reached the location of the hidden platform. When the location of the hidden platform was reached, the platform appeared beneath the participant (visible from their 1st-person perspective view) at the same time an auditory stimulus indicated that the platform had been found and that the trial was completed. After a short random interval (approximately 5 seconds) of viewing the arena from the platform, the next trial began from a new location in the maze. The last trial of each block (trial 11) was a 50 second probe trial for which the platform was not present; however, participants were instructed that the platform had 'shrunk' in size and was difficult to find. At the conclusion of the probe trial, the usual mechanical sound indicated that the trial was complete. (Participants were not made aware that the hidden

platform could not be found during this trial. They were made aware of this fact once they data collection had completed.)

At the completion of each block of 11 trials, each participant's explicit knowledge of the location of the platform was assessed for the block. Participants were asked to navigate the maze 'one more time' and indicate where they believed the location of the platform was in a task we called "Drop-The-Seed", herein referred to as the DS-probe. The location of the platform was indicated by the participant through the action of navigating the maze and as directly as possible, placing an object, a seed, on the arena maze floor where they believed the platform was located. Unbeknownst to the participant, they were scored according to how close their seed was to the location of the center of the platform.

Before navigating trials in each of the cue, place, and ambiguous trial blocks, participants were given an opportunity to 'explore' the arena maze. During exploration just prior to the place trial block, participants familiarized themselves with the features of the room. Similarly, during exploration just prior to the cue trial block, participants explored the cue maze. Prior to commencing trials for the ambiguous condition, an exploration trial was also provided. Exploration in each case continued until participants indicated that they had thoroughly explored the space. The paradigm intentionally allows for natural learning of the environment; participants are not explicitly told which visual features are important for navigation and doing so provides for the presence of learning and strategy selection during cue, place, and ambiguous trial blocks.

Description of Each Trial Type

Participants were provided with different visual information in each condition to be used to find the location of the hidden platform and complete each trial. Figures depicting an example of the cue and place trials from the perspective of study participants are provided in Appendix A. The arena maze for cue condition trials had 8 objects placed on the arena wall at equal intervals around its circumference which served as the proximal

stimuli by which participants could navigate using an egocentric strategy. One of these objects (a golden urn) always marked the location of the hidden platform, and to complete these trials, participants were required to simply navigate towards this cue object. The allocentric information in the cue condition was not useful for finding the hidden platform in the cue maze because the cue object and the platform, together, changed location on each trial. The arena maze for the place condition did not have objects; participants were required to navigate towards the hidden platform based on distal characteristics and features of the landscape outside the windows of the arena (the perspective of these features changed appropriately as participants navigated in the maze as their perspective change for their view outside the window). These distal stimuli facilitated navigation to the location of the hidden platform using an allocentric strategy. In the ambiguous condition, 8 objects were placed on the arena wall in the same manner as for the cue condition. One of these objects, a metal box, always marked the platform location, similarly as had the golden urn marked the location of the platform for trials of the cue condition. The metal box and the platform remained in the same location throughout the trial block, and thus, the distal information provided by the room windows and features outside the room remained in agreement and were constant across these trials. Therefore participants could find the platform either by using an egocentric strategy based on travelling directly to the metal box cue object, or by using the allocentric properties of the room.

Since the purpose of this pilot study was to identify the feasibility of finding meaningful differences between the cue and place trials only, the data collected for the ambiguous trials were not used to make comparisons. Data from the ambiguous condition however were used with data from the cue and place conditions in the EEG data mining process to identify brain activity related components from the EEG.

Latencies from the commencement of each trial to reaching the location of the hidden platform were recorded for use as a metric to evaluate performance on each individual trial. This is a conventional measure adopted from the original MWM paradigm (Morris, 1981).

Acquisition of EEG Data

The EEG data were acquired using a 32-channel Active-II Biosemi EEG acquisition system and ActiView 600 software (Biosemi B.V., Amsterdam, Netherlands), configured to sample data at 512 samples per second. Data were recorded while participants navigated the virtual space.

The first stage of EEG analysis incorporated de-referencing and segmentation of the data. The EEG data were de-referenced by calculating the average across channels for each individual time sample and subtracting this value from each channel (Yao, 2001). Data segments were extracted from the recorded continuous EEG data to provide for analysis around the onset of each trial. EEG data from only the first 10 trials of the cue, ambiguous, and place conditions were used in analysis. These data were segmented as -1000 to 2500 ms with the trial onset designated as 0 ms for each condition. Each trial of data was digitally band-pass filtered 8-80 Hz, using a 300 point zero-phase linear filter, and then down-sampled to 256 samples per second providing for 897 samples x 32 electrodes per trial of data. There being 3 conditions (cue, place, and ambiguous) and 12 study participants, the number of data samples totalled 322920 (12 participants x 10 trials x 3 conditions x 897 samples per condition) for each of 32 electrodes.

The second stage of EEG analysis involved application of the MCST algorithm. The MCST algorithm consists of 4 main processing steps: data mining, volume projection of identified EEG components, validation of components, and volumetric estimation of validation components. Since this is a relatively new algorithm, some extra analysis has been provided in the current study to substantiate steps of the MCST algorithm.

DATA ANALYSIS

EEG Data Mining

The Spectral Shaping ICA (SS-ICA) EEG data mining process, a component of the MCST algorithm, was used to identify components of the EEG dataset as waveform activities and topographies. The SS-ICA method differs from standard ICA methods such as runica (Makeig et al., 1997) because the source separation criterion of statistical independence is not applied equally at all frequencies; a subset of frequencies is permitted to be correlated and dependent. To do so combines characteristics of the BS-ICA algorithm of Zhang and Chan (2006) and the runica algorithm of Makeig et al. (1997). The improvement provided by the SS-ICA method over runica has been demonstrated in prior work (Zeman et al., 2008e).

The SS-ICA algorithm automatically calculates an appropriate filter by which to shape the EEG frequency spectrum and calculate spatial separation matrices. The shaping filter characteristics are determined by identifying frequencies of statistical independence that provide reduction of the overall dependence measured among EEG components. The magnitude spectrum of this filter indicates which frequencies have the greatest independence and which frequencies have the least independence. Our prior work examining EEG data found that the frequencies less than 20 Hz and in the interval 45-55 Hz had the least independence, while the frequencies in the intervals 20-45 Hz and 60-75 Hz had the greatest independence (Zeman et al., 2008e) and we expected that the shaping filter will be similar in the current study. Once the coefficients of this filter were calculated, they were used to shape the prepared EEG data, emphasizing frequencies of independence and uncorrelatedness by which to calculate spatial separation matrices. The spatial separation matrices were then used to separate the original unshaped EEG data into components and determine the topographical characteristics of these components.

This SS-ICA data mining process was applied as described above to the prepared EEG data in the current study. The magnitude of the shaping filter automatically calculated by the algorithm was plotted for inspection and is provided in Appendix B. Plots of the component topographies were created for visual inspection and are also provided in Appendix B.

Volume Projection

To characterize each component by its volume-domain properties for subsequent steps of component validation and brain source volume estimation, the volumetric spectrum of each component was calculated. The volumetric spectrum (Zeman et al., 2008b) is a 3-dimensional volume-domain representation of the topographical scalp surface field and is calculated via a process of projecting the topographical characteristics of each component into a mathematically defined head model. This process maps the spatial variance measured at the scalp surface, described by each component topography to a volume-domain representation using a closed-form mathematical solution (Van Veen et al., 1997). In the current study, a three-shell head model, created using the BrainStorm software package (Baillet et al., 2000), comprised of 5588 voxels, was used to describe the variance at every location in the head model. Each voxel was defined as cube with the length of each side equal to 5 mm. The levels of projected variance at each of these voxels, when arranged as a 1 x 5588 vector, defined the volumetric spectrum.

Validation and Classification of Components

Components calculated via the data mining process were validated using two methods, first by physical modeling of component characteristics in the volume-domain, and second, by waveform frequency characteristics.

The first validation method using physical modeling of the volume-domain characteristics of components, rated components according to how well they could be represented as volumes within a model head. Each component was rated according to

two properties: the specificity of representation of components at a single voxel in the head and the volume-domain overlap of each component with other components of the decomposition. Previous work describing this validation method is available in Zeman et al., (2008d). The voxel specificity property is determined as the value of the largest coefficient that defines the volumetric spectrum of each component and is herein referred to as the peak spectral value (PSV). The second property, the volume overlap of components, was calculated via a 2-step procedure. This procedure essentially estimates the uniqueness of the volumetric spectra of components. First the pair-wise overlap of the volumetric spectrum of the component under evaluation with the volumetric spectra of all other components of the decomposition is estimated. Each pair-wise overlap estimate is calculated as the Euclidean normalized dot product of the pair of volumetric spectra. Second, to provide a summary of overlap for the component under evaluation, the median of the dot products calculated in the previous step is calculated and is herein referred to as the median volume overlap (MVO) of that component. In the current study, the PSV and MVO were determined for each component of the decomposition. To assign a rank to each component by which to identify possible 'brain' components from 'artefact' components of the decomposition, the PSV and MVO values calculated for each component were sorted and compared against the values of all other components. The distinction between possible 'brain' component representations and 'artefact' component representations was determined by defining a threshold at the knee of the curve of these sorted PSV and MVO values. Those components that were ranked just below the knee of the curve were noted as 'uncertain'. The sorted MVO and PSV scores have been plotted and are provided in Appendix B.

Since the volume-domain validation procedure described above is relatively new, a second validation method examining component waveform frequency characteristics was used to corroborate the results of the first method. Using the Welch method (Cantero et al., 2003), the frequency spectrum of each component was estimated. Visual inspection and evaluation of the frequency characteristics of components was and used to classify each component as containing brain activities or artefact activities. Those components with frequency spectra similar to the standard scalp EEG spectrum were noted as 'brain'

and those with frequency spectra that are unlike a standard scalp EEG brain activity spectrum were noted as 'artefact'. Those components with frequency spectra that were not easily distinguished as brain or artefact (or were a mixture of both) were noted as 'uncertain'.

While validation by frequency characteristics does indicate which components have spectra that are 'brain-like', it does not provide information indicating how well each component pertains to unique anatomical areas of the brain (i.e., how well brain activities are separated). This procedure is detailed in Appendix B. The result of the volume-domain criterion based validation of components was compared to validation of components by visual inspection of their frequency content. A table summarizing the comparison between methods is given in Appendix B.

Volume Estimation of Components

Components of the EEG calculated via data mining were linked to anatomy by estimating the physical volumes inside the head from which the waveforms of components originate. These volumes were determined by estimating and removing the noise in the volumetric spectra calculated for each individual component. The variance contained in the volumetric spectrum that is not accounted for by the noise estimate is assumed to relate to the actual brain source. Noise thresholds were determined for both 4 and 5 standard deviations above the mean (STDM) noise-level. Prior work using simulated and real EEG data has shown that 4 or 5 STDM provides a reasonable depiction of the brain volumes from which component activities originate (Zeman et al., 2008b; Zeman et al., 2008e). Plots were created depicting the volumes occupied by validated brain sources. For completeness, the volumes of components that were not validated as having good volume-domain representations (those that were previously scored as 'uncertain' or 'artefact') were also plotted and are provided in Appendix B for inspection.

While component locations do provide information describing which areas of the brain have activities relating to the paradigm, this component location information does not

differentiate the activities of each condition, cue versus place. Hence, the waveform activities of each component were examined to make comparisons among the cue and place conditions.

Comparison of Effect and Conditions

The remainder of the analysis in the current work used only validated components to examine brain function associated with this spatial navigation paradigm. Component waveform activities and behavioural data obtained during data collection provided evaluation of the conditions of the paradigm.

To EEG and behavioural data, statistics were calculated using both non-standardized and standardized data. By making both types of comparisons, it was possible to determine if there was a significant difference between the cue and place conditions, while including and excluding between-subject variability. Doing so illustrates how comparisons might be made in a larger experiment investigating classification of brain activities as either egocentric or allocentric. In the current study, the approach described by Masson and Loftus (2003) was used to standardize EEG data and latency data.

Since the current study is a feasibility study, statistics used to evaluate results in the current paper are intended to infer trends that might be confirmed in a larger study. Thus, in the current study, there has been no allocation of statistical power among multiple statistical tests. Any statement of significance is an inference that a significant result might be found for a larger sample size. Differences were viewed as statistically significant for $p < 0.05$ for one-way, single-factor ANOVA comparisons using Microsoft Excel 2003. Error bars for plots were computed for the 95% confidence level.

Because the current study utilizes a small sample size (12 participants) and is a study of feasibility, an approach to significance for measures of correlation is considered noteworthy if the magnitude of correlation is greater than 0.4. In a larger study with greater than 24 participants, the standard correlation critical values table indicates that a

correlation of 0.4 would be significant, assuming all else remains constant. For evaluation of correlative relationships, three levels of significance were noted to identify trends: $p < 0.05$ relating to $r > 0.567$, $p < 0.02$ relating to $r < 0.658$, and $p < 0.01$ relating to $r < 0.708$. Analysis of waveform activities and behavioural measures utilized data from trials of the last half of each block (trials 6 to 10). This assumes that by the last half of each block, on average, participants will have established their strategy for that trial type. This assumption is based on findings in our prior work (Livingstone and Skelton, 2007).

Latency to Complete Trials

The average latency to trial completion for the last half of each of the cue and place blocks was calculated for each participant and plotted. To identify differences between the conditions for the group while including between-subject variance, an ANOVA was used on the non-standardized group latencies. To identify any effect of condition on latencies that includes between subject variance, the standardized latencies were used in an ANOVA to test for a significant effect. For comparison purposes, the standardized average and non-standardized average latencies were plotted. The standardized latencies were calculated as indicated above using the method of Masson and Loftus (2003).

Explicit Knowledge of Platform Location

Scores from the DS-probe trials were used as a measure to indicate the explicit knowledge of participants for the correct location of the hidden platform for the cue and place trials. A score of 1 was assigned if the participant placed the seed in the correct quadrant of the maze, and increasing with accuracy to the center of the platform to a maximum score of 7. A score of 0 was assigned if the participant did not place the seed in the correct quadrant of the maze. The scores for each participant were individually plotted for the cue and place conditions and were used to identify correlative relationships with the activities of components of the EEG. Following the methods of Hesterberg et al. (2003), a matched-pair permutation test was applied to the DS-probe

data to identify differences between conditions for the group. The matched-pair permutation test does not require that the data fit a Gaussian or Normal distribution and was applied because the DS-probe scores were found to be highly skewed. The test accounts for within-subject characteristics of the paradigm by maintaining the matched-pair characteristics of the cue-place data. This test assumes that the data acquired in both the cue and place condition are from the same distribution and identifies the probability of the observed mean difference between the cue and place conditions actually occurring. If the measured mean difference is unlikely to occur ($p < 0.05$), then the DS-probe scores for the cue and place conditions are considered to be from different distributions. The average of the cue and place groups were plotted for inspection. Confidence intervals were not calculated because they are known to be unreliable when data are skewed and the sample is small (n=12) (Hesterberg et al., 2003).

Brain Activations

To examine brain activations of the first second of navigation in the last half of each block of trials for the cue and place conditions, the 8-30 Hz root-mean-square (RMS) activities of each component were computed. First, component waveforms were band-pass filtered 8-30 Hz separately for each trial (trials 6 to 10) and condition using a zero-phase 300-point FIR band-pass filter. Next, an epoch of samples corresponding to the first second of navigation (0 ms to 1000 ms) was selected from each trial. These samples were then squared to provide an estimate of instantaneous power. The square-root of the mean of the squared samples was calculated to yield the RMS activation for each epoch. RMS activations of the last half of each block were averaged together to compute the average RMS activation for that condition. This was repeated separately for each participant, component, and condition. These activations for each component were plotted for each condition.

Standardized RMS activation values for each component and participant were calculated from the RMS activations determined above.

Brain Activations by Condition

To determine if there was a difference between conditions for activities of each brain area, the data were evaluated using both standardized and non-standardized RMS activations. These were compared between cue and place conditions using an AVOVA. A comparison of the RMS activations for each component by condition for both the standardized and non-standardized data was plotted.

Brain Activations and Behaviour Latencies

Brain area RMS activations were compared to latencies to identify possible relationships between brain activities in the first second of navigation and navigation performance in cue and place trials. Correlation values were computed between the RMS activation of each component and average latency to reach the platform across participants for the last half of each block for the place and cue conditions separately. The correlative relationships for each component and condition were plotted.

Paired RMS Brain Activation

Correlations between RMS activation values of components were calculated in a standard correlation matrix for each condition separately. Pair-wise relationships were determined as the correlation of each component's RMS activation with other component RMS activations, across the participant group. These paired RMS activations were calculated to identify consistencies across the participant group in the pair-wise activation of components. These calculations were made separately for each condition using the pre-calculated non-standardized RMS activations. This was calculated for all possible pair combinations of components for each condition separately. Scatter plots were created to illustrate the pair-wise relationships between components so that the position of each participant on the plot served to identify trends and outliers in the data.

A block diagram illustrating significant pair-wise relationships indicating consistency across the group, calculated for each condition overlaid on anatomical information was created. Two ranges of significant correlation were provided in the figure to show a range of confidence (the roll-off of values from most confident). These pair-wise relationships were compared to significant relationships between behavioural latency and RMS activation as well as relationships between RMS activation and measures of explicit knowledge of platform location were included in the diagram.

Coordination Among Brain Areas (Zero-Lag Correlations)

The pair-wise zero-lag correlation between components was calculated to identify which brain areas have coordinated activities separately for each participant. This was accomplished through multiple steps using trials 6 to 10 for the cue and place conditions separately. First the data of each trial were band pass filtered 8-30 Hz for each brain activity component. Second, for each pair of brain activity components, a 50% overlap sliding analysis window 500 ms wide was used to estimate the correlation between the components for multiple time intervals during each trial.

For each analysis window the data were multiplied with a Hanning window to reduce spectral leakage. Doing so reduces distortion of the data caused by processing only a segment of the continuously recorded data. The windowed data were then normalized to have unit autocorrelation, prior to estimating the cross-correlation between the activities of component pairs. The cross-correlation value was then transformed using the atanh function to map the correlation sample distribution to a distribution closer to Gaussian. After calculating the correlated activities of all pairs at all time intervals, for each participant and condition, the correlated activities were plotted. A sample zero-lag correlation measured between pairs of brain area components that differ between behavioural conditions is provided in the Results section. Error bars were calculated as 1 standard deviation of random samples of the mean (2000 random samples of the mean; to calculated each mean, 4 participants were randomly selected from the group).

To summarize the pair-wise zero-lag results for the time-window around the onset of navigation, the above chance ($p < 0.05$) zero-lag correlations that differed significantly between conditions were indicated by connecting lines on a model cortex.

(III) RESULTS

EEG DATA MINING

The first step of the data mining procedure yielded a shaping filter implicating frequencies of relative independence. The shape of the magnitude spectrum of the shaping filter (automatically calculated) identified frequencies of independence in the band 25-45 Hz and frequencies around 70 Hz. Frequencies in the 34-64 Hz band and frequencies less than 25 Hz were de-emphasized suggesting the activities in these regions of the frequency spectrum have low statistical independence. The magnitude spectrum of this shaping filter is provided in Appendix B. The magnitude spectrum is similar to the magnitude spectrum used to mine EEG data in our prior research that were acquired using a different paradigm and different recording equipment (Zeman et al., 2008e).

Upon completion of the data mining procedure, 31 components had been calculated with associated topographies and waveform activities. Each component is represented by a scalp topography plotted and provided for inspection in Appendix B numbered 1 through 31 in no particular order.

VALIDATION

Of the 31 components calculated via data mining, 14 of them were validated as representations of distinct brain activity sources by the volume-domain validation algorithm. These are components 2, 4, 7, 9, 17, 18, 22, 23, 25, 26, 28, 29, 30, and 31. The validation curves used to rank of components according to PSV and MVO, and a

comparison of the volume-domain validation results to evaluation of components by their waveform frequency spectra are provided in Appendix B.

VOLUME ESTIMATION

Estimated brain volume source origins for each of the 14 validated components (Figure 2) illustrate that numerous brain areas have activities involved this visuospatial navigation paradigm. A visual comparison of the localized brain source volumes to the features of the white matter model onto which the brain volumes have been localized suggests activities in specific cortical areas. The active brain areas of the right hemisphere include the: dorsolateral prefrontal cortex, ventral extrastriate visual cortex, anterior parietal cortex (somatosensory cortex), medial anterior parietal cortex, primary visual striate cortex, posterior parietal cortex, primary motor cortex, superior parietal lobule, and the superior medial parietal lobule. The active brain areas of the left hemisphere include the: dorsolateral prefrontal cortex, primary visual striate cortex, posterior inferior temporal cortex, dorsal extrastriate visual cortex, ventral extrastriate visual cortex, and the superior parietal lobule.

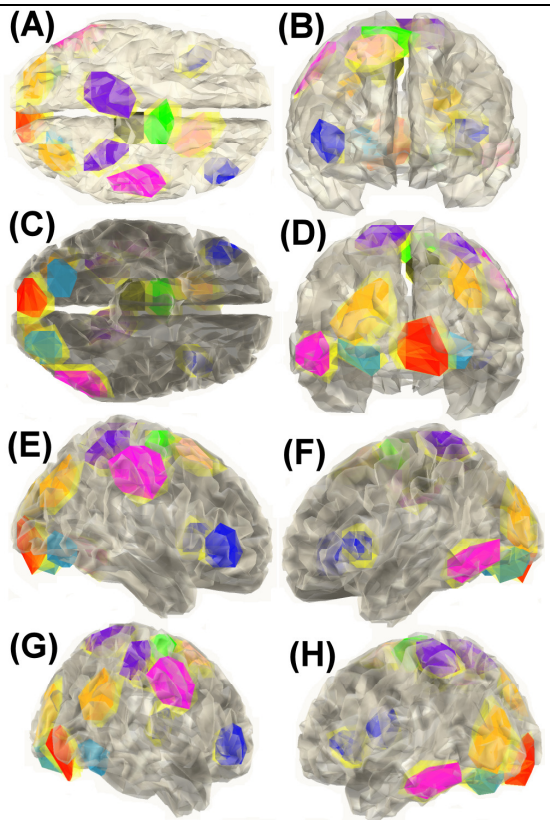

Figure 2. Volume regions estimated for component source origins calculated from the EEG data of the participant group illustrated on a canonical cortex. Colored areas represent the estimated source volumes pertaining to activities of the brain for 5 standard deviations above the mean (STDM) volume-domain noise estimate. A yellow region surrounds each of the coloured volumes estimates providing volume estimates for 4 standard deviations above the noise mean (STDM) for each component. Colors are used to differentiate components in each hemisphere.

The relative proximities and positions of volume locations of activation suggest the presence of cortical pathways. Notably, the data suggest the presence of a pathway projecting from posterior areas dorsally to prefrontal areas of the cortex in the right hemisphere, generally believed to be involved in processing spatial relationships. The dorsal pathway in the left hemisphere is evidently shorter. Similarly, a ventral pathway is present in both hemispheres, however in the right hemisphere, the ventral pathway is notably shorter. Activity of the ventral pathways has been generally attributed to object

perception. The presence of these pathways was anticipated in the introduction when highlighting the various known cortical processing streams (Goodale et al., 1998).

Summary of Active Brain Areas

The locations of components, determined by visual inspection of localization results of components on a model cortex, are summarized in Table 1.

Comp.	Color	Hemi.	Location
2	blue	L	dorsolateral prefrontal cortex (DLPFC)
4	blue	R	dorsolateral prefrontal cortex (DLPFC)
7	cyan	R	ventral extrastriate visual cortex
9	cyan	L	ventral extrastriate visual cortex
18	magenta	L	posterior inferior temporal (PIT)
22	magenta	R	anterior parietal cortex (somatosensory cortex)
23	green	R	medial anterior parietal cortex, or superior medial post-central gyrus
25	orange	L	dorsal extrastriate visual cortex
26	purple	L	superior parietal lobule
28	red	L+R	primary striate visual cortex
29	orange	R	posterior parietal cortex (PPC)
30	pink	R	primary motor cortex
31	purple	R	superior parietal lobule
17	black	R	superior medial parietal lobule

Table 1. Component numbers, color reference, possible brain locations. Secondary name or acronym is given in parenthesis. Components were linked to specific brain location descriptions by visual comparison of the localized brain source volumes to the features of the white matter model onto which the brain volumes have been localized.

COMPARISON OF EFFECT AND CONDITIONS

Latency to Complete Trials

A summary of the latencies to trial completion is provided in Figure 3. The figure shows the average latencies to trial completion for each participant (Figure 3a), a comparison of group latencies for cue and place (Figure 3b), and a comparison of the standardized latencies for the cue and place illustrating the effect of condition (Figure 3c). The individual latencies to trial completion show that the latency to complete the place trials for most participants is longer than the latency to complete cue trials. The latencies for participant numbers 9 and 11 are an exception; the average latency for cue was greater than the average latency for place. Visual inspection revealed that place trial latencies for 3 participants differed from the group; for participants 7, 10, and 12, latencies are much greater than those of other participants suggesting they had difficulty with the place trials. The cue latencies for these same participants were short suggesting successful navigation in the cue trials. Participant number 7 has the greatest latency in the place condition as compared to other study participants suggesting that this participant had the greatest amount of difficulty with the place trials.

There are some interesting trends in the latency data of participants showing differences between navigation conditions. Comparison of the cue and place data using ANOVA on non-standardized latencies in Figure 3b shows that they provide no clear difference between the conditions ($p=0.088$; $F=3.2$; $Fcrit=4.3$). ANOVA comparison using standardized latencies in Figure 3c shows a significant effect of condition ($p=0.010$; $F=6.4$; $Fcrit=4.3$).

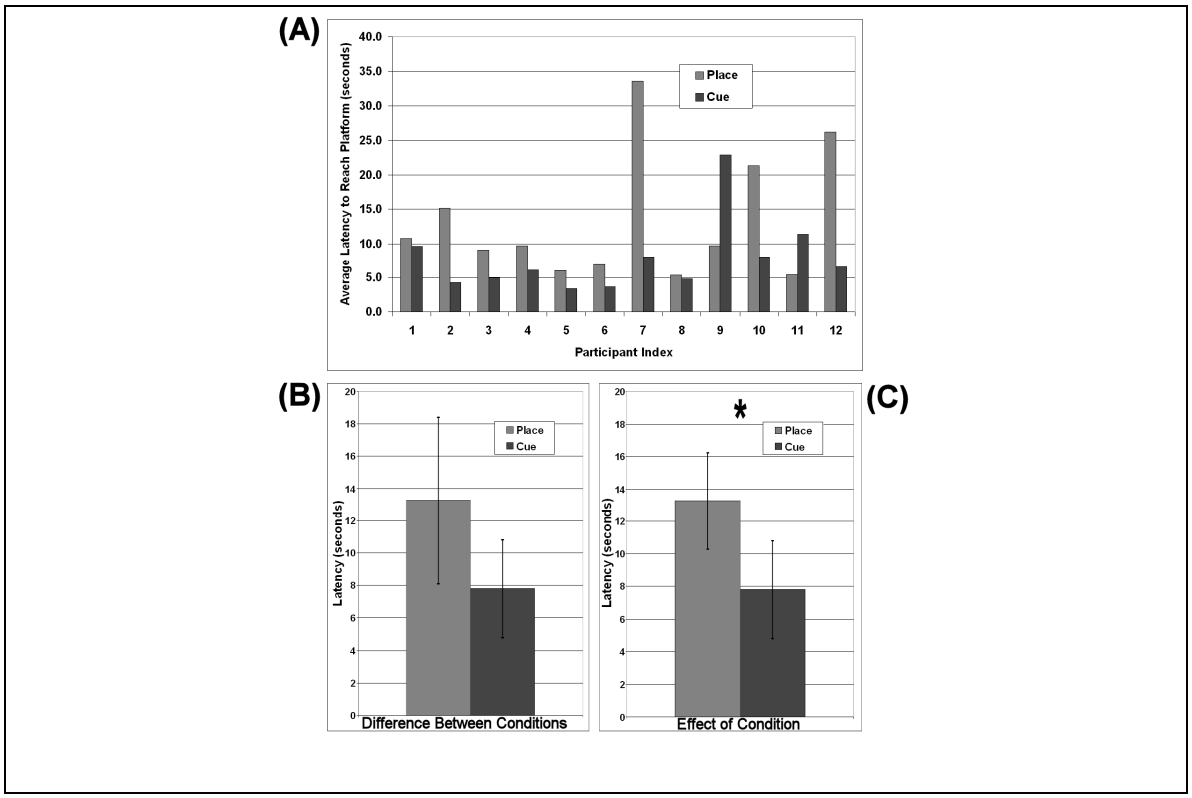

Figure 3. Latency to trial completion for trials 6 to 10 of each block for the cue and place conditions. (A) for each study participant; (B) comparing the non-standardized latencies; (C) comparing the standardized latencies. Error bars indicate the 95% confidence interval. A significant difference calculated via ANOVA of standardized latencies is indicated by (*).

Explicit Knowledge of Platform Location

The DS-probe scores which provide a measure of each participant's explicit knowledge of the correct location of the hidden platform reveals that more participants explicitly knew the location of the platform for cue trials than for place trials (Figure 4a). On cue trials: participants 1, 2, 3, 6, 7, 8, 10 had explicit knowledge of platform location. In contrast, participants 3, 5, 9, and 12 did not know the location of the cue platform when asked to identify its location. Participant 11 was close to knowing the approximate location. On place trials: participants 1, 2, 3, 6, and 8 knew the location (correct quadrant or better relating to a score greater than 3) of the hidden platform. In contrast, results showed participants 5, 7, 10, 11, and 12 did not have explicit knowledge of the platform

location for place trials. Participants 4 and 9 were close to knowing the approximate location.

Analysis of the DS-probe scores for the participant group demonstrated a significant difference between conditions ($p < 0.05$). This result is presented in Figure 4b. Paired permutation tests revealed that DS-probe scores for the cue condition were significantly greater than for the place condition ($p = 0.049$). This suggests that generally participants had greater explicit knowledge and were more confident of the location of the hidden platform in the cue condition than in the place condition.

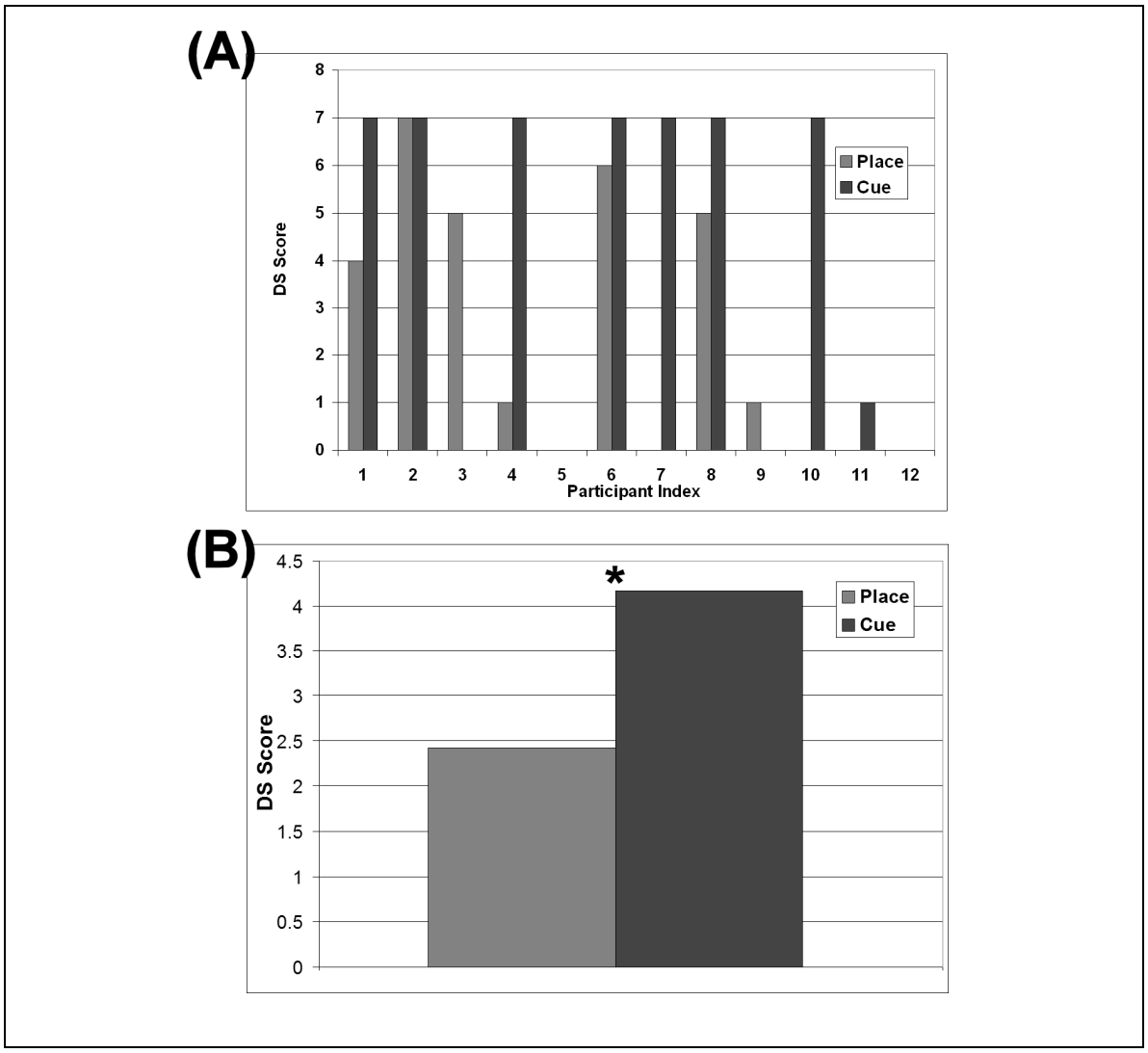

Figure 4. 'Drop-the-seed', DS-probe scores estimating the explicit knowledge of the location of the hidden platform for each participant in the cue and place navigation conditions. 'DS' on the vertical axis denotes the score for the 'Drop-the-seed' probe trial. (A) scores for individual participants for cue and place conditions; (B) a comparison of the scores for the cue and place conditions indicating a significant difference (*). Since the density functions of these data are non-Gaussian and skewed, the significant difference was determined via pair-wise non-parametric permutation methods. Because these data are skewed and the sample size is small (n=12), error bars cannot be accurately calculated (Hesterberg et al., 2003) and have not been provided.

Brain Activations by Condition

Comparison of the RMS activations of brain areas in the first second of trials is given in Figure 5 using both non-standardized and standardized RMS data. Evaluation of the difference between conditions by applying ANOVA to non-standardized data (Figure 5a) does not reveal any significant differences in activation between cue and place conditions for the group. However, differences between the RMS activations for brain areas (Figure 5b) applying ANOVA to standardized data indicate an effect of condition for some brain area activities. (Standardization of the data as described in the Methods section estimates and removes between subject variability.) In particular, ANOVA reveals a significant effect ($p = 0.015$; $F = 6.9$; $F_{crit} = 4.3$) of condition for component number 29 that was found to be located in the posterior parietal cortex of the right hemisphere indicating that this brain area is more active in the place condition than in the cue condition.

Analysis using standardized RMS activations also reveals that components approaching a significant difference between conditions, with more activity in the cue condition than the place condition, are components 17 (superior medial parietal lobule), 4 (dorsolateral prefrontal cortex), 23 (medial anterior parietal cortex), 31 (superior parietal lobule).

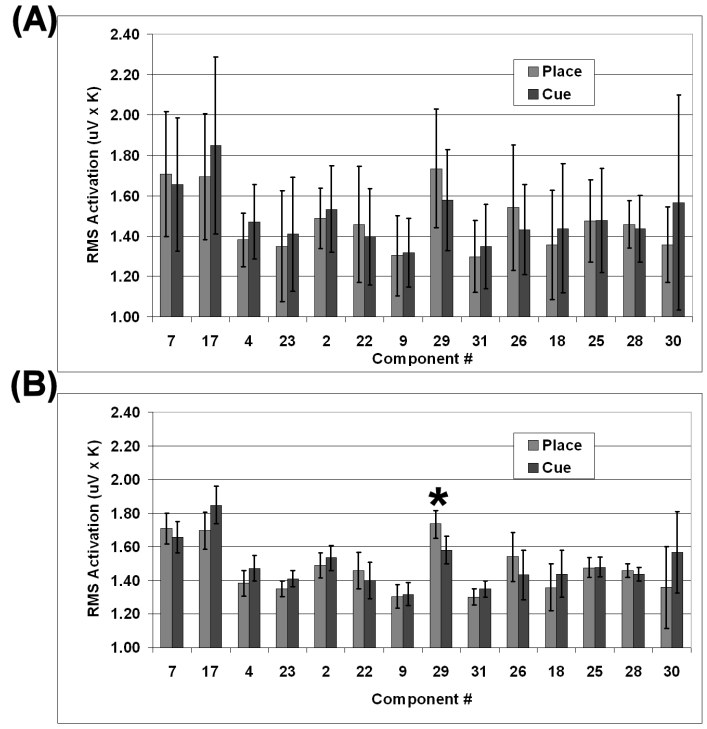

Figure 5. Comparisons of RMS activation levels for the first second of spatial navigation for each component between the cue and place conditions. Error bars are the 95% confidence interval. (A) activation for non-standardized data; (B) activation for standardized data. A significant effect of condition is present for component 29 for standardized data. Significant differences are indicated by (*).

Brain Activations and Behaviour

Correlation analysis presented in Figure 6a shows some significant relationships between RMS activation of brain areas and trial completion latencies suggesting activation of these areas relates to poor navigation performance for place trials. This correlation is positive and significant for components 7 (right extrastriate visual cortex), 4 (right dorsolateral prefrontal cortex), 9 (left extrastriate visual cortex) ($p < 0.05$). This result might indicate that some participants navigating place trials were not using the appropriate allocentric strategy but were actually using an inefficient egocentric strategy leading to increased latency to complete the place trials.

Figure 6a also reveals some possible relationships between activities in specific brain areas and poor place performance that might be revealed as significant in a larger study. For example, components 17 (right superior medial parietal lobe), 2 (left dorsolateral prefrontal cortex), 25 (left dorsal extrastriate visual cortex), and 28 (primary striate visual cortex) are approaching a significant relationship with trial latency in the place condition. In the cue condition, component 26 (left superior parietal lobule) is approaching a significant positive correlation with latency suggesting that activity in this area might contribute to poor navigation in cue trials.

Correlation analysis of brain activation with DS-probe scores calculated across study participants shows no significant correlations but does suggest some possible trends of interest that might be significant in a larger study. In the place condition, activity of component 22 (right anterior parietal cortex) is positively correlated with the measure of explicit knowledge of the platform location. A significant finding here would suggest that when this area is active for place trials, participants can identify the location of the hidden platform when asked. Brain area activities approaching a significant positive correlation with explicit knowledge of platform location in the cue condition include components 4 (right dorsolateral prefrontal cortex), and 9 (left ventral extrastriate visual cortex). This suggests that in the cue condition, if these areas are active, the participant can identify the location of the hidden platform when asked, and presumably, could identify which cue is important.

Component 29 (right posterior parietal cortex) in the cue condition approaches a significant negative correlation with explicit knowledge indicating that a larger study might find that in the cue condition, if a participant can not show where the location of the platform is when asked, they might have been utilizing their right posterior parietal cortex in the task. Conversely, if they can show where the platform is when asked in the cue condition, then the activity of their right posterior parietal cortex is expected to have decreased activity.

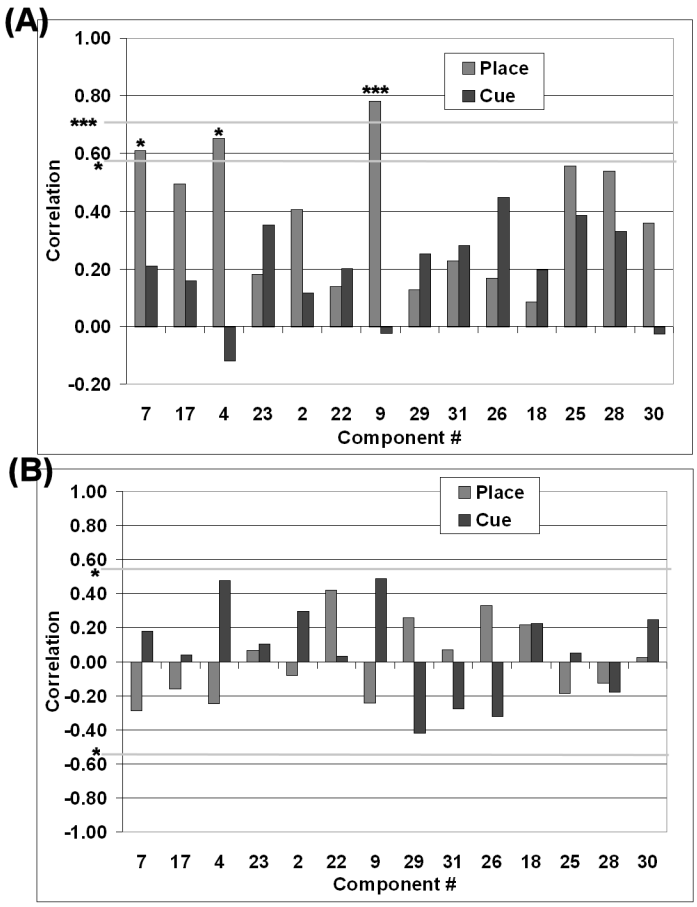

Figure 6. Correlation of 8-30 Hz RMS brain activations with behavioural measures. (A) Correlation of behavioural trial completion latencies with RMS activations of each component across study participants. (B) Correlation of RMS brain activations with DS measures of explicit knowledge of platform location. Significant correlation ($p < 0.05$; $r > 0.576$) is indicated by (*) in the figure. (***) indicates significant correlation ($p < 0.01$; $r = 0.708$).

Distribution of Brain Activations by Condition

The distribution of samples for some pair-wise component relationships suggests significant correlation among activations for different brain areas. These significant correlations indicate consistency across the participant group in the activation characteristics of pairs of brain areas. Scatter plots for a subset of these components are given in Figure 7. For a correlation to be significant for 12 minus 2 degrees of freedom

(for a 12-participant study), the correlation must be greater than or equal to 0.58 for $p < 0.05$.

Significant relationships ($p < 0.05$) for the cue condition were found between components: 9 (left extrastriate visual cortex) and 25 (left dorsal extrastriate visual cortex) (r=0.68) , 2 (left dorsolateral prefrontal cortex) and 7 (right extrastriate visual cortex) (r=0.58), 26 (left superior parietal lobule) and 29 (right posterior parietal cortex) (r=0.78), and 9 (left extrastriate visual cortex) and 18 (left posterior inferior temporal cortex) (r=0.80) (Figures 7a, b, c, and d, respectively).

For these same components, relationships for the place condition are not all significant. The only significant correlative relationship was between components 2 (left dorsolateral prefrontal cortex) and 7 (right extrastriate visual cortex) (r=0.71). Non-significant correlations were found between components 9 (left extrastriate visual cortex) and 25 (left dorsal extrastriate visual cortex) (r=0.40), 26 (left superior parietal lobule) and 29 (right posterior parietal cortex) (r=0.57), and 9 (left extrastriate visual cortex) and 18 (left posterior inferior temporal cortex) (r=0.42).

In Figures, 7a, b, and d, participant 7 may or may not to be an outlier in the distribution of samples. Participant 7 has been marked in the figure to demonstrate the scenario where it is regarded as an outlier. With the removal of this participant from the distributions of Figures 7a, b and d, the non-significant correlations become significant for 11 minus 2 degrees of freedom ($p < 0.05$; $r > 0.60$). Specifically, component pairs 9 and 25 in the place condition change from r= 0.40 to 0.62 (Figure 7a), component pairs 7 and 2 in the cue condition change from r= 0.58 to 0.74 (Figure 7b), and component pair 9 and 18 in the place condition change from r= 0.42 to 0.63 (Figure 7d).

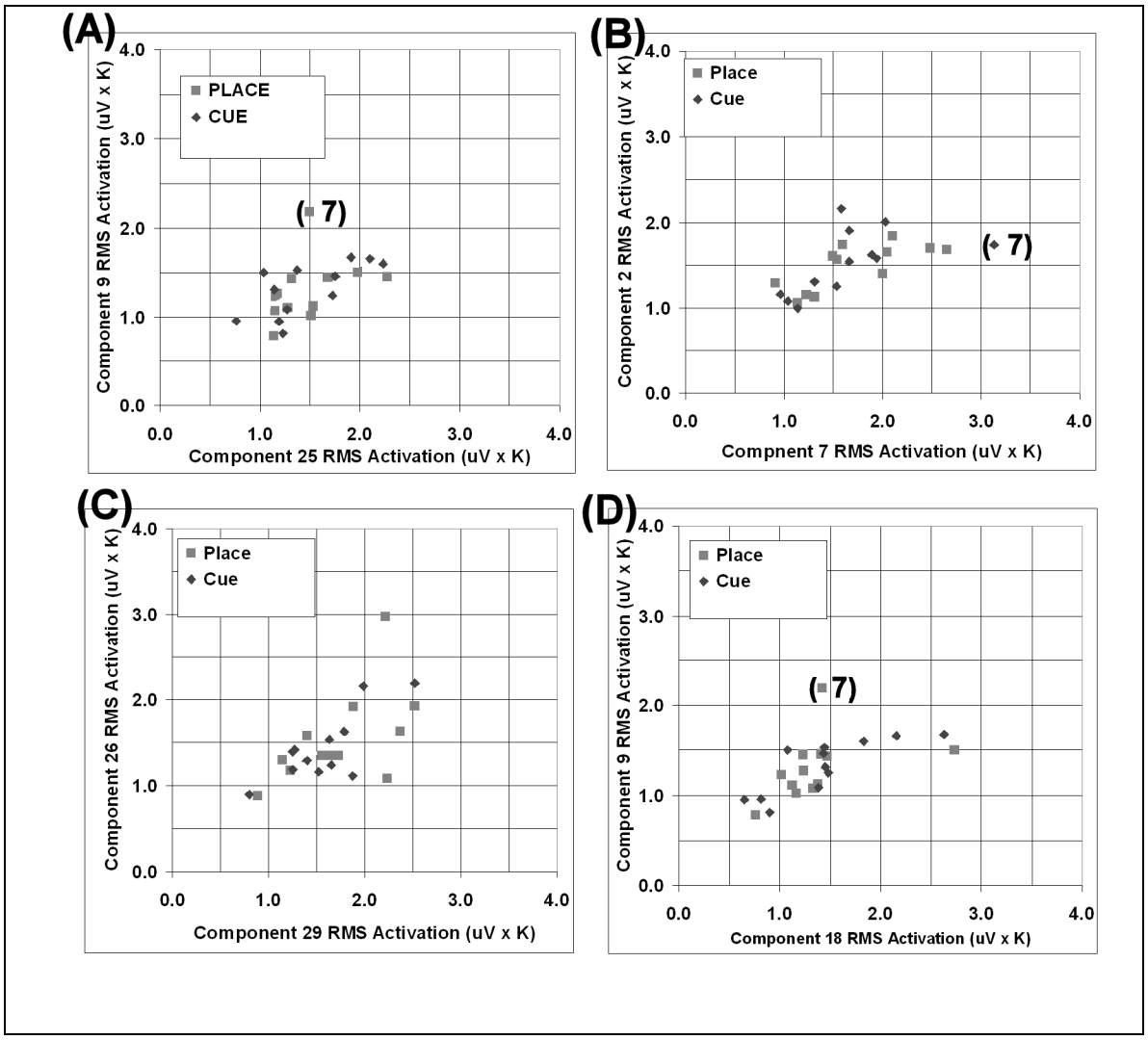

Figure 7. Scatter plots depicting RMS activations of a selection of paired components for the first second of spatial navigation demonstrating components that are correlated across study participants for one of the behavioural conditions. (A) relationship of components 9 and 25 is significant for cue but not for place; (B) relationship of components 2 and 7 is significant for cue and for place; (C) relationship of components 26 and 29 is significant for cue but not for place; (D) relationship of components 9 and 18 is significant for cue but not for place. Plots (A, B, D) illustrate a possible outlier (participant 7, indicated in the plots) that has been included in these significance calculations and has not been rejected because it is difficult to determine if this participant is a true outlier given the small sample size.

To emphasize that the activation of some component pairs is more consistent across the participant group than others, Figure 8 depicts two cases where there is no consistency of activation between components. This is the case for pairs: 29 (right posterior parietal cortex) and 25 (left dorsal extrastriate visual cortex) (Figure 8a) for both the cue condition (r=0.49) and the place condition(r=0.33), and 29 (right posterior parietal cortex) and 28 (primary visual cortex) (Figure 8b) for both the cue condition (r=0.54) and the place condition (r=0.20). The distribution of samples for both conditions is 'box-like', and is not elongated as would be expected for a correlative relationship.

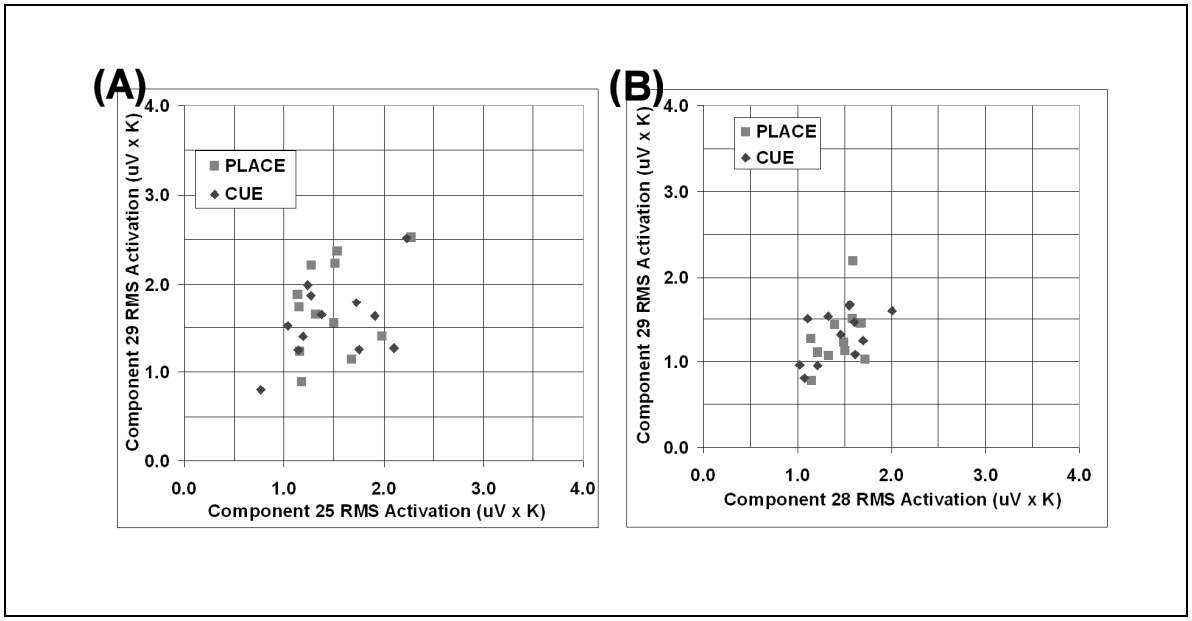

Figure 8. Scatter plots depicting RMS activations of a selection of paired components for the first second of spatial navigation demonstrating components that are not correlated across study participants for both the cue and place conditions. (A) components 29 and 25; (B) components 29 and 28.

Map of Pair-Wise Activation Relationships by Condition

A summary of the correlative relationships some of which were previously given in scatter plots is given in Figure 9. The correlative relationships calculated in this way indicate which pairs of components have an activation relationship that is consistent across the participant group and which pairs do not have this relation. Lines that connect blocks in the diagram indicate consistency of the relationship between those blocks across the group of study participants. The degree of consistency indicated by the level of correlation is reflected by the thickness of the line. This representation of pair-wise relationships for all components provides an estimation of the coordination of the brain as a system for each of the behavioural conditions. In the cue condition thick connecting lines dominate the left posterior ventral region, while in the place condition thick connecting lines dominate the right parietal region in the figure.

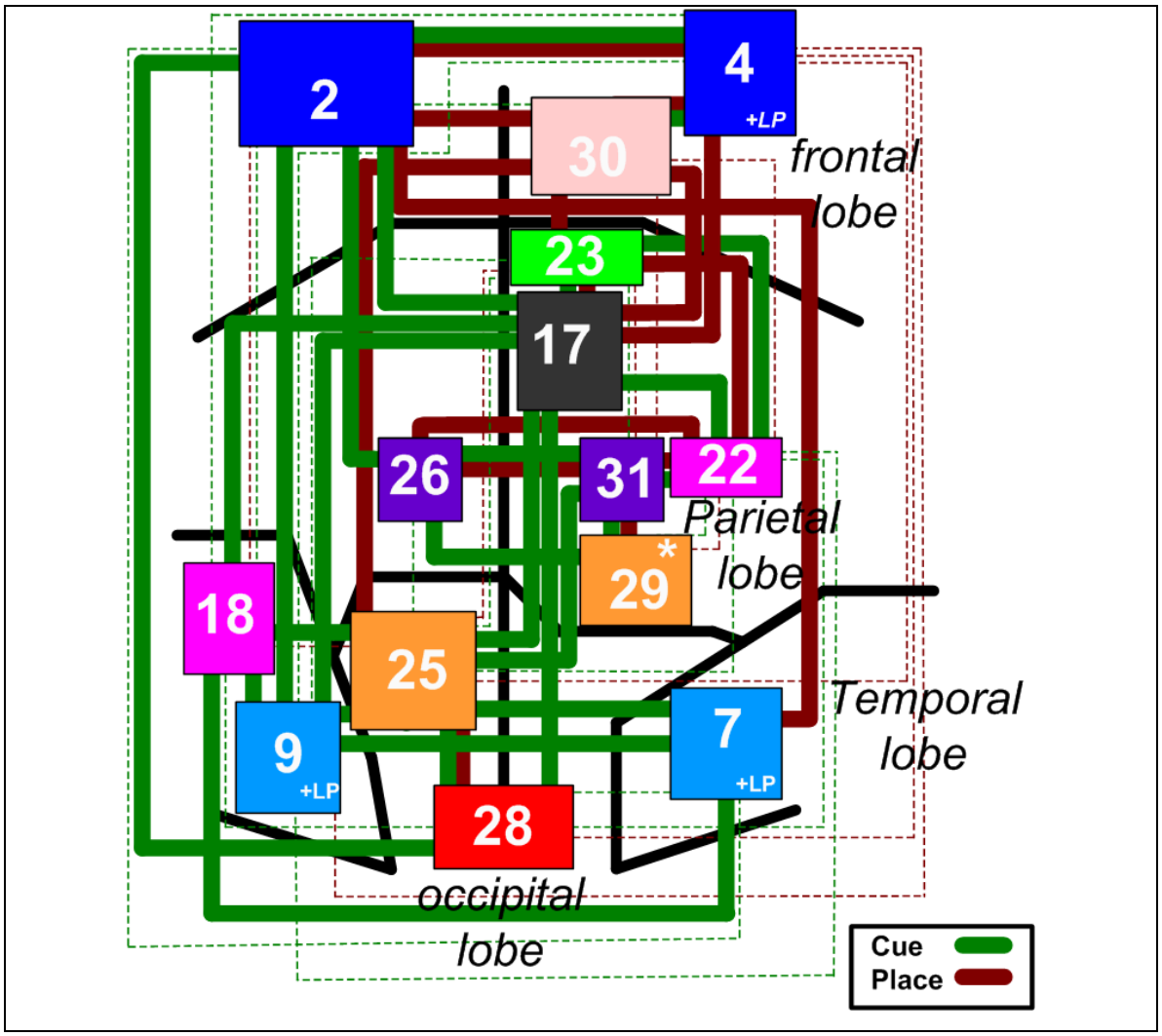

Figure 9. Block diagram of pair-wise correlation relationships calculated across the participant group (including possible outlier participant number 7) for the cue and place conditions. Relationships were calculated using the non-standardized RMS activations for the first 1 second of cue and place behavioural trials. Significance levels for this figure provide thresholds by which relationships between components are represented. Thick lines correspond to correlation greater than 0.71 ($p < 0.01$), while thin dashed lines correspond to correlation greater than 0.66 and less than 0.71 ($p < 0.02$). Only lines indicating relationships greater than $p < 0.02$ are given so that only primary relationships are represented. Block numbers correspond to component numbers. Blocks have been spatially arranged in the figure to represent their relative locations in a dorsal view of the cortex. Black lines represent divisions of the cortex: occipital, temporal, parietal, and frontal for each hemisphere. The primary visual cortex (component 28) is represented at

the bottom of the figure as a single block. (The primary visual striate cortex was not split into a left hemisphere component and a right hemisphere component by data mining.) Filled colors of blocks correspond to the colors of the estimated volumes in Figure 2. Blocks have been annotated to show additional information. (*) indicates the RMS activation is significantly greater in the place condition than in the cue condition. LP indicates activity in this area has a correlation relation to place latency measured across the participant group. (+/-) indicates positive and negative correlation, respectively. Italic LP indicates an approach to significance ($0.576 > |R| > 0.4$) while non-italicized annotation indicates a significant correlative relation ($|R| \geq 0.576$; $p < 0.05$)

Coordination Among Brain Areas (Zero-Lag Correlations)

Zero-lag evaluation of component activities revealed relationships in the time-varying activations of components in the interval around the trial onset. An example of the zero-lag correlation calculated between component pairs is given in Figure 10 for components 29 and 31 showing a difference between conditions around the interval of trial onset.

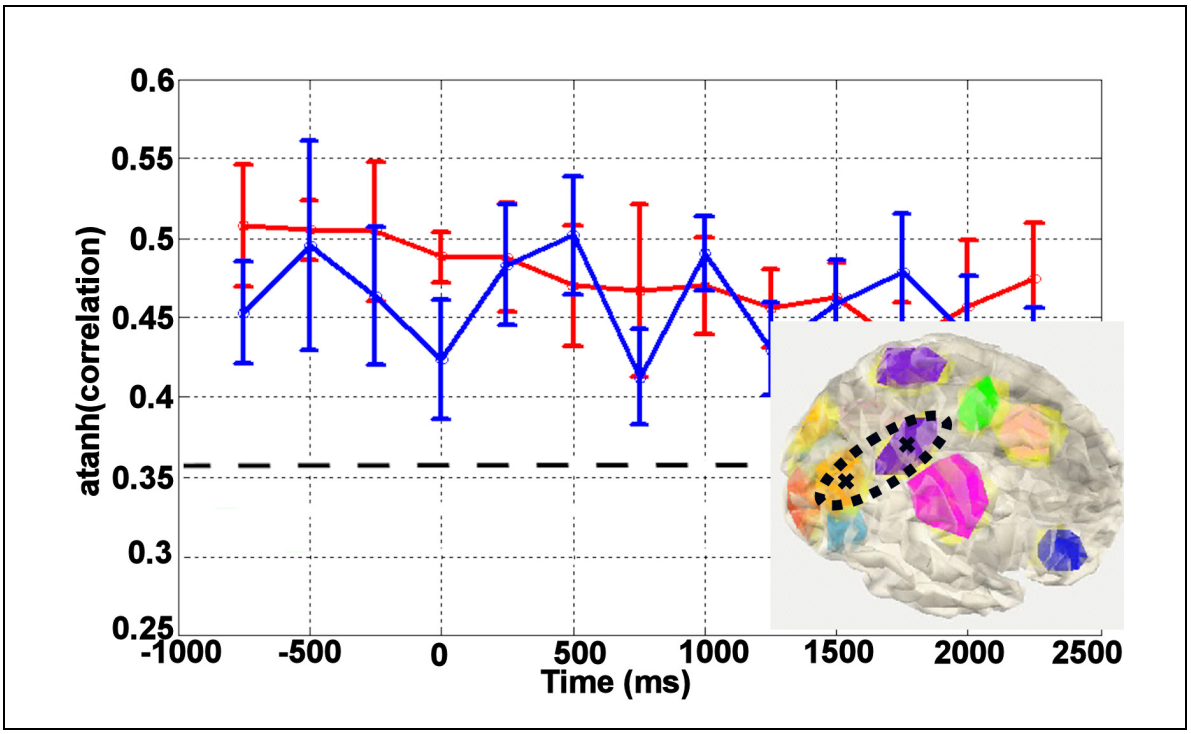

Figure 10. Zero-lag correlation between components 29 (posterior parietal cortex) and 31 (superior parietal lobule) estimating coordination among brain areas (8-30 Hz). Main Figure: Cue condition is indicated in blue. Place condition is indicated in red. Horizontal dashed line indicates the ($p < 0.05$) significant correlation level. Error bars indicate 1 standard deviation of random samples of the mean. Figure Inset: Isometric view of posterior right hemisphere of the head model showing the location of components 29 and 31. The region of components 29 and 31 in the head model are highlighted with a dashed ellipse.

A summary of zero-lag correlations for the interval around trial onset (-500 to 500ms) is plotted on the model cortex of Figure 11. Connecting lines on the figure indicate components having a significant difference in the level of correlation between conditions. Component pairs with zero-lag correlation having greater correlation for place trials than cue trials are: Left dorsolateral prefrontal cortex (2) and right ventral extrastriate visual cortex (7), right posterior parietal cortex(29) and right superior parietal lobule (31), left dorsal extrastriate visual cortex (25) and right posterior parietal cortex (29), left dorsal extrastriate visual cortex (25) and right superior parietal lobule (31), left posterior inferior temporal cortex (18) and right primary motor cortex (30). Component pairs with zero-lag

correlation having greater correlation for cue trials than place trials are: right ventral extrastriate visual cortex (7) and right anterior parietal cortex (22).

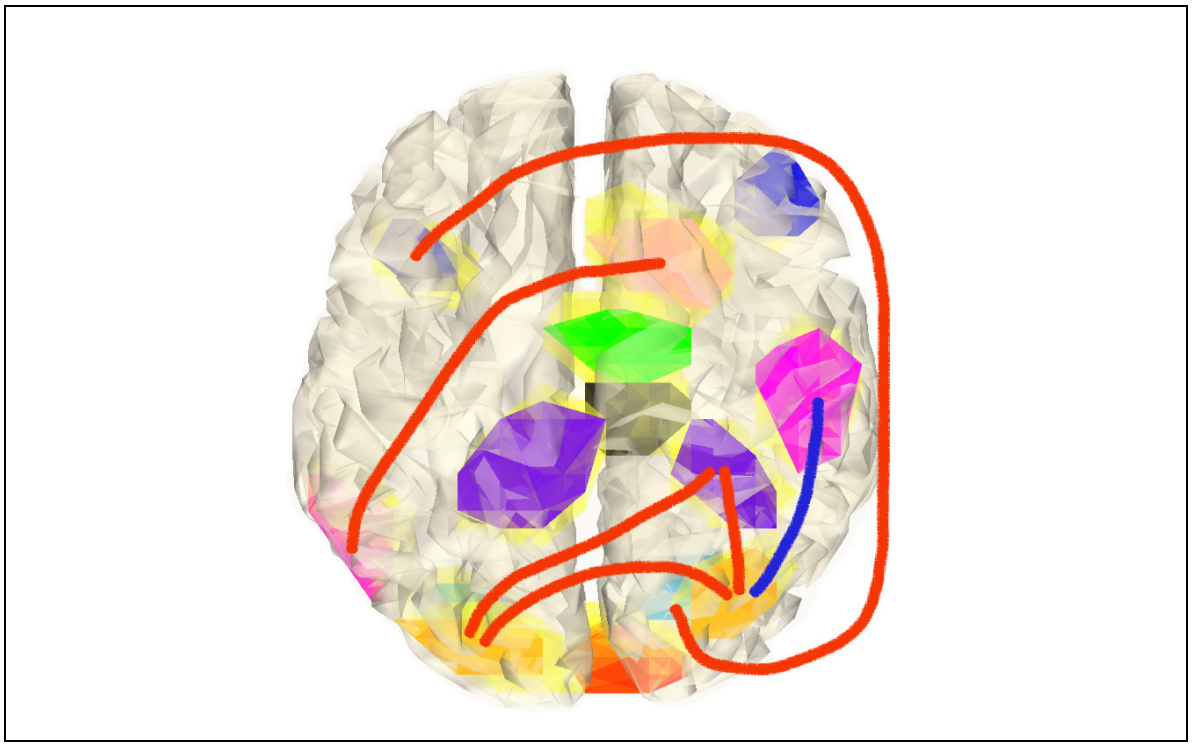

Figure 11. Coordination among brain areas measured via zero-lag correlation estimates for the interval around trial onset, -500ms to 500ms, 8-30 Hz instantaneous power. Red lines indicate component pairs having significantly greater correlation in the place condition than in the cue condition. Blue lines indicate component pairs in the cue condition with significantly greater correlation than in the place condition.

(IV) DISCUSSION

The current study has demonstrated that the MCST analysis methodology and a relatively inexpensive 32-channel EEG system can be used to describe functional brain activity associated with spatial navigation. Analysis by this methodology facilitates examination of the activities of the brain as a system comprised of multiple parts, where these parts each have a designated function in the behaviour examined. The processing methodology was used to successfully relate characteristics of scalp-EEG, collected in a

spatial navigation experiment, to specific anatomy. Comparison of the activities of specific anatomical areas of the brain with respect to behavioural conditions and in relation to each other revealed meaningful results that are congruent with prior literature using other methods. Representation of the data that the MCST methodology facilitates allows for comparison of individual brain activity characteristics of study participants to characteristics of the group. This provides a means to identify participants with specific brain activities that are dissimilar to the group. The evidence provided in this paper suggests that the MCST methodology has promise for use in analyzing EEG and brain activity in neurodiagnostic applications.

EEG data were collected while study participants navigated multiple virtual arena mazes in search of a hidden platform. The visual features of these mazes were arranged so that optimum navigation performance could be achieved using either an allocentric navigation strategy (in place mazes) or an egocentric navigation strategy (in cue mazes). The collected EEG data were separated into components using the SS-ICA (Zeman et al., 2008e) algorithm, a method of independent component analysis (ICA) that utilizes specific frequencies for source identification and separation. Components of the EEG data that were validated as originating from distinct modular areas of the brain (Zeman et al., 2008d) were used to examine brain activities associated with the paradigm. The specific origins of brain activities were estimated using a source volume estimation algorithm (Zeman et al., 2008b,c) and were depicted on a model cortex. To identify which areas of the brain were most related to each navigation strategy, the activities of brain areas were compared between the cue and place task conditions. To link estimated activities of areas of the brain to behavioural measures, two correlative relationships were examined. First examined was the relationship of brain area activation with the time required to complete trials. Second, the relationship of brain area activation with explicit knowledge of platform location was examined. Finally, to identify functional relationships among areas of the brain, pair-wise relationships between brain area activations were calculated via zero-lag cross correlation of component activities. To identify consistencies across the group, cross correlation of brain activation between component pairs was calculated across study participants, for each condition separately.

Using these relationships, maps implicating functional coordination among areas of the brain were created to compare and contrast group brain activities for the cue and place task conditions.

BRAIN AND BEHAVIOR

Source Volume Estimation

Brain volume estimations indicated that brain activities contained in the EEG originated from the superior medial parietal lobule, primary motor, posterior parietal, anterior parietal, medial anterior parietal areas of the right hemisphere, and the dorsal extrastriate visual, posterior inferior temporal cortex of the left hemisphere. Activations were also recorded from the dorsolateral prefrontal cortices, superior parietal lobules, ventral extrastriate visual cortices, and primary striate visual cortices, bilaterally. These source volume findings show what is active above the noise-level and visible in the EEG, while participants navigated in the cue and place trials indicating what brain areas were active in the paradigm. However, the source volume estimation results do not directly describe the role of each brain area in each of the paradigm conditions. An analysis of component waveform activities is required to identify relative activation differences of each brain area by condition.

These findings have an important caveat. That is, the absence of a finding of activity originating from a given brain area is not sufficient proof that the area was not active. For example, artefact in the data can easily obscure potentially visible activation of areas of the brain in the EEG. Moreover, activation of some areas of the brain is difficult to detect in the EEG due to (1) orientation of neurons in the region of interest, or (2) depth of the location within the brain. In the current study, the hippocampus was expected to be active while participants navigated the maze environment however it was not directly implicated by volume estimation results. The absence of a finding a component of the EEG that originates in the hippocampus may simply be due to its location deep within the anterior medial temporal lobes, making its activities difficult to detect in the EEG.

Fortunately, many areas of the cortex were found to be active in this navigation paradigm and interpretation can be made from activities of these areas.

The finding of distinct dorsal and ventral pathways in the current study, evident by volume estimation results, is in agreement with expectations of cortical areas active for visually-guided navigation. The dorsal pathway in the current study, known to be involved with visually guided movement and localizing objects in space (Glover 2004; Goodale, 1993), extends much farther anteriorly in the right hemisphere than in the left hemisphere indicating that right hemisphere spatial processing dominates the EEG data. Prior research using Single Photon Emission Computed Tomography (SPECT) imaging methods has linked activation of the right dorsal pathway with walking in humans. Hanakawa et al. (1999), investigating compensatory mechanisms for impaired dopamine systems relating to caudate, basal ganglia, and pedunculopontine (Pahapill and Lozano, 2000) dysfunction in persons with Parkinson's Disease (PD) found increased activation of the dorsal cortical pathway associated with visually mediated stepping across transverse lines on a treadmill. While participants in that study do not represent healthy human behaviour and brain function, the findings do present the possibility that healthy persons can, when required, use their dorsal system in relation to locomotion. To our knowledge, the current study is the first to show activation of the dorsal stream using EEG methods for navigation. It is likely that activation of the dorsal stream has not previously been demonstrated in related literature because prior research using fMRI has used a subtractive approach to data analysis. Together, the results of the current study and the study of Hanakawa et al. (1999) suggest the possibility that healthy persons participating in the vMWT, navigating a 1st-person environment, use their dorsal cortical systems for aspects of locomotion in the environment.

Activation Difference Between Conditions

The finding that significantly greater activation of the posterior parietal cortex of the right hemisphere (component 29) was present in the allocentric condition versus the egocentric condition is congruent with prior research naming the posterior parietal cortex as an

important location for processing spatial information. In a review of prior literature that brings together hippocampal research and research examining the posterior parietal cortex, Whitlock et al. (2008) suggest that the posterior parietal cortex is critical for translating coordinate information from spatial maps encoded in place cells and grid cells in the hippocampus and entorhinal cortex, respectively, into body-centered representations that can be used to direct allocentric navigation. Research examining the posterior parietal cortex typically uses non-human primate models to examine spatial stimuli, and limb and eye-movement, and how these stimuli relate to movement preparation and the movement itself. In contrast, research examining the cognitive aspects of spatial navigation and locomotion typically uses rat models, where rats are free to navigate presented mazes. The characteristics of primary research and those of rat research have not been examined together in a single experiment of human navigation.

While the current study employs spatial navigation behaviour it does so via a virtual 1st-person environment while participants are seated; thus the component of actual leg-moving locomotion is missing from the paradigm. However, there are two 'motor' activities afforded by the paradigm: movement of the right-side hand and arm while navigating using the joy-stick controller, and movement of the eyes. (Each participant's head movement was constrained by a chin-rest.) Movement of the eyes, head, and limb have been linked to activation of the posterior parietal cortex. Neurons in the posterior parietal cortex have been found to fire transiently in response to a target onset and specific movement of the eyes or limb to the target (Snyder et al., 1997; Cui and Andersen, 2007). Bastista and Andersen, (2001) and Mazzoni et al., (1996) found cells in posterior parietal cortex that fire according to properties of the next movement to be made in the task in response to a stimulus, suggesting activity of the posterior parietal cortex is important for planning of an imminent movement. The posterior parietal cortex is believed to serve as the point of interaction of spatial calculations and goal-directed movement. Hence, the motor element of locomotion that would normally be assumed by the legs in actual maze navigation is suitably provided by goal-directed movement of the eyes and limb.

While the posterior parietal cortex was more active in the place condition than in the cue condition, no areas of the brain were found to be more active in the cue condition than in the place condition. Specifically, we did not find significantly greater activation of ventral stream areas between in the cue condition than in the place condition that would be expected for object recognition and identification in the cue condition versus no object processing in the place condition. Both the cue and place conditions contained visual information in the form of a ring around the arena maze and four widows with each window providing a different perspective view of a lake and mountain scene. Visually speaking, the cue condition was unique in that it contained actual objects, identifiable by shape color and name, placed on the arena maze wall, while in the place condition. The reasons for not finding greater ventral stream activity in the cue condition are twofold. First, the place condition could use areas of the brain that are related to cue navigation and thus the ventral stream might have been active in the place condition, but was not differentially active between conditions. Object identification processes might continue to be used in the place condition even though no particular proximal objects were located in the place maze. The visual features included in the place maze intended to be used for distal allocentric navigation might have been instead utilized as cues, or 'objects' themselves: windows, a lake, and a mountain. The second reason why no ventral difference was found could be that activation of the ventral areas were not visible in the data by how we analyzed the data. A large analysis window encompassing the first second of navigation was used and it is possible that the activation of these ventral areas related to object recognition was averaged out of the data.

Latencies to Complete Trials and Explicit Knowledge

The result that some participants exhibited long trial completion latencies could be related to many factors. First, our present latency data suggest that some participants did not learn how to use the allocentric strategy in the allocentric condition, which would increase the group latency in this condition such to make the latency between conditions significantly different. The long latencies for some participants suggest that they were having difficulty finding the hidden platform and were perhaps finding the location of the

hidden platform by chance. These participants may have been still learning how to navigate the maze and might have been navigating using an idiopathic or egocentric strategy using the visual feature information (the lake and mountain scene viewed through the windows) as 'cues'. The second factor to explain the difference between egocentric and allocentric latencies could be that allocentric navigation takes longer than egocentric navigation. While this is the direct interpretation of the significant finding that latencies were longer in the allocentric condition than in the egocentric condition, given the number of participants in this study and evidence that some of them were not using allocentric navigation, the first possibility is more likely.

The result that measures of explicit knowledge using DS-probe scores showed more participants did not have explicit knowledge of the location of the platform in the allocentric condition than in the place condition supports latency findings. That is, more participants in the allocentric condition were not employing a strategy that provided them with specific, explicit knowledge of the location of the hidden platform than in the egocentric condition.

A comparison of DS-probe scores with trial completion latencies reveals a possible dissociation of explicit knowledge, and locating the platform while navigating a sequence of trials in a block. One would expect if a participant's DS-probe score is low (indicating no explicit knowledge of platform location) then latencies would be large (indicating the participant was finding the platform by chance). This however was not the case for a subset of the participants. These participants had DS-probe scores less than 1 and trial completion latencies less than 10 seconds (reaching the hidden platform by chance usually takes more than 10 seconds). This is the case for participants 3, 5, and 12 for cue trials and participants 5 and 11 for place trials. The result suggests that participants were using a strategy whereby they could efficiently navigate over the hidden platform, triggering it to appear but would navigate to the incorrect quadrant of the maze when required to align their position using visual information provided in the drop the seed task. This result suggests there might be dissociation between locating the platform in a small amount of time and the ability to explicitly identify the location of the platform.

Had this result occurred simply as a result of learning in the last trial of the block, the DS-probe scores should be consistently better than the average latencies of the last half of the block.

Activation, Latency to Reach Platform, Explicit Knowledge

Latencies to complete trials and DS-probes scores indicated that not all participants were efficient in using allocentric information to navigate mazes in the place condition. This was similarly the case for the egocentric condition however to much less a degree. Having a spread of performance scores as demonstrated by latencies in the current study allowed for some informative correlation analysis of these scores with brain activation to begin to understand the characteristics of effective and ineffective navigation. Correlative analysis of behavioural performance scores with activation of brain areas across participants demonstrated effects that show activities of ventral object recognition areas of the brain might indicate egocentric navigation in the place trials.

The result that activities of the bilateral ventral extrastriate visual cortices and the right-hemisphere dorsolateral prefrontal cortex were positively correlated with latency to complete place trials has two related interpretations. First, it might be interpreted that participants with large activation of these areas during place trials were using an egocentric strategy when an allocentric strategy would have been more effective and led to shorter trial completion latencies. The ventral stream involving the ventral extrastriate visual cortex is known to be involved with processing object properties (for example, color) for the purpose of object perception. There were however no 'objects' in the place mazes. The only relevant stimuli were windows on each of the 4 walls and the mountain and lake scene that could be viewed through the windows. It is possible that some participants used the windows and features outside the windows as cues by which to navigate through the room using an egocentric strategy and failed to, or chose not to, integrate these multiple cues into a spatial map. Unfortunately for the navigator, the individual locations of these visual features did not reveal the location of the hidden platform. Hence, reaching the hidden platform late in each trial very likely occurred by

chance for these participants. Second, this correlative relationship might also be interpreted such that inactivity of these areas in place trials was related to short latencies (and successful navigation in place trials) because participants were not using these areas to process the features of the allocentric maze as object cues. They were instead integrating them spatial information for allocentric navigation.

Relating brain activities with a behavioural measure of explicit knowledge of platform location did not reveal significant correlations, however the activities of a small number of areas approached a significant relationship with the explicit knowledge scores. Such results might become significant in a study with more participants and thus it is worth some discussion. Activities of the right dorsolateral prefrontal cortex and left ventral extrastriate visual cortex were positively correlated with DS-probe scores in the cue condition (requiring egocentric processing) indicating that activity of these areas might have a relation to a navigator's explicit knowledge of platform location. The relationship with the left ventral extrastriate visual cortex suggests a link between explicit knowledge of platform location and object processing. The relationship with the right dorsolateral prefrontal cortex suggests a link between this explicit knowledge and executive function relating to motor planning. Activities of the dorsolateral prefrontal cortex have been linked to working memory. In contrast, activities of the posterior parietal cortex were negatively correlated with DS-probe scores in the cue condition suggesting that activation of this area is related to navigators not being able to indicate the correct location of the cue condition platform when asked. This is in agreement with our previous finding that the posterior parietal cortex is more active in the place condition than in the cue condition and our conclusion that in this task it was used for allocentric navigation in the place condition. In the place condition (requiring allocentric processing) activation of the right anterior parietal cortex was found to be positively correlated with DS-probe scores suggesting activation of this area relates to explicit knowledge of platform location. Prior research has demonstrated that anterior areas of the parietal cortex are involved with eye movement and somatosensory processing (Balslev and Miall, 2008).

Activation Relationships (Across Participants)

Consistency of activation relationships of brain areas calculated across study participants show that consistent brain activation relationships were found primarily in left hemisphere areas of the brain for cue trials. Specifically, relationships were found in the left temporal and occipital regions of the cortex. In contrast, relationships between brain areas for place trials were in right hemisphere in parietal regions of the cortex. These results indicate relatively consistent co-activation of primary striate visual and left hemisphere object perception processing areas across the group that is most present in the cue condition.

The lack of relationship between activation of the primary striate visual cortex and right-hemisphere parietal region activities suggests use of the right hemisphere dorsal and ventral pathways (believed to be used for object localization and object recognition, respectively) indicates that use of those pathways was inconsistent across the participant group. This was the case for both the cue and place conditions. RMS activation results however demonstrated the posterior parietal cortex was active in the allocentric condition suggesting that it was being used for navigation in the place task. Effective use of the posterior parietal cortex however necessitates that it receives some form of sensory (in this case visual) information. It is possible that the subcortical pathway from the retina to the superior colliculus, pulvinar to the posterior parietal cortex provided the posterior parietal cortex with this visual information in some participants. Use of this pathway in place trials relates to non-conscious use of visual information for spatial processing. Use of this pathway is consistent with our hypothesis of dissociation between explicit knowledge of platform location and the ability to find the platform in short trial latencies.

Scatter plots illustrating the pair-wise relationships of brain area activations revealed one study participant (#7) as a possible outlier based on unusual activity in what was modeled as their ventral visual processing streams. The possibility that this participant's visual processing physiology might be different from the group was supported by our behavioural data and our lab notes. Behavioural latency measures showed this

participant was the slowest member of the group for place trials suggesting poor allocentric navigation. Moreover, DS-probe scores indicated this participant did not have explicit knowledge of the correct location of the platform. The most interesting information was from our lab notes which indicated that this participant has a large esotropia of the right eye which is known to result in poor retinal correspondence between the left and right eyes. This changes how visual information can be processed because, visual information received by the problem eye is suppressed when detail processing of visual stimuli is behaviourally important.

Discussion of participant #7 as an outlier in the present work is given primarily as an example to illustrate how the MCST methodology can be used to identify atypical brain activities. Given there are only 12 participants, analysis of outliers for this dataset of this size is not recommended and our analysis in this instance should be taken in context; the true distribution of samples is not clearly evident by the small sample size. This said, the data of this study suggest that outlier analysis on a larger sample is feasible and outliers could be (1) removed to better characterize the group data, and (2) studied to better understand what characteristics of their brain function and behaviour make them outliers such as lateralization of spatial function and brain pathology.

Activation Relationships (Zero-Lag Correlation)

Pair-wise relationships as determined by zero-lag correlations should provide stronger evidence towards functional links among brain areas than the measure of consistency across participants. The pair-wise relations calculated across participants implicitly include variables other than brain area co-activation such as between-subject differences in brain activation amplitudes. In contrast, zero-lag correlations provide a measure of coordination among brain areas that is independent of between-subject amplitude differences.

Results show a greater number of component pairs with significantly greater zero-lag correlation in the place condition than the cue condition suggesting more areas of the

brain are coordinated for allocentric navigation than for egocentric navigation. Our expectation is that these differences would be more profound had more participants successfully navigated allocentrically in the place condition. Measured correlation and coordination could be caused via multiple mechanisms. The first and simplest case is that coordination results could be indicative of information transported via direct pathways between cortical areas. Second, an unknown brain area could send information to multiple brain areas in parallel causing those areas to be active together (or modulated together), even if no actual direct connection between them exists. This could occur via changes in neuromodulator projections to multiple areas of the cortex or could be directly related to gating of cortical projections from subcortical areas via the thalamus. Finally, multiple areas that are not necessarily connected to each other but do receive the same or related inputs might have correlated activities. For example, auditory stimulus presented at both ears would generate correlated activities in bilateral auditory areas. Similarly would be the case for input to the visual system. In this case, multiple brain areas process the same (or similar) stimulus input at the same time.

General Discussion of Spatial Navigation

The results of this investigation have revealed some topics for further debate, discussion, and future investigation. Failure to utilize allocentric information to find the platform location in place trials does not necessarily mean that the allocentric system was not active. It is plausible that brain areas that process allocentric visual information were active and acquiring allocentric information unconsciously while navigators moved about the maze; even when they chose to navigate using an idiosyncratic or egocentric strategy. When an environment is new, the navigator is required to build an spatial map while using a non-allocentric strategy to navigate the environment. Eventually, when allocentric relationships become conscious, allocentric navigation becomes an available conscious strategy. For a participant to 'spontaneously' identify relationships among stimuli, there must be some processing that occurs without the participants explicit effort. This suggests that the allocentric system acquires allocentric relationships in parallel with non-allocentric navigation systems.

It was also described that some participants might have navigated by unconsciously employing an allocentric strategy indicating that use of a strategy does not have to be conscious. This is supported by our inferences that (1) there might be a dissociation between the ability to quickly navigate to the location of the hidden platform in regular place trials and explicit knowledge of platform location and (2) subcortical pathways were used by some participants to provide visual information to areas of the brain important for spatial navigation directly, bypassing the primary striate visual cortex.

BEHAVIOURAL AND NEURODIAGNOSTIC APPLICATIONS

A number of characteristics of brain function were revealed by the methodology that could be used to identify successful and unsuccessful use of the allocentric navigation strategy. In animal studies, unsuccessful allocentric navigation has been related to injuries of the hippocampal system. Our prior research investigating traumatic brain injury using the vMWT paradigm has provided evidence that in persons with TBI demonstrate large trial completion latencies in the allocentric condition while there is no difference in the egocentric condition compared to controls (Livingstone and Skelton, 2007). However, we have not been able to implicate specific structures of the brain that are dysfunctional or alternatively, participate in mechanisms of compensation. The results of the current feasibility study indicate that the MCST methodology in conjunction with the vMWT could be used to implicate specific brain structures. Our future work will compare how the brain activities of persons with navigational deficits relating to brain injury differ from the activities of a healthy control population.

MEETING TECHNICAL CHALLENGES

Some important challenges were overcome in achieving the analysis of brain activity provided in this study. Foremost was that it was demonstrated that data collected from this paradigm, using an inexpensive 32-channel EEG machine, yielded meaningful results. Extra analysis provided in Appendix B indicates that the MCST methodology

performed as expected; the data mining algorithm, volume-domain validation algorithm, and the volume estimation algorithm all performed similarly as in our prior investigations (Zeman et al., 2008a, 2008c, 2008e). The data mining algorithm yielded components with volumes that could be related to specific brain anatomy. Evaluation of these components by their frequency spectra indicated the volume-domain validation algorithm was successful in identifying good brain-activity related components from poor ones. Moreover, the volume estimates were found to implicate activities in areas of the brain that are meaningful for the spatial navigation paradigm.

CAVEATS AND NOTES

In some cases it was difficult to determine by visual inspection the precise brain atlas-referenced location of each component. This is a drawback of using a canonical cortex that does not fit the data exactly. Hence, only approximate locations were named. In addition, component volumes appear blurred in some cases. This occurred for two reasons. First, application of data mining to calculated spatial separation filters using group data (where each study participant has small anatomical variations from the canonical representation) leads to spatial separation filters that pertain wider regions of the cortex than one would expect if they were trained from the data of a single participant. Second, a low-density electrode array was used to collect these data and thus there is some blurring of location expected due to the low-density spatial sampling it provides. However, even given these characteristics, the volume estimation algorithm has provided results that are very supportive in linking specific brain anatomy to the brain activities extracted from the EEG.

RECOMMENDATIONS FOR FUTURE STUDIES

Future studies employing this paradigm and analysis methodology should use a greater number of electrodes for EEG data collection. In the current study we demonstrated that the MCST methodology can be successfully used to analyze the EEG of spatial navigation using 32 channels; however there is little room for artefact in the data.

Considering there were 32 channels (31 degrees of freedom) 14 good brain components and 17 artefacts, the artefact/channel ratio was approximately 0.5. Should there have been a larger number of artefacts in these data, the results obtained in the current study would not have been so clear. A larger study with a greater number of participants is expected to have a greater ratio of artefacts/channels. Moreover, a larger study is expected to have a greater number of brain sources related to various spatial processing lateralization schemes or idiosyncratic differences that might be strongly represented in the data.

In the current study it is not clear if it is movement of the eyes or movement of the limb that relates to activity of the posterior parietal cortex. Future work should examine the time activities of the posterior parietal cortex in relation to movement of the eyes and limb to reveal the motor relation to posterior parietal cortex activation in this paradigm.

Outliers in future analysis should be excluded when constructing models or participant results should be arranged in multiple clusters to separate differing activities and strategies. Presumably, future studies will use a larger pool of participants from which to collect EEG data allowing for outlier removal. Participants could also be clustered or classified according to their performance scores to generate a set of multiple brain activity models that can be compared and contrasted. By bringing analysis to this level of detail, our knowledge of lateralization of brain function and use of idiosyncratic navigation strategies may be improved.

Acknowledgements:
Funding for this study was provided in part by the Natural Sciences and Engineering Research Council of Canada, CanAssist, and the University of Victoria. Thanks also to Robert Sutherland and Patricia Sorensen at the Canadian Centre for Behavioural Neuroscience for providing data for the development of the MCST methodology, and thus, making the current feasibility study possible. Finally, thanks to Sunny Mahajan for his help in developing the MCST analysis methodology.

(V) CONCLUSIONS

The analysis presented in the current study indicates that it is possible to study the brain activity associated with navigation of virtual space using 32 channels of scalp EEG and the MCST analysis method. This study also demonstrated that the MCST methodology can be used to construct a meaningful model of brain function that differentiates allocentric and egocentric navigational cognitions. That is, the EEG data can be related to specific anatomy and the activities of the specific anatomy can be compared between conditions and in relation to each other facilitating system-level analysis of the brain function. Because of these characteristics, the MCST methodology shows promise as a tool for investigations of functional neuroanatomy. Moreover, because this methodology can be used to compare the brain activities of participants in terms of the activation of specific areas of the brain and the coordination among areas of the brain, this methodology is suitable for making comparisons between individual persons in neurodiagnostic applications.

(VI) REFERENCES

Andersen RA, Buneo CA. Intentional maps in posterior parietal cortex. Annu Rev Neuroscience 2002;25:189-220.

Anderson RA, Essick GK, Siegel RM. Neurons of area-7 activated by both visual-stimulated and occulomotor behaviour. Experimental Brain Research 1987;67:316-322.

Astur R, Ortiz ML, Sutherland RJ. A characterization of performance by men and women in a virtual Morris water task: A large and reliable sex difference. Behavioural Brain Research 1998;93(1-2): 185-190.

Astur R, Taylor LB, Mamelak AN, Philpott L, Sutherland RJ. Humans with hippocampus damage display severe spatial memory impairments in a virtual Morris water task. Behavioural Brain Research 2002;132(1):77-84.

Baillet S, Mosher JC, Leahy R. BrainStorm beta release: a Matlab software package for MEG signal processing and source localization and visualization. Proceedings of the 16th Annual Meeting of the Organization for Human Brain Mapping, San Antonio, Texas, 2000.

Balslev D, Miall RC. Eye Position Representation in Human Anterior Parietal Cortex. The Journal of Neuroscience 2008; 28(36):8968-8972.

Bastista Ap, Andersen RA. The parietal reach region codes the next planned movement in a sequential reach task. Journal of Neurophysiology 2001;85:539-544.

Bohbot V, Iaria G, Petrides M. Hippocampal Function and Spatial Memory: Evidence From Functional Neuroimaging in Healthy Participants and Performance of Patients With Medial Temporal Lobe Resections. Neuropsychology 2004;18(3):418-425.

Bohbot VD, Lerch F, Thorndycraft B, Iaria G, Zijdenbos AP. Gray Matter Differences Correlate with Spontaneous Strategies in a Human Virtual Navigation Task. The Journal of Neuroscience 2007;27(38):10078-10083.

Brandeis R, Brandys Y, Yehuda S. The use of the Morris Water Maze in the study of memory and learning. International Journal of Neuroscience; 1989;48: 29-69.

Burgess N. Spatial Cognition and the brain. In: Year in Cognitive Neuroscience 2008 (vol. 1124, pp.77-97). Oxford: Blackwell Publishing.

Cantero JL, Atienza M, Stickgold R, Kahana MJ, Madsen JF, Kocsis B. Sleep-Dependent Oscillations in the Human Hippocampus and Neocortex. The Journal of Neuroscience 2003;23(34):10897-10903.

Cui H, Andersen RA. Posterior parietal cortex encodes autonomously selected motor plans. Neuron 2007;56:552-559.

Danckert J, Revol P, Pisella L, Krolak-Salmon P, Vighetto A, Goodale MA, Rossetti Y. Measuring unconscious actions in action-blindsight: exploring the kinematics of pointing movements to targets in the blind field of two patients with cortical hemianopia. Neuropsychologia 2003; 41:1068-1081.

Delorme A, Makeig S. EEGLAB: an open source toolbox for analysis of single-trial EEG dynamics including independent component analysis. J. Neuroscience Methods 2004;134:9-21.

D'Hooge R, De Deyn PP. Applications of the Morris water maze in the study of learning and memory. Brain Research Reviews 2001;36:60-90.

DiMattia BD, Kesner RP. Spatial cognitive maps: Differential role of the parietal cortex and hippocampal formation. Behav Neuroscience 1988;102:471-480.

Farah M. Visual Agnosia: Disorders of object recognition and what they tell us about normal vision 1990. (The MIT Press, Cambridge, MA).

Fyhn M, Molden S, Witter MP, Moser EI, Moser MB. Spatial representation in the entorhinal cortex. Science 2004;305:1258-1264.

Glover S. Separate visual representations in the planning and control of action. Behavioural and Brain Sciences 2004;27:3-78.

Goodale M. Visual pathways supporting perception and action in the primate cerebral cortex. Current Opinion in Neurobiology 1993;3:578-585.

Grave de Peralta Menendez R, Andino SG, Lantz G, Michel CM, Landis T. Noninvasive Localization of Electromagnetic Epileptic Activity. I. Method Descriptions and Simulations. Brain Topography 2001;14(2):131-137.

Hamilton DA, Kodituwakku P, Sutherland RJ, Savage DD. Children with Fetal Alcohol Syndrome are impaired at place learning but not cued-navigation in a virtual Morris water task. Behavioural Brain Research 2003;143:85-94.

Hanakawa T, Fukuyama H, Katsumi Y, Honda M, Shibasaki H. Enhanced Lateral Premotor Activity During Paradoxical Gait in Parkinson's Disease 1999;45:329-336.

Hartley T, Maguire EA, Spiers HJ, Burgess N. The Well-Worn Route and the Path Less Traveled: Distinct Neural Bases of Route Following and Wayfinding in Humans. Neuron 2003;37(5): 877-888.

Hesterberg T, Monaghan S, Moore DS, Clipson A, Epstein R. Bootstrap Methods and Permutation Tests. W.H. Freeman, N.Y. Library of Congress: 2002108463, RR Donnelley & Sons Company, 2003.

Husain M, Nachev P. Space and the parietal cortex. Trends in Cognitive Science 2007;11:30-36.

Iaria G, Petrides M, Dagher A, Pike B, Bohbot VD. Cognitive strategies dependent on the hippocampus and caudate nucleus in human navigation: variability and change with practice. The Journal of Neuroscience 2003; 23(13):5945-5952.

Kallai J, Makany T, Karadi K, Jocobs WJ. Spatial orientation strategies in Morris-type virtual water task for humans. Behavioural Brain Research 2005;159(2):187-196.

Kolb B, Sutherland RJ, Whishaw IQ. A comparison of the contributions of the frontal and parietal association cortex to spatial localization in rats. Behav Neuroscience 1983;97:13-27.

Kolb B, Walkey J. Behavioural and anatomical studies of the posterior parietal cortex in the rat. Behav Brain Research 1987;23:127-145.

Livingstone S, Skelton R. Virtual environment navigation tasks and the assessment of cognitive deficits in individuals with brain injury. Behavioural Brain Research 2007;185(1):21-31.

Makeig S, Jung TP, Ghahremani D, Bell AJ, Sejnowski TJ. Blind separation of auditory event-related brain responses into independent components. Proc Natl Acad Sci USA 1997;94:10979-10984.

Masson EJM, Loftus GR. Using Confidence Intervals for Graphically Based Data Interpretation. Canadian Journal of Experimental Psychology 2003;57(3):203-220.

Mazzoni P, Bracewell RM, Barash S, Andersen RA. Motor intention activity in the Macaque's lateral intraparietal area. 1. Dissociation of motor plan from sensory memory. Journal of Neurophysiology 1996;76:1439-1456.

Michel CM, Murray, MM, Lantz, G, Gonzalez S, Spinelli L, de Peralta, RG. EEG source imaging. Clinical Neurophysiology 2004;115:2195-2222.

Moffat R, Garrud P, Rawlins JN, O'Keefe J. Place navigation impaired in rats with hippocampal lesions. Nature 1982;297(5868):681-683.

Morris R. Spatial localization does not require the presence of local cues. Learning and Motivation 1981; 12:239-260.

Morris R, Garrud P, Rawlins JN, O'Keefe J. Place navigation impaired in rats with hippocampal lesions. Nature 1982;297(5868): 681-683.

Nadel L. The hippocampus and space revisited. Hippocampus 1991;1:221-229.

Nadel L, Hardt, O. The Spatial Brain. Neuropsychology 2004;18(3): 473-476.

Nitz DA. Tracking route progression in the posterior parietal cortex. Neuron 2006;49:747-756.

Ojemann,G Ojemann J., Lettich E., Burger M. Cortical language organization in left, dominant hemisphere. Journal of Neurosurgery 1989; 71: 316-326.

O'Keefe J, Dostrovsky J. The hippocampus as a spatial map: Preliminary evidence from unit activity in the freely-moving rat. Brain Research 1971;34:171-175.

O'Keefe J, Nadel L. The hippocampus as a cognitive map 1978; Oxford: Oxford University Press

Pahapill PA, Lozano AM. The pedunculopontine nucleus and Parkinson's disease. Brain 2000;123:1776-1783.

Rasmussen T, Milner B. The role of early left brain injury in determining lateralization of cerebral speech function, Annals of the New York Academy of Sciences 1997;299:355-369.

Ross, S, Skelton, R, Mueller, S. Gender differences in spatial navigation in virtual space: Implications when using virtual environments in instruction and assessment. 2006.

Sandstrom NJ, Kaufman, J, Huettel SA. Males and females use different distal cues in a virtual environment navigation task. Cognitive Brain Research 1998;6(4):351-360.

Snyder LH, Bastista AP, Andersen RA. Coding of intention in the posterior parietal cortex. Nature 1997;386:167-170.

Snyder LH, Grieve KL, Brotchie P, Andersen RA. Separate body- and world-referenced representations of visual space in parietal cortex. Nature 1998;394:887-891.

Taira M, Mine S, Georgopoulos AP, Murata A, Sakata H. Parietal cortex neurons of the monkey related to the visual guidance of hand movement. Experimental Brain Research 1990;83:29-36.

Tolman EC. Cognitive maps in rats and men. Psychological Review 1948;55:189-208.

Ungerleider LG, Mishkin M. Two cortical visual systems. Analysis of Visual Behavior 1982, Eds: Ingle DJ, Goodale MA, Mansfield RJW (The MIT Press, Cambridge, MA), pp 549-586.

White NM, McDonald RJ. Multiple Parallel Memory Systems in the Brain of the Rat. Neurobiology of Learning and Memory 2002;77(2):125-184.

Whitlock JR, Sutherland RJ, Witter MP, Moser MB, Moser EI. Navigating from hippocampus to parietal cortex. PNAS 2008;105(39):14755-14762.

Yao D. A method to standardize a reference of scalp EEG recordings to a point at infinity. Physiological Measurement 2001;22:693-711.

Zeman PM, Mahajan SV, Livingstone SA, Driessen PF, Skelton RW, Livingston NJ. Beamform Volume Projection of EEG ICA Topographies. (for publication) 2008b.

Zeman PM, Mahajan SV, Sorensen PL, Driessen PF, Skelton RW, Livingston NJ. Beamform Volume Projection of ICA Components of Scalp EEG: Volume-Domain Uniqueness of Components. (for publication) 2007c.

Zeman PM, Mahajan SV, Livingstone SA, Driessen PF, Skelton RW, Livingston NJ. Volume Domain Validation of ICA-Derived EEG Sources. (for publication) 2008d.

Zeman PM, Mahajan SV, Livingstone SA, Livingston NJ, Skelton RW. Spectral Shaping to Relax ICA Assumptions to Facilitate Decomposition of EEG. (for publication). 2008e.

Zeman PM, Livingstone SA, Livingston NJ, Skelton RW. Building a Multi-Component Spatio-Temporal Model Using Scalp-EEG Data. (for publication) 2008f.

APPENDIX A – EXTENDED DESCRIPTION OF THE EEG PARADIGM

The current appendix provides supplemental materials describing the spatial navigation task and paradigm used in the current study.

Screen captures of the 1st-person perspective view of the maze have been provided in Figure A1 illustrating differences between the place and cue mazes. In the place condition, no objects are present in the arena maze and navigation can only be guided using the distal features of the environment outside the room viewed through four windows on each of four arena maze walls. The configural information provided by these multiple features can be used to identify the correct location of the hidden platform located on the floor of the arena maze. The location of the hidden platform remains constant in each of the place trials; the starting location of the navigator is randomized in each trial. The allocentric information in the place trials has been made as realistic as possible; as the participant navigates within the arena maze, the perspective of the features of the environment change with respect to the boarders of the windows of the maze. In the cue condition, objects and distal features are present and are available to guide navigation. However, only the object information provides the correct location of the hidden platform. For each of the 10 trials in the cue condition, the location of the hidden platform remains constant with respect to a single object in the maze (the golden urn). This object and the platform are moved to a different position in the room in each trial so that the distal information in the room does not provide the location of the hidden platform.

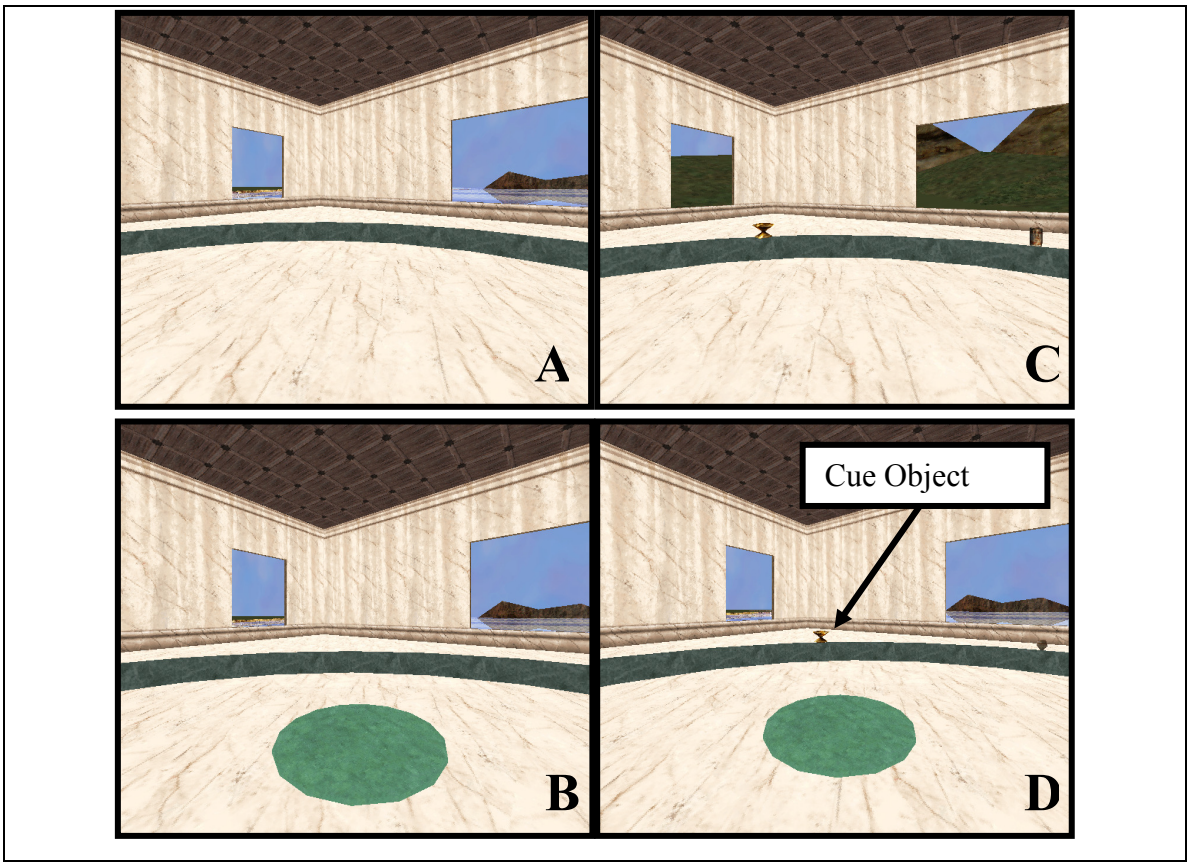

Figure A1. First person perspective views of the cue and place arena mazes showing platform locations (here, the platforms are visible) and available features inside and outside of the maze by which to navigate. **(A)** the maze used for place trials where only distal features are available for navigation. **(B)** the location of the platform for all trials during place trials. The platform is invisible until the participant's avatar steps on it. **(C)** the environment for cue trials showing objects perched proximally on the maze ring wall. **(D)** the location of the platform with respect to the object (golden urn) marking the location of the (hidden) platform. Both the platform and the object (golden urn) together, change places for each trial of the cue maze making the distal features of the maze irrelevant to locating the platform.

APPENDIX B – DETAILED METHODS

This appendix provides supplemental materials describing results related to the data mining and validation methods used in the current study. In addition, volume estimation plots of those components that failed the validation process are provided for inspection.

DATA MINING

The Spectral Shaping ICA (SS-ICA) data mining algorithm was used to identify the independent activities of the brain present in the scalp EEG data collected from participants while they navigated a virtual arena maze environment. The SS-ICA algorithm mines the EEG data via three main steps. First, the algorithm identifies a frequency shaping filter that maximizes the frequencies of independence in the EEG data. Second, EEG data shaped by the filter, (emphasizing frequencies of independence) are used to calculate spatial separation matrices. These spatial separation matrices are then used in the third step to separate the original unshaped EEG data into parts. The details of this process are described by Zeman et al. (2008e).

The magnitude spectrum of the shaping filter calculated as the second step in the data mining algorithm is given in Figure B1. The peaks of the magnitude spectrum of this shaping filter indicate that the frequencies of greatest independence are those around 70 Hz and also those in the interval 25 to 45 Hz. The frequencies of least independence are indicated by drops in the magnitude spectrum for the intervals 34 to 64 Hz and for frequencies less than 25 Hz. These results are in agreement with our prior work using a different EEG dataset acquired using a different spatial navigation paradigm (Zeman et al., 2008e). For those data, the a frequency band around 70 Hz was also emphasized, as was the a frequency band of 27 to 42 Hz indicating that these are the frequencies of greatest independence. Similarly as in the current study, those frequencies below 27 Hz were de-emphasized indicating that activities with frequencies below 27 Hz have the least independence.

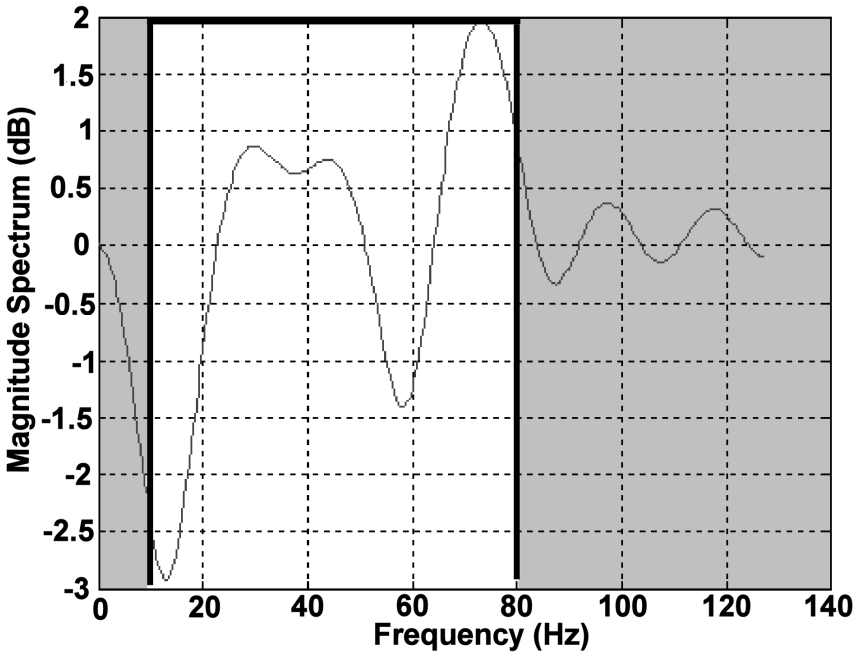

Figure B1. Magnitude spectrum of the shaping filter calculated during the data mining procedure. Peaks in the magnitude spectrum indicate which frequencies were found to have the greatest independence. The frequencies relevant to filter shaping are inside the frequency window of the band-pass filter, 8 to 80 Hz used to prepare the EEG data prior to data mining. This band-pass filter is represented in the figure as a shaded region representing an idealized 'brick-wall filter'.

Topographies of the 31 components of EEG data calculated by the data mining algorithm are illustrated in Figure B2. Visual inspection of these topographies does not provide clear discrimination between which of these might be good brain activity estimates and which of these are artefacts. The quality is ambiguous because many of the component topographical foci are at single electrodes; when a high density electrode array is used, good brain activity components usually have topographies with foci that span multiple electrodes.

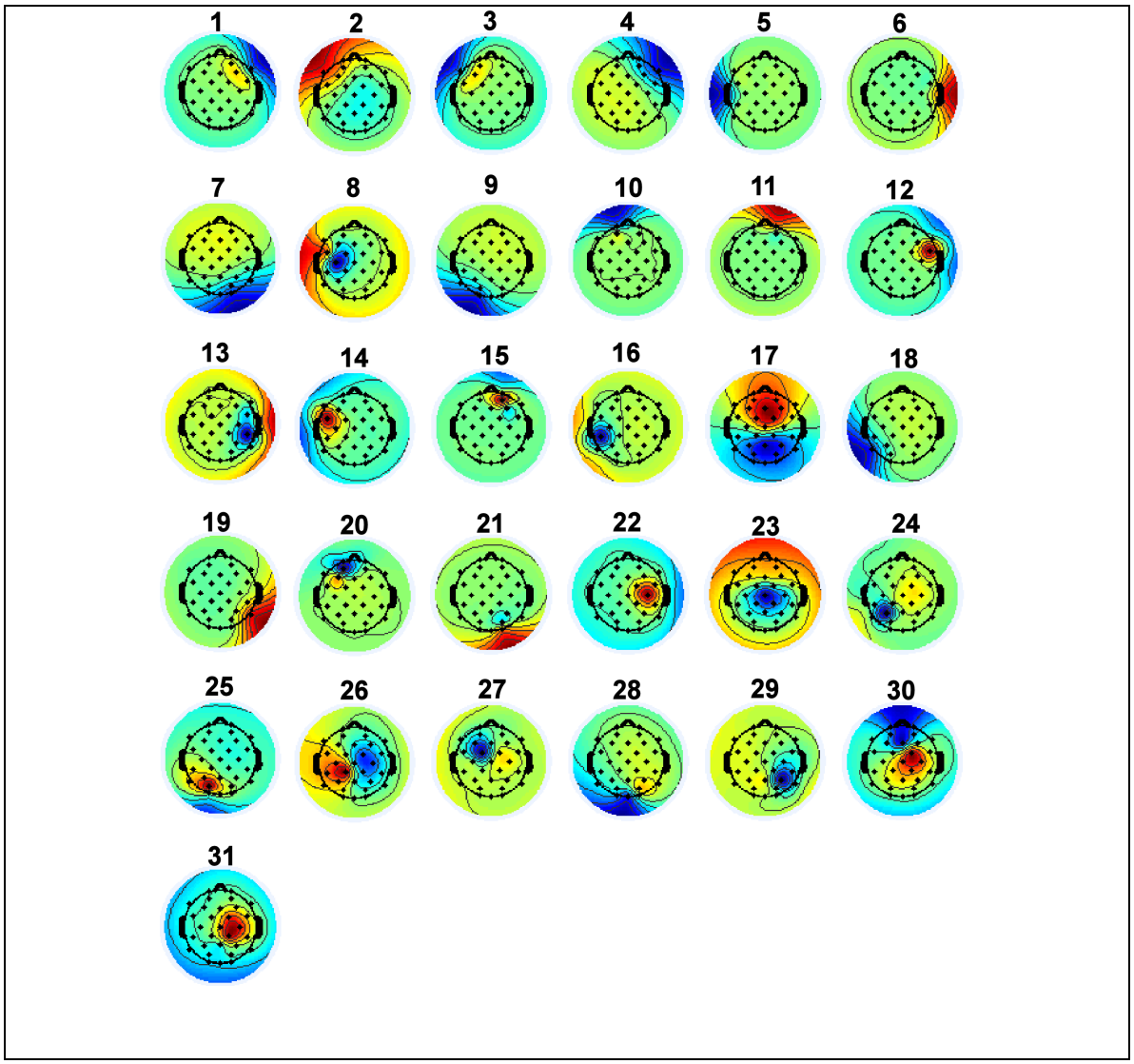

Figure B2. Topographies calculated by the data mining algorithm. Areas of focal intensity are indicated by either blue (negative) or red (positive) foci, transitioning through green (neutral). The mathematical sign (negative/positive) of these foci however are inconsequential because the topography of the component must be multiplied by the sign of the components waveform at each moment in time to determine the actual scalp polarity at a given moment in time. Dark points marked on the scalp topographies indicate the location of scalp electrodes.

VALIDATION

The validation curves used to determine which components of the decomposition likely pertain to artefacts or are poorly separated brain activities that were not suitable for analysis are given in Figure B3. Figure B3-A illustrates the sorted PSV scores and Figure B3-B depicts the sorted MVO scores. The knee of each of these curves was used to determine two thresholds. The first threshold separated possible brain activity components from those that may or may not be components that provide good representations of brain activities of specific locations of the brain. The second threshold separated those components that may or may not be good components from those with the lowest ranking and are very likely artefacts. These thresholds are indicated in the figure by horizontal lines.

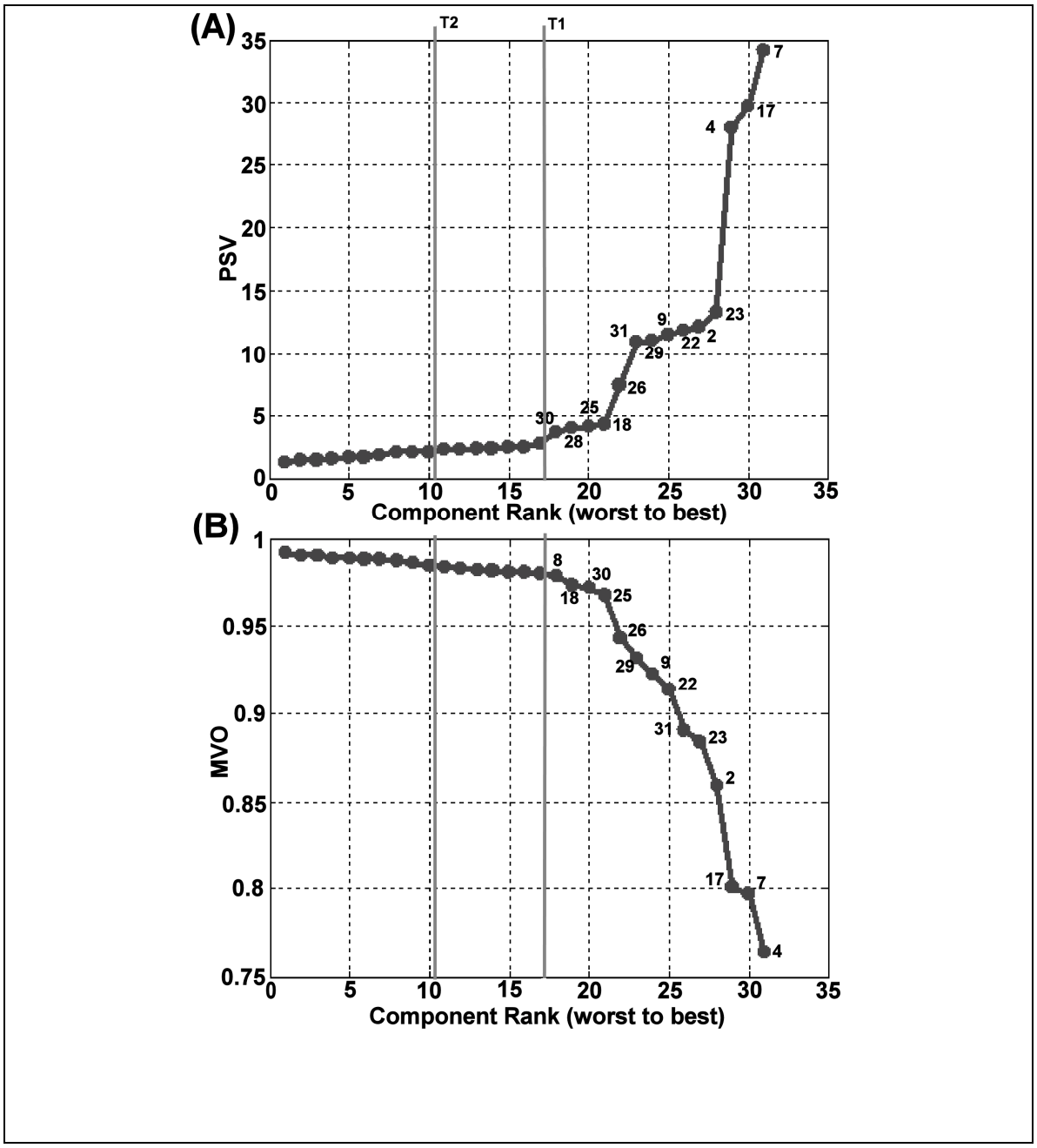

Figure B3. Validation curves for the volume-domain validation algorithm. (A) Sorted Peak Spectral Values (PSVs) of components. (B) Sorted Median Volume Overlap (MVO) of components. The threshold labelled T1 separates the good components from these that may or may not be good components. The threshold labelled T2 separates those components ranked as artefacts from those that that may or may not be good components.

The sorted PSV and MVO scores illustrated in Figure B3 have been tabulated for inspection in Table B1. Component 28 was scored by the MVO ranking as 17th while the PSV scoring method ranked it as 13th meaning that the overlap is non-idea but still has a reasonably good voxel specificity. Our prior work has shown that the component relating to the primary visual cortices typically has greater overlap than other components (Zeman et al., 2008e; Zeman et al., 2008f). We believe this occurred for two main reasons. First, the low density of the scalp electrodes very likely contributed to blurred component volume estimates. Second, the primary striate visual cortices are anatomically folded beneath secondary visual cortices and thus variability of the anatomy of the occipital lobe in humans when components are computed as a group 'average' will lead to overlaps in the group spatial mappings. For these reasons, we have retained component 28 for use in the model.

PSV	**MVO**
7	4
17	7
4	17
23	2
2	23
22	31
9	22
29	9
31	29
26	26
18	25
25	30
28 *	18
30	*8*
19	*19*
16	*1*
3	28 *
8	*3*
27	*13*
1	*27*
24	*14*
11	*16*
13	*24*
14	*11*
10	*6*
6	*10*
20	*20*
12	*12*
21	*5*
5	*15*
15	*21*

Table B1. Ranking of components by PSV and MVO scores, sorted in descending order from best score to worst score. The PSV score ranking of components is not exactly the same as the MVO score ranking because the PSV and MVO measure different component properties. Those components that score high by both measures are considered possible distinct modular brain activity sources. Those components that were identified as weak or as artefacts are given in italics. Component 28 (marked by *) was localized and found to pertain to the primary visual cortex. Our prior studies have demonstrated that the component that represents the primary visual cortex usually has a large overlap with adjacent volumes (Zeman et al., 2008e; Zeman et al., 2008f).

Component validation by the volume-domain validation algorithm was compared to ‘expert’ evaluation of components according to their frequency spectra. This ‘expert

evaluation', which was done to provide more confidence in the volume validation methods, involved visual inspection of component waveform frequency spectra and comparison of these spectra to typical brain activity frequency characteristics. The results of this comparison are given in Table B2. While validation can be done via inspection of the frequency content of component waveforms, validation by the volume-domain characteristics is generally preferred over validation by frequency content. Validation of components by inspection of frequency characteristics is not generally recommended as the soul means of validation for two reasons. First, evaluation by frequency spectra is somewhat subjective even following expert opinion. Second, it does not provide an evaluation of how well spatially distinct brain sources have been separated and it does not indicate how well they represent the activities of distinct modular areas of the brain.

Comp #	Expert Score	PSV and MVO Score
7	brain	brain
17	brain	brain
4	uncertain	brain
23	brain	brain
2	uncertain	brain
22	uncertain	brain
9	brain	brain
29	brain	brain
31	brain	brain
26	uncertain	brain
18	brain	brain
25	brain	brain
28	brain	brain
30	brain	brain
19	brain	uncertain
16	artefact	uncertain
3	artefact	uncertain
8	artefact	uncertain
27	artefact	uncertain
1	artefact	uncertain
24	brain	uncertain
11	uncertain	artefact
13	uncertain	artefact
14	artefact	artefact
10	uncertain	artefact
6	artefact	artefact
20	uncertain	artefact
12	uncertain	artefact
21	artefact	artefact
5	artefact	artefact
15	uncertain	artefact

Table B2. Comparison of automated classification by the volume-domain validation algorithm and 'expert' classification components by the shape of the frequency spectrum. Components have been sorted in descending order of goodness as determined by PSV scores. Components have been classified by an expert and by the validation algorithm as either 'brain' indicating they are a good estimate of brain activity, 'artefact' indicating the component is an artefact, or as 'uncertain' indicating the appropriate classification was not clear to the expert or that for the component was at the threshold of artefact and brain activity for the automated validation algorithm.

VOLUME ESTIMATION

Plots of volume localization and estimation of those components that were classified by the volume-domain algorithm as 'uncertain' are given in Figure B4. Those that were classified as artefact are given in Figure B5. These have been provided so that comparisons can be made between the weak components and artefact components found in this study between components calculated in futures studies using this paradigm and analysis method. Such comparisons can serve to better understand the all of the contributors to the EEG.

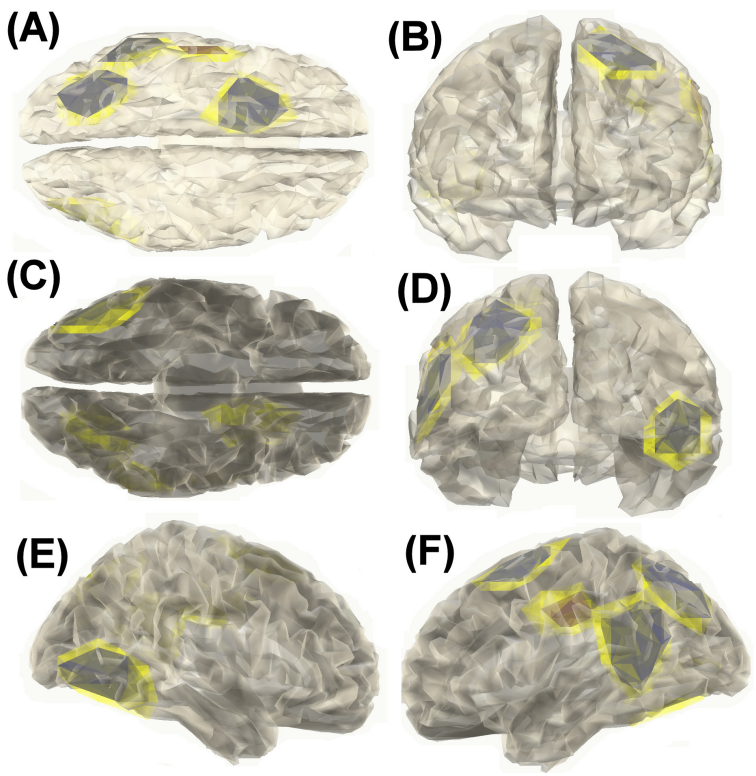

Figure B4. Volume localization and estimation for weak or 'uncertain' brain source components identified from the scalp EEG data. The volumes of components estimated for thresholds of 5 STDM have been plotted in grey. To illustrate roll-off of the volumetric spectrum coefficients that define the volume, volumes have also been plotted in yellow for a threshold of 4 STDM.

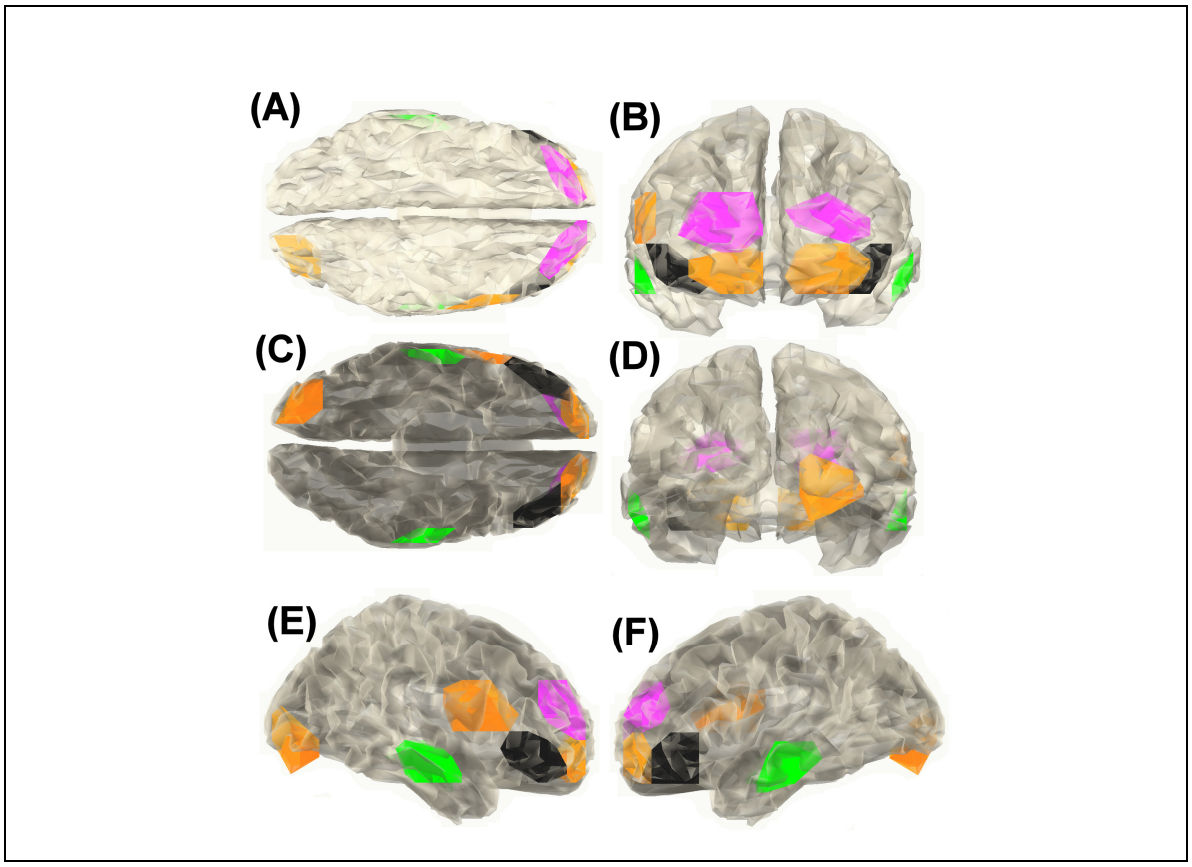

Figure B5. Volume localization and estimation for artefact or brain source components identified from the scalp EEG data. The volumes of components estimated for thresholds of 5 STDM have been plotted in various colors.

Section VI: Discussion and Conclusions

The current section provides a discussion of the collective results of studies presented in each of the previous sections of this dissertation. These results are reviewed to show how the primary research question has been investigated through a logical progression of results and findings. The current section also provides discussion of how the research described in this dissertation fits within the larger context of clinical application of EEG data to examine brain activity. Following these remarks is a statement of general conclusions.

Chapter 9: General Discussion and Conclusions

DISCUSSION

The research described in this dissertation has examined the feasibility of using scalp-acquired EEG data to construct a multi-component spatio-temporal model (MCST) of brain activity. Chapters 1 through 5 of the dissertation have described the challenges associated with generating such a model and have offered a set of technical solutions to overcome these challenges. These technical solutions were demonstrated two ways using the brain activities of spatial navigation. First, in chapter 7, the transformation of the time-varying scalp EEG into a realistic estimate of the location of multiple active areas of the brain and their associated time-domain activities was demonstrated using a single EEG dataset, collected from an individual person. Finally, in Chapter 8, investigation of the functional relationships of multiple areas of the brain using the MCST methodology was demonstrated in a group study.

The research presented in this dissertation provides novel technical contribution and novel empirical contribution to our understanding of brain function. From the technological standpoint, three novel tools have been developed for analyzing EEG data. First, a new data mining algorithm was created and tailored to separate scalp EEG data into anatomically relevant component parts. Second, a new localization and volume estimation algorithm was developed to estimate the regions of the brain from which the source waveforms found via data mining originate. Third, a validation algorithm was developed that provides researchers with an objective measure of how well the individual components of the mined EEG data relate to distinct areas of the brain. Together, these tools facilitate a new methodology for investigating brain function. This methodology encompasses three sequential, non-iterative steps: (1) data mining, (2) validation, and (3) volume estimation. Application of this methodology and associated algorithms has provided for a novel empirical representation of the brain activity of spatial navigation. This methodology has allowed for the simultaneous study of the activities of multiple areas of the brain, how the activities of these areas relate, and how they relate to behavior in a navigation paradigm. Such analysis was not possible using established analysis methods. The investigation of brain activities of spatial navigation, included in Chapter

8, demonstrated differential brain activation relationships among the cognitive conditions of spatial navigation, and linked activation of specific areas of the brain with varied navigation performance. For the first time, the brain activity associated with spatial navigation was represented as a system of functional brain activity showing what actually occurred in the brain during each navigation condition rather than only the differences between conditions provided by standard methods. The research direction that led to these novel technical contributions was inspired from an investigation of an EEG-based brain-computer interface (BCI).

Chapter 1, Section I of the dissertation was opened with a discussion of the development of a BCI and what features in the EEG might be suitable for BCI control. The choice of features to use is important because the performance of a BCI is bounded by the quality of the brain activity features by which it operates. Chapter 1 described the significant challenges that exist in ascertaining what scalp EEG features might provide the best BCI performance. Ideally, such features should relate to specific behavior and specific cognitive function that make sense for controlling the BCI. For example, if the objective is to control the location of a cursor on a computer screen, the BCI should be designed around brain activities related to spatial cognition; if the objective is to make language-based menu selections presented on a computer screen, the BCI should be designed around the brain activities related to language processing. However, detection of such brain activities requires a robust method of detecting detailed features contained in the EEG.

Current standard EEG analysis methods are not well-suited to identify detailed EEG features that would provide a high-fidelity, robust basis for BCI operation; rather, they are designed to identify average features pertaining to average brain activities. Identification of features using standard methods utilizes multiple trials of an EEG/brain activity event to generate an average result. By standard methods, the collective results of multiple experiments and manipulations are considered together in order to relate characteristics of the EEG to brain function. This process limits the utility of the EEG analysis to describing only the average brain function of the population and does not

easily allow for understanding the functional brain activities of individuals. For example, the group average of an experiment, or the average result of multiple experiments, does provide for canonical representations of brain function that are easily described, however, the functional details of the brain are generally absent. It is thus worthwhile to devise a methodology by which to extract detailed information from the scalp EEG from individual persons and construct a model of brain function around which one can build a high-fidelity BCI designed around a specific control paradigm.

Chapter 1 also describes that when it comes to understanding the relationship between brain function and behavior, it is the detail of the EEG and the brain activity contained within it that may provide for new discoveries about brain function. Current methods obscure differences in the EEGs of study participants and focus primarily on what is common among participants. However, it may be those differences that provide new insights into brain function and it is thus worth while examining them. Consideration of these details also provides for characterization of the activities of the brain as a system. An analysis approach that examines brain function as a system may be revealing of brain pathologies involving coordination among brain areas and be useful in neuroscience diagnostic applications.

The research program described in this dissertation has been structured to address the primary research question of whether or not, through a procedure of data mining, validation, and source volume estimation, it is possible to construct a meaningful, objective, and informative model of brain activity from scalp-acquired EEG data. Moreover, this research has investigated creating such models from the EEG of both single participant experiments and group experiments. Given that a methodology to construct such models could be created, the secondary question investigated was whether or not the sources derived from the EEG data could be used to construct a physiologically accurate model of the complex brain function of spatial navigation.

The present work examines brain function associated with spatial navigation using two virtual Morris Water Task paradigms, one paradigm developed at the University of

Lethbridge, and the other developed at the University of Victoria. Spatial navigation was chosen as the behavior of study for two main reasons. First, our associate lab at the University of Lethbridge had been investigating the EEG of spatial navigation prior to our involvement and had been unsuccessful using current analysis methods. Second, the brain activity of spatial navigation is expected to be complex, involving the activation and coordination of multiple brain systems. For this reason, spatial navigation is a suitable behavior around which to develop and test a methodology for examining complex brain function. The present work sought not only to contribute an analysis methodology, but to also show the usefulness of the methodology by providing successful analysis of complex EEG data in an application were existing methods have failed. The tools for analyzing EEG data developed during this research program have been evaluated in a series of papers using the University of Lethbridge EEG data and are presented in this dissertation as multiple chapters and sections. In a final study, correct operation of the analysis tools developed is confirmed using a spatial navigation dataset collected at the University of Victoria. While in both cases, paradigms based on the original MWT paradigm of Morris (1981) were used, subtle variations among the two adaptations were present.

BRAIN ACTIVITY AND EEG ANALYSIS

The data mining methods developed in the current work are based on a relatively recent algorithm in the EEG literature called Independent Component Analysis (ICA). During the development and peer-review process of the tools to address the research objectives outlined, I've had multiple correspondences with a variety of researchers who use scalp EEG data to study brain function. These correspondences revealed that there are two widely-held and related assumptions about data mining EEG using ICA methods that are not exactly correct. The first assumption is that by adding more trials to the dataset for ICA decomposition, the decomposition of the EEG into parts will improve; that increasing the number of trials will reduce the 'noise' that is leading to poor ICA separation of brain activities. The second, more general assumption is that the natural 'random' nature of EEG data will contribute to the statistical independence of brain

source activities in the EEG and that this will satisfy the ICA assumption that the contributors to the EEG are statistically independent; that we can take it for granted that if enough data are available, ICA assumptions will be automatically met. In the context of these assumptions, some fundamental characteristics of brain activity and scalp EEG were highlighted and compared to the assumptions of ICA in Section II, Chapter 2.

A survey of Event-Related Potential (ERP) literature identified some important properties of brain activity contained in scalp EEG data that impact ICA results and therefore should be considered when applying ICA. First, it is important to acknowledge that there are moments in time when activities of distinct areas of the brain are likely to be correlated because multiple areas of the brain function together to facilitate human behavior. It is this typical characteristic of brain function that makes correlation a barrier to accurate source estimation using ICA. While correlation among the activities of multiple areas of the brain is present in EEG data, because of the non-stationary statistical properties of brain function, there are moments in time when this correlation is larger and moments in time when this correlation is small. This is why some studies are more successful than others at separating the EEG into anatomically distinct parts. Depending on characteristics of the study paradigm, some time epochs (such as around the trial onset) will contain brain activities of distinct brain areas that are more correlated than in other epochs. Thus, both the time-domain location of the data analysis window and the duration of the data analysis window have a direct impact on brain source estimation error. If the activities of two distinct brain sources are highly correlated in the data analysis window, ICA will not identify them as two distinct entities but will instead consider them as a single, non-separable component of the EEG. Second, the ERP survey highlighted evidence that the statistical activation relationships among distinct areas of the brain in different EEG frequency bands are likely to vary according to the frequency band examined. Hence, some frequency bands will contain more correlated (and statistically dependant) activities than others. Moreover, since it is believed that some frequency bands are used for long-distance synchronization among brain areas (global activities) while other frequencies are involved with processes in columnar regions of the cortex (local activities) (Nunez 1989, 1995) it is logical to conclude that a

given area of the brain should concurrently possess both local and global activities. For the purposes of source separation, it is the frequencies of local activities which might be used to isolate and identify physically distinct regions of the brain that facilitate human behavior.

A logical argument was also presented in Chapter 2 that trial-to-trial variability found in the EEG (perceived EEG 'randomness') may not be best described as a characteristic of brain function per se, but better described as a characteristic of behavior. The distinction made here is that parameters that are named as brain activity characteristics should not be parameters that are under control of the experimenter. Those factors that can be controlled somewhat (such as attention, learning, arousal) should be considered a parameter of behavior and accounted for in the paradigm. For example, trial-to-trial variability might be partially due to varied level of distraction and attention, which can be modulated by parameters of the task. In addition, learning is another possible cause of variability among trials and is also a parameter that can be adjusted in the task.

Whether or not the EEG and underlying brain activities have a predictable, deterministic time-structure has also been a topic of debate. While earlier research examining scalp EEG has concluded that EEG is non-deterministic (Jeong et al., 2002; Stepien, 2002), more recent research has shown that the EEG itself has both a stochastic and deterministic nature. For example, Meghdadi et al., (2006) concluded that some aspects of the brain activities themselves contained in the EEG are deterministic and that these activities are corrupted by stochastic, non-deterministic noise. The EEG is stochastic in that some contribution to the EEG has no time structure and can only be explained by time-independent statistical variables. It is also deterministic in that a part of the EEG is comprised of activities that can be predicted given known initial conditions. Thus, any modeling of the EEG should be comprised of both deterministic and stochastic components.

In Chapter 2, after the literature review, simulation using synthetic EEG data (comprised of deterministic model brain activities and non-deterministic noise) was used to model

the interaction momentary correlated activities with ICA source estimation error. Results showed that as long as the correlative relationships between areas of the brain are maintained from one trial to the next, the addition of more trials to the dataset does not reduce the source estimate error caused by correlation among sources. In terms of analysis of real EEG data, this means that adding more trials containing brain activities that are naturally correlated does not improve the identification and estimation of the activities of distinct areas of the brain, beyond the reduction of the effect of external random noise processes. Deterministically speaking, the visual presentation of a stimulus in the center of the visual field, if all behavioral variables are held constant, should evoke correlated activation of the visual cortices, bilaterally. In this case, standard ICA can not separate these bilateral brain activities from each other. Simulation also demonstrated that manipulation of characteristics of the frequency spectrum of the modeled EEG does improve brain source estimates. Our model was used to demonstrate that a simple notch filter could be used to reduce the error associated with correlated activities. It is of course necessary to know the precise frequency at which the offending correlated activities appear. For this model, the offending frequency was known. In the case of real EEG data obtained as a result of real brain activity, the frequencies of maximum correlation, least statistical independence, and the time intervals in which they occur are not generally known.

This simple example led to the idea of developing an EEG processing methodology that automatically identifies frequencies of greatest correlation and reduces their influence on source separation and was eventually examined in Chapter 6 of the dissertation. However before this idea could be examined, it was necessary to develop a set of tools to identify source separation improvement for real EEG data. Such tools are necessary because the time-varying activities of bona fide brain sources are not generally known and therefore source separation error can generally not be quantified.

CREATION OF EEG ANALYSIS TOOLS

Development and testing of EEG analysis tools utilized both synthetic EEG data created in our lab and real EEG data obtained from the study of spatial navigation at the University of Lethbridge as described in Section III. These tools were developed as a series of multiple projects which are described over a series of 4 Chapters illustrating the principles upon which each tool is based and demonstrating their performance.

Results obtained using these tools for an investigation of Fetal Alcohol Spectrum Disorder (FASD) at the University of Lethbridge are provided in Appendix A. Analysis and paper preparation for their study is still underway at the University of Lethbridge. However results of the MCST analysis methodology applied at the University of Victoria to the Lethbridge dataset are given in the Appendix to illustrate successful application of these tools.

Source Volumes

Two main conceptual models of brain function, developed in the early days of neuroscience, have differing philosophies as to how human behavior is represented in the brain. The first model considers function of the brain as being diffusely represented such that the anatomy supporting any one behavioral characteristic is non-specific. The second model of brain function attributes behavioral function to specific distinct areas of brain anatomy. A more recent view attributes behavioral function to being diffusely represented within specific anatomical brain locations. It is viewed that the brain is comprised of many units of processing, or modules, that are each responsible for a specific functional process. Behavior however, is complex, and generally requires multiple processing modules. Hence, modern neuroscience attempts to identify how modules of brain operate together to facilitate human behavior.

Many functional modules of the brain exist in specific locations that are similar across the population. This consistency has provided a basis for our modern understanding of brain function. Functional magnetic resonant imaging (fMRI) methods, which are designed around the principle of modularity of brain function, exploit this characteristic. A

difference in activation of a specific brain area between experimental behavioral conditions is generally interpreted to indicate that a processing module of the brain was differentially active between the conditions. When neurons become active, they consume oxygen carried by hemoglobin in the blood supply. Local changes in oxygen uptake, or local hemodynamic response, are seen approximately 1-5 seconds after a population of neurons changes its firing properties. While fMRI does have very good spatial resolution to identify foci brain activity, its usefulness in characterizing the time characteristics of brain activity is limited. An alternative to fMRI for measuring the activities of the brain is provided by scalp-electroencephalographic (EEG) methods. Scalp-EEG methods utilize the time-varying electric field at the scalp cause by neuron action potentials and secondary neuron currents generated by populations of neurons in the brain.

Relating scalp-EEG to specific brain anatomy has long been a goal of EEG research methods and many algorithms have been proposed. Separation of the EEG into activities originating from distinct areas of the brain provides an engineering simplification of the EEG analysis problem; that is, to maximize the signal-to-noise ratio of the EEG so that functional brain processes contributing to the EEG can be identified. Source separation provides for a simple means of separating noise from the EEG and explaining the EEG in terms of the activities of anatomically distinct functional units. Algorithms for relating the EEG to specific brain anatomy have been generalized under the term ‘source localization’. While localization is the goal, the mechanism by which it is met entails two steps, (1) source separation (or source simplification), and (2) localization of the separated parts. Some algorithms accomplish these steps simultaneously while other methods accomplish each step separately. However, each method has inherent weaknesses. Michel et al., (2004) has generally classified source localization methods in terms of overdetermined and underdetermined methods.

Dipole modeling methods are classified as overdetermined because the method assumes that a small number of dipole sources can be used to explain the scalp field. It is assumed there are more independent measures, (electrodes) than unknown parameters describing the sources. These scalp fields usually result directly from very simple averaged event-

related potential (ERP) data, or are the result of an *a priori* step of source separation. By this localization method, a dipole (or dipoles) is placed at a specified location inside a model head and a forward solution (the simultaneous projection of these dipoles to the surface of a model scalp) is compared to the actual topography to be accounted for. The specific location and orientation of this dipole is determined using a minimization algorithm that iteratively searches for locations that provide a forward solution with the least amount of difference from the actual EEG scalp topography. However, there are three main weaknesses associated with dipole modeling methods. First, the number of dipoles to model the scalp topography is unknown, thereby providing an infinite number of solutions. Second, algorithms that minimize the error between the modeled forward solution and the actual scalp field often have a solution space with multiple minima, leading the minimization algorithm to become 'stuck' at incorrect solutions. Hence, as the number of dipoles increases, the complexity of the solution space increases, as does the likelihood of finding incorrect solutions. Third, due to the presence of noise in the data, the global minimum solution is not always the correct solution.

In contrast to the overdetermined method, dipole modeling, underdetermined modeling methods are based on reconstruction of the brain activity measured at the scalp at points on a 3-dimensional grid inside a head model. Unlike overdetermined methods such as dipole modeling, the methods of this class are linear and do not require an iterative optimization process. This class of methods is called underdetermined because the number of measured points (electrodes) is much lower than the number of solution points on the grid. Each point on the grid is considered a solution point. Hence, there is no assumption as to the number of sources. The goal is to find a single configuration of sources that exactly explain the scalp topography. Unfortunately, there are an infinite number of distributions of sources that can lead to exactly the same scalp topography. This class of methods thus requires some a priori assumptions and constraints to identify the most likely solution. The validity of the a priori constraints arising from these assumptions defines the validity of the source localization solution (Michel et al., 2004). Three well-known underdetermined modeling methods that are relevant to the current

discussion are: Minimum Norm, Weighted Minimum Norm, and Laplacian Weighted Minimum Norm.

The primary assumption of the Minimum Norm solution (Hämäläinen and Illmonemi, 1984, 1992) is that the best brain source localization estimate has a 3-dimensional current distribution that has the least overall intensity. This assumption constrains all possible arrangements of solutions to a single unique solution. A unique solution can be found because only one combination of sources can have (1) least overall intensity, and (2) exactly fit the data. However, there is a solution bias towards sources at the outer edges of the brain because less intensity is required for solution points located at the surface of the cortex to fit the data. A second and important assumption is that the activities of distinct brain sources are uncorrelated (or have little to no covariance). This method uses a correlation/covariance matrix to determine how to allocate data in a head volume; the method assumes that distinct contributors to the EEG have activities that are uncorrelated. However, this assumption is rarely completely valid (as described earlier in this discussion) because activities of distinct areas of the brain are not necessarily uncorrelated. Hence, contributors with correlated activities are inherently difficult to localize using this method. To address the issue of source location bias, two types of algorithms, Weighted Minimum Norm and Laplacian Weighted Minimum Norm (LORETA) were created and have been somewhat successful in compensating for the bias of the standard minimum norm solution.

Weighted Minimum Norm solutions compensate for the superficial location bias of the standard minimum norm solutions. For example, in the PROMS solution (Greenblatt, 1993) the covariance (zero-mean correlation) matrix is used to construct a weighting function to compensate for bias. Similarly, the FOCUSS (Focal Underdetermined System Solution) method (Gorodnitsky et al., 1995) iteratively changes weights compensating for bias comprising an iterative, non-linear solution. A third weighted minimum norm algorithm, the RWMN (radially weighted minimum norm) method (Grave de Peralta Menendez and Gonzalez Andino, 1998) imposes bounds in the model brain volume such that variance associated with radial components goes to zero when

approaching the surface of the brain. The problem with these methods of bias compensation is that they are not physiologically based but are purely a mathematical adjustment.

The Laplacian Weighted Minimum Norm Solution (LORETA) (Pascual-Marqui et al., 1994) takes a different approach than those described above to address minimum norm bias. In contrast to standard weighted minimum norm methods, this method has some physiological basis; it is assumed that activity in neurons in neighboring patches of cortex is correlated and not statistically independent (i.e., not functionally distinct). The method selects a solution by minimizing the Laplacian of weighted sources: The Laplacian is a mathematical description of smoothness. Using the Laplacian, the method provides a limit on the spatial roughness of the source estimate. However, LORETA is not without localization weaknesses. Functionally different areas of the brain can be anatomically very close and this algorithm generally provides blurred and over-smoothed solutions that can combine two functionally different and anatomically adjacent sources into a single source solution (Fuchs et al., 1999; Grave de Peralta and Gonzalez, 2000; Trujillo-Barreto et al., 2004).

Chapter 3 of the dissertation describes how our own localization and source volume representation algorithm relates the topographies of components calculated via ICA to volume-domain representations within a model head to overcome some of the limitations of existing source localization algorithms. The purpose of creating this algorithm was to determine if physical characteristics could be related to the topographies and waveforms yielded by ICA of real EEG data to make sense of the sources calculated; ICA only provides unmixing of the EEG and does not inherently provide localization. Thus, it is a necessity to create an algorithm to relate ICA results to anatomy. The volume-estimation algorithm proposed in Chapter 3 utilizes beamforming, an underdetermined modeling method which is combined with the source separation pre-processing characteristics of ICA. The pre-processing source separation step attempts to provide ideal circumstances for beamform source estimation solutions. When source separation results are ideal, each component should pertain to a single distinct source in the brain. This ideal case allows

for the estimate of source volume. The proposed volume-estimation algorithm corrects for standard beamform bias which places sources towards the top and center of the head due to the absence of spatial sampling in the inferior ventral areas of the head (at the neck and chin) by generating surrogate data using the ICA-derived topographies and additive noise with known spatial characteristics. The major weakness is that the accuracy of the source localization method is inherently dependent on the accuracy of the source separation, or data mining result.

The investigation in Chapter 3 uses synthetic data that satisfy ICA source assumptions to evaluate the volume-domain projection and volume estimation algorithm for ideal source separation conditions. Evaluation of the algorithm using synthetic EEG data showed that, for a 124-electrode scalp array, it is possible to estimate the modeled volume occupied by simulated brain sources and, furthermore, that adjacent simulated sources can be resolved at a spacing of 0.5 cm. Additional investigation of the characteristics of the volume-domain projection of components revealed that simulated sources that have been well-separated by ICA have small overlaps, while those components that have been poorly separated by ICA, have large overlaps. These results suggest that examining the overlap characteristics of sources in the volume domain might provide a means for source validation.

In contrast to Chapter 3, in which the volume-projection algorithm was examined using 'ideal' synthetic data, Chapter 4 assessed the volume-domain projection and volume estimation algorithm was assessed using notoriously 'non-ideal', real EEG data. The data examined were those acquired using a spatial navigation paradigm developed at the University of Lethbridge and were used to demonstrate volume estimation of nine ICA-derived EEG components. To maximize our success in obtaining components that pertain to distinct parts of the brain, the EEG data for this study were band-pass filtered (8-30 Hz) prior to ICA decomposition to remove low frequencies which we suspected to contain activities with the greatest correlation between spatially distinct areas of the brain. Low frequencies are suspect because our experimentation with these data found

that separation improves when the influence of the low frequencies on the source separation process are removed.

The results of this analysis showed that volume estimation provided a representation of components in areas of the brain that are reasonable for spatial navigation behavior. While localization of activities in reasonable areas of the brain is encouraging, it is not sufficient to demonstrate the accuracy of the method. It does however demonstrate that, in principle, results obtained via ICA decomposition of real EEG data can be projected to volume-domain representations. The results also demonstrated that characteristics of the volume-domain representation of components provide a metric of the physical separation of component activities determined as a measure of source volume overlap.

Together, the results of the investigations of Chapters 3 and 4 suggest that by using this algorithm, it is possible to estimate the effective region from which an ICA waveform originates. These results also show that the algorithm provides an objective measure of the physical separation that can be used to demonstrate a pair of components are physically distinct. Such a measure is useful when evaluating the correlation of activities between brain source pairs because it provides evidence that measured correlation is not likely attributed to volume conduction.

Source Validation

The study presented in Chapter 5 of Section III used both synthetic and real EEG data to describe and evaluate a new algorithm to differentiate ICA-derived artifact components of EEG data from components that might represent the activities of the brain. This algorithm, based on the findings of Chapters 3 and 4, presumes that those brain activity components of interest by neuroscientists are ideally modular, and do not overlap with the representations of other distinct sources comprising the EEG data. The algorithm evaluates components according to how well they can be represented as originating from distinct modular regions inside a model head.

Synthetic EEG data were used to demonstrate how the algorithm should perform for brain sources with ideal waveform and volume characteristics. Five sources comprising the synthetic EEG modeled distinct contributors to the EEG located in the brain with waveform activities that fit the statistical assumptions of ICA. Three artifacts were modeled: an electrode artifact that was statistically independent from other sources, and two artifacts that represented partial correlation of bona fide sources. Three metrics were devised to identify artifacts. These methods utilized the projection of component topographies into volumetric quantities called volumetric spectra to evaluate components. (1) The first metric, an estimate of the voxel specificity of components, was determined from the value of the largest coefficient of the volumetric spectrum, and was referred to as the peak spectral value (PSV). (2) The second metric, the volume overlap characteristic of components, was determined by calculating the overlap of the volumetric spectrum of the component of interest with all other components of the decomposition and was referred to as the median volume overlap (MVO). (3) The third metric, a measure of the stability of component representation, was determined as a measure of how far the center of mass of a component travels over iterations of ICA. This final metric was referred to as the total distance traveled (TDT). The changes in these for components of the synthetic EEG were evaluated over iterative steps of maximizing independence.

Results demonstrated that during ICA estimation, the volume-domain characteristics of synthetic brain sources improved and converged in a meaningful way. That is, on successive iterations, the voxel specificity (PSV) increased, the volume overlap (MVO) decreased, and the distance traveled by the component's center of mass decreased. This indicated that as the statistical independence of components was increased, the volume-domain characteristics of the estimated components that relate to the modeled source volumes improved. Interestingly, the volume-domain improvement of components reached an asymptote prior to the standard ICA algorithm reaching its default stopping value, suggesting that the ICA algorithm at some point begins to iterate on noise and no-longer offers improvement in separating the activities of the modeled brain sources.

These convergence results demonstrate that if brain sources do in fact meet the assumptions of ICA, then as the statistical independence of the EEG is maximized, the volume characteristics of components representing activities of distinct brain areas will improve. Furthermore, because the evaluation of the volume-domain characteristics (PSV, MVO, and TDT) of components for the final iteration of the ICA process provided a distinction between the model brain sources and the artifacts, it is possible that they might also provide a distinction between artifacts and brain sources for real EEG data. This however assumes that the assumptions of ICA will be met by brain sources comprising the EEG. (The investigation of this assumption in Chapter 6 revealed that, with some modifications to the ICA algorithm, it can be used to separate brain activities into physically distinct contributors.)

The result of applying the validation algorithm to real EEG data obtained from the University of Lethbridge showed that the peak value of the volumetric spectrum (PSV) is an appropriate measure to characterize source separation improvement. The voxel specificity for a subset of the components was found to improve over successive ICA iterations on real data suggesting that these particular components, at least somewhat, meet the assumptions of ICA and do originate from modular regions inside the head. In contrast, the measure of volume overlap (MVO) used successfully on the model data was found to be unstable for real EEG data. The MVO for real EEG data is unstable, compared to the case when model EEG data were used, because the real EEG data contains many more artifacts than the model data that were used. A new method to calculate the median volume overlap was introduced that is less sensitive to artifacts contained in the EEG. The new method characterizes the volume-domain uniqueness of each component as a normalized vector comparison of the volumetric spectra instead of the zero-mean normalized vector comparison of the volumetric spectra used for the model data. This new method of estimating the volume-domain overlap was found to be more stable than the previous method and showed that the overlap of a subset of brain activity components (that was similar to the components with improved PSV) improved over iterations of ICA. Evaluation of the PSV, MVO, and TDT of components for the final iteration revealed that only the PSV and new MVO method (excluding the TDT)

provides a distinction between artifact and possible brain activity components. It also revealed that ocular artifact components are not necessarily distinguished separately from the brain activity components. The inability to distinguish ocular motor activity from brain activity using volumetric properties makes sense because both active brain areas and the muscles of the eye that contribute activities to the EEG are located inside the head.

Taken together, the above results mean that the volume-domain validation method can be used to determine which components are artifacts that can not be represented as volumes inside the head. Those components that have origins inside the head and that are not brain activities (such as ocular sources) are not necessarily distinguished by the automated process. However, this isn't a problem in most cases because such artifacts are generally easily characterized and can thus be identified from the other brain activity components that originate from inside the head. This was demonstrated in the next chapter, Chapter 6, that by using a new ICA data mining algorithm, the ocular artifacts can be clearly identified from brain activities by properties of their physical volume. In addition to providing a means of classifying components, it provides a rank of the relative goodness of components so that weak or poorly separated brain sources can be distinguished from good ones.

Data Mining

The research described in the final chapter of Section III, Chapter 6, used real EEG data obtained from the University of Lethbridge to investigate an alternative to the strict assumptions of uncorrelatedness and statistical independence of ICA with the goal of separating the EEG into components representing distinct parts of the brain that are distinct functional units. This particular investigation further developed the idea of an EEG processing methodology that automatically identifies frequencies of greatest correlation and reduces their influence on source separation first described in Chapter 2, with the goal of reducing brain source estimation error. The method proposed, called Spectral Shaping ICA (SS-ICA), allows for some correlation and dependence between

sources and can identify contributors to the EEG that are not necessarily uncorrelated or statistically independent. Because this new source separation method deviates from the strict assumptions of ICA, the more general term, data mining, is used to describe the process of identifying the parts that comprise the EEG mixture.

A comparison of source separation results obtained using the SS-ICA method and results obtained using the standard ICA method showed two main distinctions. First, the SS-ICA method yielded two anatomically correct components of the ocular muscles that the standard ICA method (runica, Makeig et al., 1997) allocates in an anatomically inappropriate way. Second, results indicated that SS-ICA was successful at separating brain activity components while still preserving the correlative properties of their waveform activities. The most compelling evidence supporting the use of SS-ICA over the standard method was that SS-ICA separated the EEG into brain activity components with activities having most correlation between sources in the low frequency EEG spectrum and having uncorrelated activities in the high frequency EEG spectrum. Most of the correlation was demonstrated to be at frequencies below 30 Hz. Moreover, with these changes in the correlation characteristics of waveforms of components, there were no significant changes in their physically modeled overlap indicating that source volume accuracy was not sacrificed to in allowing for correlated source waveforms.

The results of Chapter 6 provided evidence, using real EEG data, of the varied statistical characteristics of brain activities contained in the EEG that was predicted by the study in Chapter 2. The investigation of Chapter 2 used theoretical evidence to anticipate that correlation among the activities of distinct areas of the brain varies according to the frequency band examined. The investigation of Chapter 6 calculated a spectral shaping filter (used by the proposed SS-ICA algorithm) which showed that frequencies in the band 27-42 Hz had activities with greater statistical independence than frequencies less than 30 Hz did. The shape of the filter also implicated the frequency band 65-80 Hz as having greater statistical independence than lower frequencies of the EEG spectrum. This result is also expected because this frequency band is largely dominated by noise unrelated to activities of the brain.

The results of this investigation demonstrate that the *bona fide* correlative structure of brain source activities can be preserved by using the SS-ICA method. Because correlated activities are permitted by the SS-ICA algorithm, it is better at separating partially correlated source activities in an anatomically meaningful way than the standard method. In terms of understanding how the brain functions as a system, being able to preserve the correlative properties of brain activity estimates makes it possible to use measures of time-domain correlation to evaluate the coordination between areas of the brain.

CREATION OF THE MCST METHODOLOGY

In Section IV, Chapter 7, the tools developed in Section III were described as parts of a toolkit providing for a methodology to examine the functional relationships of multiple areas of the brain called Multi-Component Spatio-Temporal (MCST) modeling. A step-wise description was given for how to use the tools for analyzing EEG data. The philosophy of the methodology was discussed and analysis results obtained in a case study of EEG data acquired from an individual person were used to demonstrate its capabilities. Finally, to facilitate future use of the MCST methodology by other researchers, a step-wise description of how to use the tools to analyze EEG data was given.

In Chapter 7, results from a case study demonstrated that the MCST methodology can be used to identify activities of the ventral cortical visual processing stream of the brain associated with visuospatial navigation and that this processing stream can be represented by multiple components. A depiction of the time-varying activities of these distinct parts of the visual pathways was provided to illustrate how they can be used to make comparisons between two different behavioral conditions. In addition, a depiction of the time-varying correlation of activities of distinct parts of the brain was provided to show that time-varying correlation can be used to estimate the coordination between areas of the brain and to make comparisons between behavioral conditions.

This collection of algorithms provides a toolkit that other researchers can use in their own EEG research to examine how activities of distinct parts of the brain relate to each other and how these relations differ between behavioral conditions. The methodology facilitates study of the brain as a system because it attempts to account for all active areas of the brain and how they relate to each other in a given behavioral paradigm. In contrast, fMRI experiments usually examine only the activities of specific parts of the brain that are determined *a priori*, as part of a hypothesis testing strategy and rarely examine the direct activation relationships among brain areas. The data mining component of the MCST methodology attempts to identify the activities of all the brain areas involved so that they can all be studied in relation to each other. Because fMRI analysis uses subtractive methods to evaluate the data, only the difference between conditions can be studied. This subtractive method is similar to how scalp EEG data would be studied using standard ERP-based methods, however, without the knowledge of brain activity origins. In contrast, the MCST method provides a depiction of all detectible activities that occurred during the data collection paradigm for each condition separately.

EXAMINING GROUP DATA USING THE MCST METHODOLOGY

In Section V, Chapter 8 of this dissertation, the MCST methodology was used to study the brain activity associated with spatial navigation using scalp EEG data collected at the University of Victoria. This study was approached as a pilot investigation using the MCST methodology to examine brain activity and behavioral differences associated with allocentric versus egocentric navigation strategy. If feasibility was demonstrated in this pilot, it would be followed-up by a larger study directed by the spatial navigation group at the University of Victoria. For the purpose of this dissertation, the University of Victoria study served 5 functions. It provided context within which to: (1) demonstrate the MCST methodology (2) make contrasts of the estimated brain activities of a group between behavioral conditions, (3) show that the brain activities estimated using the MCST methodology can be related to behavioral measures, (4) demonstrate how the EEG might be used to study the coordination of areas of the brain, and (5) show how the brain

activities of individual persons can be meaningfully compared to group data to identify anomalous brain activities and behavior.

Demonstrating that the tools can be successfully applied to new data collected using different equipment than was used to develop the tools helps validate them. Application of the tools and methodology to the University of Victoria dataset provided results that were comparable to those found using data from the University of Lethbridge. First, both datasets revealed the dorsolateral prefrontal cortices, ventral visual cortices, and primary striate visual cortices were active in their respective paradigms. Second, the validation curves were similar across datasets. That is, the PSV and MVO curves separating artifact components from components that could be well-represented in the head model bared a remarkable resemblance in shape across datasets. Unfortunately, the two datasets examined had differing numbers of electrodes (112 versus 32) and thus the actual values of the PSV and MVO scores were not comparable between studies. Third, the shape of the spectral shaping filter calculated for the Victoria dataset was similar to that of the spectral shaping filter calculated for the Lethbridge dataset. That is, specific bands of frequencies, identified by the shaping filter as having high statistical independence, were common among the datasets. A comparison of the log spectra of Chapter 6, Figure 2 and Chapter 8 Figure B1 (12-point correlation, 15 Hz to 70 Hz in steps of 5 Hz) reveals a significant ($p = 0.64$) correlation between the shaping filter spectra. This not only demonstrates that the SS-ICA algorithm can be successfully applied to new data, but also demonstrates that this SS-ICA algorithm identified consistent statistical properties of the EEG data collected in differing lab settings using comparable behavioral paradigms.

Analysis of the University of Victoria group EEG dataset identified meaningful differences between spatial navigation conditions that are in agreement with prior literature. The main result of this study relating brain function and behavior was that a region of the right hemisphere we identified as the posterior parietal cortex was differentially active by condition. This area was significantly more active when study participants where navigating place trials than when they were navigating cue trials. The finding of greater activation for this brain area in place trials is in agreement with prior

literature because the posterior parietal cortex is believed to be important for the allocentric navigation strategy (Goodale, 1993, 1998), which by design of the paradigm, is the required strategy for successful completion of place trials (Livingstone and Skelton, 2007). Hence, by applying the MCST methodology to this spatial navigation problem, brain activation differences between behavioral conditions were successfully identified.

Some interesting brain activation properties were revealed by relating brain activities to behavioral measures such as latency to complete trials and a test of explicit knowledge of the correct location of the hidden platform. For some participants, latencies for navigating place trials were large suggesting that they had difficulty finding the location of the hidden platform using the allocentric information provided in those trials. For other participants latencies were short, indicating mastery of the task. Further, analysis showed that the latency to reach the location of the hidden platform for these place trials was significantly correlated with activity levels of particular areas of the brain (right ventral extrastriate visual cortex, right dorsolateral prefrontal cortex, and the left ventral extrastriate visual cortex); participants with large activation in these areas tended to be poor navigators (as indicated by latency) in place trials. This suggests that either the activation of these areas caused knock-on brain activities that made navigation in the place condition difficult, or that participants with large activation in these areas were using a cognitive strategy that was not the most efficient for place trials. For example, participants with large latencies might have been navigating using an egocentric strategy (best for cue trials) instead of allocentric strategy. This is plausible because prior literature cites use of egocentric navigation in place trials as a possible cause of poor navigation performance (Livingstone and Skelton, 2007). Moreover, these areas are part of the ventral stream and are expected to be active in a scenario when object identification is required. In this context, it appears that the MCST methodology revealed a reasonable relationship between behavioral measures and brain area activation that fits within the context of prior literature.

The measure of explicit knowledge of platform location via the drop-the-seed trials also revealed a relationship between activation of specific brain areas and behavior.

Correlative analysis showed that participants who were able to use explicit knowledge to accurately identify the location of the center of the platform for place trials, requiring an allocentric navigation strategy, tended to have larger activities of the right anterior parietal cortex. Participants who were able to use explicit knowledge to identify the location of the center of the platform for cue trials (requiring an egocentric strategy) tended to have larger activities of the right dorsolateral prefrontal cortex and the left ventral extrastriate visual cortex, while having smaller activity in the right posterior parietal cortex. This finding is similar to the finding that activity of the right dorsolateral prefrontal cortex and left ventral extrastriate visual cortex related to increased latency suggesting in some cases, poor performance in place trials was due to egocentric navigation instead of the allocentric navigation for which they were optimized. These relationships are new and have not direct comparison in established literature. The revelation of these novel correlative findings means that use of the MCST methodology has facilitated a contribution to neuroscience in the field of spatial navigation research.

Following from the analysis of brain area activation, the results presented in this study showed two different ways to construct a model of the functional relationship between parts of the brain for a group dataset. The first method used the pair-wise activation of brain areas calculated across components, separately for the cue and place conditions. This method provided a measure of the consistency of coordinated activation of brain areas across participants in this study and a way to identify outlier participants. For cue trials, optimized for egocentric navigation, the components with volumes in regions implicating the left ventral stream showed consistent pair-wise activation relationships across the participant group. In contrast, in place trials optimized for allocentric navigation, there was a lack of consistent pair-wise relationships among the same brain areas. However, some notable relationships were present in the right parietal region. To the credit of the MCST methodology, the characteristics of the model constructed from the EEG data fit with what is already known about spatial navigation and object identification using the visual system. Namely, the evidence suggesting that object identification involves the ventral visual streams (Goodale, 1998) and spatial navigation involves parietal areas of the cortex (Witlock et al., 2008).

In contrast to examining consistency across the group, the second method for model construction examines specific pair-wise zero-lag correlation of activities among brain areas, separately for each participant. Application of this method around the onset of navigation revealed that more significant correlative activation relationships were present among brain areas in the allocentric navigation condition than in the egocentric condition.

Results also demonstrated how the MCST methodology can be used to identify anomalous brain activation and behavior. A possible outlier participant was identified as having unusual activity of the ventral visual processing streams of both the left and right hemispheres. Inspection of participant information revealed that this outlier participant has an esotropia which is known to alter the way the brain processes visual information. This result suggests that this analysis methodology might provide for meaningful identification of brain activities that deviate from the norm.

The results derived from this spatial navigation study are exciting because this is the first time that brain activities related to spatial navigation have been examined using scalp EEG. They are also exciting because they revealed so many characteristics of functional activities. The results of this study were easy to interpret—specific areas of the brain and specific processing stream were implicated by the results. It is worthwhile mentioning that, while I have done much of the research for this dissertation in the context of spatial navigation, I am not an expert in the field and my knowledge is limited. For this reason, my interpretation of results is largely driven by what has become visible from the EEG data and is less influenced by any desire to validate prior findings in spatial navigation research. I find it fabulously rewarding that characteristics of brain activity implicated by the algorithm support both well-established theories (O'Keefe and Nadel, 1978) and newer theories of spatial navigation (Nadel and Hardt, 2004; Witlock et al., 2008).

APPLICATIONS

Practical Contribution for Researchers

The algorithms developed for this dissertation provide a very practical toolkit for neuroscience researchers and diagnosticians examining neurophysiology. In its current state, the toolkit consists of multiple scripts of Matlab code customized for analysis of the University of Lethbridge and University of Victoria datasets and requires some modification to make it useable for general applications by persons unfamiliar with Matlab programming. The toolkit will provide researchers with a 'black-box' approach to EEG analysis that has herein been termed Multi-Component Spatio-Temporal (MCST) modeling. The data mining, validation, and volume estimation algorithms are fully automated, requiring virtually no user selection of algorithm parameters with the exception of selecting confidence intervals for component validation and volume estimation. These confidence intervals can be objectively determined based on the parameters established in this dissertation. For example, validation thresholds are determined by identifying the knee of the validation curves (Chapter 8) and volume estimation thresholds are determined by required confidence in volume location (Chapters 3 and 4). Readers of this dissertation, who are able to grasp only a basic understanding of the signal processing and neuroscience concepts presented, are well-suited to apply the methodology in their own work.

The MCST methodology can be applied in any number of areas of research, both in paradigms where standard EEG analysis methods have been successful and in paradigms that have used methods other than EEG. For example, D'Arcy et al. (2004), in an EEG investigation of language, found numerous areas of the brain active for language processing. Application of this methodology in similar research would not only reveal what areas of the brain are active for language processing but also how brain areas involved with language processing coordinate their activities over time. Prior research investigating compensatory mechanisms for impaired dopamine systems conducted by Hanakawa et al. (1999) used Single Photon Emission Computed Tomography (SPECT) imaging methods to identify areas of the cortex that persons with Parkinson's disease use

while walking on a treadmill. This method of imaging required participants to ingest a radiotracer prior to walking on the treadmill. Participant's then performed the behavior of interest, (walked on the treadmill), and then were required to lie inside a SPECT imager so that the areas of the brain that metabolized the tracer could be identified. Application of the MCST method in a study such would allow for the use of scalp EEG, recorded while participants walked on the treadmill, to reveal what areas of the brain were active during the behavior of interest. In addition, the MCST method could reveal how the active areas of the brain identified coordinate their activities.

Functional Anatomy and Clinical Neuropathology

It is my opinion that the MCST methodology should be far more sensitive to some aspects of brain activity than standard methods. The methodology provides a representation of brain function in terms of areas of the brain operating (or not operating) together. Because of this property, the MCST methodology should prove useful to detect brain pathologies described as 'disconnection syndromes' better than standard methods that examine activities of areas of the brain in isolation of each other. For this reason, I expect that the MCST methodology will be useful for research into functional brain anatomy and pathologies that are more evident as a functional deficit rather than an anatomical deficit.

With additional testing using synthetic and real EEG data, it might be possible to use the MCST methodology to evaluate pathological brain activities against a normative. Furthermore, the methodology might be suitable to detect and meaningfully represent subtle changes in brain activity such as changes related to recovery after a stroke, and differentiate injury compensation versus actual recovery from injury. Presumably, compensation would appear in a functional analysis of the brain as an outlier strategy indicated by outlier activation of areas of the brain when compared to normative group data, much like was found in the group study of Chapter 8. In contrast, other human studies infer recovery versus compensation from behavioral measures and are never certain as to the mechanism of improvement in behavioral performance. Actual recovery

of function would be seen in a longitudinal study showing gradual increases of activation and/or coordination between areas that have been affected by injury. Using this information we should be able to speculate on therapies or provide alternate strategies to persons with brain injuries to compensate for problems.

MCST METHODOLOGY AND BCI

It was described earlier that the reliability of a BCI is generally limited by the reliability and specificity of the EEG features upon which the BCI is based. Thus, it is important to identify a set of specific EEG features that relate to the specific brain function and specific cognitive behavior that will drive the BCI. The ability to obtain such features has a bearing on how well the EEG, behavior, and brain function of a given BCI control paradigm are understood.

The MCST methodology provides a means to determine what specific features might be available in the EEG for a given behavioral task. For example, features useable for BCI control might exist at the presentation of certain visual stimuli on a computer screen in a neural-response to stimulus BCI paradigm. For example, given a particular stimulus provided by a computer, a set of 'go/no-go', brain activity responses useable in a BCI might be generated. The MCST methodology would serve to study and characterize the cognitive processes, brain activities, and human behaviors related to the BCI scenario. However, while many aspects of brain activity are generally consistent across the population, differences in the brain physiology such as lateralization of function make it necessary to characterize the brain activities of each individual BCI user. From this characterization, a real-time system could be created to detect the features of interest and account for some of the likely interferers identified in the characterization process. Such interferers include both muscle artifacts and normal cognitive processes that interfere with BCI control.

There is a continuum of brain activity and cognitive complexities around which a BCI can be designed. In the simplest case, the BCI might be controlled by the activity of a

single brain area. Presumably, the activation of multiple areas serves as a better, more detailed basis, by which to construct a BCI controller and would be more resilient to interferers; it would be able to reject spurious activation of single brain areas, and reject artifacts that appear to be activation of single brain areas. Moreover, should the activation of multiple areas occur at zero-lag as correlated activities, or as predictable lagged correlated activities (as in a sequence of events), then the co-occurrence of such events and their timing can could be characterized for BCI control. Simply, a BCI that provides a link to a computer that is based on complex brain processes has the potential for some very abstract and artifact resilient computer control.

CAVEATS AND CONDITIONS

While the results of the study in Chapter 8 demonstrated that the MCST methodology can be successfully applied using a low density 32-channel electrode array, a high-density electrode array is recommended. In that study, the low number of degrees of freedom by which to separate sources contributing to the EEG was an issue because there were very likely more sources comprising the EEG data than dimensions for source separation. It is a necessity to count all noise sources with the possible brain sources in the dimension required for good source separation. Noise sources that might have been separated as other components if more electrodes were available were not separated from the estimated activities of some brain areas. This failure to separate noise might have led to some of the weak component representations that were provided for inspection in Appendix A of the study. The low density array also did not allow for the spatial sampling that a high density array could have provided to provide more confidence in the source location and volume estimates of active brain areas.

An important limitation to the MCST methodology is that if the data mining algorithm fails to separate distinct brain sources contained in the EEG data, the localization and volume estimation algorithm will fail to identify the correct anatomical brain regions contributing to the EEG data. The special circumstance under which the volume-projection and estimation algorithm can find the correct is when the topography

calculated via data mining only contains the characteristics of a single distinct source inside the head volume. The volume-domain validation algorithm addresses this weakness somewhat by providing a measure of the volume-domain voxel specificity of components and in theory (which has been somewhat demonstrated in Chapter 3 using simulated data) will identify poorly separated sources. The research presented in Chapter 5 demonstrates that components of the EEG that are poor representations of sources in the head volume will be identified by the validation algorithm.

While the brain anatomy and activity results found by the spatial navigation research paradigms described in Chapters 7 and 8 are plausible and fit within current knowledge of brain function, they were not sufficient to completely validate the MCST methodology and associated tools. This is because validation of the methodology and tools has not yet been done using simple, well-known paradigms with well-known brain activities and neural systems. The spatial navigation EEG paradigm used to validate the methodology in the current work has not been sufficiently characterized by other methods by which to compare the results of our proposed method. The task itself is well-established in behavioral literature, as are the brain activities associated with spatial navigation, but analysis and description of the brain activities as a system have not previously been provided. This comes of no coincidence because prior EEG methods analyzing spatial navigation have not been successful in identifying the brain system underlying the paradigm and thus a new methodology was created in the current work to address this problem. In sum, analysis of the behavior of spatial navigation was selected (1) out of the necessity to address a current ongoing research problem that could not be addressed using prior analysis methods, and (2) because it elicits complex systems of brain function and studying such complex systems is a current direction of neuroscience research.

FUTURE WORK

The MCST methodology and toolkit described in this dissertation requires additional (1) user interface development, (2) refinement of the algorithms and software implementation, and (2) testing. User interface development is required to make the

toolkit and methodology available to persons who are not experts in Matlab programming. Currently, the tools exist as a set of text-based Matlab scripts and functions. Refinement of the data mining algorithm would involve increasing the number of coefficients that define the spectral shaping filter to more precisely identify frequency bands of statistical independence. The volume estimation algorithm can also be significantly improved with the addition of a robust noise estimation algorithm that automatically determines the most suitable noise threshold for each brain source volume estimate. Finally, testing using both synthetic data and real EEG data is required to better validate the methodology. Synthetic EEG data should be used to examine estimation error for a variety of electrode configurations, brain source configurations, and artifact configurations. Using real EEG data, numerous behavioral paradigms of varied complexity should be examined to identify limitations of the methodology and underlying algorithms.

The present work also demonstrated varied statistical characteristics across the EEG frequency spectrum which should be explored further and quantified. Quantification should use root-mean-difference measures consistency of the shaping filter calculated between studies to identify regions of the frequency spectrum that have varied statistical independence among experiments.

Future work should also generalize the current analysis software so that it can be used for other datasets in other research labs.

CONCLUSIONS

The main contributions of this body of work are 5 fold. The contributions are: (1) a new data mining algorithm tailored for EEG, (2) an EEG component validation algorithm that identifies noise components via their poor representation in a head model, (3) a volume estimation algorithm that estimates the region in the brain from which each source waveform found via data mining originates, (4) a new procedure to study brain activities associated with spatial navigation, and (5) a contribution to the understanding of brain

function from evidence of specific functional systems within the brain that are used while persons participate in the vMWT paradigm (Livingstone and Skelton, 2007).

The research presented in this dissertation demonstrates that, through a procedure of ICA-based data mining, validation, and source volume estimation, it is feasible to construct a meaningful, objective, and informative model of brain activity from EEG data. The brain activity model is meaningful because it describes the brain activity that actually occurred rather than only reporting a difference between conditions. It is objective because the methods used to construct the model minimize researcher bias. It is informative because it relates waveforms measured at the scalp to specific anatomy and implicates specific pathways of information transfer and coordination. The final studies described in Chapters 7 and 8 showed that the methodology developed can be used to study the cognition of spatial navigation using a vMWT paradigm; it can be used to compare the brain activities of an individual person, or a group, between behavioral conditions. The study of Chapter 8 showed that this methodology can be used to provide a comparison of the brain activities of individual persons against a group to identify anomalies in brain function and cognitive strategy. That is, the activities of specific areas of the brain and their functional relationships for an individual can be compared against the group. Taken together, the collective evidence presented in this dissertation suggests that the methods developed can be refined and customized for use in clinical diagnostic tests evaluating functional brain activity.

The last key contribution of this work is in demonstrating the principle that when presented with an analysis problem, a customized analysis methodology can be created to study the process of interest rather than be limited by standard analysis methods. In this case, the characteristics of EEG and brain activity were examined and established tools were modified and combined to create a new analysis tool to examine the brain as a functional system.

REFERENCES

American Psychiatric Association. Diagnostic and Statistical Manual of Mental Disorders, 4th Ed. American Psychiatric Association, 1400 K Street, N.W.,Washington, DC, 1994.

Amari S, Cichocki A. A New Learning Algorithm for Blind Signal Separation. In: Advances in Neural Information Processing Systems 8, Editors D. Touretzky, M. Mozer, and M. Hasselmo, pp757-763, MIT Press, Cambridge MA, 1996

Andersen RA, Buneo CA. Intentional maps in posterior parietal cortex. Annu Rev Neuroscience 2002;25:189-220.

Anderson RA, Essick GK, Siegel RM. Neurons of area-7 activated by both visual-stimulated and occulomotor behaviour. Experimental Brain Research 1987;67:316-322.

Andrew CM, Pfurtscheller G. On the existence of different alpha band rhythms in the hand area of man. Neuroscience Letters 1997;222:103-106.

Andrew C. Quantification of event-related coherence (ERCoh). In: Pfurtscheller G, Lopes da Silva FH (Eds). Handbook of electroencephalography and clinical neurophysiology. Revised Series, v6. Amsterdam, The Netherlands: Elsevier, 1999:119-137.

Andrew CM, Pfurtscheller G. On the existence of different alpha band rhythms in the hand area of man. Neuroscience Letters 1997;222:103-106.

Anemueller J, Sejnowski TJ, Makeig S. Complex independent component analysis of frequency domain electroencephalographic data. Neural Network 2003;16:1311-1323.

Antoniou A, Lu W-S. Practical Optimization: Algorithms and Engineering Applications, 1st ed. New York: Springer Science and Business Media, 2007.

Astur R, Ortiz ML, Sutherland RJ. A characterization of performance by men and women in a virtual Morris water task: A large and reliable sex difference. Behavioural Brain Research 1998;93(1-2): 185-190.

Astur R, Taylor LB, Mamelak AN, Philpott L, Sutherland RJ. Humans with hippocampus damage display severe spatial memory impairments in a virtual Morris water task. Behavioural Brain Research 2002;132(1):77-84.

Baillet S, Mosher JC, Leahy R. BrainStorm beta release: a Matlab software package for MEG signal processing and source localization and visualization. Proceedings of the 16th Annual Meeting of the Organization for Human Brain Mapping, San Antonio, Texas, 2000.

Bell A, Sejnowski TJ. An information-maximization approach to blind separation and blind deconvolution. Neural Comp, 1995;7:1129-1159.

Berg P, Scherg M. A fast method for forward computation of multiple-shell spherical head models. Electroencephalography and Clinical Neurophysiology, 1994;90:58-64.

Baddeley AD, Hitch G. (1974). Working memory. In: Bower GH (Ed). The psychology of learning and motivation: Advances in research and theory, v8. New York: Academic Press 1974:47-89.

Baddeley A. The episodic buffer: a new component of working memory? Trends in Cognitive Sciences 2000;4(11):417-423.

Baddeley A, Della Salla S. Working memory and executive control. Philosophical Transactions R. Soc. Lond 1996;351:1397-1404.

Başar, E. Memory as the “whole brain work”: a large-scale model based on “oscillations in super-synergy”. International Journal of Psychophysiology 2005;58:199-226.

Bastista Ap, Andersen RA. The parietal reach region codes the next planned movement in a sequential reach task. Journal of Neurophysiology 2001;85:539-544.

Bibbig A, Middleton S, Racca C, Gillies MJ, Garner H, LeBeau FEN, Davies CH, Whittington MA. Beta rhythms (15-20 Hz) generated by non-reciprocal communication in the hippocampus. Journal of Neurophysiology 2007;97:2812-2823.

Birch GE, Lawrence PD, Hare RD. Extraction of motor related activity from single trial EEG. Departments of Electrical Engineering and Psychology, University of British Columbia, Vancouver, B.C., Canada. 1988.

Bland B H, Oddie S D. Theta band oscillation and synchrony in the hippocampal formation and associated structures: the case for its role in sensorimotor integration. Behavioural Brain Research 2001;127:119-136.

Bohbot V, Iaria G, Petrides M. Hippocampal Function and Spatial Memory: Evidence From Functional Neuroimaging in Healthy Participants and Performance of Patients With Medial Temporal Lobe Resections. Neuropsychology 2004;18(3):418-425.

Borisoff JF, Mason GS, Bashashati A, Birch GE. Brain-computer Interface Design for Asynchronous Control Applications: Improvements to the LF-ASD Asynchronous Brain Switch. IEEE Transactions on Biomedical Engineering 2004; 51(6):985-992.

Brandeis R, Brandys Y, Yehuda S. The use of the Morris Water Maze in the study of memory and learning. International Journal of Neuroscience; 1989;48: 29-69.

Bressler SL. Large-scale cortical networks and cognition, Brain Research Reviews 1995;20;288-304.

Brown P, Day BL. Eye acceleration during large horizontal saccades in man. Experimental Brain Research 1997; 113:153-157.

Collette F, Van der Linden M. Brain imaging of the central executive component of working memory. Neuroscience and Biobehavioral Reviews, 2002;26:105-125.

Contreras-Vidal JL, Kerick SE. Independent component analysis of dynamic brain responses during visuomotor adaptation. NeuroImage, 2004;21(3):936-945.

Cui H, Andersen RA. Posterior parietal cortex encodes autonomously selected motor plans. Neuron 2007;56:552-559.

Cureton EE, Mulaik SA. The weighted varimax rotation and the promax rotation. Psychometrika 1975;40(2):183-195.

Danckert J, Revol P, Pisella L, Krolak-Salmon P, Vighetto A, Goodale M, Rossetti Y. Measuring unconscious actions in action-blindsight: exploring the kinematics of pointing movements to targets in the blind field of two patients with cortical hemianopia. Neuropsychologia 2003; 41:1068-1081.

D'arcy RCN, Connolly JF, Service E, Hawco CS, Houlihan ME. Separating Phonological and Semantic Processing in Auditory Sentence Processing: A High-Resolution Event-Related Brain Potential Study. Human Brain Mapping 2004;22:40-51.

Delorme A, Makeig S. EEGLAB: an open source toolbox for analysis of single-trial EEG dynamics including independent component analysis. J. Neuroscience Methods 2004;134:9-21.

De Lucia M, Fritschy J, Dayan P, Holder D. Detection of spikes in EEG recordings using features derived from ICA. Clinical Neurophysiology, 2006;117(1):139-140.

D'Hooge R, De Deyn PP. Applications of the Morris water maze in the study of learning and memory. Brain Research Reviews 2001;36:60-90.

Dien J. Issues in the application of the average reference: review, critiques, and recommendations. Behaviour Research Methods, Instruments & Computers 1998;30:34-43.

Dien J, Wayne K, George RM. Evaluation of PCA and ICA of Simulated ERPs: Promax vs. Infomax Rotations. Human Brain Mapping, 2007;28:742-763.

DiMattia BD, Kesner RP. Spatial cognitive maps: Differential role of the parietal cortex and hippocampal formation. Behav Neuroscience 1988;102:471-480.

Donchin E. A multivariate approach to the analysis of average evoked potentials. IEEE Transactions on Bio-Medical Engineering 1966; BME-13:131-139.

Donchin E, Heffley EF. Multivariate analysis of event-related potential data: A tutorial review. In Otto DA (Ed), Multidisciplinary Perspectives in Event-related Brain Potential Research. Washington, DC: U.S. Gov Printing Office. Pp. 555-572, 1978.

Dyrholm M, Makeig S, Hansen LK. Model Selection for Convolutive ICA with an Application to Spatiotemporal analysis of EEG. Neural Computation 2007;19(4):934-955.

Farah M. Visual Agnosia: Disorders of object recognition and what they tell us about normal vision 1990. (The MIT Press, Cambridge, MA).

Fellman DJ, Van Essen DC. Distributed hierarchical processing in the primate cerebral cortex. Cereb Cortex, 1991;1:1– 47.

Fuchs M, Wagner M, Kohler T, Wischmann HA. Linear and nonlinear current density reconstructions (Review). Journal of Clinical Neurophysiology 1999;16:267-295.

Fyhn M, Molden S, Witter MP, Moser EI, Moser MB. Spatial representation in the entorhinal cortex. Science 2004;305:1258-1264.

Gevins AS, Bressler SL, Morgan NH, Cutillo BA, White RM, Greer DS, Illes J. Event-related covariances during a bimanual visuomotor task. I. Methods and analysis of stimulus- and response-locked data. Electroencephalography and clinical Neurophysiology 1989;74:58–75.

Ghahremani D, Makeig S, Jung T-P, Bell AJ, Sejnowski TJ. Independent Component Analysis of Simulated EEG Using a Three-Shell Spherical Head Model. Technical Repoft INC-9601, Institute for Neural Computation, University of California San Diego. La Jolla CA, 1996.

Glover S. Separate visual representations in the planning and control of action. Behavioural and Brain Sciences 2004;27:3-78.

Goodale M. Visual pathways supporting perception and action in the primate cerebral cortex. Current Opinion in Neurobiology 1993;3:578-585.

Gorodnitsky IF, George JS, Rao BD. Neuromagnetic source imaging with FOCUSS: a recursive weighted minimum norm algorithm. Electroencephalography and Clinical Neurophysiology 1995; 95:231-251.

Grave de Peralta Menendez R, Gonzalez Andino SL. A critical analysis of linear inverse solutions. IEEE Trans Biomed Eng 1998;45:440-448.

Grave de Peralta Menendez R, Gonzalez SL. Discussing the capabilities of Laplacian minimization. Brain Topography 2000;13:96-104.

Grave de Peralta Menendez R, Andino SG, Lantz G, Michel CM, Landis T. Noninvasive Localization of Electromagnetic Epileptic Activity. I. Method Descriptions and Simulations. Brain Topography 2001;14(2):131-137.

Greenblatt RE, Probabilistic reconstruction of multiple sources in the neuroelectromagnetic inverse problem. Inverse Prob. 1993;9:271-284.

Hämäläinen MS, Ilmoniemi RJ. Interpreting measured magnetic fields of the brain: estimates of current distributions. Technical report TKK-F-A559, Helsinki University of Technology, Espoo; 1984

Hämäläinen MS, Ilmoniemi RJ. Interpreting magnetic fields of the brain—minimum norm estimates. Med. Biol. Eng. Comput. 1994;32:35-42.

measured magnetic fields of the brain: estimates of current distributions. Technical report TKK-F-A559, Helsinki University of Technology, Espoo; 1984

Hamilton DA, Kodituwakku P, Sutherland RJ, Savage DD. Children with Fetal Alcohol Syndrome are impaired at place learning but not cued-navigation in a virtual Morris water task. Behavioural Brain Research 2003;143:85-94.

Hartley T, Maguire EA, Spiers HJ, Burgess N. The Well-Worn Route and the Path Less Traveled: Distinct Neural Bases of Route Following and Wayfinding in Humans. Neuron 2003;37(5): 877-888.

Haykin S. Adaptive Filter Theory, 4th ed. New Jersey: Prentice Hall, 2002.

Hensen RN, Rugg MD. Neural resonse suppression, haemodynamic repetition effects, and behavioural priming. Neuropsychologia 2003;41(3):263-270.

Holzner B. Event-related correlation of EEG activity. MSc. Thesis, Graz University of Technology.

Husain M, Nachev P. Space and the parietal cortex. Trends in Cognitive Science 2007;11:30-36.

Hyvärinen A. Fast and Robust Fixed-Point Algorithms for Independent Component Analysis. IEEE Transactions on Neural Networks. 1999;10(3):626-734.

Hyvärinen A, Oja E. A fast fixed-point algorithm for independent component analysis. Neural Computation 1997;9(7):1483-1492.

Hyvärinen A, Karhunen J, Oja E. Independent Component Analysis. New York: John Wiley & Sons, 2001.

Hyvärinen A, Oja E. A fast and Robust Fixed-Point Algorithm for Independent Component Analysis. IEEE Transactions on Neural Networks, 1999;10(3):626-634.

Hyvärinen A, Oja E. Independent component analysis: algorithms and applications. Neural Networks, 2000;13(4-5):411-430.

Iaria G, Petrides M, Dagher A, Pike B, Bohbot VD. Cognitive strategies dependent on the hippocampus and caudate nucleus in human navigation: variability and change with practice. The Journal of Neuroscience 2003; 23(13):5945-5952.

Jackson GM, Eberly DA. Facilitation of performance on an arithmetic task as a result of the application of a biofeedback procedure to suppress alpha wave activity. Applied Psychology and Biofeedback 1982;7(2):211-221.

Jentzsch I. Independent Component Analysis Separates Sequence-Sensitive ERP Components. International Journal of Bifurcation and Chaos, 2004;14(2):667-678.

Jeong J, Gore JC, Peterson BS. A method for determinism in short time series and its application to stationary EEG. IEEE Transactions on Biomedical Engineering 2002;49(11):1374-1379.

Jung TP, Makeig S, Mckeown MJ, Bell AJ, Lee TW, Sejnowski TJ. Imaging Brain Dynamics Using Independent Component Analysis. Proceedings of the IEEE, v89, no7, 2001.

Jung TP, Makeig S, Westerfield M, Townsend J, Courchesne E, Sejnowki TJ. Analysis and visualization of single-trial event-related potentials. Human Brain Mapping, 2001;14(3):166-85.

Kaiser HF. The Varimax Criterion for Analytic Rotation in Factor Analysis. Psychometrika 1958;23(3):187-200.

Kim YJ, Grabowecky M, Paller KA, Muthu K, Suzuki S. Attention induces synchronization-based response gain in steady-state visual evoked potentials. Nature Neuroscience 2007;10:117-125.

Klimesch W. EEG alpha and theta oscillations reflect cognitive and memory performance: a review and analysis. Brain Research Reviews 1999;29:169-195.

Knoblauch A, Sommer FT. Synaptic plasticity, conduction delays, and inter-areal phase relations of spike activity in a model of reciprocally connected areas. Neurocomputing 2003; 52(44):301-306.

Kobayashi K, Akiyama T, Nakahori T, Yoshinaga H, Gotman J. Systematic source estimation of spikes by a combination of independent component analysis and RAP-MUSIC. I: Principles and simulation study. Journal of Clinical Neurophysiology, 2002;113(5):713-724.

Kolb B, Sutherland RJ, Whishaw IQ. A comparison of the contributions of the frontal and parietal association cortex to spatial localization in rats. Behav Neuroscience 1983;97:13-27.

Kolb B, Walkey J. Behavioural and anatomical studies of the posterior parietal cortex in the rat. Behav Brain Research 1987;23:127-145.

Koles ZJ, Soong ACK. EEG source localization: implementing the spatio-temporal decomposition approach. Electroencephalography and Clinical Neurophysiology, 1998;107:343-352.

Kopp F, Schroger E, Lipka S. Neural networks engaged in short-term memory rehearsal are disrupted by irrelevant speech in human subjects. Neuroscience Letters 2004;354:42-45.

Kosslyn SM, Pascual-Leone A, Felician O, Camposano S, Keenan JP, Thompson WL, Ganis G, Sukel KE, Alpert NM. The Role of Area 17 in Visual Imagery: Convergent Evidence from PET and rTMS. Science 2 1999, vol 284 no 5411, 167-170.

Languis ML, Miller DC. Luria's Theory of brain functioning: A model for research in cognitive psychology. Educational Psycologist 27(4), 493-511, 1992

Law I, Svarer C, Rostrup E, Paulson O. Parieto-occipital cortex activation during self-generated eye movements in the dark. Brain 1998:121;2189-2200.

Leal AJR, Dias AI, Vieira JP. Analysis of the EEG dynamics of epileptic activity in gelastic seizures using decomposition in independent components. Clinical Neurophysiology, 2006;117(7):1595-1601.

Lee T-W, Girolami M, Bell AJ, Sejnowski TJ. A unifying information-theoretic framework for independent component analysis. Computers and Mathematics with Applications, 2000;39:1-21.

Lee T-W, Girolami M, Sejnowski T. Independent component analysis using extended infomax algorithm for mixed sub-Gaussian and super-Gaussian sources. Neural Computation, 1999;11(2):609-633.

Leocani, L, Locatelli T, Martinelli V, Rovaris M, Falautano M, Filippi M, Magnani G, Comi G. Electroencephalographic coherence analysis in multiple sclerosis: correlation with clinical, neuropsychological, and MRI findings. Journal of Neurology, Neurosurgery, and Psychiatry 2000;69:192-198.

Livingstone S, Skelton R. Virtual environment navigation tasks and the assessment of cognitive deficits in individuals with brain injury. Behavioural Brain Research 2007;185(1):21-31.

Luria, AR. The working Brain. Harmondsworth, England: Penguin, 1973.

Maguire EA, Burgess N, Donnett JG, Frackowiak RSJ, Frith CD, O'Keefe J. Knowing Where and Getting There: A Human Navigation Network. Science 1998;280:921-924.

Makeig S, Jung TP, Ghahremani D, Bell AJ, Sejnowski TJ. Blind separation of auditory event-related brain responses into independent components. Proc Natl Acad Sci USA 1997;94:10979-10984.

Makeig S, Bell A, Jung T, Sejnowski, T. Independent component analysis of electroencephalographic data. In: Touretzky D, Mozer M, Hasselmo M (Eds). Advances in Neural Information Processing Systems. MIT Press, 1996;8:145-151.

Makeig S, Jung T-P, Ghahremani D, Sejnowski TJ. Independent Component Analysis of Simulated ERP Data. In: Nakada T (Ed). Integrated Human Brain Science: Theory, Method, Applications (Music). Elsevier, 2000.

Makeig S, Delorme A, Westerfield M, Jung TP, Townsend J, Courchesne E, Sejnowski TJ. Electroencephalographic Brain Dynamics Following Manually Responded Visual Targets. Public Library of Science Biology, 2004;2(6);747-762.

Makeig S. Beyond Blind Averaging: Analyzing Event-Related Brain Dynamics. Institute for Neural Computation, University of California San Diego, La Jolla, CA. Retrieved April 17, 2007 from http://cogimage.dsi.cnrs.fr/documents/MBM2005_MEEGCourse/Makeig.pdf

Makeig S, Bell A, Jung T, Sejnowski, T. Independent component analysis of electroencephalographic data. In: Touretzky D, Mozer M, Hasselmo M (Eds). Advances in Neural Information Processing Systems. MIT Press, 1996;8:145-151.

Marosi E, Harmony T, Becker J, Reyes A, Bernal J, Fernandez T, Rodriguez M, Silva J, Guerrero V. Electroencephapographic coherences discriminate between children with different pedagogical evaluation. International Journal of Psychophysiology 1995;19:23-32.

Masson EJM, Loftus GR. Using Confidence Intervals for Graphically Based Data Interpretation. Canadian Journal of Experimental Psychology 2003;57(3):203-220.

Mazzoni P, Bracewell RM, Barash S, Andersen RA. Motor intention activity in the Macaque's lateral intraparietal area. 1. Dissociation of motor plan from sensory memory. Journal of Neurophysiology 1996;76:1439-1456.

McCarthy G, Wood CC. Scalp distributions of event-related potentials: an ambiguity associated with analysis of variance models. Electroenceph. Clin. Neurophysiol., 1985;62: 203-208.

Meghdadi AH, Fezel-Rezai R, Aghakhani Y. Detecting Determinism in EEG Signals using Principal Component Analysis and Surrogate Data Testing. Proceedings of the 28th IEEE EMBS Annual International Conference 2006

Menendez RGP, Andino SG. Comparison of Algorithms for the Localization of Focal Sources: Evaluation with Data and Analysis of Experimental Data. V4 n?. International Journal of Bioelectromagnetism

Mesulam MM. From sensation to cognition. Brain 1998;121(6),1013-1052.

Michel C M, Seeck M, Landis T. Spatiotemporal Dynamics of Human Cognition. News Physiol. Sci, 1999;14:206-214.

Michel MC, Murray MM, Lantz G, Gonzalez S, Spinelli L, de Peralta RG, Invited Review: EEG source imaging. Clinical Neurophysiology, 2004;115:2195-2222.

Morris R. Spatial localization does not require the presence of local cues. Learning and Motivation 1981; 12:239-260.

Morris R, Garrud P, Rawlins JN, O'Keefe J. Place navigation impaired in rats with hippocampal lesions. Nature 1982;297(5868): 681-683.

Mosher JC, Leahy RM. EEG and MEG Source Localization using Recursively Applied (RAP) MUSIC. Proceedings Thirtieth Annual Asilomar Conference on Signals, Systems, and Computers, Pacific Grove, CA, Nov 3-6, 1996

Mulholland TB. The concept of attention and the electroencephalographic alpha rhythm. In: Evans CR, Mulholland TB (Eds.) Attention in Neurophysiology. London Butter-worths, 1969.

Nadel L. The hippocampus and space revisited. Hippocampus 1991;1:221-229.

Nadel, L, Hardt, O. The Spatial Brain. Neuropsychology 2004;18(3): 473-476.

Nishitani N, Schürmann M, Amunts K, Hari R. Broca's Region: From Action to Language. Physiology 2005. 20:60-69.

Nitz DA. Tracking route progression in the posterior parietal cortex. Neuron 2006;49:747-756.

Nunez PL. Generation of Human EEG by a Combination of Long and Short Range Neocortical Interactions. Brain Topography 1989;1(3):199-215.

Nunez PL, Srinivasan R, Westdorp AF, Wijesinghe RS, Tucker DM, Silberstein RB, Cadusch PJ. EEG coherency I: statistics, reference electrode, volume condition, Laplacians, cortical imaging, and interpretation at multiple scales. Electroencephalography and Clinical Neurophysiology 1997;103(5):499-515.

Nunez PL, Neocortical Dynamics and Human EEG Rhythms. New York: Oxford University Press, 1995

Ojemann,G Ojemann J., Lettich E., Burger M. Cortical language organization in left, dominant hemisphere. Journal of Neurosurgery 1989; 71: 316-326.

O'Keefe J, Dostrovsky J. The hippocampus as a spatial map: Preliminary evidence from unit activity in the freely-moving rat. Brain Research 1971;34:171-175.

O'Keefe J, Nadel L. The hippocampus as a cognitive map 1978; Oxford: Oxford University Press

Onton J, Delorme A, Makeig S. Frontal midline EEG dynamics during working memory. NeuroImage 2005;17(2):341-356.

Onton J, Makeig S. Information-based modeling of event-related brain dynamics. In: Neuper C, Klimesch W, editors. Event-Related Dynamics of Brain Oscillations. Progress in Brain Research vol.159. Amsterdam: Elsevier, 2007.

Pahapill PA, Lozano AM. The pedunculopontine nucleus and Parkinson's disease. Brain 2000;123:1776-1783.

Parra L, Sajda P. Converging Evidence of Linear Independent Components in EEG, Proc 1st Int'l IEEE EMBS Conf. Neural Eng 2003;525-528.

Parvizi J, Van Hoesen GW, Buckwalter J, Damasio A. Neural connections of the posteromedial cortex in the macque. PNAS 2006;103(5):1563-1568.

Pasqual-Marqui RD, Michel CM, Lehmann D. Low resolution electromagnetic tomography: a new method to localize electrical activity in the brain. International Journal of Psychophysiology 1994;18:49-65.

Pfurtscheller G, Neuper C. Simultaneous EEG 10 Hz desynchronization and 40 Hz synchronization during finger movements. Neuroreport 1992;3(12):1057-1060.

Pfurtscheller G, Neuper C. Event-Related synchronization of mu rhythm in the EEG over the cortical hand area in man. Neuroscience Letters 1994;174:93-96.

Raghavachari S, Kahana MJ, Rizzuto DS, Caplan JB, Kirschen MP, Bourgeois B, Madsen JR, Lisman JE. Gating of Human Theta Oscillations by a Working Memory Task. The Journal of Neuroscience 2001;21(9):3175-3183.

Rasmussen T, Milner B. The role of early left brain injury in determining lateralization of cerebral speech function, Annals of the New York Academy of Sciences 1997;299:355-369.

Rodriguez E, George N, Lachaux JP, Martinerie J, Renault B, Varela FJ. Perception's shadow: long-distance synchronization of human brain activity. Letters to nature 1999;397:430-433.

Roelfsema, PR, Engel AK, Konig P, Singer W. Visuomotor integration is associated with zero time-lag synchronization among cortical areas. Nature 1997; 385:157-161.

Ross, S, Skelton, R, Mueller, S. Gender differences in spatial navigation in virtual space: Implications when using virtual environments in instruction and assessment. 2006. Virtual Reality (Downloaded on the 15th of November, 2008, http://portal.acm.org/citation.cfm?id=1183181)

Rugg MD, Coles MGH. Electrophysiology of Mind: Event-Related Brain Potentials and Cognition. Oxford University Press, Oxford, New York, 2002.

Scherg M, Berg P. New concepts of brain source imaging and localization. In: Barber C, Celesia G, Comi GC, Maguiere F, eds. Functional Neuroscience. Amsterdam: Elsevier Science B.V. 1996; 127-137.

Schmidt RO. Multiple Emitter Location and Signal Parameter Estimation. IEEE Transactions on antennas and propagation, 1986;AP-34(3).

Shepherd GM. The Synaptic Organization of the Brain. 5th ed. Oxford, NY: Oxford University Press, 2004

Silberstein P, Pogosyan A, Kuhn AA, Hotton G, Tisch S, Kupsch A, Dowsey-Limousin P, Hariz MI, Brown P. Cortico-cortical coupling in Parkinson's disease and its modulation by therapy. Brain 2005,128:1277-1291.

Sklar B, Hanley J, Simmons WW. An EEG experiment aimed toward identifying dyslexic children. Nature 1972;240:414-416.

Snyder LH, Bastista AP, Andersen RA. Coding of intention in the posterior parietal cortex. Nature 1997;386:167-170.

Snyder LH, Grieve KL, Brotchie P, Andersen RA. Separate body- and world-referenced representations of visual space in parietal cortex. Nature 1998;394:887-891.

Sorensen PL, Zeman PM, Sutherland RJ. Differing patterns of synchronous cortical activity during a virtual spatial navigation task. Canadian Society for Brain, Behaviour and Cognitive Science, 16th Annual Meeting. Paper presentation. 2006.

Spencer KM, Dien J, Donchin E. A componential analysis of the ERP elicited by novel events using a dense electrode array. Phychophysiology 1999;36:409-414.

Spiers HJ, Maguire EA. Thoughts, behaviour, and brain dynamics during navigation in the real world. NeuroImage 2006;31:1826-1840.

Streletz LJ, Katz L, Hohenberger M, Cracco RQ. Scalp recorded auditory evoked potentials and sonomotor responses: an evaluation of components and recording techniques. Electroencephalography and Clinical Neurophysiology 1977;43:192-206.

Stepien R. Testing for non-linearity in EEG signal of healthy subjects. Acata Neurobiol. Exp. 2002;62:277-281.

Stone JV. Independent component analysis: an introduction. Trends in Cognitive Sciences, 2002;6(2): 59-64.

Suffczynski P, Pijn J P M, Pfurtscheller G, Lopes da Silva F H. Event-related dynamics of alpha band rhythms: a neuronal network model of focal ERD/surround ERS. In: Pfurtscheller and Lopes da Silva Eds. Handbook of Electroencephalography and Clinical Neurophysiology: Event-Related Desynchronization. Revised Series, v6. Amsterdam, The Netherlands:Elsevier, 1999.

Summerfield C, Mangels JA. Functional coupling between frontal and parietal lobes during recognition memory. Brain Imaging 2005;8;16(2):117-122.

Taira M, Mine S, Georgopoulos AP, Murata A, Sakata H. Parietal cortex neurons of the monkey related to the visual guidance of hand movement. Experimental Brain Research 1990;83:29-36.

Takada M, Tokuno H, Nambu A, Inase M. Corticostriatal projections from the somatic motor areas of the frontal cortex in the macaque monkey: segregation versus overlap of input zones from the primary motor cortex, the supplementary motor area, and the premotor cortex. Experimental Brain Research 1998;120:114-128.

Tikhonov AN. Solution of incorrectly formulated problems and the regularization method. Soviet Doklady 1963; 4, pp. 1035-1038.

Townsend J, Courchesne E. Parietal damage and narrow “spotlight” spatial attention. J Cogn Neurosci 1994;6:220–232.

Trenado C, Haab L, Strauss DJ. Modeling Neural Correlates of Auditory Attention in Evoked Potentials using Corticothalamic Feedback Dynamics. Proceedings of the 29th Annual International Conference of the IEEE EMBS. Cite Internationale, Lyon, France. Aug. 2007.

Trujillo-Barreto NJ, Aubert-Vazquez E, Valdes-Sosa PA. Bayesian model averaging in EEG/MEG imaging. NeuroImage 2004;4:1300-1319.

Ungerleider LG, Mishkin M. Two cortical visual systems. Analysis of Visual Behavior 1982, Eds: Ingle DJ, Goodale MA, Mansfield RJW (The MIT Press, Cambridge, MA), pp 549-586.

Urrestarazu E, LeVan P, Gotman J. Independent component analysis identifies ictal bitemporal activity in intracranial recordings at the time of unilateral discharges. Clinical Neurophysiology, 2006;117(3):549-561.

Van Veen BD, van Drongelen W, Yuchtman M, Suziki A. Localization of Brain Electrical Activity via Linearly Constrained Minimum Variance Spatial Filtering. IEEE Transactions on Biomedical Engineering 1997;44:867-880.

Varela F, Lachaux JP, Rodriguez E, Martinerie J. The Brainweb: Phase synchronization and large-scale integration. Nature Neuroscience Reviews 2001;2:229-239.

Vigário R, Särelä J, Jousmäki V, Hämäläinen M, Oja E. Independent Component Approach to the Analysis of EEG and MEG Recordings. IEEE transactions on biomedical engineering 2000; 47(5):589-593.

Von Stein A, Sarnthein J. Different frequencies for different scales of cortical integration: from local gamma to long range alpha/theta synchronization. International Journal of Psychophysiology 2000;38:301-313.

Weiss S, Muller HM. The contribution of EEG coherence to the investigation of language. Brain and Language 2003;85:325-343.

White NM, McDonald RJ. Multiple Parallel Memory Systems in the Brain of the Rat. Neurobiology of Learning and Memory 2002;77(2):125-184.

Wilenius-Emet M, Revonsuo A, Ojanen V. An electrophysiological correlate of human visual awareness. Neuroscience Letters, 2004;354:38-41.

Witlock JR, Sutherland RJ, Witter MP, Moser MB, Moser EI. Navigating from hippocampus to parietal cortex. PNAS 2008;105(39):14755-14762.

Yao D. A method to standardize a reference of scalp EEG recordings to a point at infinity. Physiological Measurement 2001;22:693-711.

Yao D, Wang L, Oostenveld R, Nielsen KM, Arendt-Nielsen L, Chen ACN. A comparative study of different references for EEG spectral mapping: the issue of the neutral reference and the use of the infinity reference. Physiological Measurement 2005; 26:173-184.

Zani A, Proverbio AM. Attention modulation of C1 and P1 components of visual evoked potentials. Electroencephalography and Clinical Neurophysiology 1997;103(1):97-97.

Zeman PM, Mahajan SV, Livingstone SA, Driessen PF, Skelton RW, Livingston NJ. Beamform Volume Projection of EEG ICA Topographies. (for publication) 2008b.

Zeman PM, Mahajan SV, Livingstone SA, Driessen PF, Skelton RW, Livingston NJ. Volume Domain Validation of ICA-Derived EEG Sources. (for publication) 2008d.

Zeman PM, Mahajan SV, Livingstone SA, Livingston NJ, Skelton RW. Spectral Shaping to Relax ICA Assumptions to Facilitate Decomposition of EEG. (for publication). 2008e.

Zeman PM, Livingstone SA, Livingston NJ, Skelton RW. Building a Multi-Component Spatio-Temporal Model Using Scalp-EEG Data. (for publication) 2008f.

Zeman PM, Livingstone SA, Livingston NJ, Skelton RW. Feasibility of System Analysis of Brain Activity for Spatial Navigation using Scalp-EEG. (for publication). 2008g.

Zeman PM, Mahajan SV, Sorensen PL, Driessen PF, Skelton RW, Livingston NJ. Beamform Volume Projection of ICA Components of Scalp EEG: Volume-Domain Uniqueness of Components. (for publication) 2007c.

Zeman PM, Sorensen PL, Livingstone SA, Skelton RW, Livingston NJ. Understanding and Improving ICA Source Separation of EEG Data. (for publication) 2008a.

Zhang K, Chan L-W. An Adaptive Method for SubBand Decomposition ICA. Communicated by Hyvarinen, A. Neural Computation 2006:18;191-223.

APPENDIX A. VOLUME ESTIMATION AND VALIDATION: UNIVERSITY OF LETHBRIDGE STUDY

The figures in this appendix demonstrate results calculated for the University of Lethbridge study of Fetal Alcohol Spectrum Disorder (FASD) using the tools developed in this dissertation. These results demonstrate three important points that emphasize the practicality and effectiveness of these tools. First, the results demonstrate that the ICA rotation of the data provided by the runica algorithm, on average, offers improved brain activity estimates over the initial PCA separation of data into uncorrelated parts. Second, the results demonstrate that the volume-domain validation methodology described in Chapter 5, when applied to a real EEG data analysis problem, provides useful and relevant criteria to help determine which components might relate to real brain sources and be used in further analysis. Third, brain source volumes that were found from real EEG using the volume estimation algorithm of Chapter 3 are also depicted in this appendix. Taken together, these results demonstrate the value of these tools to research being conducted at the University of Lethbridge. A description of their data collection paradigm and descriptions of the results calculated for each of these tools are provided in the sections below.

DATA COLLECTION PARADIGM

Approval for this study was granted by the ethics committee of the University of Lethbridge. Participants in the study belonged to one of two groups: persons with an FASD rating based on neuropsychological scoring (10 persons), and a socially matched FASD control group (10 persons). The data for both groups were pooled to comprise a dataset of 20 female participants.

A 1st-person perspective computer-based virtual Morris Water Task paradigm (Sorensen et al., 2006) was used to elicit and capture brain activities related to spatial navigation. This EEG collection paradigm is similar to the behavioral paradigm used by Hamilton et

al., (2003). The paradigm uses two different behavioral conditions corresponding to two types of trials, cue and place. To complete each type of trial successfully, participants were required to select and use the appropriate of the two behavioral strategies. For each type of trial, participant's avatars are placed inside an arena maze and are required to navigate to the 'correct' platform to escape the maze. During the place condition, the two platforms were visually identical; navigation was possible via wall-mounted pictures. For the cue condition, the platforms displayed visually distinctive color patterns.

Participants were seated approximately 180 cm from a 40 cm CRT computer screen. The two strategies to complete the task were described to each participant. For each of the behavioral conditions examined, participants were given practice trials until it was clear they understood how to complete the task.

The paradigm consisted of multiple visual stimuli for which each subject was required to interpret and to respond. The virtual environment consisted of a round pool placed in a square room. A unique image, framed as a picture, was placed on each of the four walls. The two visible square platforms were placed in different quadrants of the pool. To navigate in the virtual pool, participants pressed the left/right arrow keys on a keyboard. For each trial, participants began in a random starting location along the pool wall. When the participant reached the incorrect platform, forward motion would continue and the participant would appear to "swim through the platform". When the participant reached the correct platform, forward motion would stop and the phrase "Platform Found" was presented on the screen. Different sets of wall-mounted pictures (place condition) and platform colors (cue condition) were presented for each block of trails. Each participant completed 20 blocks of each condition. Each block consisted of four trials during which the platform locations remained constant. The distal cues on the four walls remained constant during each block. Place and cue blocks alternated throughout the session. Prior to the commencement of each block, the participants viewed a blank screen with a fixation point, '+' in the center of the screen, for 2000 ms. They then viewed a pre-trial signal, "Place" or "Cue" for 1000 ms to indicate which navigation strategy should be used to complete the impending block of trials. Between trials within each block,

participants viewed a blank screen with a fixation point, '+' in the center of the screen, for 2000 ms.

DATA ANALYSIS

Components were calculated from a single ICA decomposition of a grand EEG dataset. Each participant contributed 29 trials for each of the 2 behavioral conditions. To reduce the memory requirements to process the data, the sampling rate was reduced. The data of each trial were band-pass filtered from 3 Hz to 80 Hz using a 60-point zero-phase FIR filter and then down-sampled to 250 samples/second. Each of the datasets were concatenated to provide for a single grand dataset of 112 channels with 1015000 samples (i.e. 29 trials x 875 samples/trial x 20 subjects x 2 conditions). While the concatenation of datasets from multiple subjects does weaken the assumption of spatial stationarity, our experience is that this effect is more than offset by the overall increase in the quantity of data.

The runica algorithm was used to compute component activities and topographies. Using the runica 'PCA' parameter, the rank of the data was reduced to 60 dimensions.

The validation methodology described in Chapter 5 was used to determine which components of the decomposition likely represent activities of the brain. This analysis was done by examining both the convergence of averages of various volume characteristics and the convergence of volume characteristics of each component separately. These characteristics include the peak spectral value (PSV), the median volume overlap (MVO), the average volume overlap (AVO), and the center of mass travel distance (DT) at each iteration of the runica algorithm. Component validation was based on ranking each component by their corresponding PSV and MVO scores. The center of mass total distance traveled (TDT) of each component and the variance of the DT over runica iterations was also calculated. Each of these values was derived from the topographies of each component via projecting their variance into the head model using

the volume projection algorithm described in Chapter 3. This volume projected variance is herein referred to as the volumetric spectrum.

The PSV was derived as the largest value of all the coefficients defining the volumetric spectrum. The MVO and AVO were derived as dot products of the normalized volumetric spectrum coefficients. The DT was calculated by estimating the center of mass of each component at each successive iteration of the algorithm and subtracting the difference between iterations.

The volumes of each of the validated components that did not pertain to eye-movement or eye-blink artifacts were estimated. The volume estimation algorithm described in Chapter 3 was used to estimate the physical boundary of each brain source for a confidence of 3 standard deviations above the mean (3 STDM) volume-domain noise estimate. These volumes were plotted on a canonical white matter head model in various colors for easy identification.

RESULTS

The 60 topographies plotted in Figure A1 calculated via the ICA decomposition of EEG data illustrate that it is not an easy task to manually determine which components might relate to activities originating from distinct modular areas of the brain. Further, each component has a varied amount of noise contamination and the relative quality of estimates is not clear.

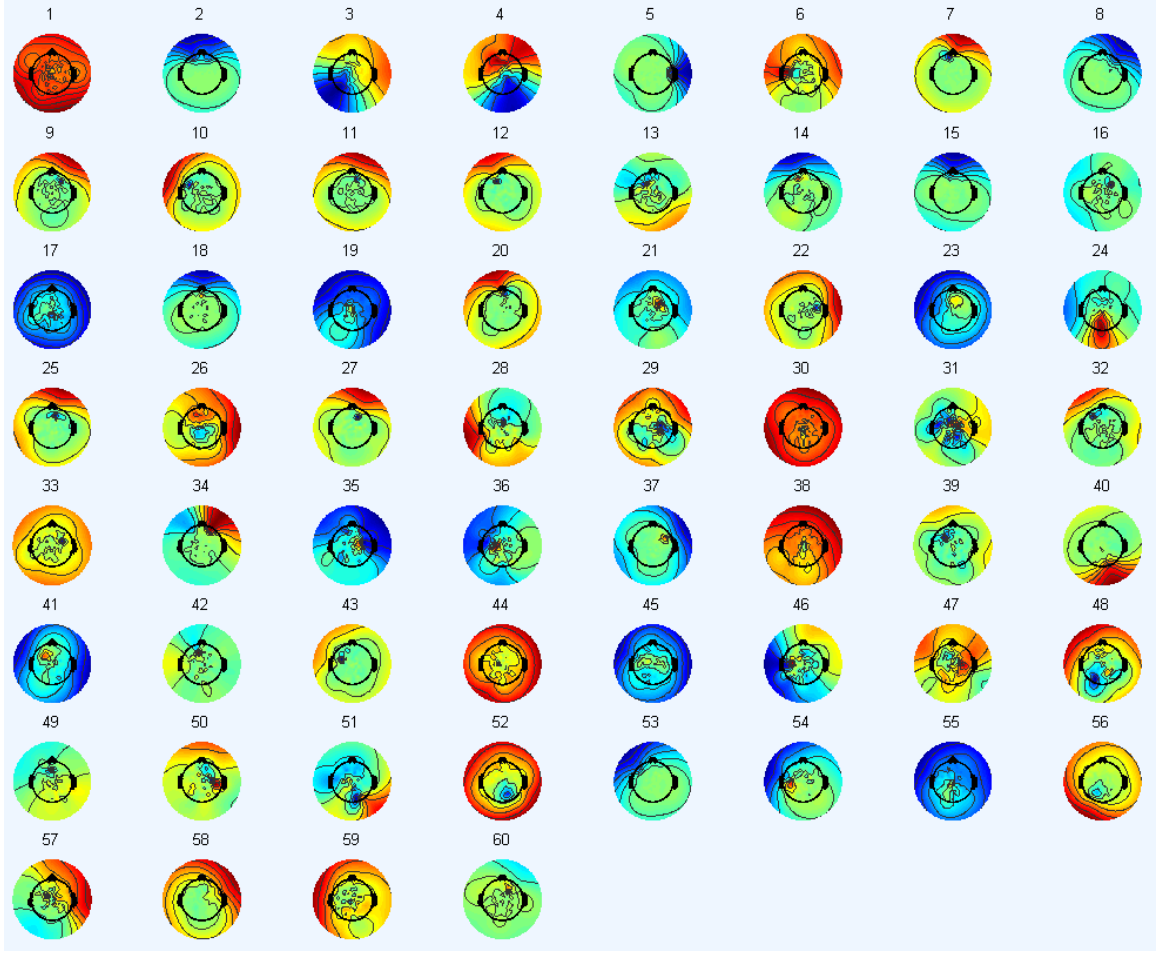

Figure A1. Topographies calculated via the ICA decomposition of EEG data. Colors represent relative electrode weights: blue indicates most negative weights; red indicates most positive weights.

The waveforms plotted in Figure A2 illustrate that while runica iterates and improves the estimate of statistically independent sources, the average and median volume characteristics of components of the EEG improve. The average and median PSV illustrated in Figure A2a shows that by iteration 200, brain sources have been appropriately estimated. This is similarly represented by the median and average curves for the MVO and the AVO. Changes in these curves occurring after iteration 600 suggest some overtraining of the runica source separation matrix on noise.

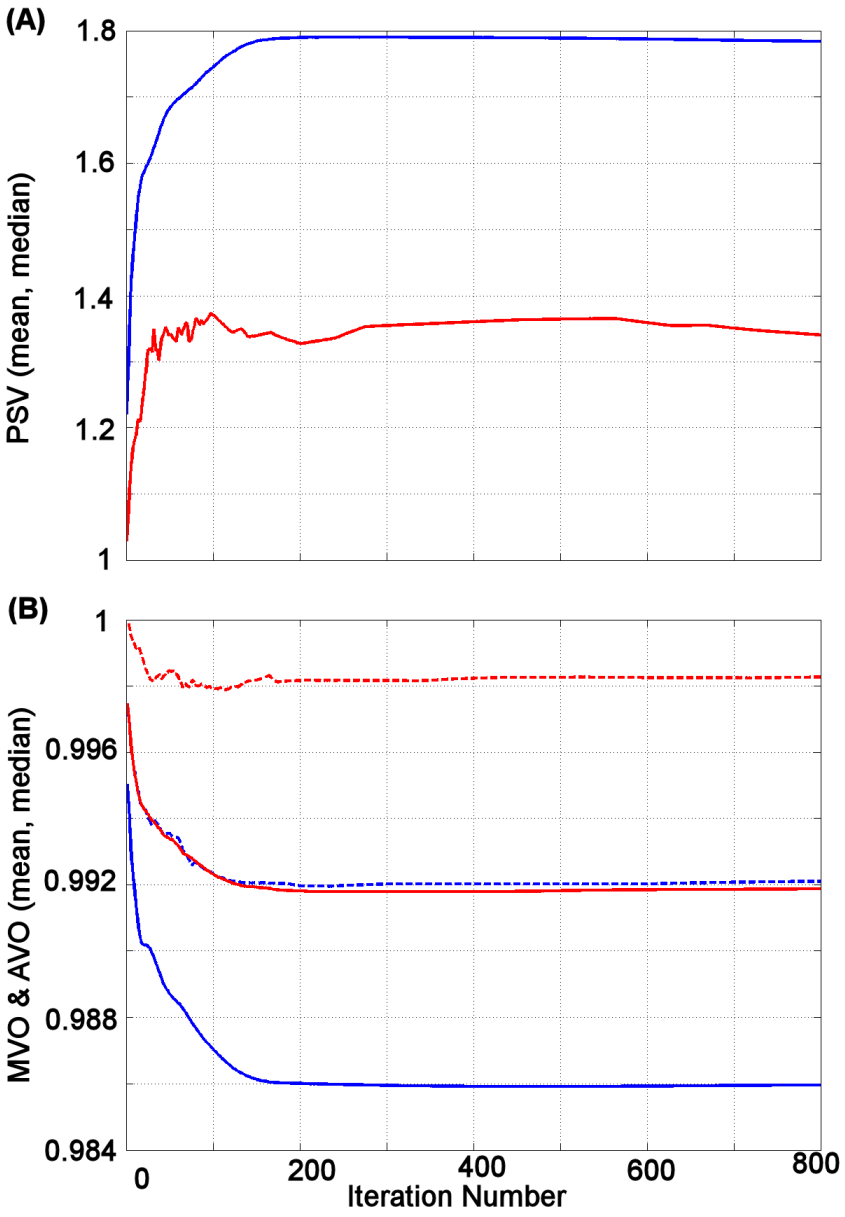

Figure A2. Plot showing average and median convergence characteristics of source estimates over iterations of the runica algorithm. (A) the average and median PSV represented in blue and red, respectively. (B) the average MVO represented by the red solid line; the median MVO represented by the red dashed line; the average AVO represented by the blue solid line; the median AVO represented by the blue dashed line.

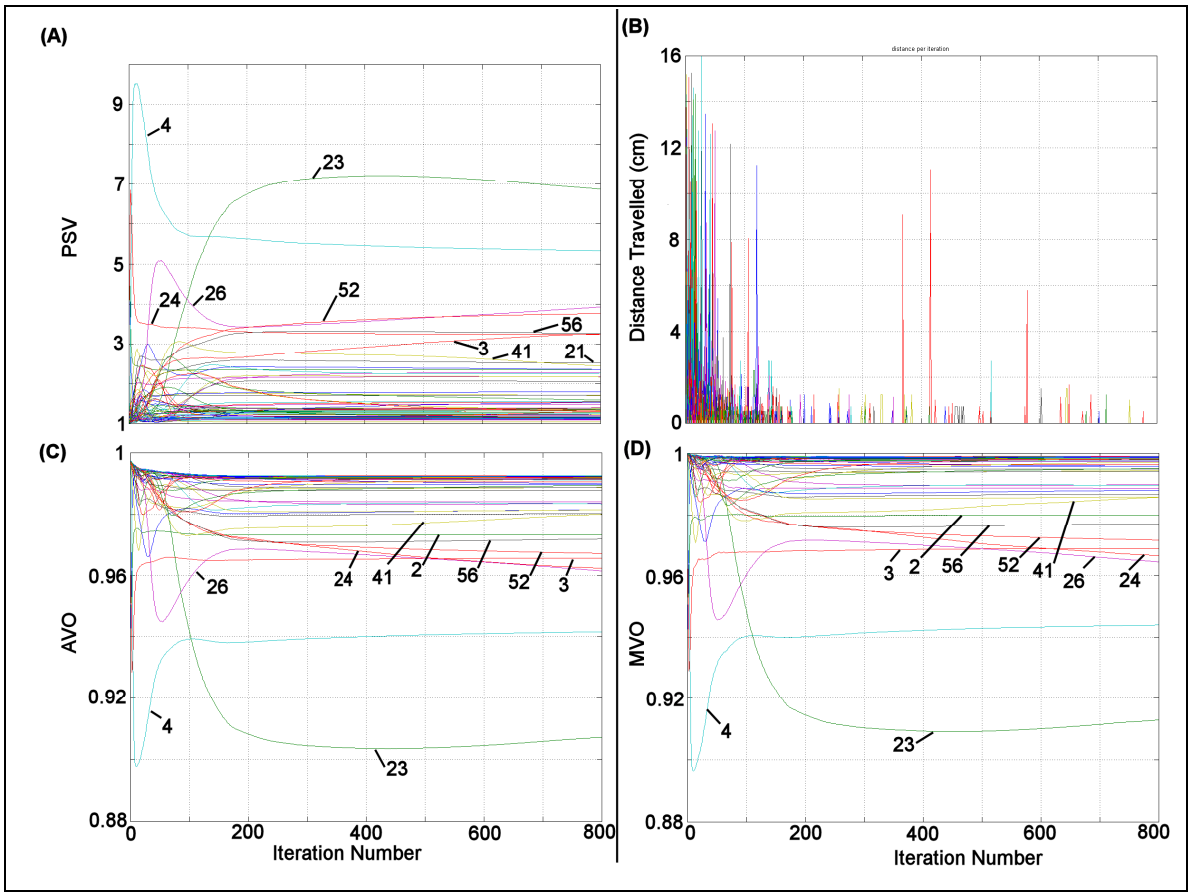

Figure A3. Individual convergence curves of each component. (A) the peak spectral value (PSV); (B) the center of mass distance traveled (DT); (C) the average volume overlap (AVO); (D) the median volume overlap (MVO). Where there separation of curves allows, components have been numbered with the same labels as in Figure A1.

Since it is difficult to place component numbers of Figure A3b, those components that had non-zero distance traveled for iteration 300 to 800 have been indicated in Table 1. The iteration numbers for which each late-converging component had a non-zero distance are indicated.

Component #	Iteration Number
1	306, 352, 442
13	373
21	605
24	448
25	520
26	354
28	321, 459, 460, 461, 462, 463, 466, 470, 472, 473
37	681
41	306, 333, 334, 335, 385
45	370, 417, 425, 506, 519, 577, 581, 652, 689
48	647, 648, 549, 755
51	306, 715
57	376, 703
58	314, 376, 415
59	314, 454, 500, 638, 675, 778

Table 1. A list of the components with late iterations and corresponding iteration numbers.

The plots of Figures A4 and A5 contain the sorted final scores for each component. These plots illustrate the relative goodness of each component as originating from inside the head. They may also represent brain activities from distinct areas of the brain and the reliability of the estimate according to the movement of the center of mass of each component over iterations of the runica algorithm.

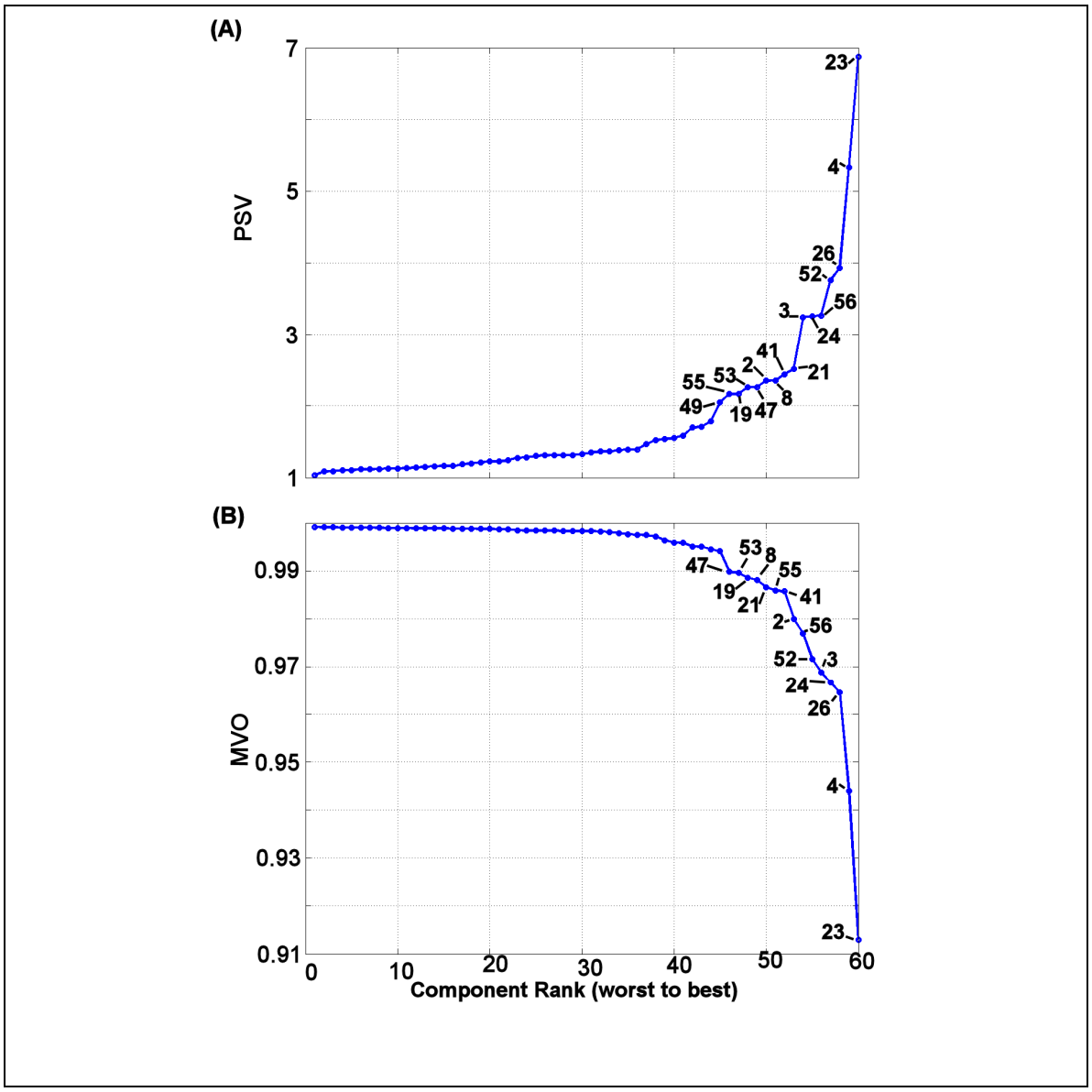

Figure A4. Sorted PSV and MVO scores for the final runica iteration. Component numbers are provided for those components with scores beyond the knee of each curve. A complete list of the ranked component scores for the PSV and MVO is provided in Table 1.

Figure A5 illustrates the relative scores calculated for the movement of the center of mass of each component over iterations. The sorted TDT scores of Figure A5a shows which components moved by small amounts versus those that move large distances around the head. For example, components 49, 45, 18, 53, 38, 36 are the 6 components that moved the greatest distance over iterations. The sorted DT variance scores of Figure A5b

provide another indication of which components had the greatest and least variability of location during runica iterations. For example, components 49, 18, 53, 45, 43, and 38 are the 6 components with the greatest variability of center of mass compared to other components.

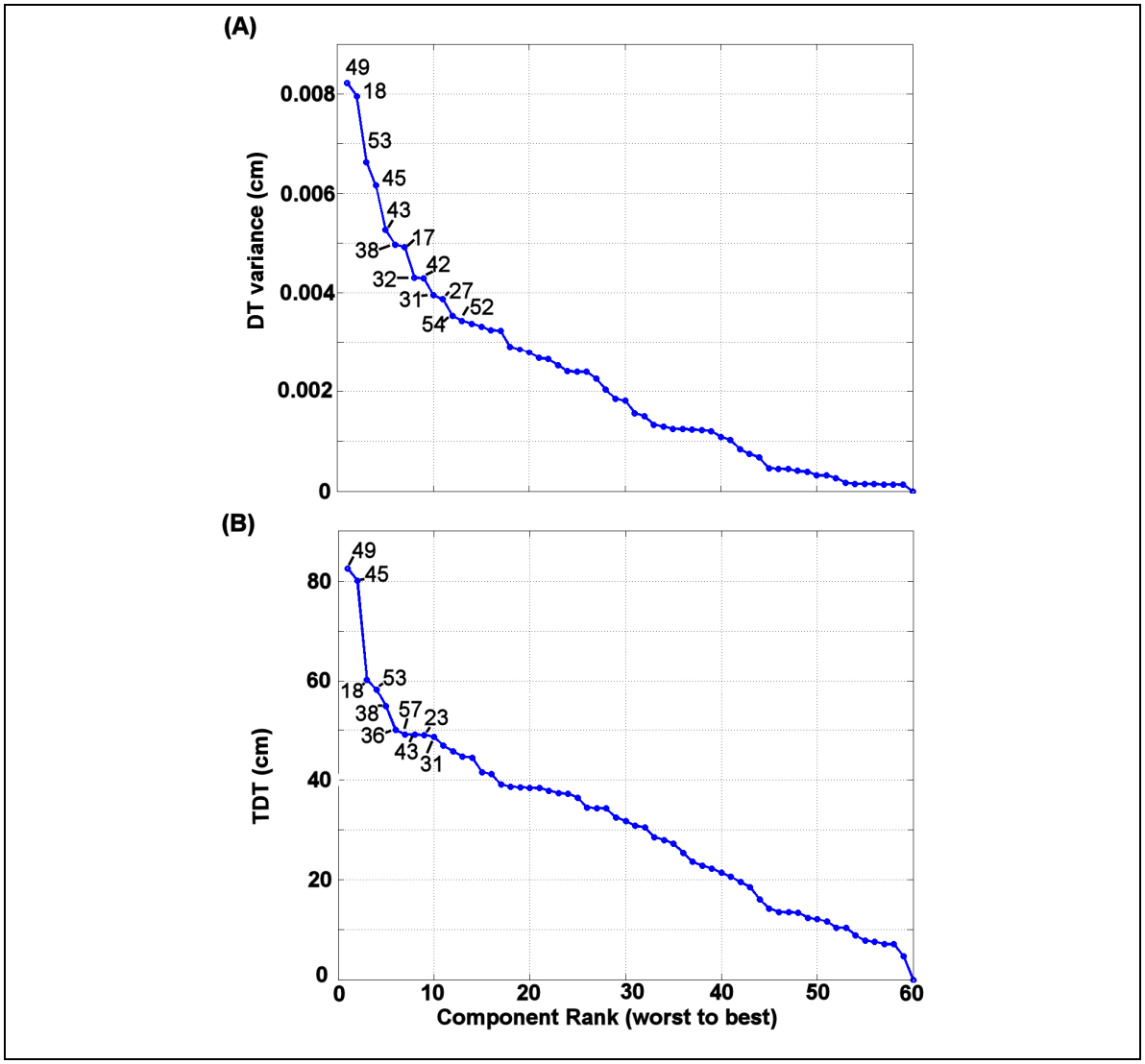

Figure A5. Sorted TDT and DT variance scores for the final runica iteration. Component numbers are provided for those components with scores beyond the knee of each curve. A complete list of the ranked component scores for the TDT and DT variance is provided in Table 1.

The tabulated components are listed in order of best to worst for each measure in Table 1.

PSV			**MVO**			**TDT**			**DT variance**		
23	4	26	23	4	26	11	20	29	11	15	29
52	56	24	24	3	52	5	7	9	20	4	2
3	21	41	56	2	41	15	3	19	3	9	7
8	2	47	55	21	8	2	4	6	6	5	1
53	19	55	19	53	47	25	22	56	14	8	25
49	15	35	35	6	49	14	60	12	19	58	22
6	58	32	58	36	15	35	10	8	35	12	47
38	36	54	38	48	30	26	46	1	26	24	55
40	34	30	54	32	40	34	16	30	44	60	51
37	17	28	37	59	34	44	58	13	33	48	10
48	59	10	28	10	17	28	37	33	59	56	36
44	25	45	9	16	44	55	40	24	41	37	28
9	16	39	25	27	57	41	42	21	46	50	39
1	27	14	39	51	46	39	32	47	21	34	16
12	42	46	1	29	13	51	48	52	30	23	57
13	50	31	42	14	45	59	54	17	13	40	52
51	43	57	50	12	31	50	27	31	54	27	31
22	60	11	60	20	18	23	43	57	42	32	17
29	7	5	7	11	43	36	38	53	38	43	45
33	18	20	33	5	22	18	45	49	53	18	49

Table 1. Component number scores sorted from best (top) to worst (bottom) for the PSV, MVO, TDT, and DT variance. For each measure, the descending order of components is from top left to the top right and then down to the following line. For example, the PSV in descending is 23, 4, 26, 52, 56, 24, 3, …, 5, 33, 18, 20.

The component scores for the PSV and the MVO implicate components 32, 4, 26, 52, 56, 24, 3, 21, 41, 8, 2, 52 as related to activities originating from inside the head. Component

numbers 8, 2, and 52 likely relate to eye-artifacts, leaving components 32, 4, 26, 52, 56, 24, 3, 21, and 41 as sources originating from the brain. The volumes of the non-ocular related components were plotted in Figure A6. These volumes illustrate the set of components found that relate to the brain activity most represented in the all-subjects concatenated EEG dataset that were present during the vMWT paradigm.

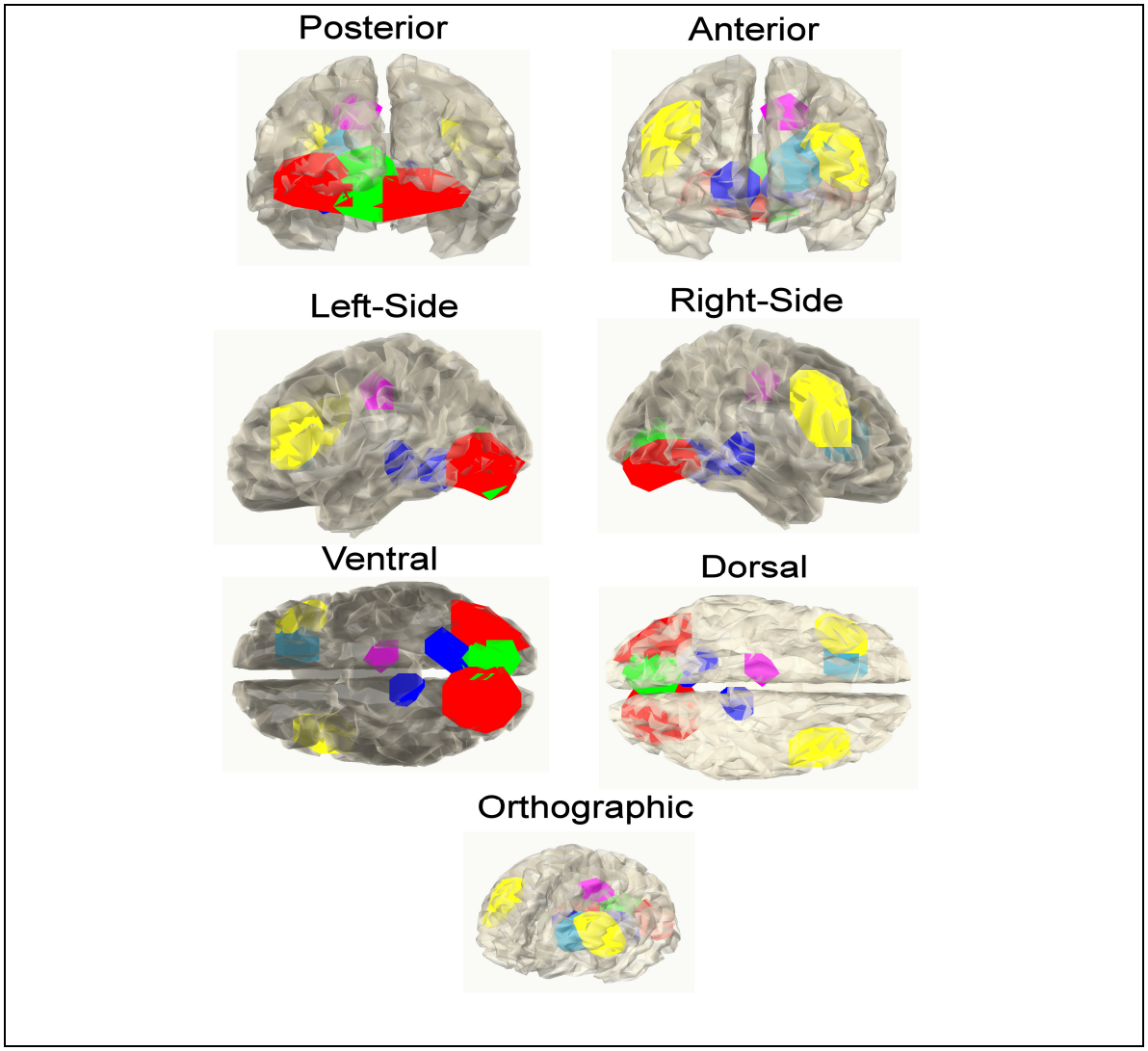

Figure A6. Estimated Volumes for validation components of the ICA (runica) decomposition of EEG data. Red (LEFT) is component 56; red (right) = component 52; cyan = component 23; blue (LEFT) = component 3; blue (right) = component 4; green = component 24; yellow (right) = component 21; yellow (left) = component 41; purple = component 26.

Explanation of the areas with respect to the colored volumetric representation is as follows. All references to plotted data refer to Figure A6.

RED BILATERAL (Components 52 and 56)

Volumes marked in red relate to the left and right hemisphere extrastriate visual cortex (V2) reflecting processing of visual information and its segregation into form, movement, and color information that is relayed to higher-level areas of processing through the ventral stream.

GREEN MEDIAL (Component 24)

The green region in the figure is likely related to the primary visual cortex (known as V1), also referred to as striate cortex, which is located medially in both hemispheres. As a volumetric representation it extends laterally and ventrally in both hemispheres. It is unlikely that the primary visual cortices of each hemisphere would be separated into distinct components by any measure of statistical independence of activities as it is believed that they both receive continuous and correlated visual information under normal conditions. (A visual field study with uncorrelated presentation of stimuli might be used dissociate these two cortices.) In these low resolution blurry depictions of the primary visual cortex in the figure, the volume of the primary visual cortex should appear to penetrate the extrastriate volumes because the related anatomy of the primary visual cortex wraps beneath the extrastriate cortex.

BLUE BILATERAL (Components 3 and 4)

These components are generally located in the ventro-medial temporal areas of the cortex. The modeled volume is more anterior in the right hemisphere than in the left hemisphere. Medial structures on the right include hippocampus and surrounding regions such as the parahippocampal cortex and the entorhinal cortex. These areas of the brain are thought to contribute to the integration of sensory information and the encoding of memories. Processing of this type related to spatial information is thought to be

predominantly in the right hemisphere. The volume located in the right hemisphere is more posterior than the volume in the left and is directly adjacent to the red and green areas identified as primary visual and high-level visual processing, respectively. Thus, the volume on the left appears to be part of the ventral stream that processes information about form and color.

PURPLE MEDIAL (Component 26)

The component relating to the purple volume in the figure is located in the left hemisphere and appears to be just superior to the corpus callosum on the medial aspect of the cortex. It could be located in the posterior-ventral part of the anterior cingulated cortex. This area is thought to be involved in emotional processing and learning.

CYAN MEDIAL (Component 23)

The region marked by the cyan volume is located medially in the frontal cortex and implicates activity in Brodmann areas 32 and/or 24, the most anterior part of the cingulate cortex. This region of the cortex is believed to be involved in episodic encoding and recognition. There is evidence that the anterior cingulate is involved in reinforcement learning via dopamine pathways.

YELLOW BILATERAL (Components 21 and 41)

These areas are located in the dorsolateral prefrontal cortex of both hemispheres. On the right side, the volume appears to also include the pre-motor cortex. These areas are known for what is called executive function and working memory.